Bayerische Julius-Maximilians-Universität Würzburg

Fakultät für Biologie

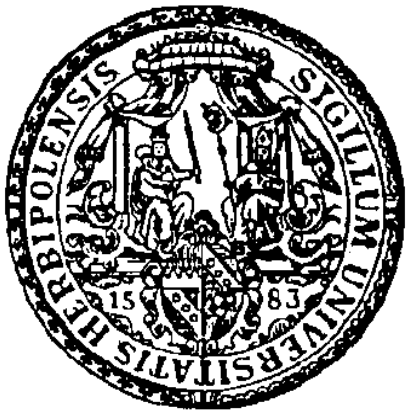

Vaccinia
Virus-mediated MR Imaging of Tumors in Mice: Overexpression of Iron-binding Proteins in Colonized Xenografts

Dissertation

Zur Erlangung des naturwissenschaftlichen Doktorgrades der bayerischen Julius-Maximilians-Universität Würzburg

vorgelegt von
Ulrike Geißinger
aus Aalen

Würzburg, 2010

meiner Familie

Eingereicht am:.....

Mitglieder der Promotionskommission:

Vorsitzender: Prof. Dr. T. Dandekar
Gutachter: Prof. Dr. A. A. Szalay
Gutachter: Prof. Dr. G. Krohne

Tag des Promotionskolloquiums:.....

Doktorurkunde ausgehändigt am:.....

Erklärung gemäß § 4 Absatz 3 der Promotionsordnung der Fakultät für Biologie der Bayerischen Julius-Maximilians-Universität Würzburg:

Hiermit erkläre ich, die vorgelegte Dissertation selbständig angefertigt zu haben und keine anderen als die von mir angegebenen Quellen und Hilfsmittel verwendet zu haben.

Des Weiteren erkläre ich, dass die vorliegende Arbeit weder in gleicher noch in ähnlicher Form bereits in einem anderen Prüfungsverfahren vorgelegen hat.

Zuvor habe ich neben dem akademischen Grad “Diplombiologin, Univ.” keine akademischen Grade erworben oder zu erwerben versucht.

Würzburg, 2010

Ulrike Geißinger

Contents

Summary

Vaccinia virus plays an important role in human medicine and molecular biology ever since the 18th century after E. Jenner discovered its value as a vaccination virus against smallpox. After the successful eradication of smallpox, vaccinia virus, apart from its use as a vaccine carrier, is today mainly used as a viral vector in molecular biology and increasingly in cancer therapy. The capability to specifically target and destroy cancer cells makes it a perfect agent for oncolytic virotherapy. Furthermore, the virus can easily be modified by inserting genes encoding therapeutic or diagnostic proteins to be expressed within the tumor.

The emphasis in this study was the diagnosis of tumors using different vaccinia virus strains. Viruses with metal-accumulating capabilities for tumor detection via MRI technology were generated and tested for their usefulness in cell culture and *in vivo*.

The virus strains GLV-1h131, GLV-1h132, and GLV-1h133 carry the gene encoding the two subunits of the iron storage protein ferritin under the control of three different promoters. GLV-1h110, GLV-1h111, and GLV-1h112 encode the bacterial iron storage protein bacterioferritin, whereas GLV-1h113 encodes the codon-optimized version of bacterioferritin for more efficient expression in human cells. GLV-1h22 contains the transferrin receptor gene, which plays an important role in iron uptake, and GLV-1h114 and GLV-1h115 contain the murine transferrin receptor gene. For possibly better iron uptake the virus strains GLV-1h154, GLV-1h155, GLV-1h156, and GLV-1h157 were generated, each with a version of a ferritin gene and a transferrin receptor gene. GLV-1h154 carries the genes that encode bacterioferritin and human transferrin receptor, GLV-1h155 the human ferritin H-chain gene and the human transferrin receptor gene. GLV-1h156 and GLV-1h157 infected cells both express the mouse transferrin receptor and bacterioferritin or human ferritin H-chain, respectively. The virus strains GLV-1h186 and GLV-1h187 were generated to contain a mutated form of the ferritin light chain, which was shown to result in iron overload and the wildtype light chain gene, respectively. The gene encoding the Divalent Metal Transporter 1, which is a major protein in the uptake of iron, was inserted in the virus strain GLV-1h102. The virus strain GLV-1h184 contains the *magA* gene of the magnetotactic bacterium *Magnetospirillum*

magnetotacticum, which produces magnetic nanoparticles for orientation in the earth's magnetic field.

Initially the infection and replication capability of all the virus strains were analyzed and compared to that of the parental virus strain GLV-1h68, revealing that all the viruses were able to infect cells of the human cancer cell lines A549 and GI-101A. All constructs exhibited a course of infection comparable to that of GLV-1h68.

Next, to investigate the expression of the foreign proteins in GI-101A and A549 cells with protein analytical methods, SDS-gelelectrophoresis, Western blots and ELISAs were performed. The proteins, which were expressed under the control of the strong promoters, could be detected using these methods. To be able to successfully detect the protein expression of MagA and DMT1, which were expressed under the control of the weak promoter, the more sensitive method RT-PCR was used to at least confirm the transcription of the inserted genes.

The determination of the iron content in infected GI-101A and A549 cells showed that infection with all used virus strains led to iron accumulation in comparison to uninfected cells, even infection with the parental virus strain GLV-1h68. The synthetic phytochelatin EC20 was also shown to enhance the accumulation of different heavy metals in bacterial cultures.

In vivo experiments with A549 tumor-bearing athymic nude mice revealed that 24 days post infection virus particles were found mainly in the tumor. The virus-mediated expression of recombinant proteins in the tumors was detected successfully by Western blot. Iron accumulation in tumor lysates was investigated by using the ferrozine assay and led to the result that GLV-1h68-infected tumors had the highest iron content. Histological stainings confirmed the finding that iron accumulation was not a direct result of the insertion of genes encoding iron-accumulating proteins in the virus genome.

Furthermore virus-injected tumorous mice were analyzed using MRI technology. Two different measurements were performed, the first scan being done with a seven Tesla small animal scanner seven days post infection whereas the second scan was performed using a three Tesla human scanner 21 days after virus injection. Tumors of mice injected with the virus strains GLV-1h113 and GLV-1h184 were shown to exhibit shortened T2 and T2* relaxation times, which indicates enhanced iron accumulation.

In conclusion, the experiments in this study suggest that the bacterioferritin-encoding virus strain GLV-1h113 and the *magA*-encoding virus strain GLV-1h184 are promising candidates to be used for cancer imaging after further analyzation and optimization.

Zusammenfassung

Das Vaccinia Virus spielt in der Humanmedizin und Molekularbiologie eine wichtige Rolle seit E. Jenner im 18. Jahrhundert seinen Nutzen als Impfvirus entdeckt hat. Nach der erfolgreichen Ausrottung der Pocken, wird das Vaccinia Virus heutzutage neben der Anwendung als Impfstoffträger hauptsächlich als viraler Vektor in der Molekularbiologie und in zunehmendem Maße in der Krebstherapie verwendet. Die Fähigkeit Krebszellen gezielt zu zerstören, macht es zu einem perfekten Wirkstoff für die onkolytische Virotherapie. Des Weiteren kann das Virus durch das Inserieren von Genen, die für therapeutische oder diagnostische Proteine kodieren, und im Tumor exprimiert werden, modifiziert werden.

Der Schwerpunkt dieser Arbeit war die Tumordiagnose mit Hilfe verschiedener Vaccinia Virusstämme. Viren mit der Fähigkeit, Metalle anzureichern wurden zur Tumordetektion mittels Kernspintomographie hergestellt und auf ihre Nutzbarkeit in Zellkultur und *in vivo* getestet.

Die Virusstämme GLV-1h132, GLV-1h132 und GLV-1h133 tragen das Gen, welches für die zwei Untereinheiten des Eisenspeicherproteins Ferritin kodieren unter der Kontrolle von drei verschiedenen Promotoren. GLV-1h110, GLV-1h111, und GLV-1h112 tragen das Gen, welches für das bakterielle Eisenspeicherprotein Bacterioferritin kodiert, wohingegen das inserierte Gen in GLV-1h113 für die codon-optimierte Version dieses Proteins kodiert, die eine effizientere Expression in humanen Zellen ermöglichen soll. GLV-1h22 beinhaltet das Transferrin-Rezeptor-Gen, welches eine wichtige Rolle in der Eisenaufnahme spielt, und GLV-1h114 und GLV-1h115 beinhalten das murine Transferrin-Rezeptor-Gen. Für eine möglicherweise bessere Eisenaufnahme wurden die Virusstämme GLV-1h154, GLV-1h155, GLV-1h156 und GLV-1h157 mit je einer Version eines Ferritin-Gens und eines Transferrin-Rezeptor-Gens generiert. GLV-1h154 trägt die Gene, die für Bacterioferritin und den humanen Transferrin Rezeptor kodieren, GLV-1h155 trägt die Gene für die humane Ferritin H-Untereinheit und den humanen Transferrin Rezeptor. Zellen, die mit GLV-1h156 und GLV-1h157 infiziert wurden, exprimierten den Maus-Transferrin-Rezeptor und Bacterioferritin beziehungsweise die humane Ferritin-H-Untereinheit. Die Virusstämme GLV-1h186 und GLV-1h187 wurden

mit einer mutierten Form der leichten Untereinheit von Ferritin, für die eine Überladung mit Eisen gezeigt wurde, beziehungsweise mit der leichten Untereinheit des wildtypischen Gens ausgestattet. Das Gen, das für den Divalenten Metal Transporter 1 kodiert, welches ein bedeutendes Protein für die Aufnahme von Eisen darstellt, wurde in den Virusstamm GLV-1h102 inseriert. Der Virusstamm GLV-1h184 trägt das *magA* Gen des magnetotaktischen Bakteriums *Magnetospirillum magnetotacticum*, welches magnetische Nanopartikel zur Orientierung im Erdmagnetfeld produziert.

Zunächst wurde die Infektions- und Replikationsfähigkeit aller Viren analysiert und mit der des Ausgangsstammes GLV-1h68 verglichen, was zeigte, dass alle Viren in der Lage waren humane Krebszellen der Zelllinien GI-101A und A549 zu infizieren. Alle Konstrukte zeigten einen vergleichbaren Infektionsverlauf zu GLV-1h68.

Als nächstes, um die Expression der fremden Proteine in GI-101A und A549 Zellen zu untersuchen, wurden SDS-Gelelektrophorese, Western Blots und ELISAs durchgeführt. Die Proteine, welche unter der Kontrolle von starken Promotoren exprimiert wurden, konnten mit diesen Methoden detektiert werden. Um die Expression von MagA und DMT1 zu detektieren, welche unter der Kontrolle des schwachen Promotors exprimiert wurden, wurde die sensitivere Methode RT-PCR angewendet, mit der zumindest die Transkription der Gene nachgewiesen werden konnte.

Die Bestimmung des Eisengehaltes in infizierten GI-101A und A549 Zellen zeigte, dass die Infektion mit allen Viren im Vergleich zu uninfizierten Zellen zu einer Eisenanreicherung führte, sogar die Infektion mit dem Ausgangsstamm GLV-1h68. Für das synthetische Phytochelatin EC20 wurde auch eine Anhäufung von verschiedenen Schwermetallen in Bakterienkulturen gezeigt.

In vivo Experimente mit A549 tumor-tragenden athymischen Nacktmäusen ergaben, dass Viruspartikel 24 Tage nach der Infektion hauptsächlich im Tumor gefunden wurden. Die von den Viren vermittelte Expression der rekombinanten Proteine in den Tumoren wurde erfolgreich mit Hilfe von Western Blots detektiert. Die Eisenansammlung in Tumorlysaten wurde mit dem Ferrozine Assay untersucht und führte zu dem Ergebnis, dass Tumore, die mit GLV-1h68 infiziert wurden, den höchsten Eisengehalt vorwiesen. Histologische Färbungen bestätigten die Erkenntnis, dass die

Eisenansammlung nicht ein direktes Resultat der Insertion von eisenansammelnden Genen in das Virusgenom war.

Darüberhinaus wurden tumortragende Mäuse, denen Virus injiziert wurde, mittels Kernspintomographie analysiert. Zwei verschiedene Messungen wurden durchgeführt, wobei die erste Messung sieben Tage nach Virusinjektion mit einem sieben Tesla Kleintier-Scanner durchgeführt wurde und die zweite Messung mit einem humanen drei Tesla Scanner 21 Tage nach Virusinjektion. Tumore von Mäusen, die mit den Virusstämmen GLV-1h113 und GLV-1h184 injiziert wurden, zeigten verkürzte T2- und T2*-Relaxationszeiten, was auf eine verbesserte Eisenakkumulation hinweist.

Zusammenfassend deuten die Experimente dieser Studie darauf hin, dass der Virusstamm GLV-1h113, welcher für Bacterioferritin kodiert, und der Virusstamm GLV-1h184, welcher für MagA kodiert, nach weiterer Untersuchung und Optimierung vielversprechende Kandidaten für die Krebs Bildgebung sind.

1 Introduction

1.1 Iron Metabolism

1.1.1 Iron

Iron is the sixth most abundant element in the universe and the fourth most abundant element in the earth's crust. Pure iron is rarely found on the surface of the earth because it oxidizes easily in the presence of oxygen and moisture. Iron is classified as a transition metal. Transition metals are defined by the IUPAC as elements whose atom has an incomplete d sub-shell, or which can give rise to cations with an incomplete d sub-shell. There are a number of properties shared by the transition elements which result from the incomplete *d* shell. These include the formation of colored compounds, the formation of compounds in many different oxidation states, and the formation of paramagnetic compounds (Matsumoto, 2005).

Almost all organisms depend on iron for survival. Iron forms compounds mainly in the +2 and +3 oxidation states. Under conditions of neutral or alkaline pH, iron is found in the Fe^{3+} state and at acidic pH in the Fe^{2+} state and can therefore accept or donate electrons, respectively. When in the Fe^{3+} state, iron will form large complexes with anions, water and peroxides. These large complexes have poor solubility. Fe^{2+} compounds are called ferrous and Fe^{3+} compounds ferric. The ability to exist in two redox states makes iron useful in many biochemical reactions serving as a cofactor for many enzymes. It is important for multiple metabolic processes including oxygen transport, cell proliferation, DNA synthesis, and electron transport. However, its redox reactivity can also lead to the generation of oxidative radicals that can damage essential cellular components such as lipids, proteins, and DNA. To avoid harm, organisms have to regulate their iron levels appropriately by iron transport, storage and regulatory proteins.

The average adult human contains 2-4 mg of iron. Most of the iron is in hemoglobin of blood erythrocytes. The supply of iron to erythrocyte precursors in the bone marrow and other tissues is largely maintained by daily recycling of about 20 mg of iron from senescent erythrocytes. Only 1-2 mg a day needs to be absorbed from the diet to

replace iron losses due to mucosal and skin epithelial cell sloughing (Nemeth and Ganz, 2006).

Good sources of dietary iron for the human body include red meat, fish, poultry, lentils and beans. Dietary iron can be in the heme (10%) or in the non-heme form (90%) (Munoz *et al*., 2009). Heme iron (iron from meat) is more easily absorbed than non-heme iron. There is no regulated physiological way of excreting iron and only small amounts of iron are lost daily. Therefore iron levels are controlled mostly by regulating iron uptake.

1.1.2 Iron Absorption and Transport

Iron absorption involves two steps: the uptake of iron form the intestinal lumen into the mucosa and the transfer across the mucosal cells into the circulation. Dietary iron can be taken up in either a heme or a non-heme form. Enterocytes in the epithelian cell layer of the duodenum and proximal jejunum are specialized for iron absorption. They express a number of proteins that are related to the uptake of iron. The majority of the food iron is in the ferric state that is not bioavailable. In the first step of the absorption the iron is taken up from the lumen of the intestine across the apical membrane and into the enterocyte (Frazer and Anderson, 2005). Non-heme iron in the ferric form is reduced by a ferric reductase (Dcytb = duodenal cytochrome B) in the duodenum before being transported into the enterocyte by the transmembrane transporter DMT1 (divalent metal transporter 1), which is also known as Nramp2 or DCT1 (Sargent *et al*., 2005). DMT1 transports iron only in the ferrous form. Most of the dietary iron is in the ferric form and has to be reduced before it can be taken up. Once inside the cell the iron (Fe^{2+}) has two fates depending on iron requirements. If iron is not required in the body it is stored by the iron storage protein ferritin and will be lost when enterocytes are sloughed from the villus some days later. If iron demand is high, it passes through the basolateral membrane through the iron exporter ferroportin. After reoxidation by the ferroxidase hephestin the Fe^{3+} is sequestered by apo-transferrin and circulates in the plasma (Sargent *et al*., 2005). When iron is not bound to transferrin it is called apo-transferrin and with iron it is called holo-transferrin. Transferrin is the main iron transport

protein in the body and it provides all cells in the organism with iron from the liver or the gut.

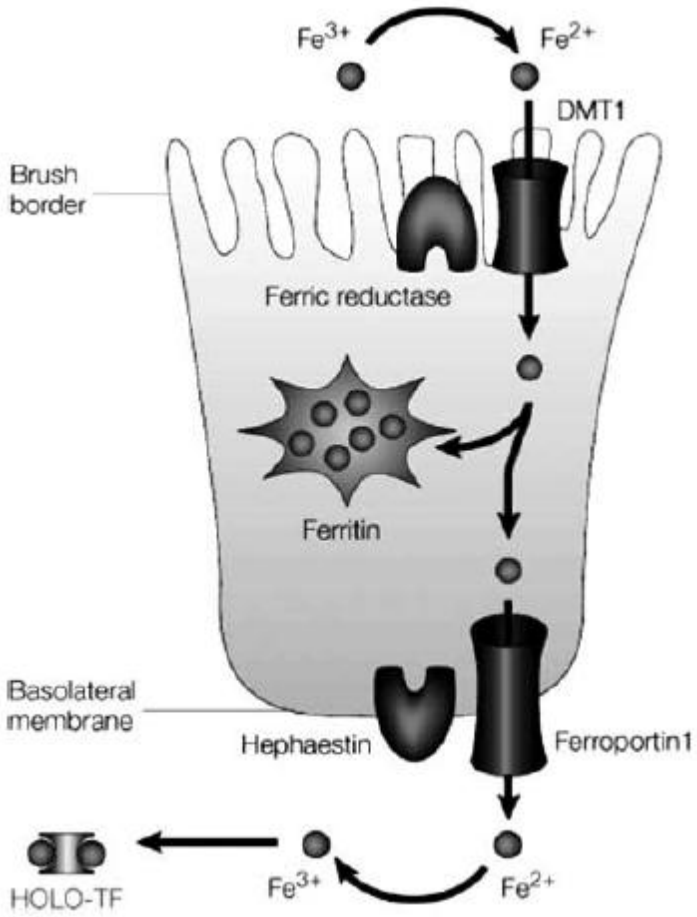

Fig. 1.1 Iron Absorption (from Andrews, 2000)

When the ferrous form of iron and protoporphyrin IX are complexed the structure is referred to as heme. Dietary heme iron has better bioavailability than non-heme iron but there is not as much known about it than about the absorption of non-heme iron. It was shown that heme from hemoglobin and other heme-containing proteins must be separated from protein fragments and then be absorbed as free heme. Heme enters the enterocytes as an intact molecule. The mechanisms by which heme binds to and enters

the enterocytes are largely unknown. Studies showed that the cells internalize heme through a not totally identified membrane protein (Munoz *et al*., 2009). After internalization into enterocytes, heme is degraded by a heme oxygenase into iron, biliverdin, and carbon monoxide (Testa, 2002). Inside the enterocytes most dietary heme-iron is released as ferrous iron and enters a common pathway with dietary non-heme iron (Munoz *et al*., 2009). The iron can be stored in intestinal enterocytes bound to ferritin. The transport protein ferroportin (also called IREG1= iron-regulated gene 1 or MTP-1) transports iron across the basolateral membrane of intestinal enterocytes into the circulation. Ferroportin is a highly conserved protein that is expressed and can export iron in organs like liver, spleen, kidney, heart, placenta and duodenum (Wessling-Resnik, 2006). Overexpression of ferroportin in tissue culture cells confirmed its role in iron release because depletion of cytosolic iron can be shown by decreased levels of ferritin (Abboud and Haile, 2000). Associated with ferroportin is the enzyme hephestin which is a copper-containing ferroxidase that oxidizes the ferrous form back to the ferric form. Once in the circulation, the ferric form of iron is bound to plasma transferrin.

The process of iron absorption is affected by different factors, for example variations in body iron stores, inflammation and pregnancy. These factors lead to changes in the expression of iron transport molecules in the duodenum at mRNA level and protein level (Frazer and Anderson, 2005).

1.1.3 Cellular Iron Uptake

The main protein that is involved in iron uptake into the cell is the plasma membrane transferrin receptor (TfR) (De Freitas *et al*. 2001). This receptor is a homodimeric glycoprotein. It binds diferric transferrin (Tf) in a pH dependent manner and delivers iron to the cells. Transferrins are single chain glycoproteins with two similar iron-binding sites that bind the majority of iron in the plasma. For that reason transferrin iron is the primary source of iron for non-intestinal cells. The process by which transferrin-bound iron is taken up into the cell is called receptor-mediated endocytosis. It can be distinguished into 6 main steps: binding, internalization, acidification, dissociation and

reduction, translocation, and cytosolic transfer of iron into intracellular compounds like ferritin (Qian and Tang, 1995). The first step in the process is the binding of transferrin to the extracellular part of the receptor. One transferrin molecule can bind to each subunit of the receptor. At physiological pH, the transferrin receptor has a high binding affinity for diferric serum transferrin. Apotransferrin binds transferrin receptor with a much lower affinity than diferric transferrin (Conrad *et al*., 1999). After the binding of the two proteins the complex internalizes through clathrin-coated pits into specialized endosomes. After clathrin is removed, the endosomes become acidified through an ATP-dependent proton influx, which leads to a conformational change in transferrin and transferrin receptor. This leads to the release of iron. After iron is released from the transferrin-transferrin receptor complex, it is still located in the endocytic vesicles and has to be transported through the vesicle membrane. Free Fe^{3+} has to be reduced to Fe^{2+} before transported out of the endosome by DMT1. The iron can either be stored or utilized by the cell. The transferrin-transferrin receptor complex is then recruited back to the cell surface. At physiological pH apo-transferrin dissociates from the receptor and returns to the circulation (Sargent *et al*., 2005). Transferrin can be reused between 100-200 times during its life time (Aisen *et al*., 2001).

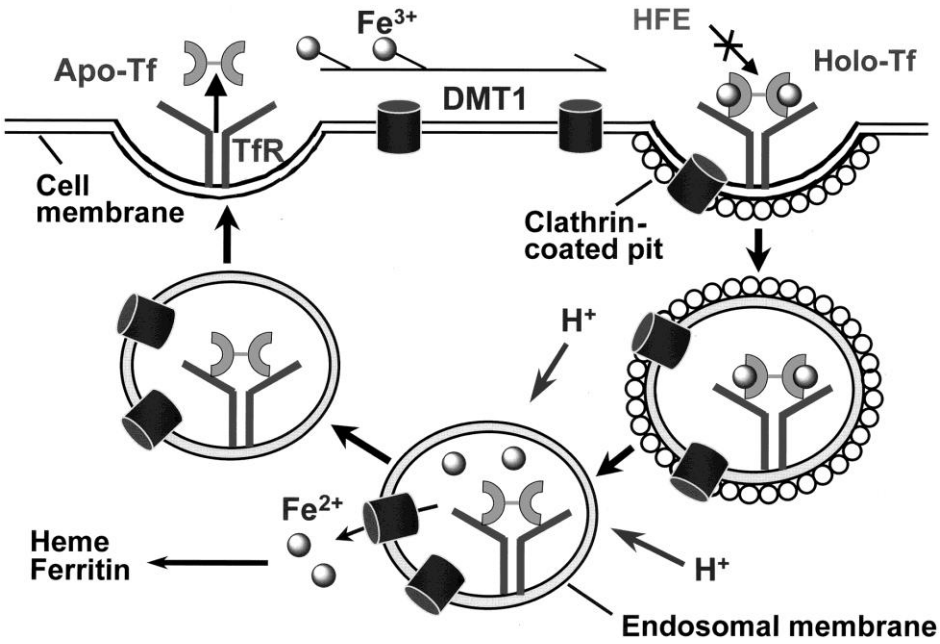

Fig. 1.2 Transferrin-transferrin Receptor: Receptor-mediated Endocytosis (from Qian *et al*., 2002)

1.1.4 Iron Storage and Release

Not all body iron is used in metabolic processes. To prevent free iron to accumulate to toxic precipitates it is stored in ferritins or hemosiderins. Ferritin is a highly conserved iron storage protein. It is constructed from 24 identical or very similar subunits that are folded in a four-helix bundle and contain a ferroxidase site, located within the four-helix bundle of individual subunits, and micelle nucleation sites facing the internal cavity. The subunits are assembled in a way that small hydrophobic and hydrophilic channels are formed at the 4-fold and 3-fold symmetry axes. These channels allow the passage of iron and other small molecules. Iron passes through the 3-fold channels by a negative electrostatic gradient and reaches the ferroxidase site (Douglas and Ripoli, 1998). Although ferritins store iron in the Fe^{3+} form, it is bound as Fe^{2+} and oxidized at the ferroxidase site. After oxidation, iron moves to the internal cavity of the ferritin shell which is rich in carboxylate residues that provide the nucleation sites of the ferric oxy-hydroxide micelles. When it is required for intracellular metabolism, ferritin iron can be mobilized by reduction of the oxy-hydroxide core (Chiancone *et al*., 2004).

Hemosiderin is a poorly defined complex that forms an insoluble iron storage system, which is thought to arise from the degradation of ferritin in lysosomes (Testa, 2002). The iron stored in hemosiderin is not easily available to supply iron when needed. Hemosiderin is mainly present in macrophages and is especially found after hemorrhage, which indicates that its formation is related to phagocytosis of red blood cells and hemoglobin. Hemosiderin can accumulate in different organs in various diseases.

1.1.5 Regulation of Iron Homeostasis

Most of the proteins of the iron metabolism are under tight genetic control. Their expression is up- or down-regulated dependent on the availability of iron. This control involves modulation of transcription, mRNA stability, translation, and posttranslational modification.

The posttranscriptional regulation is the best characterized. Its main components are the iron regulatory proteins (IRPs) and iron responsive elements (IREs). IRP1 and IRP2 are involved in the posttranscriptional regulation of iron metabolism by binding to IREs (Wang *et al*., 2002). These IREs are stem shaped structures located in the 5‘ and 3‘ untranslated regions of mRNA encoding proteins. Their structure includes a terminal hexanucleotid loop region with the sequence 5‘-CAGUGX-3‘, where X can be A, C or U, but never G and a base-paired stem structure that is interrupted by a conserved unpaired cytosine, six nucleotides down from the loop (Sargent *et al*., 2005). The binding of IRPs to single IREs in the 5‘UTRs of mRNA were found to block translation, whereas binding of IRPs to IREs in the 3‘UTRs stabilizes the mRNA and having a positive effect on translation (Sargent *et al*., 2005). The IRP/IRE regulated mRNAs include the transferrin receptor, ferritin, one isoform of DMT-1, and ferroportin (Nemeth and Ganz, 2006).

Figure 1.3 shows the effect iron levels have on the translation of mRNAs. The binding of IRPs to IREs is regulated by a number of different factors. When iron levels are high, a cubane iron sulphur cluster assembles in IRP1, inhibiting IRE binding and converting IRP1 to an aconitase (Pantopoulos *et al*., 2004). Under iron-limiting conditions this iron

sulphur cluster does not form, and IRP1 is able to bind IREs. This is different for IRP2 because this protein does not contain an iron sulphur cluster. IRP2 contains an iron-dependent degradation domain. In the presence of iron, proteasomes bind to this protein and degrade it and prevent its interaction with IREs. It has been shown that these two proteins do not differ in their ability to regulate ferritin and TfR1 expression (Erlitzki *et al*., 2002). However, it has been suggested that IRP2 dominates post-transcriptional regulation of iron metabolism in mammals (Meyron-Holtz *et al*., 2004).

In general it can be stated that through the IRE/IRP system iron deprivation in the cell leads to increased transferrin receptor expression, decreased iron storage through ferritin, and a decreased hemoglobin synthesis by the protein ε-ALAS. An increased concentration of iron in the cell results in increased expression of ferritin, reduced expression of transferrin receptor on the cell surface and augmentation of hemoglobin synthesis by ε-ALAS (Thomas *et al*., 2008).

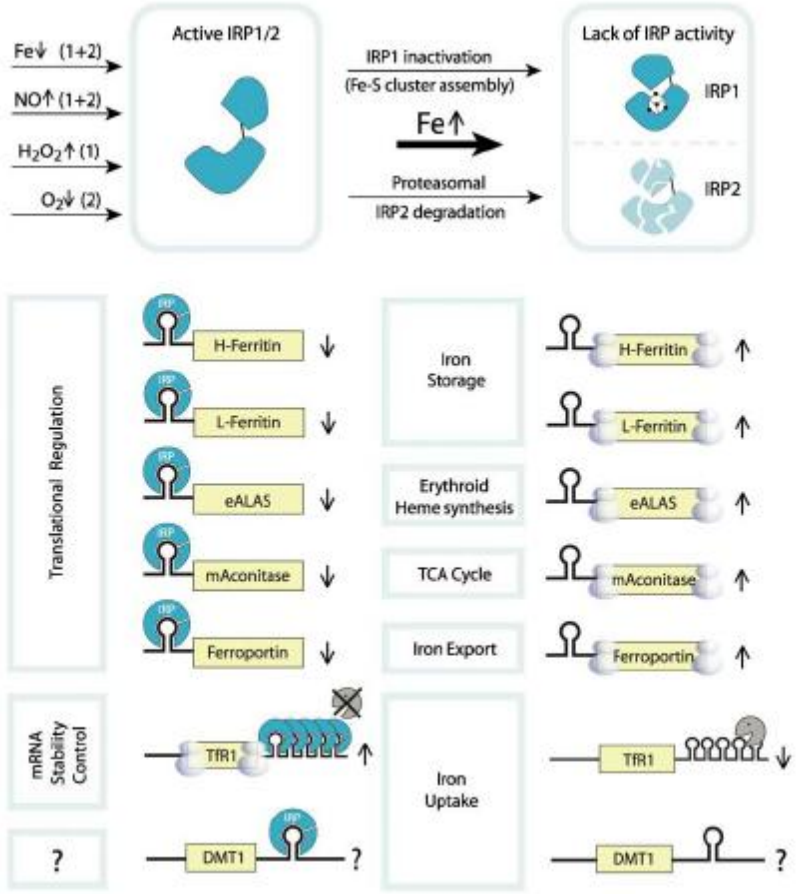

Fig. 1.3 Regulation of iron metabolism (from Hentze *et al*., 2004)

There are also mechanisms that are independent of the IRE/IRP system. Some cytokines has been shown to have an effect on the expression of some of the proteins involved in iron homeostasis. For example tumor necrosis factor-α, interleukin-1, interleukin-6 and interferon-γ all stimulate H-chain ferritin expression but reduce TfR1 expression (Torti and Torti, 2002).

The liver derived peptide hepcidine was also identified to play a part in iron homeostasis (Andrews, 2008). Hepcidine is a small peptide synthesized in the liver, which controls extracellular iron by regulating its intestinal absorption, placental transport, recycling by macrophages, and release from iron stores (Ganz and Nemeth, 2006). Its expression is related to body iron demand and it is increased in times when there is enough iron and

decreased when iron requirements are high. Hepcidine influences its downstream target cells to regulate how much iron they release into the plasma. Important cellular targets are intestinal enterocytes, macrophages and hepatocytes. Hepcidin controls cellular iron efflux by binding to the iron exporter ferroportin and causing its internalization and degradation. The hepcidine-encoding gene is controlled by factors like changes in body iron stores, changes in the rate of erythropoiesis, hypoxia and inflammation (Anderson *et al*., 2009). It was shown that hepcidine, hemojuvelin (HJV), HFE and TfR2 are all parts of the same regulatory pathway and upstream regulators of hepcidine (Camaschella *et al*., 2008). The upstream regulators respond to external signals and change hepcidine expression through one or more signal transduction pathways. Also proinflammatory cytokines such as IL-6 can induce expression of the hepcidine encoding gene through the janus kinase signal transducers and activators of transcription (JAK-STAT) pathway (Verga Falzacappa *et al*., 2007). Hepcidine expression can also be induced by hypoxia (Peysonnaux *et al*., 2007).

Another component of iron homeostasis is the hemochromatosis protein HFE. HFE is a heterodimeric membrane protein which has the ability to form non-covalent binding with β-microglobulin and has been shown to bind TfR1. Two molecules of HFE can bind to the dimeric TfR1 or one molecule together with diferric Tf. When both proteins are bound, HFE was shown to reduce the binding affinity of Tf for TfR. The reason for that can be either a structural change transmitted through the binding or HFE competing with Tf for the TfR1 binding site (Gianetti *et al*., 2004). The HFE gene is only slightly influenced by changes in cellular iron status (Theurl *et al*., 2005). It is also proposed that HFE participates in the regulation of intestinal iron absorption by modulating the expression of hepcidin. It was shown that the loss of HFE results in decreased hepcidin expression (Fleming and Britton, 2006).

1.1.6 Iron-accumulating Proteins Used in this Study

1.1.6.1 Ferritin

Ferritin is one of the major proteins of iron metabolism. It is an almost ubiquitous protein and its main functions are the sequestration and storage of iron (Harrison *et al*., 1996). Biochemical and structural properties of ferritin are largely conserved from bacteria to man. The peptide chains fold into four helix bundles with a long loop between helices B and C and a fifth short helix at the C-terminus. Twenty-four subunits assemble in large, highly stable complexes (Arosio and Levi, 2002).

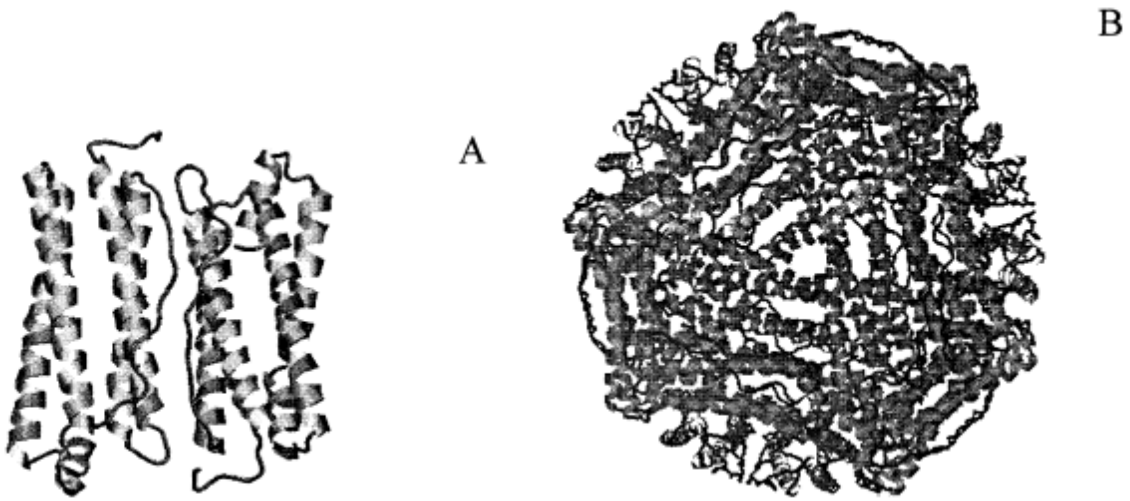

Fig. 1.4 A: Subunit dimers of human ferritin H-chain B: Assembled 24-mer protein (from Arosio and Levi, 2002)

Ferritin genes are present in almost all organisms, with the exception of yeast, which uses alternative mechanisms to store excess iron. Mammalian ferritin consists of a protein shell that can accommodate up to 4500 atoms of iron in its internal cavity. The protein shell has a molecular mass of around 450 kDa and is made up of 24 symmetrically arranged subunits of two types, a light subunit (L subunit) of approximately 19 kDa and a heavy subunit (H subunit) of approximately 21 kDa (Ponka,

1999). The H subunit has a ferroxidase activity that is necessary for iron incorporation into the ferritin molecule. The L subunit is required for iron mineralization inside the ferritin cavity (Testa, 2002). It was shown that a deletion of the H-chain is lethal in mice (Missirlis *et al*., 2007). Different proportions of the two subunits are the reason for the heterogeneity of ferritin in different tissues. The entry and exit of iron happens via channels in the protein shell. Once within the protein shell, iron is stored in the ferric state as ferric oxyhydroxide phosphate (Ponka, 1999).

All the ferritins have the property to interact with Fe^{2+} ions in solution under aerobic conditions and to induce iron oxidation and aggregation inside the cavity. The reaction with iron starts with the binding of Fe^{2+} to a specific site inside ferroxidase center. Iron interacts with oxygen, is oxidized to Fe^{3+} and then migrates to the cavity where it aggregates to form the iron core. In *in vitro* reactions the oxidation step is fast and completed in seconds, and the hydrolysis-mineralization step is slower and completed in minutes (Harrison and Arosio, 1996).

1.1.6.2 Bacterioferritin

The ferritins from bacteria and plants consist of 24 subunits of the same type. Ferritins from bacteria can be heme-free or contain heme. If they contain heme they are called bacterioferritins (Bfr). Ferritins and bacterioferritins have the same architecture, consisting of a 24mer cluster to form a hollow, spherical construction. The main function of ferritins is storage of iron and detoxification of iron is a secondary function. It is suggested that bacterioferritin has similar roles (Andrews *et al*., 2003). In general the iron storage cavity can accumulate 4500 iron ions as an inorganic complex core. In bacterioferritins the heme is located between the two subunits (Carrondo, 2003). There are normally 12 heme groups per 24mer. The heme is located in a pocket towards the inner surface of the protein shell, with the heme facing the inner cavity. The heme iron atom is coaxially ligated by two methionine residues, which is unique to the bacterioferritins. The purpose of the heme group is not clear. Heme-free Bfr variants from *E.coli* were shown to take up iron *in vitro* at a comparable rate as the wild type which leads to the conclusion that heme is not required for the iron uptake. However in

the study heme-free variants accumulated approximately four fold more iron *in vivo* than the heme-containing protein which shows that the heme group might be involved in the release of iron from Bfr (Andrews *et al*., 1995).

1.1.6.3 Transferrin Receptor

The transferrin receptor (TfR) has been characterized by Sutherland *et al*. in 1981. TfR is a major surface membrane component which is present in high levels on most fast proliferating normal and transformed cells (Larric and Cresswell, 1979). Because of that fact the TfR is known as a specific surface marker for rapidly growing cells like cancer cells. The main function of the TfR is the binding and internalizing iron into the cell by binding iron-bound transferrin (Klausner *et al*., 1983). The process by which transferrin receptors bind and facilitate entry of ferrotransferrin into cells is called receptor-mediated endocytosis. The TfR is a transmembrane, homodimeric, glycoprotein with a molecular weight of 180 kDa. Each identical 90 kDa subunit is covalently bound through a single disulfide bridge (Trowbridge and Omary, 1981) and organized in three domains, extracellular, transmembrane, and intracellular. The TfR is synthesized in the endoplasmatic reticulum, but it goes through several co- and posttranslational modifications during its synthesis and localization at the level of the cell membrane. The mature TfR is a glyco-phosphoprotein with covalently attached fatty acids (Omary and Trowbridge, 1981). The primary sequence contained in each functional monomer consists of about 760 amino acids. The C-terminus region of the polypeptide is facing the extracellular environment and the N-terminus domain represents the cytoplasmic tail of the receptor. The extracellular fragment contains the transferrin ligand-binding domain (Schneider, 1982; Schneider, 1984). After ligand-binding, trypsin treatment of cells was shown to lead to two molecules of labeled transferrin, which are recovered per molecule of receptor dimer, indicating that each monomer subunit binds a single transferrin molecule. Two moles of transferrin can be internalized by each mole of receptor. Since two moles of iron can bind to each mole of transferrin, up to four moles of iron can be transported into the cell for each transferrin receptor (Enns and Sussman, 1981; Schneider *et al*., 1982).

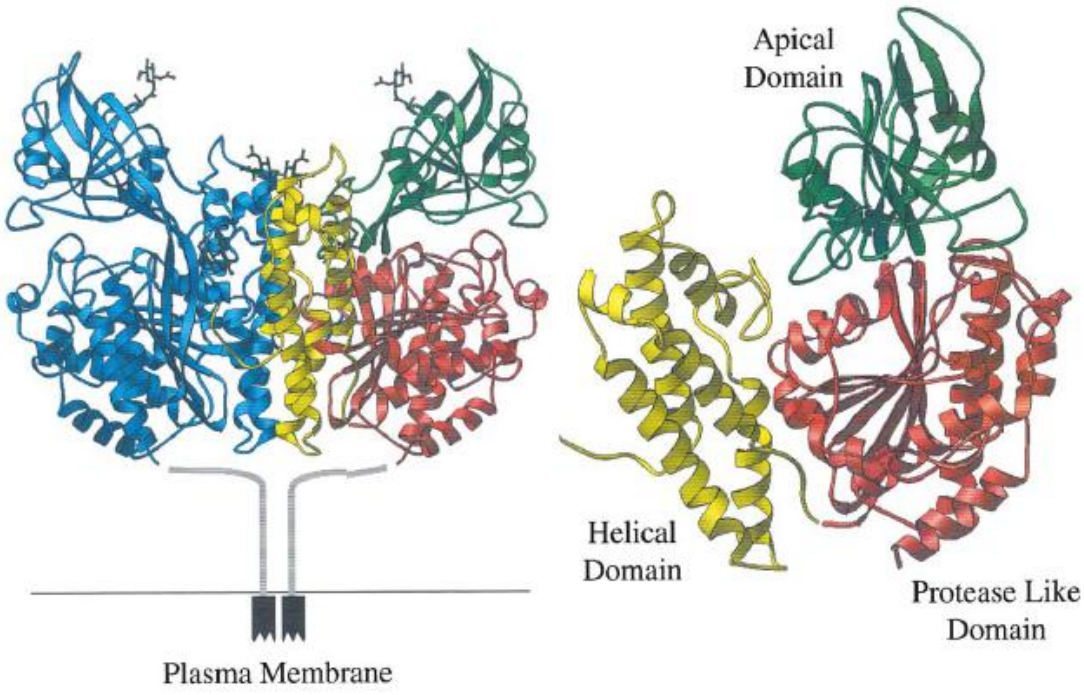

Fig. 1.5 Crystal structure of TfR (from Lawrence *et al*., 1999)

1.1.6.4 Divalent Metal Transporter

The divalent metal transporter (DMT1) is a ferrous ion transporter that is energized by the H^+ electrochemical potential gradient. It does not transport ferric iron. Its main location is on the brush border membrane of mature villous enterocytes of the proximal duodenum. The expression of DMT1 is tightly regulated by body iron status. This same transporter is also responsible for the recovery of iron from recycling endosomes during transferrin receptor-associated cellular uptake in erythroid precursor cells and many other cell types (Garrick and Garrick, 2004; Gunshin *et al*., 1997; Mackenzie, 2004). Gunshin *et al*. showed that, in addition to Fe^{2+}, a broad range of transition metal ions (Cd^{2+}, Zn^{2+}, Mn^{2+}, Cu^{2+}, Co^{2+}, Ni^{2+} and Pb^{2+}) can be transported by DMT1.

DMT1 was first identified in 1995. The human DMT1 gene consists of 17 exons over more than 36 kb (Lee *et al*., 1998). The 64 kDa protein is highly hydrophobic, with twelve transmembrane domains. Both amino and carboxy termini are predicted to be

within the cytoplasm. There is an extracellular loop between transmembrane domains seven and eight. The expression of DMT1 in intestinal cells has been shown to be regulated in response to iron status. Rats, which were made iron deficient showed increased levels of DMT1 mRNA detectable by Northern blotting of intestinal epithelial cells (Gunshin *et al*., 1997). The promoter of the human DMT1 gene contains several potential metal response elements, which leads to the conclusion that there is transcriptional regulation in response to iron levels (Lee *et al*., 1998). There are at least two different splice variants, encoding alternative carboxy termini and alternative 3‘ untranslated regions. The IRE sequence found in the 3‘ untranslated region of one of the two alternative splice forms of DMT1 mRNA binds IRP *in vitro* (Gunshin *et al*., 1997). That means the IRP binds under low iron conditions and stabilizes the DMT1 mRNA, leading to an increase in the amount of the expressed DMT1 protein.

1.1.6.5 MagA from *Magnetospirillum magnetotacticum*

Magnetotactic bacteria are a class of bacteria which were discovered in the 1960s. They have the ability to orient themselves along the magnetic field lines of the earth’s magnetic field. To be able to do that they have organelles, called magnetosomes, that contain magnetic crystals. This phenomenon is called magnetotaxis. It is believed to help these organisms in reaching regions of optimal oxygen concentration. The first description of magnetotactic bacteria appeared in 1963 in a publication of the Instituto di Microbiologia of the University of Pavia (Bellini, 1963). While he was looking at bog sediments under his microscope, Bellini discovered a group of bacteria that oriented themselves in a unique direction. He realized that these microorganisms moved according to the direction of the North Pole and called them „magnetosensitive bacteria“ (Bellini, 1963). The first peer-reviewed article on magnetotactic bacteria appeared in a 1975 article in Science by Richard Blakemore, a microbiologist who made similar observations. He realized that these organisms were following the direction of earth’s magnetic field, from south to north, and invented the term „magnetotactic“ (Blakemore, 1975).

The sensitivity of magnetotactic bacteria to the earth's magnetic field comes from the fact that the bacteria precipitate chains of crystals of magnetic minerals within their cells. Magnetotactic bacteria can be divided in two categories, according to whether they produce particles of magnetite (Fe_3O_4) or greigite (Fe_3S_4). Magnetite possesses a magnetic moment three times that of greigite (Faber, 2001). Magnetite-producing magnetotactic bacteria can be usually found in transition zones between oxygen-rich and oxygen-starved water or sediment. Many magnetotactic bacteria are only able to survive in environments with very little oxygen or in completely anaerobic environments. The evolutionary advantage of having magnetosomes might be the ability to efficiently navigate within this zone of sharp chemical gradients (Bazylinsky, 1995).

The different morphotypes found in environmental samples of water or sediment shows the diversity of magnetotactic bacteria. Mainly found morphotypes are spherical or ovoid cells (cocci), ros-shaped (bacilli), curved bacteria (vibrio) and helical (spirillum) of different sizes. All magnetotactic bacteria studied so far are moving with the use of flagella and have a cell wall structure characteristic of Gram-negative bacteria. Another difference, which shows their diversity, is the arrangement of magnetosomes inside the bacterial cell. In the majority of magnetotactic bacteria, the magnetosomes are aligned in chains of different lengths and numbers along the cell's long axis, which is magnetically the most efficient orientation.

Magnetosomes are held in place with cytoskeletal filaments and surrounded by a lipid bilayer and usually contain 15-20 crystals of magnetite and can vary with environmental conditions. The combination of each tiny magnetic dipole enables the magnetosome chain to guide the bacterium in its ideal direction. The magnetosome points the bacteria in the direction of optimal growth environment, but flagella are necessary for them to get there (Frankel and Bazylinsky, 2004).

Because the magnetite in the magnetosomes is derived from iron, there must be a way for the cell to take up iron. The *magA* gene was shown to be responsible for the iron uptake, encoding a H/Fe(II) antiporter on the cytoplasmic membrane (Matsunaga *et al*., 2005 and Suzuki *et al*., 2006). It was shown that *magA* alone is sufficient for producing magnetic nanoparticles in mammalian cells (Zurkiya *et al*., 2008).

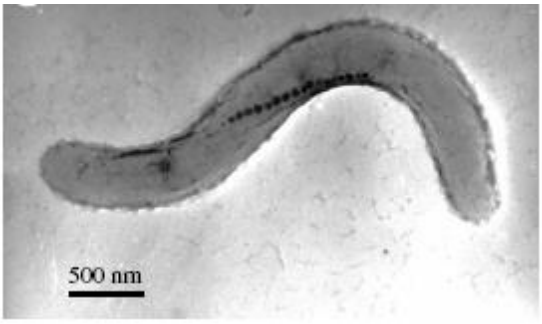

Fig 1.6 TEM image of *Magnetospirillum magnetotacticum* strain AMB-1 with magnetosomes (from Arakaki, 2008)

1.1.6.6 Synthetic Phytochelatin EC20

The contamination with heavy metals from agricultural, industrial, and military operations has serious negative effects on the environment. Higher organisms respond to the presence of heavy metals with the production of cystein-rich peptides such as glutathione, phytochelatins (PCs), and metallotheins (MTs) that bind metal ions and sequester them in biologically inactive forms (Bae *et al*., 2000). PCs are short, cysteine-rich peptides with the general structure $(\gamma Glu\text{-}Cys)_nGly$ (n=2-11) (Zenk, 1996). PCs have a higher metal-binding capacity than MTs. Suggestions have been made to use PCs for detoxification of heavy metals (Zenk, 1996). However generating organisms that overexpress PCs require a very good knowledge of the mechanisms involved in synthesis and chain elongation of these peptides. The presence of a γ-bond between glutamic acid and cysteine in PCs indicates that these peptides must be synthesized enzymatically. An alternative strategy is to develop organisms carrying synthetic genes encoding protein analogs of PC (ECs). These peptides differ from PCs because the peptide bond between glutamic acid and cysteine is the standard α peptide bond that can be synthesized on the ribosomal machinery. It was shown that several ECs bind metals in a similar way than their corresponding PCs (Bae and Mehra, 1997) and it is possible to produce large quantities of ECs with any defined chain length.

Bae *et al*. described the construction and characterization of recombinant *E. coli* strains that bind functional synthetic phytochelatins on the cell surface. It was shown that these synthetic phytochelatins give a metal-binding capability to the host cells and lead to a higher accumulation of cadmium than the wild type cells. In this study EC20, a synthetic phytochelatin with 20 cysteines, is used to accumulate different metals in bacteria. EC20 was integrated into an outer loop of the *E. coli* surface protein TolC. This concept could possibly be used in the future by generating new EC20-encoding vaccinia viruses for tumor detection with MRI technology.

1.2 Vaccinia Virus

1.2.1 History

The most famous virus of the poxvirus family in human medicine is the variola virus. This virus can cause smallpox, a once common and very lethal disease that influenced human history by killing millions of people. The English physician Edward Jenner found that an infection with a cowpox virus leads to an immunity against smallpox. As a result of these findings smallpox was eradicated in 1977 through a dedicated effort by the World Health Organization through prophylactic inoculations with cowpox virus and vaccinia virus.

Vaccinia virus is the best characterized member of the poxvirus family. Its origin is unclear but it was the first animal virus seen microscopically, grown in tissue culture, tittered accurately, purified, and analyzed (Moss, Fields Virology).

1.2.2 Taxonomy

The vaccinia virus belongs to the family of poxviruses, which are complex DNA viruses that replicate in the cytoplasm of vertebrate or invertebrate cells. Poxviridae are divided into two subfamilies, the chordopoxviridae and the entomopoxviridae. This distinction is

based on their host range, which are insects for the entomopoxviridae and vertebrates for the chordopoxviridae. The subfamily of the chordopoxviridae consists of eight genera: orthopoxviruses, parapoxviruses, avipoxviruses, capripoxviruses, leporipoxviruses, suipoxviruses, molluscipoxviruses, and yatapoxviruses. The orthopoxviruses have been studied most intensively. Both the human pathogen variola virus and the vaccinia virus belong to the orthopoxviruses whereas vaccinia virus is most studied virus of the genus.

1.2.3 Morphology

Poxviruses are large DNA viruses. They contain a double-strand DNA molecule between 130 and 300 kb (Moss, 2001) that encodes for around 200 genes. The DNA is associated with a number of virus-encoded proteins like RNA polymerase, transcription factors, and enzymes for RNA capping, methylation and polyadenylation, which are packaged within the core to enable early viral protein synthesis (Shen and Nemunaitis, 2005). In molecular biology it is very useful as a vector because up to 25 kb can be integrated in its genome (Smith and Moss, 1983).

The basic infectious form of the poxvirus is the mature virion. The virions have a barrel shape with dimensions of ~360x270x250 nm. The thickness (5-6 nm) and density of the outer layer is comparable to one lipid membrane bilayer. The internal structure of the virion consists of a dumbbell-shaped core and aggregates of heterogeneous material which are called lateral bodies between the concavities and the outer membrane. The core wall consists of two layers. The inner layer is continuous except for a few channels and has a diameter resembling a lipid membrane. The outer layer has a palisade structure that is made of T-shaped spikes that are anchored in the lower membrane.

The main components are protein (90%), lipid (5%) and DNA (3.2%). The lipid components of vaccinia virus are predominantly cholesterol and phospholipids (Sodeik *et al*., 1993; Stern *et al*., 1974).

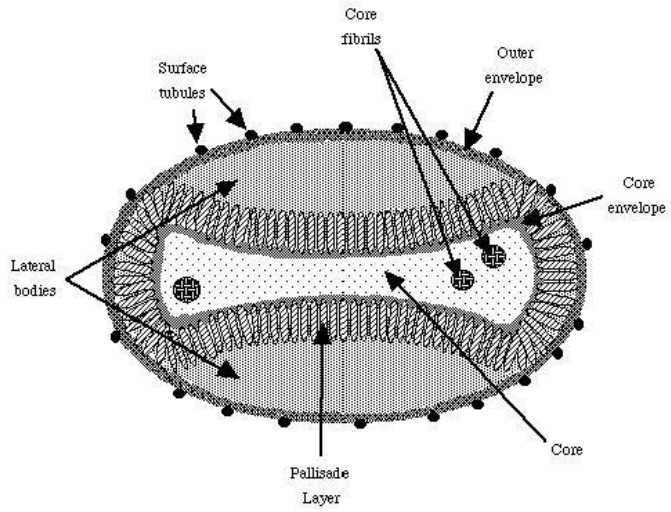

Fig 1.7 Vaccinia Virus Morphology

1.2.4 Vaccinia Virus Replication Cycle

The infection of a cell begins with the binding of a vaccinia virus particle to the cell. It is not known exactly how the virus binds the cell membrane, but the virus is thought to be taken in by membrane fusion. After the fusion of the viral and cellular membranes, the viral core that contains the necessary proteins for early replication, is released into the cytoplasm and transported further into the cell along microtubules to the cytoplasmic side of the endoplasmatic reticulum (*ER*). Unlike other DNA viruses, vaccinia remains in the host cell cytoplasm for the duration of the infectious cycle. After entry into the cytoplasm, the core partially uncoats to synthesize early viral mRNAs which resemble host cell mRNAs. This happens in a period of 20 minutes after infection of the virus particle. The cellular translational apparatus is recruited for translation of these mRNAs that encode for proteins involved in viral DNA synthesis. Other early proteins serve to modify the host cell to the advantage of the virus and destroy the viral nuclear membrane to free the genome (Sieczkarsky and Whittaker, 2005). Replication of the viral DNA starts one to two hours after infection (Moss, 2001). After the DNA replication has started in so-called mini-nuclei, which are surrounded by rough ER membranes, immediate genes and late genes are transcribed (Tolonen *et al*., 2001). Immediate genes serve mainly for the transcription of late genes, which are involved in packaging

of the new viral particles and for essential proteins that start the early gene transcription in an infected cell. After synthesis of all the necessary proteins, assembly of mature virus particles begins (Harrison *et al*., 2004). Assembly involves condensation of viral DNA, packing in the nuclear membrane and proteolytic cleavage of some capsid proteins (Smith *et al*., 2003). Intracellular mature virions (IMVs) will either be released by lysis of the cell or move away from DNA sites by binding to microtubules of the host cell and get a second double membrane from a trans-Golgi or early endosomal compartment to become intracellular enveloped virions (IEVs) (Harrison *et al*., 2004). The IEV particles use microtubules and kinesins to move towards the cell membranes and fuse with the membranes to form cell-associated enveloped virus (CEVs). CEVs can use actin from the cytoplasm to be transported to neighboring cells or dissociate from the cell membrane to become extracellular enveloped viruses (EEVs). Most of the EEVs are still bound to the cell membrane even at late stages of infection (Blasco and Moss, 1992).

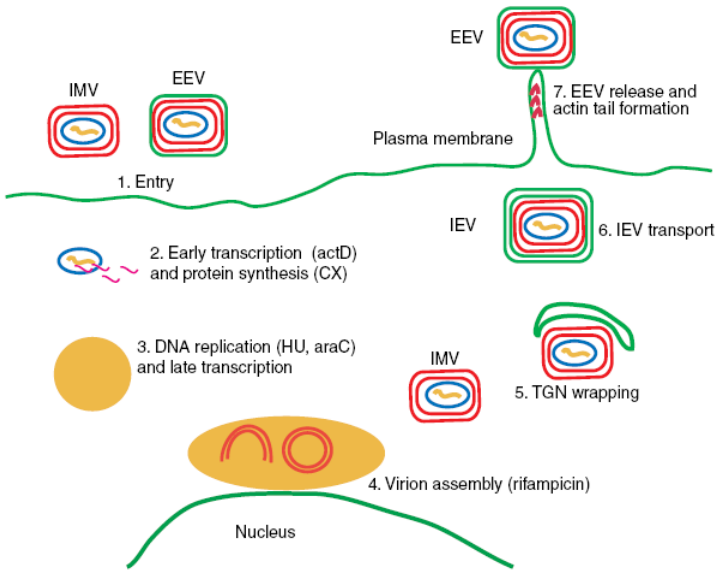

Fig 1.8 Vaccinia Virus Replication Cycle (from Schramm and Locker, 2005)

The replication and assembly of new virus particles is regulated by a time-dependent control of the gene expression. Proteins, which are used for DNA replication, nucleotide biosynthesis, and destruction of the nuclear membrane to free the DNA, are synthesized early in the infection cycle. Proteins, which are used for the morphogenesis and assembly of the new viruses, are intermediate and late gene products (Rosel and Moss, 1985).

Gene expression is mainly regulated at the initiation step of the transcription. Transcription factors for intermediate genes are synthesized as early proteins and transcription factors for late genes are products of intermediate genes. Transcription factors for early genes are made as late proteins of the previous cycle and packaged into new virions so they are brought into the cell by the infecting viruses and can start early gene transcription immediately. Around 50% of all genes belong to the early genes (Oda and Jocklik, 1967). These genes are synthesized in the viral nucleus. The intermediate and late transcription happens in the cytoplasm and uses also proteins of the host cell for initiation and termination of the transcription instead of only viral proteins in the early transcription (Broyles, 2003).

1.2.5 Oncolytic Viruses

Poxvirus strains have been used for different therapeutic purposes, for example, the modified Vaccinia virus Ankara (MVA) that was used as a smallpox vaccine is now used as a recombinant vaccine vector for immunization against a various diseases and cancers (Garber *et al*., 2009). MVA can efficiently express high levels of foreign genes and is used in clinical trials as a tool for vaccination against different infectious diseases like malaria, tuberculosis, HIV/AIDS or cancer (Moorthy *et al*., 2004, McShane *et al*., 2005, Mwau *et al*., 2004, Smith *et al*., 2005). One main advantage for the use of vaccinia virus is the long clinical experience that started with the smallpox eradication program and that also demonstrated that vaccinia virus is safe for use in humans.

Oncolytic viruses are viruses that have the capacity of infecting and replicating in tumor cells. This selective behavior can have different reasons, for example tumor specific

mutations. Many growth-stimulating factors in tumor cells lead to an increased concentration of nutrition factors. Tumor cells also lose some of the important components of the intracellular defense system. Another reason can be that some viruses use the cellular mechanisms for the production of viral proteins which can lead to cell death of the tumor cells.

Poxviruses have been used for different approaches in cancer therapy, for example gene therapy and development of cancer vaccines. The capability to replicate in and lyse human cells in comparison with other virus species makes poxviruses very promising oncolytic agents (Wein and Kirn, 2003). Additionally, poxviruses display a broad tumor tissue tropism because they infect cells by membrane fusion and not by binding to specific cell surface receptors (Thorne *et al*., 2007). This makes poxviruses easy to study in laboratory animals which is of special importance for preclinical studies. First- and second-generation oncolytic viruses have been shown to be safe and showed a high selectivity for cancer although their therapeutic potential was poor. In the next step genetically modified third-generation oncolytic poxviruses that carry therapeutic transgenes, have been engineered. Examples of the transgenes are cytokines, pro-drug converting enzymes, immunostimulating and antiangiogenic agents (Kirn *et al*., 2006, Hodge *et al*., 1999, Thorne *et al*., 2006, Frentzen *et al*., 2009). These genes can also be chosen for imaging purposes, for example optical imaging with luciferases or fluorescing proteins (Yu *et al*., 2004, Luker e*t al*., 2005, Gross and Piwnica-Worms, 2005) or deep tissue imaging by using PET (Chen e*t al*., 2009) or MRI technology. It was recently shown that vaccinia virus targets cancer cells which provide perfect conditions for its replication like blocks in apoptotic pathways, deregulation of cell cycle control and evasion from the host immune system (Yu *et al*., 2004, Kirn and Thorne, 2009). Also, vaccinia virus is able to carry a large amount of foreign genes which allows the expression of various genes. An advantage for the use in humans is that vaccinia virus replicates in the cytoplasm of the host cell and that there is no chance of DNA integration in the genome.

It is also a possibility to attenuate viruses so they can exclusively replicate in tumor cells. It has been shown that a deletion of the thymidine kinase gene in vaccinia virus leads to dependence of the virus on cellular thymidine expression, which is

overexpressed in tumor cells (Buller *et al*, 21985). Another major advantage is ability of vaccinia virus to travel within the blood and therefore reach distant tumor sites like metastases (Park *et al*., 2008).

1.2.6 Vaccinia Virus Strains Used in this Study

The recombinant vaccinia virus GLV-1h68 is a genetically stable oncolytic vaccinia virus that has been constructed by Genelux Corporation (San Diego, CA). It was shown that it is capable to locate, enter, colonize and destroy cancer cells without harming healthy cells (Zhang *et al*., 2007). GLV-1h68 was derived from the vaccinia virus Lister strain (*LIVP wt*), a European vaccine strain. Three expression cassettes were inserted into the *F14.5L*, *J2R*, and *A56R* loci of the viral genome. These three expression cassettes are the *Renilla* luciferase *Aequorea* green fluorescent protein fusion gene (*RUC-GFP*), the ß-galactosidase gene (*lacZ*), and the ß-glucuronidase gene (*gusA*). The *Ruc-GFP* fusion protein gene located in the *F14.5L* locus is under control of an early/late promoter whereas the marker gene ß-galactosidase in the *J2R* locus is under control of the $P_{7.5}$ promoter. The transferrin receptor gene (*rhTfr*) cDNA was inserted in the reverse orientation to vaccinia synthetic early/late promoter to serve as a negative control for a TFR-expressing recombinant virus (Zhang *et al*., 2007). Another marker gene coding for ß-glucuronidase was inserted into the *A56R* locus and is under control of the P_{11K} promoter.

GLV-1h68

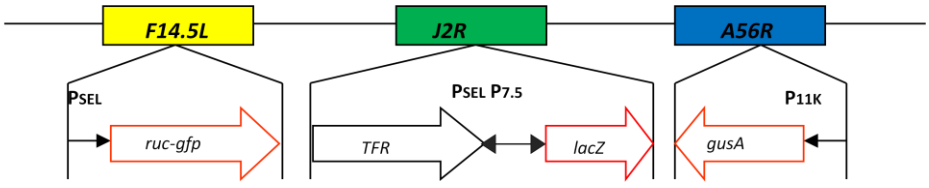

Other viruses used in this study were constructed while working on this project and are described in detail in paragraph 2.6 recombinant viral constructs.

1.3 Cancer

Cancer is a major public health problem all over the world. Currently, one in four deaths in the United States is caused by cancer. It affects people at all ages but the risk for most different cancers increase with age. Overall cancer death rates decreased in men by 19.2% between 1990 and 2005, with decreases in lung (37%), prostate (24%), and colorectal (17%) cancer rates accounting for nearly 80% of the total decrease. In women, overall cancer death rates between 1991 and 2005 decreased by 11.4%, with decreases in breast (37%) and colorectal (24%) cancer rates responsible for 60% of the total decrease (Cancer Statistics, 2009). This reduction of cancer deaths is mainly due to better and earlier detection methods.

Estimated New Cases*

Males			Females		
Prostate	192,280	25%	Breast	192,370	27%
Lung & bronchus	116,090	15%	Lung & bronchus	103,350	14%
Colon & rectum	75,590	10%	Colon & rectum	71,380	10%
Urinary bladder	52,810	7%	Uterine corpus	42,160	6%
Melanoma of the skin	39,080	5%	Non-Hodgkin lymphoma	29,990	4%
Non-Hodgkin lymphoma	35,990	5%	Melanoma of the skin	29,640	4%
Kidney & renal pelvis	35,430	5%	Thyroid	27,200	4%
Leukemia	25,630	3%	Kidney & renal pelvis	22,330	3%
Oral cavity & pharynx	25,240	3%	Ovary	21,550	3%
Pancreas	21,050	3%	Pancreas	21,420	3%
All Sites	**766,130**	**100%**	**All Sites**	**713,220**	**100%**

Estimated Deaths

Males			Females		
Lung & bronchus	88,900	30%	Lung & bronchus	70,490	26%
Prostate	27,360	9%	Breast	40,170	15%
Colon & rectum	25,240	9%	Colon & rectum	24,680	9%
Pancreas	18,030	6%	Pancreas	17,210	6%
Leukemia	12,590	4%	Ovary	14,600	5%
Liver & intrahepatic bile duct	12,090	4%	Non-Hodgkin lymphoma	9,670	4%
Esophagus	11,490	4%	Leukemia	9,280	3%
Urinary bladder	10,180	3%	Uterine Corpus	7,780	3%
Non-Hodgkin lymphoma	9,830	3%	Liver & intrahepatic bile duct	6,070	2%
Kidney & renal pelvis	8,160	3%	Brain & other nervous system	5,590	2%
All Sites	**292,540**	**100%**	**All Sites**	**269,800**	**100%**

Fig.1.9 Ten leading cancer types for estimated new cancer cases and deaths, by sex, United States, 2009 (Cancer Statistics, 2009)

Cancer is a class of diseases in which a group of cells displays uncontrolled growth, invasion, and sometimes metastasis. These three properties of malignant cancers distinguish them from benign tumors, which are self-limited and do not invade or metastasize. Most cancers form a tumor but some, like leukemia, do not.

Nearly all cancers are caused by abnormalities in the genetic material of the transformed cells. These abnormalities can originate from effects of carcinogens like tobacco smoke, radiation, or chemicals. Genetic abnormalities that cause cancer can also be randomly acquired through errors in DNA replication or can be inherited, and are as a result present in all cells from birth (Weinberg, 2007).

Genetic abnormalities in cancer cells usually have to do with two classes of genes. Cancer-promoting oncogenes are typically activated in cancer cells and are giving those cells new properties, for example overactive growth and division, protection against programmed cell death and the ability to become established in different tissue environments. The second class of genes are tumor suppressor genes and they are inactivated in cancer cells. This causes the loss of functions in these cells like correct DNA replication, control over the cell cycle, orientation and adhesion within tissues, and interaction with protective cells of the immune system (Weinberg, 2007).

D. Hanahan and R.A. Weinberg suggest six essential cell modifications that are responsible for malignant growth: self-sufficiency in growth signals, insensitivity to growth-inhibitory signals, evasion of programmed cell death (apoptosis), limitless replicative potential, sustained angiogenesis, and tissue invasion and metastasis (Hanahan and Weinberg, 2000).

1.3.1 Classification and Morphology

Cancers are classified by the type of cell that resembles the tumor and by the tissue that is the origin of the tumor. Histology and location are important factors to help identifying the tumor.

The majority of human tumors come from epithelial tissues. These cancers are called carcinomas and are responsible for more than 80% of the most common human cancer-related deaths in the Western world. Tumors coming from the epithelial cell layers of the gastro-intestinal tract, which includes mouth, esophagus, stomach and small and large intestines, skin, mammary gland, pancreas, liver, ovary, gall bladder, and urinary bladder belong to that group. Most of the carcinomas belong to two main categories that come from the two main functions of epithelia. Epithelial cells serve to protect the cells under them. Tumors that come from these protective cell layers are called squamous cell carcinomas. Many epithelia also contain specialized cells that secrete substances into the ducts or cavities that they line. This class of epithelial cells is the origin of adenocarinomas (Weinberg, 2007).

The rest of the malignant tumors originate from non-epithelial tissues throughout the body. One class of non-epithelial cancers comes from connective tissues, which are called sarcomas. Sarcomas originate from different mesenchymal cell types, for example fibroblasts, adipocytes, osteoblasts, and myocytes. Another group of non-epithelial cancers arise from the hematopoietic cells and cells of the immune system. Leukemia is a cancer of hematopoietic cells that move through the circulation. Lymphomas include tumors of the lymphoid lineages (B and T lymphocytes) that aggregate and form solid tumors, mostly found in lymph nodes (Weinberg, 2007).

The third main group of non-epithelial tumors derives from cells that are part of the central and peripheral nervous system. These are called neuroectodermal tumors to reflect their origin in the outer cell layer of the early embryo and include are gliomas, glioblastomas, neuroblastomas, schwannomas, and medullablastomas (Weinberg, 2007).

Melanomas derive from melanocytes, the pigmented cells of the skin and retina. Small-cell lung carcinomas contain cells that have many attributes of neurosecretory cells. It is unclear whether they arise from neuroectodermal cells or from endodermal cells of the lung (Weinberg, 2007).

Most cancer cells seem to have one major similar biological principle in common. They almost always keep some of the distinctive characteristics of the normal cell types from which they have developed (Weinberg, 2007).

1.3.2 Cancer Cell Lines Used in this Study

1.3.2.1 GI-101A Cell Line

The GI-101A cell line was developed and characterized as human breast epithelial (Hurst *et al*., 1993). The original GI-101 breast tumor xenograft was developed from an infiltrating ductile breast carcinoma and propagated in athymic mice for over eight years. A cell line was then developed from this tumor xenograft and has been grown in culture for over 35 passages. It was shown, that when injected subcutaneously into nude mice,

this cell line is tumorigenic and consistently metastasizes to the lung and lymph node of the murine host, a pattern similar to that seen in the original patient.
GI-101A is shown to be ER+ and responsive to estrogen for growth (Morrissey and Raney, 1998).

1.3.2.2 A549 Cell Line

The A549 cell line was initiated in 1972 by D.J. Giard *et al*. through explant culture of lung carcinomatous tissue from a 58-year old male.

1.4 MRI Technology

Magnetic Resonance Imaging (MRI) is a method of examining tissues and organs inside the body without using surgery, harmful dyes, or x-rays. The MRI scanner uses magnetism and radio waves to produce clear pictures of the human anatomy.

1.4.1 History

MRI, also called NMR (nuclear magnetic resonance) imaging is based on a phenomenon discovered in the 1930s in which magnetic fields and radio waves cause atoms to emit small radio signals. Felix Bloch, working at Stanford University, and Edward Purcell, from Harvard University, discovered NMR. NMR spectroscopy was then used to study the composition of chemical compounds. The 2003 Nobel Prize in Physiology or Medicine was given to Paul C. Lauterbur and Peter Mansfield for their discoveries concerning magnetic resonance imaging. Lauterburs imaging experiments expanded the technology from the single dimension of NMR spectroscopy to the second dimension of spacial orientation. Peter Mansfield developed the use of gradients in the magnetic field. He showed how the signals can be mathematically analyzed, which made it possible to develop a useful imaging technique. In 1970, Raymond Damadian, a

medical doctor and research scientist, discovered the basis for using magnetic resonance imaging as a tool for medical diagnosis. He found that different kinds of animal tissue emit response signals that vary in length, and that cancerous tissue emits signals that last much longer than non-cancerous tissue. Less than two years later he filed his idea for using magnetic resonance imaging as a tool for medical diagnosis with the US patent office, titled “Apparatus and Method for Detecting Cancer in Tissue”. The patent approved in 1974 and it was the world’s first patent in the field of MRI. By 1977, Damadian completed the construction of the first whole-body MRI scanner. The medical use of magnetic resonance imaging has developed rapidly. The first MRI equipment in the clinic was available at the beginning of the 1980s.

1.4.2 Principle

An MRI system consists of the following parts: a large magnet to generate the magnetic field, shim coils to make the magnetic field as homogenous as possible, a radiofrequency (RF) coil to transmit a radio signal, a receiver to detect the returning radio signals, gradient coils to provide special localization of the signals, and a computer to reconstruct an image of the signals (Hesselink).

When the body lies in a magnet, it becomes magnetized. This happens when the hydrogen nuclei in the body align with the magnetic field. When it is magnetized and gets exposed to radio waves at a certain frequency, the body sends back a radio wave signal called a spin echo. This only happens at one certain frequency (Larmor frequency) corresponding to the strength of the magnetic field. The spin echo signal consists of multiple frequencies. When the signal is analyzed and broken into its component frequencies the magnitude of the signal at each frequency is proportional to the hydrogen density at the location. An image can be constructed (Bradley).

1.4.2.1 Magnetization

The hydrogen nucleus is a single proton that is charged and it spins. It generates a small magnetic field that is called magnetic moment. Similar to the needle of a compass

all magnetic moments align when they are put in a larger magnetic field. In this magnetic field the protons align so that the same amount of protons is pointing parallel and anti-parallel to the magnetic field. The individual magnetic moments cancel each other out. In biological substances within a few seconds the protons redistribute so that there is a slightly bigger number of hydrogen nuclei aligning parallel to the field. In this state the body is said to be magnetized (Bradley). Two separate phenomena take place after a 90˚ RF pulse is applied. One phenomenon is the recovery of the longitudinal magnetization, described by the time constant T1 and called T1 relaxation. The other phenomenon is the decay of the transverse magnetization, the magnetization that is flipped into the transverse plane, which is described by the time constant T2 or T2* and is called T2 relaxation.

1.4.2.2 T1 and T2 Relaxation

T1 is the longitudinal relaxation time. It describes the recovery of longitudinal magnetization along the direction of the magnetic field, after applying an RF pulse. T1 is determined by thermal interactions between resonating protons and other protons and other magnetic nuclei in the magnetic environment. The T1 relaxation time reflects the relationship between the frequency of these molecular motions and the resonance frequency, which depends on the main magnetic field of the MR scanner. When the two are similar, T1 is short and recovery of magnetization is fast, when they are different, T1 is long. The water molecule is small and moves too fast for efficient T1 relaxation, whereas large proteins move too slowly. They have natural frequencies that are very different from the Larmor frequency and thus have long T1 relaxation times.

T2 is the transverse relaxation time. It is a measure of how long the resonating protons precess after a RF pulse. T2 decay is due to magnetic interactions that happen between spinning protons. T2 relaxation depends on the presence of static internal fields in the substance. These are usually due to protons in larger molecules.

The contrast on the MR image can be modified by changing the pulse sequence parameters. A pulse sequence determines the specific number, strength, and timing of the RF and gradient pulses. The two most important parameters are the repetition time

(TR) and the echo time (TE). The TR is the time between consecutive 90 degree RF pulses. The TE is the time between the initial 90 degree RF pulse and the echo.

There is another form of transverse relaxation. It is called T2*. T2* is shorter than T2 because it includes magnetic field inhomogeneities or magnetic susceptibility. In extremely homogenous magnetic fields T2* values are approximately equal to T2 values.

The difference in T1 values can be used to enhance contrast between the two. A short TR time allows a shorter T1 substance to recover signal between repetitions much better than a longer T1 substance. Substances with low values of T1 have the highest signal intensities on T1-weighted images. The T1-weighted sequence uses a short TR (<1000 msec) and short TE (<30 msec).

Substances with longer T2 times generate stronger signals than substances with a shorter T2 times, when both are acquired at the same TE and if proton density and T1 are comparable. Increasing the echo delay time increases the differences in the T2 decay curves between substances, increasing the T2 weighting. Images which are obtained with a long TR (>2000 msec) and TE (>80 msec) are called T2-weighted images.

In general, the strongest signal is detected from those substances with the highest proton densities (high water content), shortest T1 times (rapid recovery) and longest T2 times (slowest decay).

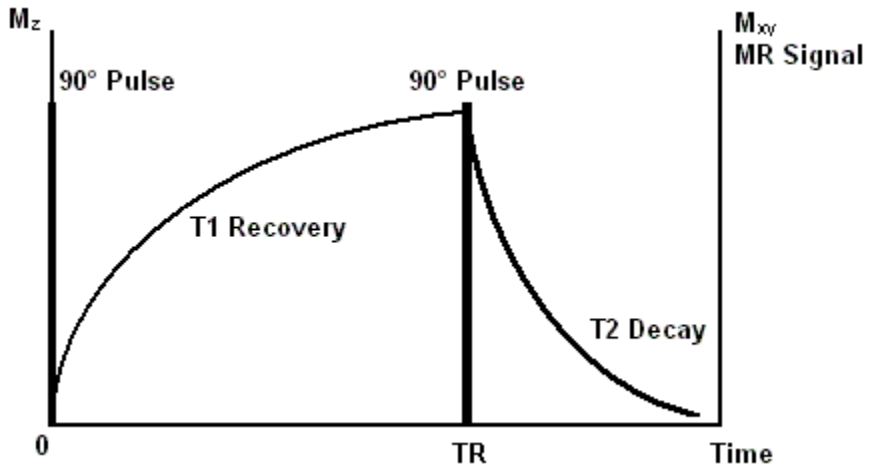

Fig 1.10 T1 and T2 relaxations (from Chan, 2006)

1.4.3 MRI Cancer Diagnosis with Iron-accumulating Proteins

Diseased tissue, such as tumors, can be detected by MRI technology because the protons in different tissues return to their equilibrium state at different rates. By changing the parameters on the scanner this effect is used to create contrast between different types of body tissues.

To enhance appearance of blood vessels, tumors or inflammation contrast agents can be used. Most contrast agents that are used in MRI have specific magnetic properties.

Recently several new approaches to get specific MRI contrast have focused on iron as a contrast agent. One advantage of genetic methods for accumulating endogenous iron is that no contrast agents have to be delivered. It has been shown that brain iron lead to darkening on T2-weighted MRI, which demonstrates that different iron levels in normal tissues can be enough to show MRI contrast (Schenk *et al*., 2003). Different components of the iron metabolism pathway have been used to try to mediate cellular iron accumulation, specifically the overexpression of iron accumulation proteins like the transferrin receptor (Weissleder *et al*., 2000) or ferritin (Genove *et al*., 2005). In one report, TfR overexpressing tumors were shown to significantly decrease T2 values (Korentsky *et al*., 1996). The most notable effect has been demonstrated by overexpressing one or both of the ferritin subunits to use the iron loaded ferritin complex as a molecular contrast agent (Cohen e*t al*., 2005, Genove *et al*., 2005). The contrast

effects of ferritin in MR imaging have been studied in detail, including the influence on iron loading factor (Vymazal *et al*., 1996) and field strength (Gossuin *et al*., 2004). Ferritin-bound iron is a much more effective contrast agent for T2 than for T1, and it has been suggested that the T2 effect is due to superparamagnetic iron in the ferritin core (Brooks *et al*., 1998). Most studies have shown a linear correlation of *R2* (=1/T2) relaxivity with increasing field strength up to 1.5 T (Gossuin *et al*., 2004) and a less clear correlation of R2 with tissue iron content (Gossuin *et al*., 2004).

1.5 Aim of this Study

It has recently been demonstrated that oncolytic virotherapy using vaccinia virus may provide a powerful new tool in cancer therapy. It is specifically targeting cancer cells and can potentially be used in combination with conventional cancer therapies. It was shown that a recombinant vaccinia virus could not only reveal the exact location of solid tumors and metastases in mice but also success-fully eradicate human breast tumors in mice xenografts (Zhang *et al*., 2007, Yu *et al*., 2004). Recently, this recombinant vaccinia virus progressed to phase I clinical trials in human cancer patients.

This study focuses on the detection of tumors by using genetically modified vaccinia virus strains. The aim of this work was to collect enough iron or other heavy metals in the tumor by infecting with a vaccinia virus that mediates expression of metal-accumulating proteins to be able to detect tumors and metastases by MRI technology. For this purpose different recombinant viruses were generated that carry genes encoding for metal-accumulating proteins, such as iron transport or iron storage proteins.

Viral replication of these newly generated viruses should be characterized and compared to replication of the parental virus GLV-1h68 in cell culture using the standard plaque assay in two different cancer cell lines. Expression of viral genes during infection in cell culture should be demonstrated in these cell lines using SDS- PAGE, Western

blot analysis and ELISA. Also the detection on a transcriptional level should be performed by RT-PCR. The metal-collecting capability should be demonstrated and compared for the different virus-infected tumor cells in cell culture by using different metal determination techniques.

In addition, the virus-mediated iron accumulation of infected tumor cells with the different viruses should be followed in a nude mouse xenograft after intravenous injection of the viruses over the course of 24 days. The viral distribution in virus-treated tumor-bearing mice should be analyzed by standard plaque assay and by immunohistochemical vaccinia virus staining at day 24 after virus injection. Samples from both, infected and uninfected tumors should be used for detection of virus induced expression of the iron-collecting proteins in the tumor lysates by immunohistochemical staining. Determination and comparison of the iron content in tumors of uninfected and infected mice should be accomplished.

Furthermore, the mice should be used for MRI studies after virus injection with several different parameters. The capability and usefulness for tumor detection or therapeutic monitoring using oncolytic vaccinia virus strains that mediate expression of iron-accumulating proteins should be evaluated.

2 Material

2.1 Chemicals and Enzymes

Materials	Manufacturer
100bp DNA Ladder	New England Biolabs
1kb DNA Ladder	New England Biolabs
2-Mercaptoethanol	Fisher Scientific
3-(2-Pyridyl)-5,6-diphenyl-1,2,4-triazine-4',4'' -disulfonic Acid Sodium Salt (Ferrozine)	Sigma
3,3',5,5'-Tetramethylbenzidine (TMB) Liquid Substrate System for ELISA	Sigma
5-bromo-4-chloro-3-indolyl-b-D-galactopyranoside (X-Gal)	Stratagene
5-bromo-4-chloro-3-indolyl-beta-D-glucuronic acid cyclohexylammonium salt (X-GLCA)	RPI Research Products
Accuprime™ Pfx SuperMix	Invitrogen
Acetic Acid	VWR
Ampicillin	Sigma
Antibiotic-Antimycotic Solution	Cellgro
Benzonase® Nuclease	Novagen
β-Estradiol	Sigma
Biorad Protein Assay Standard I	Biorad
Blocker™ Casein in PBS	Pierce
Bromphenol Blue	Aldrich Chemical Company
BugBuster® Protein Extraction Reagent	Novagen
Carboxymethyl Cellulose Sodium Salt	MP Biomedicals
Cadmium Sulfate	Sigma
Casein Blocking Solution	Pierce
Chloroform	Fisher Scientific
Citric Acid	Sigma

Clearslip Mounting Media	IMEB Inc.
Coomassie Brilliant Blue R250	Sigma
Crystal Violet	Sigma
Cupric Sulfate	Sigma
Deoxycholic Acid	Fisher Biotech
Difco™ Agar	BD
Difco™ LB Broth, Miller	BD
Difco™ Skim Milk	BD
Digitonin	Invitrogen
DMEM medium 1x	Cellgro
Diaminobenzidine	Aldrich Chemical Company
Dithiothreitol (DTT)	Invitrogen
Dulbecco's Phosphate Buffered Saline (DPBS) 1x	Cellgro
EDTA	Fisher Scientific
Eosin-Y	Richard-Allan Scientific
Ethidium Bromide	Sigma
Ferric Chloride	Sigma
Ferric Ammonium Sulfate	Sigma
Ferric Citrate	Fisher Scientific
Ferritin Protein Human	Abcam
Fetal bovine serum	Omega Scientific
Formaldehyde	EMD
Formalin 1:10 Dilution, Buffered	Fisher Diagnostics
Freund's Incomplete Adjuvant, Modified	Calbiochem
FuGENE® Transfection Reagent	Roche
Glucose	Cellgro
Glycerol	Fisher Scientific
Hematoxylin QS	Vector
HEPES	Gibco
Holo-Transferrin Human	Sigma
HyClone® HyPure™ Cell Culture Grade Water	Thermo Scientific

Hydrochloric Acid Solution 2N	VWR
Hydrogen Peroxide Solution	Sigma
Hydroxymethylaminomethanehydrochloride (Tris-HCl)	Fisher Scientific
Hypoxanthine	Sigma
Iron Dextran-100 Injection	Durvet
Iron Standard 1000µg/mL in 2% HNO_3	High Purity Standards
Kanamycin	Sigma
Ketathesia	Butler
Magnesiumchloride	J.T.Baker
Manganese(II)sulfate Monohydrate	Sigma
Methanol, Absolute	Sigma Diagnostics
Modified Mayer's Hematoxylin	Richard-Allan Scientific
Mycophenolic Acid	Sigma
Native PAGE™ 20x Cathode Buffer Additive	Invitrogen
Native PAGE™ 20x Running Buffer	Invitrogen
Native PAGE™ Sample Additive	Invitrogen
Native PAGE™ Sample Buffer	Invitrogen
Nitric Acid 70%	Sigma
NuPAGE® 20x Transfer Buffer	Invitrogen
NuPAGE® MOPS SDS 20x Running Buffer	Invitrogen
OmniPur Ethyl Alcohol Pure	EMD
OmniPur® Agarose	EMD
OPTI-MEM® Medium	Gibco
Paraplast Tissue Embedding Medium	McCormick Scientific
Paraformaldehyde	Sigma
Phenol:Chloroform:Isoamyl Alcohol 25:24:1	Sigma
Potassiumferricyanide	Fisher Scientific
Potassiumhexacyanoferrate(II)trihydrate	Sigma
Precision Plus Protein™ Standard	Biorad
Progesterone	Mediatech

Proteinase Inhibitor Cocktail Tablets	Roche
Proteinase k	Sigma
Quick T4 DNA Ligase	New England Biolabs
Restriction Enzymes	New England Biolabs
RPMI Medium 1640 1x	Cellgro
S.O.C. Medium	Invitrogen
Sodium Acetate	Fisher Scientific
Sodium Azide	Fisher Scientific
Sodium Carbonate	Fisher Scientific
Sodium Chloride	Fisher Scientific
Sodium Citrate	Fisher Scientific
Sodium Dodecylsulfate (SDS)	Fisher Scientific
Sodium Hydrogencarbonate	Fisher Scientific
Sodium Pyruvate	Cellgro
Sucrose	Sigma
TBE Buffer 10x	Sigma
Thioglycolic Acid	Sigma
TMB	Sigma
Trichloroacetic Acid	VWR
Tris (Base)	Fisher Scientific
Tris-Borate-EDTA (TBE) Buffer	Sigma
Triton-X 100	Sigma
TRIzol® Reagent	Invitrogen
Tween-20	Biorad
Xanthine	Calbiochem
Xylazine 20 Injection	Butler
Xylene Substitute	Sigma
Z-Competent™ *E. coli* DH5α Cells	Zymo Research

2.2 Cell Lines and Cell Culture Media

GI-101A-cells:	human breast carcinoma (adherent)
A549 cells:	human lung carcinoma (adherent)
CV-1-cells:	green monkey kidney fibroblasts (adherent)

Cell culture media:

GI-101A:	500ml RPMI-1640
	20% FBS
	5.6ml Glucose
	1% HEPES
	1% Sodium Pyruvate
	1% Antibiotics-Antimycotics
	5ng/ml β-Estradiol
	5ng/ml Progesterone
A549:	500ml RPMI-1640
	10% FBS
	1% Antibiotics-Antimycotics
CV-1:	500ml DMEM
	10% FBS
	1% Antibiotics-Antimycotics

2.3 Kits

Kit	Manufacturer
Biorad D_C Protein Assay	Biorad
DNA Clean & Concentrator™-5Kit	Zymo Research
DNA-free™ Kit	Ambion
ImmPACT™ DAB Diluent and Chromogen	Vector
Native PAGE® Sample Prep Kit	Invitrogen
Opti-4CN™ Substrate Kit	Biorad
PureLink™ Quick Plasmid Miniprep Kit	Invitrogen
QuantiChrom™ Iron Assay Kit	Bioassay Systems
RNase-free DNase Set	Qiagen
RNeasy® Mini Kit	Qiagen
SuperScript™ First-Strand Synthesis System for RT-PCR	Invitrogen
Vectastain ABC Kit Rabbit IgG	Vector
Zero Blunt® TOPO® PCR Cloning Kit	Invitrogen
Zymoclean™ Gel DNA Recovery Kit	Zymo Research

2.4 Synthetic Oligonucleotides

β-actin for: 5’-GAC AAC GGC TCC GGC ATG TG-3’
β-actin rev: 5’-TGG CTG GGG TGT TGA AGG TC-3’
magA for: 5’-AGC GGC TTC GGG CTG GTG ACA A-3’
magA rev: 5’-GTC CAG CTC GTC CGA GGA TTC CAG CA-3’
DMT1 for: 5’-CTT GTG GGG CTG CTG CTC-3’
DMT1 rev: 5’-CAT AAT AGT GAT GAG AAA GCC AAA AAA TGC-3’

All primers were synthesized by IDT.

2.5 Antibodies

Antibody	Source	Manufacturer
anti-bacterioferritin serum	mouse	selfmade
anti-human ferritin	rabbit	GeneTex
anti-human ferritin H-chain	rabbit	Abcam
anti-transferrin receptor	rabbit	Santa Cruz
anti-DMT1	rabbit	Abcam
anti-vaccinia A27L	rabbit	Genescript (custommade)
anti-β-actin	mouse	Sigma
anti-mouse IgG peroxidase conjugate	goat	Sigma
anti-rabbit conjugated to HRP	goat	Biorad

2.6 Recombinant Viral Constructs

The recombinant Vaccinia Virus GLV-1h68 is a genetically stable oncolytic vaccinia virus that has been constructed by Genelux Corporation (San Diego, CA). Three expression cassettes were inserted into the *F14.5L*, *J2R*, and *A56R* loci of the viral genome. These three expression cassettes are the *Renilla* luciferase *Aequorea* green fluorescent protein fusion gene (*RUC-GFP*), the ß-galactosidase gene (*lacZ*), and the ß-glucuronidase gene (*gusA*). The Ruc-GFP fusion protein located in the *F14.5L* locus is under control of an early/late promoter whereas the marker gene ß-galactosidase in the J*2R* locus is under control of the $P_{7.5}$ promoter. The transferrin receptor gene (*rhTfR*) cDNA was inserted in reverse orientation to the vaccinia synthetic early/late promoter to serve as a negative control for a TFR-expressing recombinant virus (Zhang *et al*., 2007). An additional marker gene coding for ß-glucuronidase was inserted into the A56R locus and is under control of the P_{11K} promoter.

GLV-1h68

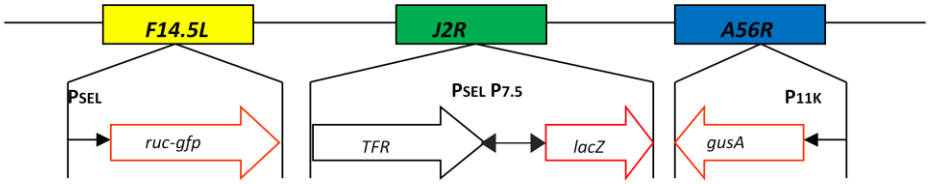

The vaccinia virus strains GLV-1h131, GLV-1h132, and GLV-1h133 were derived from GLV-1h68 as a parental virus but instead of the β-galactosidase gene in the *J2R* locus two genes encoding the human ferritin light chain and the human ferritin heavy chain were inserted. These two genes are connected by a linker sequence (2A), which is originating from the picornavirus foot-and-mouth disease virus and is often used in molecular biology to create polycistronic mRNAs for coexpression of two proteins. Insertion of picornaviral 2A sequences into mRNAs cause ribosomes to skip formation of a peptide bond at the junction of the 2A and downstream sequences, leading to the production of two proteins from a single open reading frame (Funston *et al*., 2008). It leads to approximately equal expression of the proteins upstream and downstream of the 2A site (de Felipe *et al*., 2006). In GLV-1h131 the ferritin expression cassette is under the control of a synthetic early promoter (P_{SE}), whereas in GLV-1h132 and GLV-1h133 is controlled by the synthetic early/late promoter (P_{SEL}) and synthetic late promoter (P_{SL}), respectively. These three promoters differ in promoter strength and time of activation, where P_{SE} is the weakest and P_{SEL} is the strongest promoter.

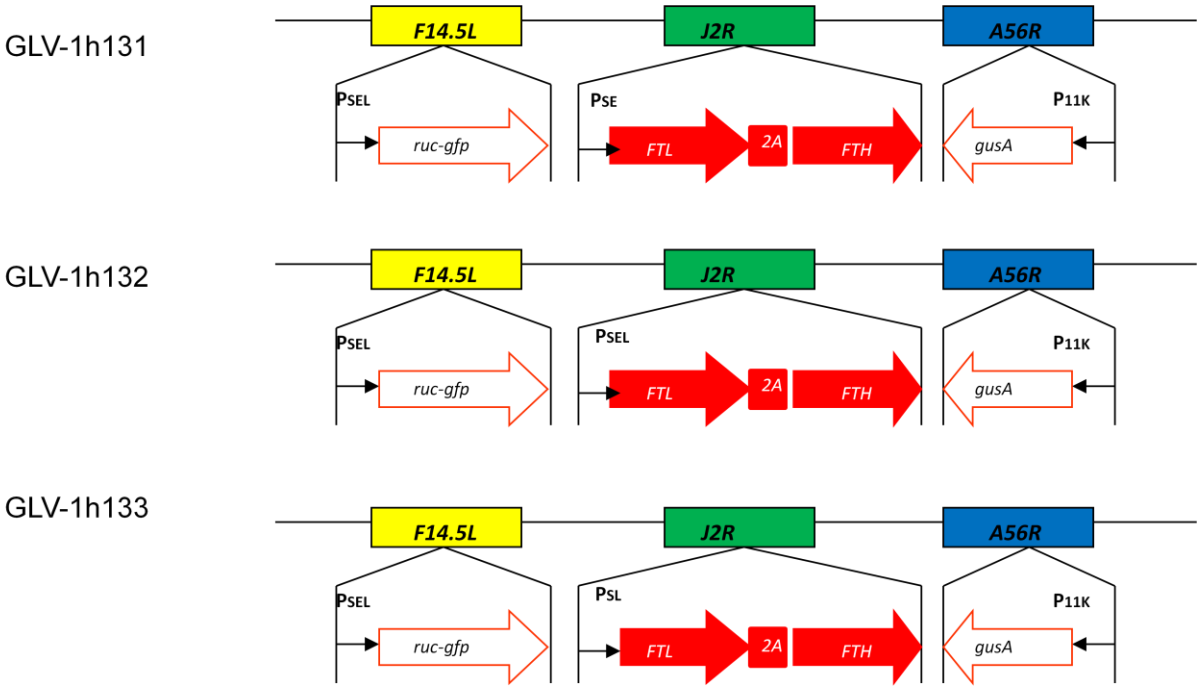

Also the virus strains GLV-1h110, GLV-1h111, GLV-1h112, and GLV-1h113 were derived from the paternal virus GLV-1h168. They carry the gene encoding for the *E. coli* bacterioferritin. This gene was brought into the *A56R* locus with three different promoters. These virus strains still express the RUC-GFP fusion protein and the β-galactosidase as marker proteins. The β-glucuronidase gene was replaced by the *bfr* gene. GLV-1h113 leads to expression of a humanized form of the bacterioferritin under control of P_{SEL}, which means the bfr gene sequence was adapted to human codon usage. This is expected to be an advantage for expression in human cells.

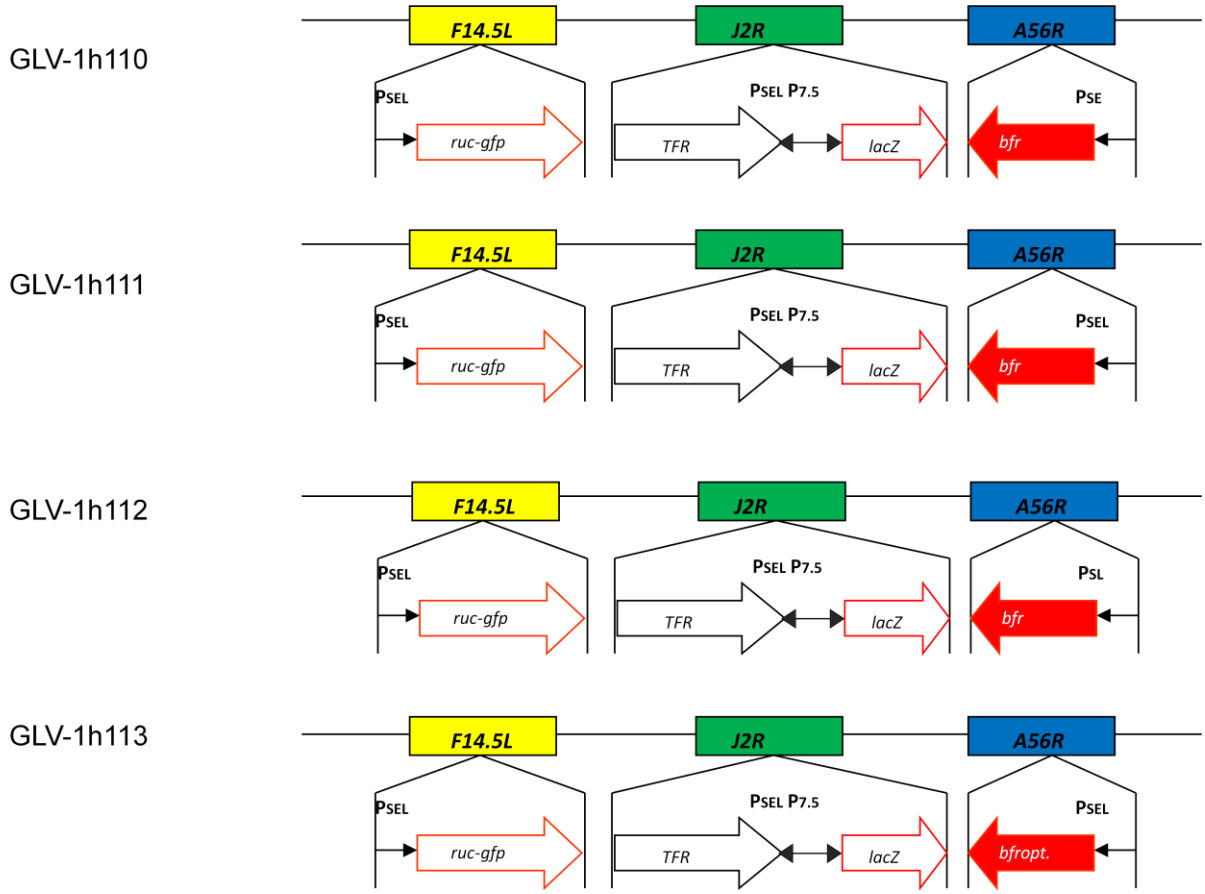

GLV-1h22 is a virus strain that mediates the expression of the human transferrin receptor in infected cells. It is very similar to the parental virus GLV-1h68 that also contains the transferrin receptor gene, only in reverse orientation. In GLV-1h22 this gene was inserted in the opposite orientation and can therefore be functionally expressed. GLV-1h114 and GLV-1h115 lead to expression of the murine version of the transferrin receptor, which should be an advantage for *in vivo* experiments in mice. This gene was inserted in the *A56R* locus with two different promoters, the synthetic early and the synthetic early/late promoter.

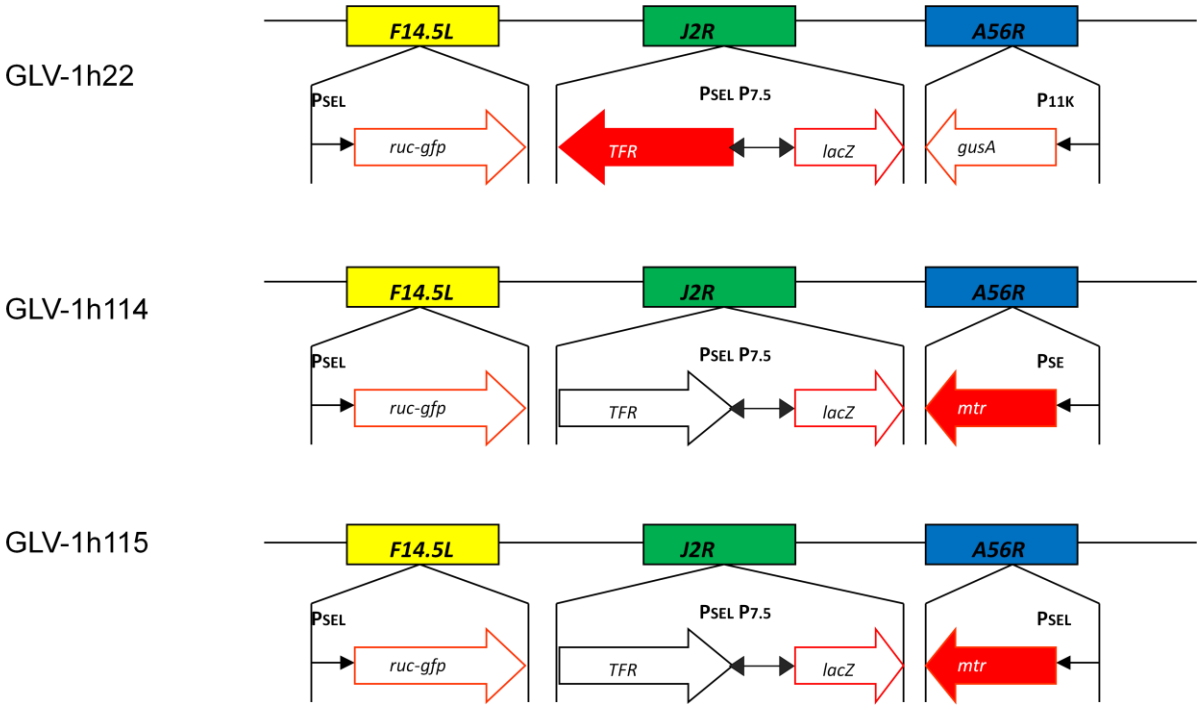

For a possibly better efficiency in iron uptake four more virus strains were engineered from the parental virus GLV-1h68, which carry each one version of a ferritin gene and one version of a transferrin receptor gene. GLV-1h154 carries genes for the human transferrin receptor in the *J2R* locus and the for the codon-optimized version of bacterioferritin in the *A56R* locus. GLV-1h155 also has the human transferrin receptor inserted in the *J2R* locus, but the human ferritin H-chain gene in the *A45R* locus. In GLV-1h156 and GLV-1h157 the mouse transferrin receptor was inserted in the *J2R* locus and the codon-optimized bacterioferritin gene and the human ferritin H-chain in the A56R locus, respectively.

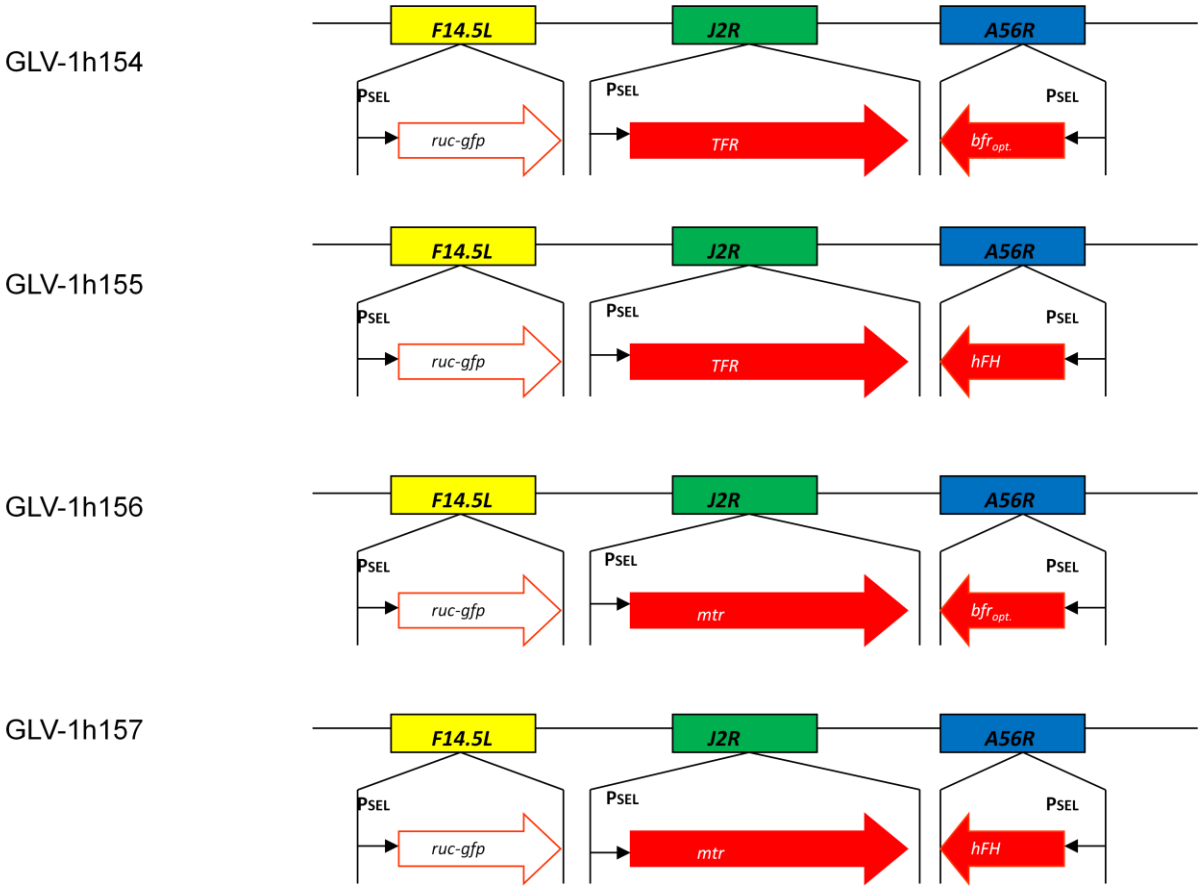

GLV-1h186 and GLV-1h187 both have the gene encoding the ferritin light chain inserted into their *A56R* locus. In GLV-1h186 this gene has an insertion of a thymidine (T) and a cytidine (C) at position 498 in its open reading frame resulting in a frameshift mutation. It was shown that expression of the ferritin light chain with this mutation leads to iron overload in mice (Vidal *et al*., 2008, Barbeito *et al*., 2009).

GLV-1h186

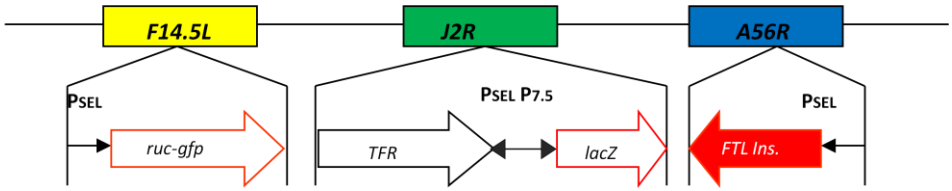

GLV-1h187

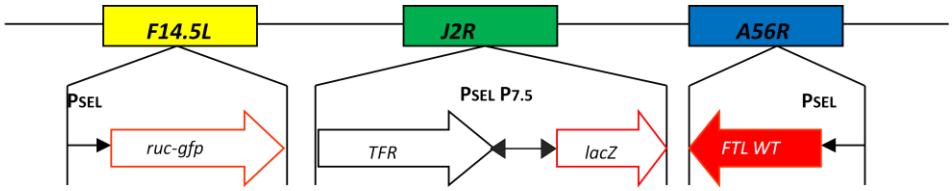

The divalent metal transporter-1 gene (*DMT1*) is another gene encoding an iron transport protein, which was inserted into the A56R locus of parental virus GLV-1h68. In GLV-1h102 it is under the control of the synthetic early promoter. It was not successful to generate a DMT-expressing virus with one of the two stronger promoters.

GLV-1h102

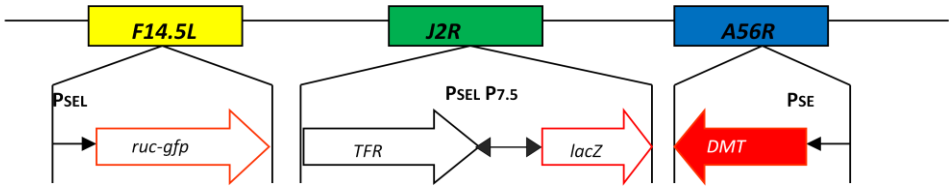

The *magA* gene from the magnetotactic bacterium *Magnetospirillum magneticum* was also inserted into the A56R locus with GLV-1h68 to generate GLV-1h184. Similar to the DMT expressing virus it was only possible to generate the virus with the weak promoter P_{SE}. *MagA* was shown to be sufficient for producing magnetic nanoparticles in mammalian cells (Zurkiya *et al*., 2008).

GLV-1h184

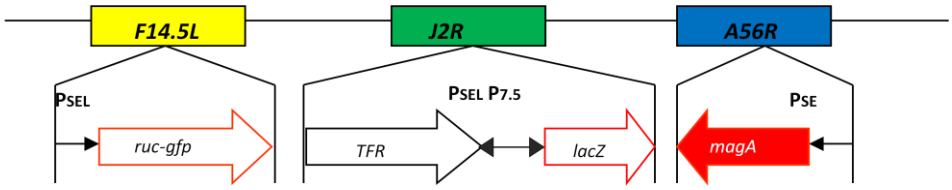

2.7 Bacterial Stains

E. coli Omnimax pTolC

E. coli Omnimax pTolC-EC20

E. coli Top10

2.8 Laboratory Animals

For in *vivo* experiments, male and female athymic nude FoxN1 mice were used. The FoxN1 mouse model is characterized by an autosomal recessive mutation in the *nu* locus on chromosome 11. This leads to a completely hairless phenotype in the mice. Additionally, these animals feature a dysfunctional and rudimental thymus which manifests in a T-cell deficiency. By contrast, B-cell function is normal in athymic nude FoxN1 mice. Due to the defects in the immune system of the mouse, athymic nude FoxN1 mice are suited as adequate laboratory animals in oncology, immunology and additional fields of biomedical research. Another advantage of the used mouse model is that xenotransplants will not be rejected by the mouse.

Fig.2.1 Phenotype of an athymic nude FoxN1 mouse (http://www.harlan.com)

BALB/c mice were used for the antiserum production. They are used as a general-purpose strain in many disciples as Immunology and the production of monoclonal antibodies.

All animals were purchased from Harlan. Mice were cared for and maintained in accordance with animal welfare regulations under the approved protocol by the Institutional Animal Care and Use Committee of Explora Biolabs (San Diego Science Center) and of the University of California, San Diego.

2.9 Laboratory Equipment and Other Materials

Equipment	Manufacturer
Balance PL1501-S	Mettler Toledo
Bio Doc-It™ System	UVP
Biosafety Cabinet	The Baker Company Inc.
Cell Culture Cluster 24-well Costar 3526	Corning Inc.
Cell Culture Cluster 6-well Costar 3516	Corning Inc.
Cell Culture Cluster 96-well Costar 3595	Corning Inc.
Cell Culture Flask 75cm^2	Corning Inc.
Cell Scraper	Corning Inc.

Cell Spreader	VWR International
Centrifuge Sorvall RC 6 Plus	Thermo
Centrifuge Centra CL2	Thermo
Centrifuge Micro CL 21	Thermo
Combitips Plus 25ml	Eppendorf
Cryotubes 2ml	Nalgene
Digital Caliper	VWR
Digital Dry Bath Incubator	Boekel Scientific
Dish 10cm	Fisher Scientific
Embedding Mold TISSUE-TEK®	IMEB Inc.
Falcon 15ml Tubes	BD
Falcon 50ml Tubes	BD
Fluorescence Microscope IX71	Olympus
Heater	VWR International
Hotplate Stirrer 375	VWR Scientific Products
Incubator HERA Cell 150	Thermo Electron Corporation
Incubator Shaker C25	New Brunswick Scientific
Insulin SyringeU-100 29G1/2	BD
MagNA Lyser	Roche
MagNA Lyser Green Beads	Roche
Microfuge Tubes 2.0ml	Avant
Microfuge Tubes Easy Open Cap 1.5ml	Saarstedt
Microplate Reader SpectraMax MS	Molecular Devices
Microscope Cover Glass	Fisher Scientific
Microslides Premium Superfrost®	VWR International
Microwave Carousel	Sharp
Mini-Sub® Cell GT	Biorad
Multipipette	Eppendorf
Parafilm Laboratory Film	Pechiney Plastic Packaging
pH Meter Accumet AR15	Fisher Scientific
Photometer Biomate3	Thermo Spectronic

Pipet Aid	Drummond
Pipet Tips 200-1000µl, 100µl, 10µl	VWR International
Pipettes 1000µl, 100µl, 10µl	Rainin
Pipettes 25ml, 10ml, 5ml	Corning Inc.
Power Pac 200	Biorad
Precast Native PAGE™ 4-16% Bis-Tris Gel	Invitrogen
Precast NuPAGE® 12% Bis-Tris Gel	Invitrogen
PVDF Membrane Filter Paper Sandwich 0.2µm	Invitrogen
Rocking Platform	VWR International
Sectioning Machine Leica RM 2125	IMEB Inc.
Slide Staining Set TISSUE-TEK®II	IMEB Inc.
Slide Warmer	Barnstaed Labline
Sonifier 450	Branson
Sterile Disposable Scalpel	Sklar Instruments
Syringe 1ml	BD
Syringe 5ml	BD
Syringe Driven Filter Unit Millex®-VV PVDF 0.1µm	Millipore
Thermocycler Mastercycler Personal	Eppendorf
Tissue Culture Dish 60mm	BD
Tissue Embedding Center	Reichert – Jung
Tissue Grinder	Kimble
Tissue Processing/Embedding Cassettes with Lid	Simport
Illumatool Tunable Lighting System	Lightools Research
Vortex VX100	Labnet
Water Bath	Boekel Scientific
Water Bath Isotemp	Fisher Scientific
X Cell Sure Lock™	Invitrogen

3 Methods

3.1 Generation of Recombinant Vaccinia Viruses

3.1.1 Cloning of Plasmids for Homologous Recombination with Virus DNA

First the DNA of the desired gene is amplified by PCR and special restriction sites are attached to the DNA sequence by designing two specific primers that are complementary to the 3' ends of each of the sense and anti-sense strand of the DNA target and contain the restriction sites. The restriction sites allow the cutting of the DNA at the exact position that is needed to ligate the sequence later with a transfer vector that is also cut with the same restriction enzymes. For the PCR a 50 µl reaction is prepared with 45 µl of Accuprime™ Pfx Supermix 1 µl of each primer and 1 µl of template DNA. The PCR cycle starts with an initialization step at 94 ˚C for five minutes. Then there are 35 repetitions of a denaturation step at 94 ˚C for 30 seconds, an annealing step at a temperature that depends on the primers (about three to five degrees Celsius below the melting temperature of the primers used) for ten seconds and an elongation step at 68 ˚C for a time that depends on the length of the DNA that is to be amplified. In the end there is a final elongation at 68 ˚C for five minutes.

After the PCR the product is purified with the PCR purification Kit (Invitrogen) according to the manufacturer's instructions. The blunt PCR product is mixed together with pCR®-Blunt II-TOPO vector in the TOPO® Cloning reaction by incubating for five minutes at room temperature. Two microliters of the TOPO® Cloning reaction are added to one vial of One Shot Chemically Competent *E. coli*. The reaction is incubated on ice for five minutes. The cells are heat-shocked for 30 seconds at 42 ˚C and then transferred back on ice. Twohundertfifty microliters of S.O.C. medium are added and the tube is shaken horizontally (180 rpm) at 37 ˚C for one hour. Fifty microliters of the transformation are spread out on a pre-warmed LB-plate containing 50 µg/ml kanamycin. Plates are incubated over night at 37 ˚C. The next day colonies are picked for overnight bacterial cultures in LB medium with 50 µg/ml kanamycin and incubated in a rotating incubator overnight at 37 ˚C and 180 rpm.

The overnight cultures are used to isolate the DNA with the PureLink™ Quick Plasmid Miniprep Kit (Invitrogen) according the manufacturer's instructions.
The isolated DNA can be digested with the restriction enzymes that were chosen before the restriction sites were brought into the sequence by PCR in the beginning of the cloning process. Restriction reactions are usually incubated for a few hours at 37 ˚C and then purified with the DNA Clean & Concentrator™-5Kit (Zymo Research) according to the instructions of the manufacturer. After that the DNA can be ligated with the desired transfer vector that is cut with the same restriction enzymes and that contains one of the vaccinia promoters (synthetic early, synthetic late or synthetic early/late promoter) and flanking regions of the vaccinia virus locus where the gene is to be inserted for the homologous recombination. Ligation is performed with the Quick T4 DNA Ligase (New England Biolabs) according to the manufacturer's instructions.

3.1.2 Co-Transfection of Plasmid DNA with Parental Virus GLV-1h68 Infection

For the infection with the parental virus GLV-1h68, CV-1 cells seeded the day before in 6-well-plates are used. First the virus is diluted to a concentration of $1x10^5$ pfu/ml and the cells are infected with 0.5 ml of virus containing medium. The plates are incubated for one hour at 37 ˚C and 5% CO_2 and shaken every 20 minutes for better distribution of the virus.
For co-transfection of plasmid DNA 30 minutes after the infection the DNA is prepared by pipetting 12 µl of FuGENE transfection reagent (Roche) to 88 µl of OPTI-MEM medium. After vortexing and incubation at room temperature for five minutes 2 µg of DNA are added. Then the mixture is vortexed again and incubated at room temperature for 20 minutes. After one hour of incubation the cells are washed twice with OPTI-MEM medium and the 1.5 ml of OPTI-MEM is added to the cells. The DNA mix is added and the plates are incubated at 37 ˚C and 5% CO_2 for one to two days until all the cells are infected. Then the cells are harvested and frozen at -80 ˚C.

3.1.3 Plaque Selection

The transfected cell lysate is frozen and thawed three times for the cells to break up. Then it is sonicated for 30 seconds with 100% power to further break up the cells and

break up virus aggregates. CV-1 cells seeded in 6-well-plates are treated with the three drugs mycophenollic acid (MPA), xanthine, and hypoxanthine the day before the infection. MPA is an inhibitor of purine metabolism and because it blocks the pathway for GMP synthesis, it interferes with the replication of vaccinia and reduces the size of the virus plaques. However, this effect can be overcome by expression of the *E. coli gpt* gene in the presence of xanthine and hypoxanthine. The *gpt* gene is inserted next to the gene of interest and outside the vaccinia DNA flanking regions. Under these conditions only the single cross-over recombinant virus will express XGPRT, which is leading to enrichment over the parental virus (Falkner and Moss, 1990). One day after pretreatment with these drugs, the cells are infected with 50, 5 and 1 µl of virus containing cell lysate. After one hour of incubation at 37 ˚C and 5% CO_2 2 ml of overlay medium are added and the cells are incubated for five days at 37 ˚C and 5% CO_2. Six single plaques are then picked by aspirating 150 µl of medium surrounding single plaques and adding them into tubes with 500 µl of DMEM medium. These samples are then frozen and thawed three times and after sonication and pretreatment of cells new plates are infected with 50 and 5 µl of cell lysate. After five days six plaques are picked again and new CV-1 cells are infected with these plaque lysates. After the first two rounds of plaque selection there is no pretreatment with MPA, xanthine and hypoxanthine. When the drugs are removed, the desired double cross-over recombinant virus without the XGPRT gene can form plaques and three more rounds of selection without the drugs follow. After the fifth round the plaque lysates are screened for recombinant viruses by their marker gene expression.

<u>MPA (400x):</u>

MPA	50 mg
NaOH 0.1 N	5 ml

filter sterilize and store at -20˚C

<u>Hypoxanthine (670x):</u>

Hypoxanthine	50 mg
NaOH 0.1 N	5 ml

filter sterilize and store at -20˚C

Xanthine (40x):	
Xanthine	500 mg
NaOH 0.1 N	50 ml
filter sterilize and store at -20˚C	

Virus Plaque Overlay Medium:	
CMC	15 g
weighed in 1 L bottle and autoclaved	
DMEM	1000 ml
Antibiotic-Antimycotic solution	10 ml
stir until dissolved	
FBS	50 ml

Crystal Violet Solution:	
Crystal violet	1.3 g
Ethanol	50 ml
37% formaldehyde	300 ml
stir overnight	

3.1.4 Screening of Marker Gene Expression

The two loci in which most of the foreign genes are inserted are the J2K and the A56R locus. In the parental virus GLV-1h68 the gene encoding the β-galactosidase is inserted in the J2K locus and the gene encoding the β-glucuronidase is inserted in the A56R locus. When the parental virus is transfected with a DNA of a new gene, it will destroy the gene that was in that locus before and therefore it will not be expressed by virus infected cells anymore. This is a simple way of testing if a new gene was inserted in one of the loci.

Ten microliters of every virus plaque lysate of the fifth round of plaque selection are used to infect CV-1 cells in 24-well plates. After two days of incubation at 37 ˚C and 5% CO_2 the cells are screened for the expression of β-galactosidase and β-glucuronidase. The cells are washed with PBS twice and then fixed with 3.7% of paraformaldehyde. After ten minutes of incubation the paraformaldehyde is aspirated and the cells are washed twice again. Then the staining solution is added to the cells

and they are incubated at 37 ˚C and 5% CO_2 for two days until stained and non-stained virus plaques can be distinguished. If a foreign gene was inserted successfully into the J2K locus β-galactosidase staining is negative and if it was inserted into the A56R locus β-glucuronidase staining should be negative.

3.7% Paraformaldehyde:	
Paraformaldehyde	18.5 g
PBS	500 ml PBS
filter through 0.45 micron filter	

Solution B:	
$MgCl_2$	2 mM
$K_3Fe(CN)_6$	5 mM
$C_6FeK_4N_6$ x 3 H_2O	5 mM

β-galactosidase staining solution:	
Solution B	1.5 ml
PBS	0.5 ml
X-Gal	30 µl

β-glucuronidase staining solution:	
Solution B	1.5 ml
PBS	0.5 ml
X-Gluc	30 µl

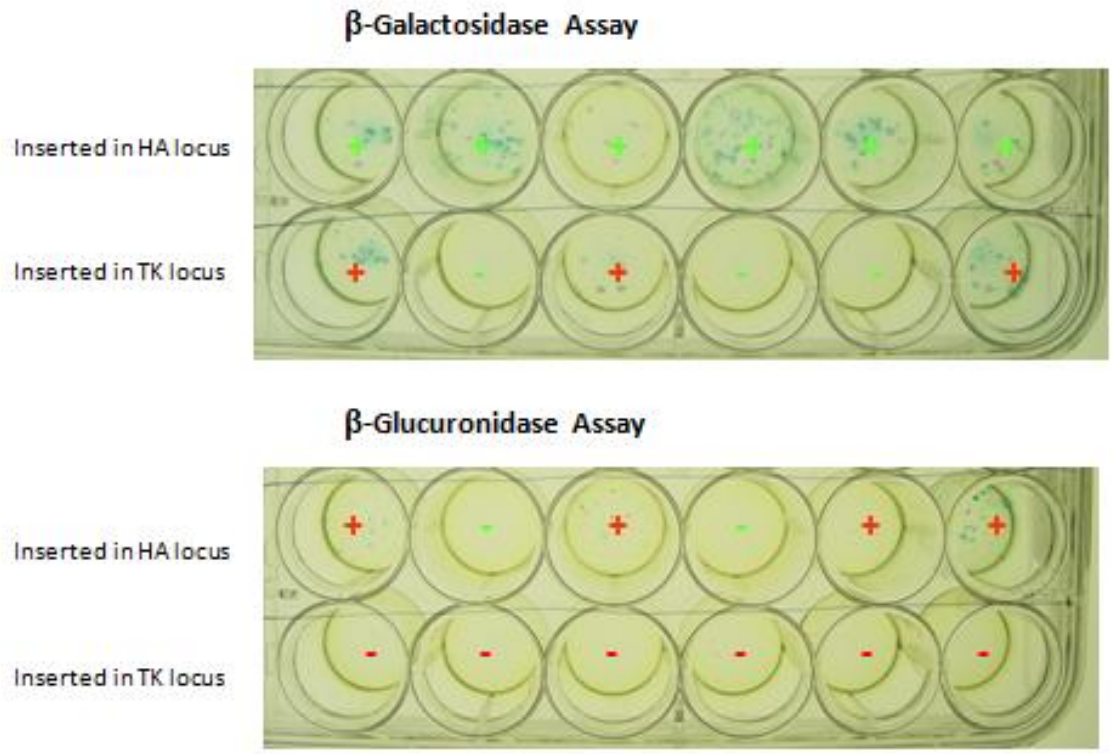

Fig. 3.1 Screening of plaque lysates by β-Galactosidase and β-Glucuronidase staining

3.1.5 *gpt* Screening

This screening is important to find out whether some of the recombinant viruses still have the *gpt* gene inserted, which means they only went through one cross-over event instead of a double cross-over.

CV-1 cells seeded in 24-well plates are treated with MPA, xanthine and hypoxanthine. After 24 hours cells are infected with 10 µl of virus plaque lysates from the fifth round. Overlay medium is added one hour after infection and plates are incubated for five days and stained with crystal violet solution. After washing the plates the wells with virus plaques can be distinguished from the wells without plaques. The plaque lysates that don't show plaques can be used to confirm the presence of the desired gene by PCR using designed primers.

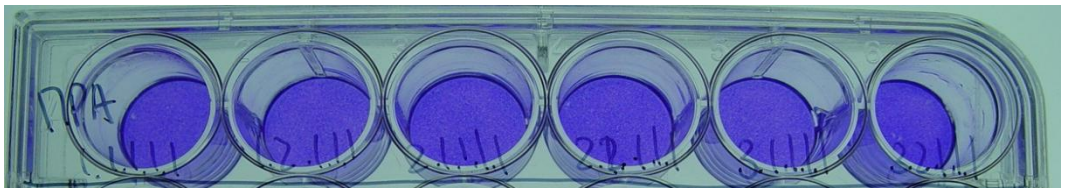

Fig. 3.2 Crystal violet staining after treatment with MPA, Xanthine and Hypoxanthine and infection with virus plaque lysates shows that double cross-over event has taken place and because the gpt gene is not present anymore.

3.1.6 Isolation of DNA to Verify Sequence

Before amplifying the virus to create a virus stock to use for experiments, the presence and the correctness of the inserted gene has to be verified by PCR. Therefore, CV-1 cells in 60 mm dishes are infected with 100 µl of virus plaque lysates from the fifth round that seem to be correct after screening of marker gene expression and gpt selection. When all the cells are infected, they are scraped with a cell scraper. Sixhundret microliters of the lysate are used for DNA isolation. The rest of the lysate is stored at -80 ˚C as a p1-stock, which is used for the amplification of the virus. The 600 µl of the lysate are frozen and thawed three times and then 600 µl of 2 x Triton X-100 buffer are added. The tubes are mixed and centrifuged at 3000 rpm for five minutes. The supernatant is transferred into a new microfuge tube and centrifuged at maximum speed for fifteen minutes. The supernatant is discarded, the pellet resuspended in 100 µl of 1 x SDS buffer and incubated at 55 ˚C for 30 minutes. After incubation the DNA is extracted twice with phenol-chloroform and the aqueous phase is saved. 1/10 volume 3.0 M sodium acetate and 2.5 volumes of 95% ethanol are added. The tube is centrifuged for fifteen minutes at top speed and the supernatant discarded. After adding 1 ml of 80% ethanol and another centrifugation step for five minutes at top speed the supernatant is discarded and the pellet air dried. Then the pellet is resuspended in 20 µl distilled water. One microliter is used as template in the PCR reaction.

2 x Triton X-100 buffer:

H_2O	90.52 ml
0.5 M EDTA	8.0 ml
Triton X-100	1.0 ml

before use, add 4.8 µl of β-mercaptoethanol per ml

1 x SDS buffer:

H_2O	83.3 ml
1 M Tris-HCl	1.0 ml
5 M NaCl	4.0 ml
0.5 M EDTA	0.2 ml
10% SDS	10.0 ml

before use, add 15 µl of 10 mg/ml proteinase K and 0.35 µl β-mercaptoethanol per ml

3.1.7 Amplification and Purification of Recombinant Viruses

After confirming the DNA sequence, CV-1 cells in ten T225 cell culture flasks are infected with $2x10^5$ pfu/ml virus. The medium in the flasks is aspirated and the cells are infected with 10 ml of virus containing medium. After two hours in a 37 ˚C and 5% CO_2 incubator and rocking the flasks every 30 minutes to ensure better distribution of the virus, 15 ml of DMEM medium containing 2% FBS are added. Two days after infection the cells in the flasks are scraped into the medium with a cell scraper and pipetted into sterile 50 ml tubes. Cells are centrifuged for five minutes at 3000 rpm and the supernatant is discarded. The pellets are then resuspended in 14 ml of 10 mM TrisCl, pH 9.0. The cell suspension is homogenized with 40 strokes in a glass homogenizer with a tight pestle. After another centrifugation step for five minutes at 3000 rpm the supernatant is saved and the pellet is resuspended in 5 ml of 10 mM TrisCl. The supernatant is saved again and pooled with the supernatant form the earlier step. The supernatant is then sonicated three times for one minute, the sonicated lysate is layered on a cushion of 17 ml of 36% sucrose in 10 mM TrisCl and centrifuged for two hours at 13,000 rpm in a HB-6 rotor, Sorvall 6 Plus Refrigerated Superspeed centrifuge. The supernatant is aspirated and discarded. The viral pellet is resuspended in 1 ml of 1 mM TrisCl, pH 9.0 and sonicated once for one minute. In centrifuge tubes sterile 24% to

40% continuous sucrose gradients are prepared the day before needed by layering 6.8 ml each of 40%, 36%, 32%, 28%, and 24% sucrose in 1 mM TrisCl and stored overnight in a refrigerator. The sucrose gradients are then overlayed with 1 ml sonicated viral pellet and centrifuged for 40 minutes at 12600 rpm at 4 ˚C. The virus band is carefully collected and saved on ice and after aspirating the remaining sucrose, the pellet is resuspended in 1 ml of 1 mM TrisCl. The resuspended pellet is sonicated once for one minute and layered on another sucrose gradient for centrifugation. The virus band is also collected and pooled with the virus band of the first centrifugation. The two volumes of 1 mM TrisCl are added. After another centrifugation step at 4 ˚C and 13000 rpm for two hours the viral pellet is resuspended in 1 ml of 1 mM TrisCl. Before making aliquots the virus is sonicated three times for one minute.

3.1.8 Determination of the Virus Titer by Plaque Assay

For determining the virus titer ten-fold serial dilutions are prepared. CV-1 cells seeded in 24-well plates are infected in duplicate with 200 µl of the virus dilutions. One hour after infection 1 ml of overlay medium is added. After two days the plates are stained with 250 µl of crystal violet solution per well and several hours after staining the plates can be washed, virus plaques can be counted, and the titer calculated with the following formula:

$$\frac{\textit{plaque forming units (pfu)} \times \textit{dilution factor}}{\textit{infection volume}} = \textit{pfu/ml}$$

3.2 Virological Methods

3.2.1 Infection of Cells with Vaccinia Virus

Cells are seeded in 6-well cell culture plates and infected at a stage of 95-100% confluence. The required amount of virus is calculated using the following formula:

$$\frac{\textit{plaque forming units (pfu) x dilution factor}}{\textit{infection volume}} = \textit{pfu/ml}$$

The virus titer is defined as plaque forming units (pfu) / ml. Prior to infection, virus aliquots are thawed on ice and sonicated for 30 seconds at 4 ˚C. This procedure prevents the formation of virus aggregates. The medium is aspirated from the cells and to 500 µl of new medium the desired amount of virus is added. After one hour of incubation at 37 ˚C and 5% CO_2 with gentle agitation every 20 minutes, fresh culture medium is added.

3.2.2 Viral Replication

For the viral replication assay, cells are grown in 6-well-plates and infected with an multiplicity of infection (MOI) of 0.01. After one hour of incubation at 37 ˚C and 5% CO_2 with gentle agitation every 20 minutes, fresh culture medium is added. The cells are harvested after 24, 48 and 72 hours by scraping the cells off the culture plate with a cell scraper. Following three freeze-thaw cycles, serial dilutions of the lysates are titered by standard plaque assay on CV-1 cells. All samples are measured in triplicate.

3.2.3 Plaque Assay

The standard plaque assay is a method to determine viral titers in a suspension. CV-1 cells are grown in 24-well-plates to 100% confluence. Samples are sonicated three times for 30 seconds and diluted depending on the expected virus titer. Then CV-1 cells are infected with 200 µl of dilutions. After one hour of incubation at 37 ˚C and 5% CO_2 with gentle agitation every 20 minutes, 1 ml of carboxymethylcellulose (CMC) overlay

medium is added and the cells are incubated at 37 ˚C and 5% CO_2 until after 48 hours the cells are stained with 250 µl of crystal violet solution per well. Several hours after the staining plates can be washed and colorless viral plaques can be identified and counted. Every viral plaque represents one infectious virus particle. All samples are measured as triplicates and the results are averaged to obtain better accuracy. The following formula is used to determine the final pfu/ml:

$$\frac{\textit{plaque forming units (pfu) x dilution factor}}{\textit{infection volume}} = \textit{pfu/ml}$$

3.3 Bacteriological Methods

3.3.1 Growth Curve

From bacterial colonies of the strains *E. coli* Omnimax pTolC and *E. coli* Omnimax pTolC-EC20 grown on LB-Plates with 50 µg/ml kanamycin overnight cultures are prepared by picking a colony with a pipette tip and putting it into 5 ml of LB medium with kanamycin. The next day the optical density is measured at 600 nm. All strains are diluted to the same density and new 20 ml cultures with kanamycin are inoculated 1:100. Every hour optical density measurements are made until the readings do not change anymore, which means the bacteria are in the stationary phase. A growth curve from the values of the measurements is generated.

3.3.2 Preparation of Bacterial Cultures for Heavy Metal ICP-MS Measurements

From bacterial colonies of the strains *E. coli* Omnimax pTolC and *E. coli* Omnimax pTolC-EC20 grown on LB-Plates with 50 µg/ml kanamycin overnight cultures are prepared by picking a colony with a pipette tip and putting it into 5 ml of LB medium with kanamycin. The next day the optical density is measured at 600 nm. All strains are diluted to the same density and new 20 ml cultures with kanamycin are inoculated

1:100. Into the media 5 µM of heavy metal supplements ($FeCl_3$, $MnSO_4$, $CuSo_4$, and $CdCl_2$) are added. Bacterial cultures are incubated for six hours at 37 ˚C and 180 rpm. After 100 µl of each culture are taken out to prepare serial dilutions until 10^{-7} and spread out on LB-plates, cultures are centrifuged for twelve minutes at 6000 rpm. The bacterial pellets are washed twice with 1 ml of cold PBS. Then the pellet is resuspended in 1.5 ml of BugBuster (Novagen). The lysate is treated three times with sonication for one minute. After that the remaining DNA is digested with 1 µl of benzonase (Novagen) per sample for 30 minutes at 37 ˚C. A treatment with1 µl of proteinase k (Sigma) at 50 ˚C overnight destroys all remaining proteins. The next day 0.5 ml of nitric acid is added to the samples and they are incubated on ice for one hour. Then the precipitated remaining proteins and cell debris are removed by centrifugation for 20 minutes at 13000 rpm. The supernatant is transferred into a new microfuge tube and is ready for ICP-MS measurement. The measurements are performed at the University of Wuerzburg by Uwe Gbureck of the Department of Functional Materials in Medicine and Dentistry.

LB plates:

LB	25 g
H_2O	1 L

autoclave

LB medium:

LB	25 g
agar	15 g
H_2O	1 L

autoclave and pour plates

3.4 Protein Analytical Methods

3.4.1 Preparation of Protein Lysates from Mammalian Cells

Cells are grown in 6-well-plates to 90-100% confluence. The supernatant is then aspirated and the cells are washed with PBS. Then 1 ml of PBS is added to the cells and cells are scraped off the plate with a cell scraper. After centrifugation at 2.5 x g for five minutes the cell pellet is resuspended in 100 µl of RIPA buffer with Proteinase Inhibitors. Cells are sonicated with 50% power for 30 seconds and incubated on ice for fifteen minutes. Then the lysate is treated with 1 µl benzonase and incubated for one hour at 37 ˚C to degrade the DNA. At this point the protein concentration is determined with the D_C Protein Assay (Biorad). After mixing 10 µg of protein with SDS-loading buffer the samples are boiled at 95 ˚C for five minutes and centrifuged for five minutes before loading the supernatants on the gel.

RIPA Buffer:

NaCl	150 mM
Tris, pH 7.2	10 mM
SDS	0.1%
Triton X-100	1.0%
Deoxycholate	1.0%
EDTA	5 mM

one tablet of proteinase inhibitors is added to 2 ml PBS. After it is dissolved 4 µl added per ml of RIPA buffer.

SDS-Loading Buffer:

1 M Tris-HCl pH 6.8	5 ml
Glycerin 20%	10 ml
SDS 4%	20 ml
Bromphenole blue	0.001 g
distilled H_2O	to 50 ml

before use 200 mM DTT are added.

3.4.2 Protein Assay

To determine the protein concentration of the samples a protein assay is performed to be able to load the exact same amount of protein in every well of the gel which is important for comparison. For this procedure the DC protein assay (Biorad) was used according to the instructions of the manufacturer. Standards were prepared with concentrations from 0.2 mg/ml to 1.2 mg/ml of lyophilized Bovine Plasma Gamma Globulin (Biorad). Five microliters of standards and samples are pipetted into a 96-well microtiter plate. Twentyfive microliters of reagent A' (prepared of 20 µl of reagent S for each ml of reagent A) are added to each well. Then 200 µl of reagent B are added and the plate is mixed. After fifteen minutes, absorbance can be read with a microplate reader at 750 nm and the protein concentrations calculated according to the standard curve.

3.4.3 SDS-Polyacrylamid Gel Electrophoresis

SDS-PAGE (sodium dodecyl sulfate polyacrylamide gel electrophoresis) is a technique to separate proteins according to their molecular weight. SDS is an anionic detergent that denatures proteins. It charges proteins homogenously negative by binding to positively charged side chains of amino acids in proteins. The intrinsic charges of polypeptides become negligible when compared to the negative charges contributed by SDS. Separation of proteins is based on the amount of SDS that is bound by a protein. The SDS in the SDS-loading buffer that is added to the protein samples prior to electrophoresis, helps degrading three-dimensional protein structures. To perform the electrophoresis the NuPAGE® precast gel system (Invitrogen) in an XCell SureLock™ Mini Cell (Invitrogen) is used. Precast NuPAGE® Bis-Tris (Invitrogen) gels are loaded with 10 µg of protein mixed with loading buffer. In the first well 10 µl of Precision Plus Protein Standard (Biorad) are loaded to compare protein sizes of the samples. The gel chamber is filled with 1 x NuPAGE® MOPS Running buffer (Invitrogen). Gel electrophoresis is conducted at a voltage of 150 V for about one hour.

3.4.4 Coomassie Staining of Protein Gels

After SDS-PAGE the gel can be stained with Coomassie Brilliant Blue R250 Solution. It is an anionic dye, which binds with proteins non-specifically. Proteins in the gel are fixed by acetic acid and simultaneously stained. The excess dye incorporated in the gel can be removed by destaining with the same solution but without the dye. The proteins are detected as blue bands on a clear background.

The gel is incubated in Coomassie Staining solution on a shaker at room temperature. After several hours the staining solution is removed and replaced by destaining solution. When the protein bands are clearly visible and the background destained the gel can be scanned or photographed.

Coomassie Staining Solution:	
Coomassie Brilliant Blue R-250	0.025%
Methanol	40%
acetic acid	7%

Coomassie Destaining Solution:	
Methanol	40%
acetic acid	7%

3.4.5 Protein Transfer to PVDF Membrane (Western Blot)

Proteins within a polyacrylic matrix are not accessible for macromolecular ligands like antibodies. To make them accessible to these ligands, proteins have to be transferred to a membrane. Degraded proteins are transferred to a polyvinylidene fluoride (PVDF) membrane through migration within an ionic gradient. The negatively charged proteins migrate towards a cathode. They bind to the membrane through hydrophobic interaction.

For protein transfer also the XCell SureLock™ Mini-Cell with a blot module (Invitrogen) is used. The proteins are blotted on a 0.2 µm PVDF membrane (Invitrogen). The blot is assembled in the following order from cathode to anode: Three buffer soaked sponges,

buffer soaked filter paper, polyacrylamide gel, membrane, buffer soaked filter paper, three buffer soaked sponges. The inner chamber is filled with 1 x NuPAGE® Transfer buffer (Invitrogen) and the outer chamber with cold water for cooling. The proteins are blotted for 50 minutes at 35 V.

3.4.6 Native PAGE

Native PAGE is a protein gel electrophoresis where the proteins keep their native form. No denaturing buffers are used. The NativePAGE™ Novex Bis-Tris Gel system (Invitrogen) is used to perform electrophoresis. It is a near-neutral pH precast polyacrylamide system to perform non-denaturing electrophoresis. It is based on the Blue Native PAGE technique developed by Schaegger and von Jagow (Schaegger and von Jagow, 1991) that uses Coomassie G-250 as a charge shift molecule instead of SDS in denaturing gels. Coomassie G-250 binds to proteins and confers a net negative charge while maintaining the proteins in their native state without any protein denaturation.

Samples are prepared according to the manufacturer's manual by mixing the cells with NativePAGE™ sample buffer (Invitrogen) and 1% digitonin. The cells are homogenized by pipetting up and down and centrifuged to clarify the lysate. Then samples are treated with one unit of benzonase. A protein assay (Biorad) is performed to determine the protein concentration. Then 5% G-250 Sample Additive (Invitrogen) is added and the volume is brought to 10 µl with water per sample. The wells are loaded with a protein marker and samples. The anode buffer is filled in the outer gel chamber and the cathode buffer in the inner chamber and the gel is run at 150 V for around 120 minutes.

Anode buffer:

NativePAGE™ Running Buffer (20x)	50 ml
deionized H_2O	950 ml

Light Blue Cathode buffer:

NativePAGE™ Running Buffer (20x)	10 ml
NativePAGE™ Cathode Additive	1 ml
deionized H_2O	189 ml

3.4.7 Colorimetric Immunodetection

After Western Blotting the membrane is blocked with 5% skim milk for 30 minutes at room temperature on a shaker. Then it is incubated with the primary antibody with using an antibody specific dilution (anti-ferritin antibody: 1:2000, anti-transferrin receptor antibody: 1:500, anti-DMT1 antibody: 1:1000) in PBS over night at 4 ˚C. The membrane is washed for 30 minutes in PBST and the secondary antibody in a 1:5000 dilution is incubated for two hours at room temperature. After a final wash of one hour in PBST the protein can be detected with a colorimetric method. For the detection the Opti-4CN kit (Biorad) is used. To 1 ml of diluent 9 ml of water are added. Then 200 µl of substrate are added and it is mixed well. Then the PBST on the membrane is replaced with the substrate solution. Protein bands are visible after 30 minutes.

PBST:

0.05% Tween-20 in PBS

3.4.8 Stripping of Membranes

Stripping of membranes makes it possible to detect different proteins on membranes after Western Blotting for more than one time. After finishing the detection of one antigen, the membrane can be scanned or photographed to save the result. Then it is incubated with stripping buffer for 50 minutes at 50 ˚C in a shaking incubator set at40 rpm. Then the membrane is washed twice in 0.05% PBST for ten minutes on an orbital shaker at room temperature. After that the membrane is blocked again in 5% skim milk and another antibody can be incubated.

Stripping Buffer:

2-Mercaptoethanol	100 mM
SDS	2%
Tris-HCl	62.5 mM
pH 6.7	

3.4.9 ELISA

ELISA (Enzyme-linked immunosorbant assay) is a biochemical technique used to detect the presence of an antibody or an antigen in a sample. In a direct ELISA the antigen is coated on a microtiter plate and detected with an antibody.

The antigen is diluted to a concentration of 10 µg/ml in carbonate buffer. The antigen dilution is pipetted in the wells of a microtiter plate and incubated over night at 4 ˚C. Then the coating solution is removed and the plate washed twice by filling the wells with 0.05% PBST. The solutions are removed by flicking the plate over a sink. Twohundret microliters of casein blocking solution are added to the wells. After two hours at room temperature the plate is washed twice. Onehundret microliters of primary antibody dilution (1:5000) in PBS are added to each well. The incubation time is one hour at room temperature. Then the wells are washed again and the secondary antibody is added in the same concentration. After another round of washes the antigen is detected by a colorimetric method. Onehundret microliters of TMB are added to each well. After sufficient color development 100 µl of 2 N HCl are pipetted into the wells as a stop solution. The absorbance is measured with a microplate reader at 450 nm.

Bicarbonate/Carbonate Coating Buffer:

Na_3CO_3	3.03 g
$NaHCO_3$	6.0 g
distilled H_2O	1000 ml
pH 9.6	

3.5 Detection of Gene Expression Mediated by Recombinant Vaccinia Virus

3.5.1 Analysis of Gene Transcription by RT-PCR

RT-PCR is an abbreviation for reverse transcriptase polymerase chain reaction. For a RT-PCR cDNA (complementary DNA) is synthesized from mRNA by specific RNA-

dependent DNA polymerases (reverse transcriptases). Synthesized cDNA can be used to analyze and compare transcription of genes by PCR with matching primers.

3.5.1.1 Isolation of RNA from Adherent Mammalian Cells

RNA is isolated from mammalian cells. Cells are grown in 6-well-plates to 95% confluence before they are infected with virus. To harvest the cells they are washed with PBS and scraped into PBS using a cell scraper. Then the cell lysates are centrifuged at 2.5 x g for five minutes and the supernatant aspirated. The pellet is frozen at -20 ˚C. RNA is isolated using the RNEasy® Mini Kit (Qiagen) following the manufacturer's protocol. Cells are homogenized with a 20G syringe. The suspension is then transferred to RNA isolation columns. After the procedure RNA is eluted in 30 µl of RNase free water. To avoid genomic DNA amplification, samples are treated with DNA-free™ Kit (Ambion) after the manufacturer's protocol for genomic DNA digestion.

3.5.1.2 Synthesis of cDNA

Isolated RNA is used to synthesize cDNA. For that a reverse transcriptase is used to transcribe RNA back to DNA. The commercially available SuperScript™ II Reverse Transcriptase Kit (Invitrogen) was used according to the manufacturer's protocol. To 1 µg total RNA Oligo(dT) primers and dNTP Mix are added. The mixture is heated to 65 ˚C for five minutes and chilled on ice. Then 5x First Strand buffer, DTT, and RNase Out are added and mixed. The mixture is incubated at 42 ˚C for two minutes. Then the reverse transcriptase is pipetted into the mixture and incubated at 42 ˚C for 50 minutes. To inactivate the reaction the tubes are heated at 70 ˚C for one minute. The cDNA is ready to be used as a template in a PCR reaction.

3.5.1.3 Polymerase Chain Reaction (PCR)

The Polymerase Chain Reaction is a very sensitive method to amplify DNA. It consists of the following steps: In the denaturation step the double-stranded DNA is separated into single strands. The annealing step serves the binding of the primers to the DNA template. In the elongation the DNA polymerase binds to the template and uses dNTPs to extend the primers and to synthesize a complementary strand.

For the PCR a 50 µl reaction is prepared with 45 µl of Accuprime™ Pfx Supermix 1 µl of each primer and 1 µl of template DNA. The PCR cycle starts with an initialization step at 94 ˚C for five minutes. Then there are 35 repetitions of a denaturation step at 94 ˚C for 30 seconds, an annealing step at a temperature that depends on the primers (about 3-5 degrees Celsius below the melting temperature of the primers used) for ten seconds and an elongation step at 68 ˚C for a time that depends on the length of the DNA that is to be amplified. At the end there is a final elongation step at 68 ˚C for seven minutes.

3.5.1.4 Agarose Gel Electrophoresis

Horizontal agarose gel electrophoresis is a method to separate DNA fragments by its size. Agarose concentration is dependent on the DNA fragment sizes. For a 1% agarose gel 0.5 g of agarose are heated in the microwave with 50 ml of TBE buffer. Ethidium bromide (0.5 µg/ml) is added to the agarose to enable detection of the DNA using UV light. Ethidium bromide intercalates between the bases of the DNA strands. To the samples DNA sample buffer is added and they are loaded into the wells of a gel. A DNA marker is used for comparison of DNA fragment sizes. After applying a voltage of 100 V the nucleic acids start moving to the anode. Larger DNA molecules need more time to migrate the same distance than smaller DNA molecules. After electrophoresis the bands can be detected under UV light and photographed.

3.6 Determination of the Iron Content in Cell Cultures

3.6.1 QuantiChrom™ Iron Assay

QuantiChrom™ Iron Assay Kit is a commercially available Iron Assay Kit that forms a blue colored complex with Fe^{2+}. Fe^{3+} in the sample is reduced to Fe^{2+}, which allows the determination of the total iron content.

The assay is performed according to the manufacturer's instructions. Cells grown in 6-well-plates are infected with virus and 24 hours after infection an iron supplement is added. This supplement is composed of 1mg/ml human holo-transferrin (Sigma) and

1 mM ferric citrate. Another 24 hours later the cells are rinsed with cold PBS, scraped into 1 ml of PBS and centrifuged at 2500 x g for five minutes to wash them. Then they are resuspended carefully in 1 ml of PBS. After repetition of the wash step the pellet is resuspended in 100 µl of 1% Triton-X. A protein assay is performed to determine the protein concentration. The working Reagent for the Iron Assay is prepared by mixing 20 volumes of Reagent A, one volume of Reagent B and one volume of Reagent C. Standards are prepared from 0 - 1000 µg/dL iron. Fifty microliters of diluted standards and samples are pipette into a 96-well microtiter plate. Twohundret microliters of working reagent are added to the wells. After 40 minutes of incubation at room temperature the absorbance at 590 nm is measured and iron concentrations are calculated by using the standard curve.

3.6.2 Ferrozine Assay

Ferrozine (the disodium salt of 3-(2-pyridyl)-5,6-bis(4-phenylsulfonic acid)-1,2,4-triazine) reacts with divalent iron to form a stable magenta complex which is soluble in water and can be used for the direct determination of iron in water (Stookey, 1970).

Cells grown in 6-well-plates are infected with virus and 24 hours after infection an iron supplement is added. This supplement is composed of 1 mg/ml human holo-transferrin (sigma) and 1 mM ferric citrate. Another 24 hours later the cells are rinsed with cold PBS, scraped into 1 ml of PBS and centrifuged at 2500 x g for five minutes to wash them. Then they are resuspended carefully in 1 ml of PBS. After repetition of the wash step the pellet is resuspended in 100 µl of 1% Triton-X. A protein assay is performed to determine the protein concentration. After that 100 µl of cell lysate are mixed with 100 µl of Protein Precipitation Buffer. The samples are heated for 45 minutes at 95 ˚C. In a cold water bath they are cooled down and the centrifuged for ten minutes at 14,000 x g. As standards 0 - 2.0 µg/ml iron dilutions are prepared. Thirty microliters of the supernatants and standards are incubated with 30 µl of Chromogen Solution. After 30 minutes incubation at room temperature the absorption at 562 nm is measured in a microtiter plate with a microplate reader. The iron concentrations are calculated with the standard curve and µg iron per mg protein are determined with the results of the protein assay.

Protein Precipitation Solution:

H_2O	25 ml
Trichloroactetic Acid	10.0 g
concentrated HCl	8.34 ml
add H_2O	to 100 ml
store at 4˚C	

Chromogen Solution:

Water	25 ml
Sodium acetate	20.4 g
Ferrozine	25.0 mg
Thioglycolic Acid	0.2 ml
add H_2O	to 100 ml

3.6.3 Inductively Coupled Plasma Mass Spectrometry (ICP-MS)

ICP-MS is an analytical technique used for elemental determinations. ICP-MS combines a high temperature inductively-coupled plasma source with a mass spectrometer. An ICP-MS consists of the following components: The sample introduction system consists of the peristaltic pump, nebulizer and a spray chamber, and gets the samples into the instrument. The ICP torch generates the plasma which serves as the ion source of the ICP-MS, converting the analyte atoms to ions. The interface links the atmospheric pressure ICP and the high vacuum mass spectrometer. The lens focuses ions into a beam for transmission into the quadrupole which acts as a mass filter to sort ions by their mass-to-charge ratio. Then the detector counts individual ions passing through the quadrupole and a computer controls the instrument and data handling to obtain final concentration results. Most samples analyzed by ICP-MS are liquid. The nebulizer converts the liquid samples into very small droplets. These droplets are carried through the spray chamber and into the tube or injector that is the center channel of the torch and then into the plasma. The plasma ionizes the elements present in the droplets. These ions then pass through the interface and the ion lens. After being focused by the ion lens, the ions are separated by their mass-to-charge ratio in the mass spectrometer

and measured by the detector. Once the detector measures the ions, the computerized data system is used to convert the measured signal intensities into concentrations of each element.

3.6.3.1 Sample Preparation for ICP-MS

Forty-eight hours after infection with different viruses and 24 hours after supplementation with iron or manganese, cells are washed twice with cold PBS and then lysed with 1% Triton-X in water. The samples are treated with 1 µl of benzonase for one hour at 37 ˚C. After that the protein concentration is determined by using the biorad protein assay. The samples are digested with proteinase k and also incubated for one hour at 37 ˚C. Fourhundret microliters of concentrated nitric acid is added to the samples and incubated for one hour on ice to precipitate all the proteins. The volume is brought to 2 ml by adding water. After sterile filtration of the samples they are ready to be measured. The measurements are done by Uwe Gbureck of the Department of Functional Materials in Medicine and Dentistry, University Würzburg.

3.7 *In vivo* Studies

3.7.1 Tumor Monitoring

Four to six weeks old male nude mice are implanted with $5x10^6$ A549 lung carcinoma cells subcutaneously in both sides of the upper hind leg area. The viruses are injected three to four weeks after tumor implantation. Five times ten to the six plaque forming units of the virus are mixed with PBS to a volume of 100 µl and injected intravenously by retro orbital injection. After injection of the tumorous mice are supplemented with 0.1 mg iron by intraperitoneal injection with iron dextran solution every other day. Tumors are measured once a week with a digital caliper. Length, height and width of the tumors are measured and written down. The tumor volume is calculated using the following formula:

$$\text{tumor volume} = \frac{\text{length} \times \text{width} \times (\text{height} - 5\text{mm})}{2}$$

Also the weight of each mouse is noted to keep track of any changes of body weight after tumor implantation and injection with the virus. By holding the mice under UV light and looking at the tumors, a successful infection can be confirmed by the visible green GFP expression mediated by the viruses and can be photographed for the records.

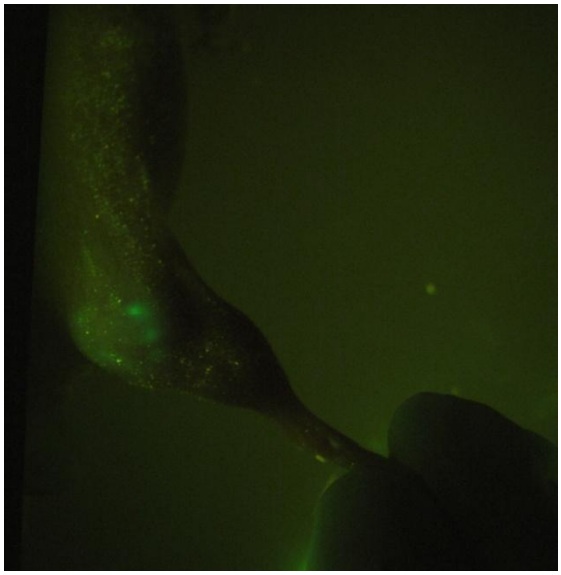

Fig 3.4 GFP expression in mouse tumor after infection with GLV-1h68

3.7.2 Preparation of Virus for Mouse Injection

Mice are infected with 5 x 10^6 pfu in 100 µl PBS. The right amount of virus is calculated for each virus that is to be injected with the titer of each virus and mixed with PBS to get 100 µl total per mouse. A small amount of virus is prepared additionally to what is needed for the injections to be able to confirm the prepared viruses titers by making dilution series and performing a plaque assay. Onehundret microliters of virus

containing PBS are injected retro orbital with insulin syringes. The remaining virus is titrated with CV-1 cells in 24-well-plates. After one hour overlay medium is added and after two days the cells are stained with crystal violet solution. Then the virus plaques are counted and virus titer is compared with the calculated numbers.

3.7.3 Production of Mouse Serum against Bacterioferritin

BALB/c mice are used for this purpose because they are not immunodeficient and therefore able to produce antibodies against an injected antigen. Fifty micrograms of the desired antigen (in this case bacterioferritin) is mixed together with 100 µl of Freund's Incomplete Adjuvant (Calbiochem) until the mixture is homogenous. The mixture is injected intraperitoneally every two weeks. After the third injection blood is taken to test the serum. The blood is stored at 4˚C over night and the next day the sample is centrifuged at 6000 rpm for five minutes to get the serum. The serum is used in a 1:10 dilution for Western Blot with bacterioferritin samples. After successful detection in the Western Blot the mice are sacrificed and all the blood is taken and refrigerated overnight. After centrifugation the serum can be used for Western Blots.

3.7.4 Tumor and Organ Preparation for Virus Titration

After dissection of the tumors and organs (spleen, liver, heart, lungs) they are weighed and placed in MagNA Lyser Green Beads tubes (Roche) containing 500 µl of PBS with proteinase inhibitors. One tablet of proteinase inhibitor cocktail is previously dissolved in 50 ml of PBS. If the weight exceeds 0.8 g additional tubes are used for the same organ. It has to be noted how many tubes are used so it can be calculated into the end result. The tubes are kept on ice at all times. After all tumors and organs are dissected they are shredded at 3000 rpm for 30 seconds with a MagNA Lyser (Roche). Then they are frozen at -80 ˚C until the day of the titration. Samples are thawed three times before further use. Then they are sonicated three times for one minute to further break up the tissue and virus aggregates. Tissues that were split into more than one tube are combined. Then the samples are centrifuged for five minutes at 6000 rpm.

CV-1 cells are infected with 10 µl of organ lysate into 200 µl of medium. Tumors are diluted until 10^{-6} and the dilutions 10^{-4} - 10^{-6} are used for infection. 200 µl of the dilutions

are added to CV-1 cells. After one hour overlay medium is added and after two days the cells are stained with crystal violet solution. After washing and drying the virus plaques are counted and titers are calculated.

3.7.5 Tumor Preparation for Western Blot

The preparation of the tumor lysates is done as previously described (paragraph 3.6.4). Then the protein concentration is determined with a Protein Assay. 10 µg of protein lysate are mixed with SDS loading buffer and loaded in the wells of a precast protein gel (Invitrogen).

3.7.6 Tumor Preparation for Ferrozine Assay

The preparation of the tumor lysates is done as previously described (paragraph 3.6.4). Then the protein concentration is determined with a Protein Assay. The remaining lysate is used for the Ferrozine Assay. The ferrozine assay is conducted as previously described (paragraph 3.5.2) for the cell culture samples.

3.7.7 Histology

After dissection of the tumors they are cut into slices no thicker than 3 mm and placed in a beaker with 10% neutral buffered formalin for fixation over night at room temperature.

3.7.7.1 Dehydration

To dehydrate the tissue is subjected to the following steps on a rocking platform for one hour per step:

1. 0.9% NaCl
2. 30% EtOH in 0.9% NaCl
3. 50% EtOH in 0.9% NaCl
4. 70% EtOH in 0.9% NaCl
5. 90% EtOH in 0.9% NaCl
6. 100% EtOH
7. 100% EtOH

At this stage the tissues are stored over night until they are embedded in paraffin the next day.

3.7.7.2 Embedding

Paraffin wax is melted ahead of time. A small aliquot of wax is heated in a beaker and mixed with an equal amount of xylene substitute. Prior to embedding the tissue is processed through the following solutions on a rocking plate, each step for one hour:

1. 100% Ethanol, at room temperature
2. EtOH/Xylene 1:1, at room temperature
3. Xylene, at room temperature
4. Xylene/wax, at 58˚C
5. Wax, three times at 58˚C

Subsequent to infiltration, the tissue is placed into an embedding mold and melted paraffin is poured into the mold to form a block. The blocks are allowed to cool and are ready for sectioning.

3.7.7.3 Sectioning

A water bath set between 45 ˚C and 50 ˚C and a slide warmer set at 38 ˚C are placed next to the sectioning machine. The blade angle is set to 10 ˚ and 5 µm slice thickness. Ribbons of sections are cut and put into the water bath. To mount the tissue, a Superfrost Plus slide is positioned underneath the ribbons and single sections are lifted out of the water. The slides are allowed to dry on the slide warmer for at least two hours, then they are stored in a cool dry place.

3.7.7.4 Deparaffinization and Rehydration of Tissue Sections

Before deparaffinization the slides are placed in a 55 ˚C oven for ten minutes to melt the paraffin. Slides are placed into a slide holder and subjected to the following steps:

1. Xylene substitute, three minutes
2. Xylene substitute, three minutes
3. Xylene substitute, three minutes
4. 100% EtOH, three minutes
5. 100% EtOH, three minutes
6. 100% EtOH, three minutes
7. 95% EtOH in H_2O, three minutes
8. 80% EtOH in H_2O, three minutes
9. deionized H_2O, five minutes

3.7.7.5 Hematoxylin and Eosin (H&E) Staining

Slide holder with slides it put through following steps:

1. Hematoxylin, three minutes
2. Slides are rinsed in deionized H2O
3. Tap water to allow the stain to develop, five minutes
4. eight to twelve dips in acid ethanol (1 ml concentrated HCl in 400 ml 70% EtOH)
5. Slides are rinsed twice for two minutes each in tap water
6. Slides are rinsed in deionized H_2O for two minutes
7. excess water is blotted from slide holder
8. Eosin, 30 seconds
9. 95% EtOH, five minutes
10. 95% EtOH, five minutes
11. 95% EtOH, five minutes
12. 100% EtOH, five minutes
13. 100% EtOH, five minutes
14. 100% EtOH, five minutes
15. Xylene substitute, fifteen minutes
16. Xylene substitute, fifteen minutes
17. Xylene substitute, fifteen minutes

The slides are cover slipped using mounting medium. A drop of mounting medium is placed on the slide using a glass rod, taking care not to leave bubbles. The coverslip is angled and placed gently onto the slide. The medium will spread beneath the coverslip, covering all tissue. The slides are dried over night.

3.7.7.6 Prussian Blue Iron Staining with DAB Intensification

After deparaffinization and rehydration of tissue slides the slides are put into a mixture of 5% HCl and 5% potassium ferrocyanide for 30 minutes, changing the solution once after fifteen minutes. After the staining the tissue sections are incubated with ImmPACT DAB Peroxidase Substrate (Vector) for ten minutes to intensify the staining. The blue areas turn dark brown. Then the slides are counterstained with hematoxylin for 30 seconds and rinsed in water before they are dehydrated with 100% EtOH, one minute each for three changes, followed by xylene substitute, three minutes each for three changes. Then coverslips are mounted on slides using mounting medium.

3.7.7.7 Immunohistochemical Staining of Vaccinia Virus

The sections are deparaffinized and rehydrated. After rinsed for five minutes in tap water they are incubated for 20 minutes in steamed citrate buffer in a steamer. Then they are cooled down at room temperature for another 20 minutes. The slides are rinsed for five minutes in tap water. Then the sections are incubated in 3% H_2O_2 for five minutes and rinsed with water again for two minutes. The slides are washed in PBS for five minutes. To block the sections are treated with diluted normal blocking serum (three drops of serum stock in 10 ml PBS) (Vector) for 20 minutes. After excess serum is blotted from the sections, they are incubated with primary antibody (Genelux custom made rabbit polyclonal antibody against vaccinia A27L) diluted 1:1000 in blocking serum for 30 minutes. Slides are washed for five minutes in PBS and incubated with diluted biotinylated secondary antibody (one drop in 10 ml diluted blocking serum) (Vector). Slides are washed for five minutes in PBS and incubated for 30 minutes with Vectastain Elite ABC reagent. After that slides are washed for five minutes in PBS and ImmPACT DAB Peroxidase Substrate is added to the sections until suitable staining develops. The slides are washed in water again and the counterstained with

Hematoxylin (Vector) for 30 seconds. Sections are rinsed in water until it is colorless. The sections are then dehydrated with 100% EtOH, one minute each for three changes, followed by Xylene substitute, three minutes each for three changes. Then coverslips are mounted on slides using mounting medium.

Citrate buffer:

Sodium citrate 0.1 M	4.1 ml
Citric Acid 0.1 ml	9 ml
H_2O	450 ml
pH 6	

3.7.7.8 Immunohistochemical Staining of Ferritin

The staining is performed as previously describes for vaccinia virus A27L (paragraph 3.6.7.7). As primary antibody the rabbit polyclonal antibody against ferritin H-chain (Abcam) diluted 1:200 in blocking serum is used. The secondary antibody and all other solutions are used as described in paragraph 3.6.7.7.

3.8 MRI Measurements

MRI scans are performed at Center for functional MRI of the University of California, San Diego, by Miriam Scadeng. For the measurements a 7 Tesla horizontal bore small animal scanner Advance II by Bruker Biospin with Paravision 4 software and a 3 Tesla human scanner by GE are used. The mice are scanned at two different time points: 7 days post infection and 21 days post infection with the viruses. Mice are anesthetized with isoflurane or by intraperitoneal injection with a ketamine - xylazine anesthesia mix and scanned by using different T2-weighted sequences.

Anesthesia mix:

PBS	2.6 ml
Xylazine (20 mg/ml)	0.1 ml
Ketamine (100 mg/ml)	0.3 ml

inject 300-350 µl per mouse

Fig 3.5 7 Tesla Bruker MRI scanner at the center for functional MRI, UCSD

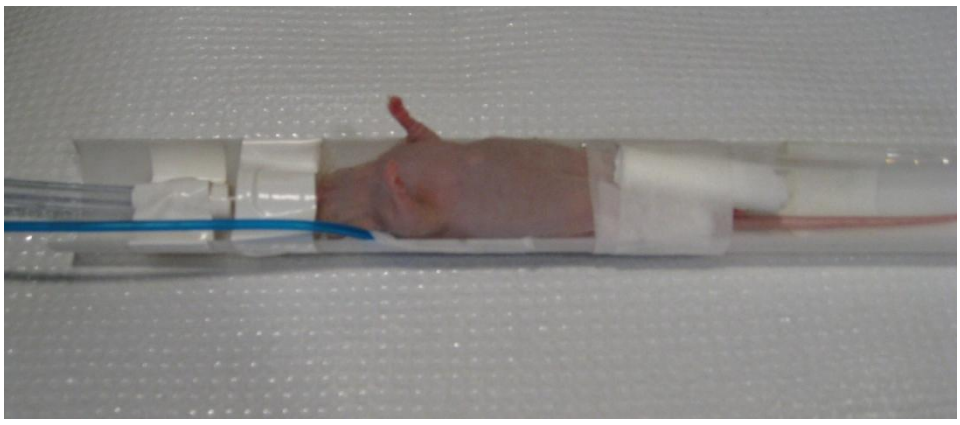

Fig 3.6 Anesthetized mouse about to be scanned in the 7T scanner

The obtained data is analyzed using Paravision 4.0 software and GE software. T2 and T2* relaxation times are determined by T2 map analysis of regions of interests drawn into the tumors. Statistical analysis of the obtained values is performed using the student’s t-test.

4 Results

4.1 Characterization of Iron-collecting Virus Strains in Cell Culture

4.1.1 Virus-mediated Ferritin Expression

GLV-1h131, GLV-1h132, and GLV-1h133 carry the genes that encode for the human ferritin H- and L-subunits linked by a 2A sequence under the control of the three different vaccinia promoters, the synthetic early promoter, the synthetic early/late promoter, and the synthetic late promoter. Ferritin is an iron storage protein and its expression in virus-infected cells and the resulting iron accumulation in tumor cells are investigated in this study. Ferritin expression was shown to provide MRI contrast in C6 glioma tumors (Cohen *et al*., 2005).

4.1.1.1 Analysis of Viral Replication in the Cancer Cell Lines GI-101A and A549

The first step after the generation of a new recombinant virus strain is to investigate the infection and replication capability of the new virus strains in the cancer cells that it is supposed to detect through iron accumulation as aim of this study in comparison to the parental virus strain GLV-1h68. Viral replication begins with the entry of the virus into a cell. The replication efficiency is dependent on the viral strain as well as on the cell line that is infected.

The replication assay was performed in the human breast carcinoma GI-101A and the human lung carcinoma A549. The same cell lines were used for protein expression studies and iron accumulation experiments described below. For analysis of the replication the respective cell lines were infected with the viruses at an MOI of 0.01, followed by determination of viral titers at the time points 24, 48, and 72 hours post infection. Average data including standard deviation are shown for all newly generated iron-accumulating virus strains in comparison to the parental virus GLV-1h68.

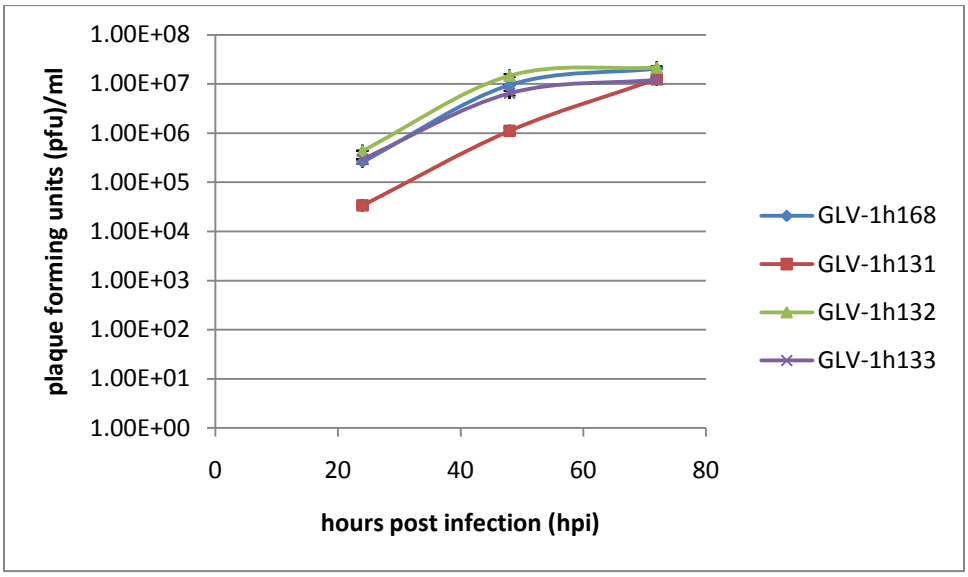

Fig. 4.1 Replication of GLV-1h131, GLV-1h132, and GLV-1h133 in comparison to GLV-1h68 in GI-101A cells

Figure 4.1 illustrates the replication efficiency of GLV-1h131, GLV-1h132 and GLV-1h133 in GI-101A cells at different time points. The x-axis shows the hours post infection and the y-axis the virus particles in plaque forming units per ml in a logarithmic scale. Viral titers in the cells increased markedly during the course of infection in the first 48 hours and then stayed on a constant level. GLV-1h131 seemed to have a slower replication in the first 48 hours but the titers increased clearly until 72 hours post infection where they were comparable to all other viruses examined. This experiment shows that GI-101A cells can efficiently be infected with the viruses GLV-1h131, GLV-1h132, and GLV-1h133.

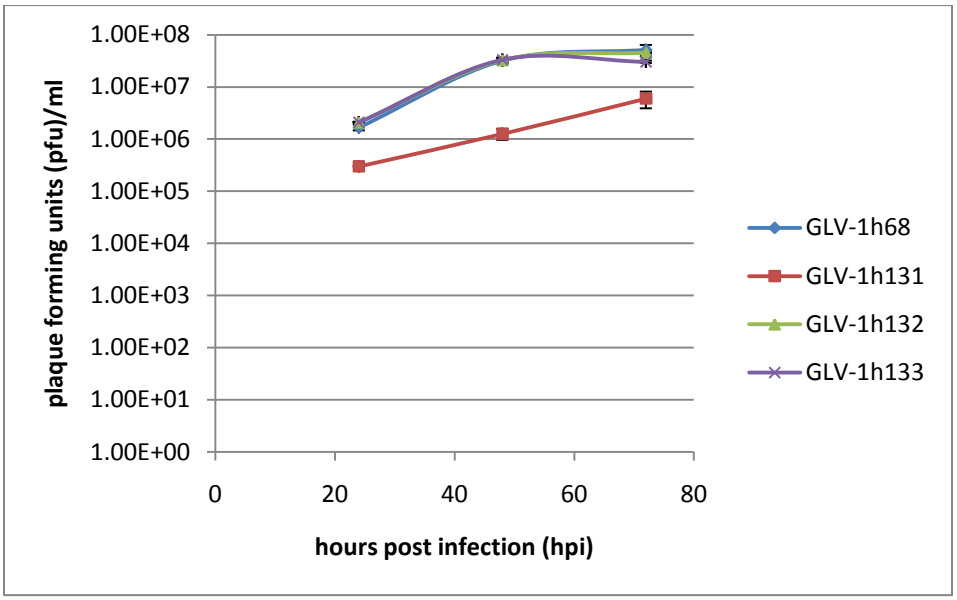

Fig. 4.2 Replication of GLV-1h131, GLV-1h132, and GLV-1h133 in comparison to GLV-1h68 in A549 cells

Figure 4.2 shows the replication efficiency of the ferritin-encoding virus strains in A549 cells. The replication rate of GLV-1h132 and GLV-1h133 was comparable to that of the parental virus GLV-1h68. Viral titers in the cells of all infected cell samples increased with the time during the course of infection. As already observed in GI-101A cells, the virus strain GLV-1h131 seemed to replicate slower in A549 cells. This experiment demonstrates that A549 cells also can efficiently be infected with the viruses GLV-1h131, GLV-1h132, and GLV-1h133 and replicate in these cells.

4.1.1.2 Analysis of Recombinant Protein Expression in Infected Cell Cultures

4.1.1.2.1 Coomassie Staining of Protein Gels

After the generation of new virus strains and the determination of the replication efficiency, it is also important to determine whether the genes, which were inserted into the viral genome are efficiently delivered to and functionally expressed by the infected mammalian cells. SDS-PAGE is a method for protein analysis. The staining of protein

gels with Coomassie Brilliant Blue shows all protein bands in contrary to Western blot, which shows as a result only the bands that are recognized by the antibody that is used. The Coomassie Blue staining is a good method to detect highly overexpressed proteins in SDS-PAGE gels like the proteins which are delivered to the cells by the virus.

For the protein expression analysis by Coomassie staining, infected cells were harvested 24 hours after infection. The protein gels were loaded with equal amounts of cell lysates after scraping the cells off the plates and cell lysis with Triton X-100. Ten micrograms of cell lysate mixed with SDS loading buffer were analyzed on the gels.

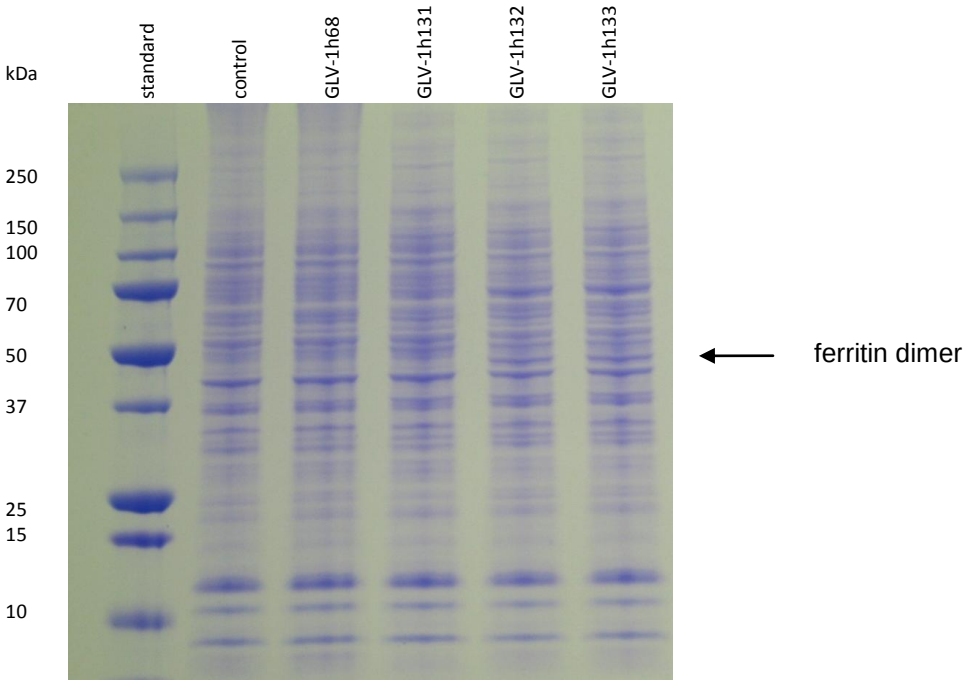

Fig. 4.3 Coomassie-stained SDS-Gel loaded with infected GI-101A cell culture samples: ferritin-encoding virus strains

Figure 4.3 shows the Coomassie-stained protein gel of uninfected, GLV-1h68 infected, and with human ferritin-encoding viruses infected GI-101A cell culture samples. The protein ladder on the left side of the gel demonstrates the protein sizes. The arrow

points to the ferritin protein band which could be clearly seen in the GLV-1h132- and GLV-1h133-infected samples. The ferritin dimer consisting of the heavy and the light ferritin chain has a size of 40 kDa. There were additional bands at 80 kDa, which represent multimers of ferritin subunits. All these bands were also slightly visible in the other samples because ferritin is expressed in a wide range of cell types and tissues (Testa, 2002). The synthetic early promoter, which controls ferritin overexpression in GLV-1h131 is to weak to express enough ferritin to make the overexpression visible on the stained protein gel.

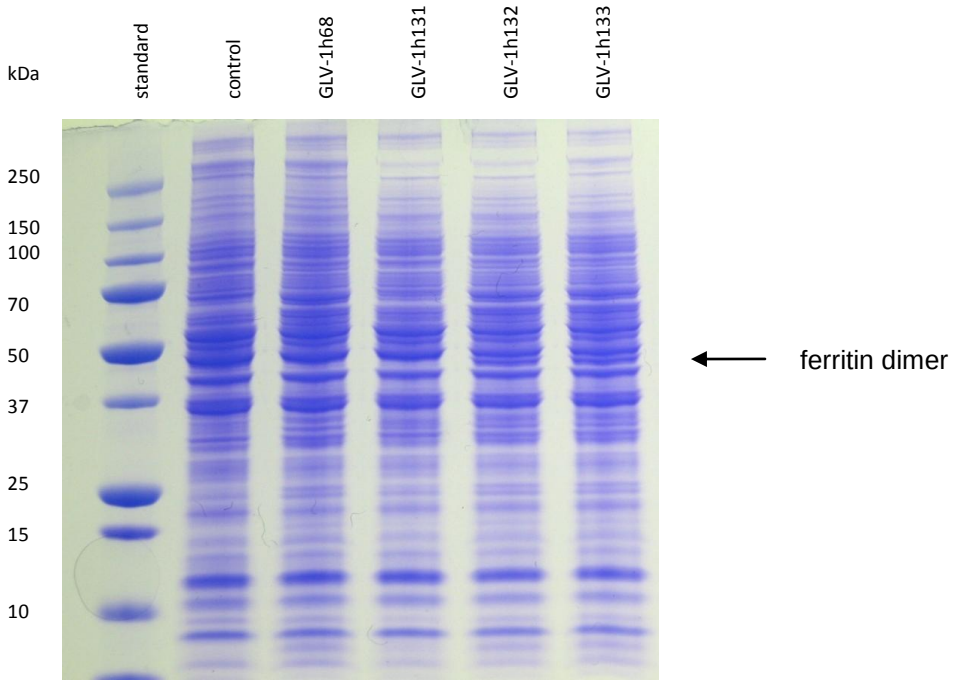

Fig. 4.4 Coomassie staining of SDS-PAGE performed with infected A549 cell culture samples: ferritin-encoding virus strains

Figure 4.4 shows the Coomassie-stained protein bands of uninfected, GLV-1h68-, and human ferritin virus-infected A549 cell culture samples. GLV-1h132 and GLV-1h133-infected samples show bands at around 40 kDa, which is the size of the ferritin dimers

as described before. These bands are also slightly visible in all other samples because of the fact that ferritin is expressed in a wide range of cell types (Testa, 2002). The synthetic early promoter, which controls ferritin expression in GLV-1h131 is to weak to express enough ferritin to be visible on the Coomassie-stained gel. The results are comparable to what was shown for infected GI-101A cells before.

4.1.1.2.2 Western Blot

Western blot analysis is a method to analyze gene expression after translation and posttranslational modification on the protein level. Specific antibodies are used to detect the protein of choice, in this case ferritin.

Cells were seeded in 6-well plates and grown until they reached 90% confluence. They were then infected with GLV-1h68 and iron-accumulating viruses, respectively, at an MOI of 5. For protein isolation and detection, cells were harvested after 24 hours. The protein samples were separated by SDS polyacrylamide gel electrophoresis (PAGE) and subsequently blotted onto a PVDF membrane. The virus-induced protein expression was detected using different antibodies, in this case ferritin antibodies, or serum and with a colorimetric detection method.

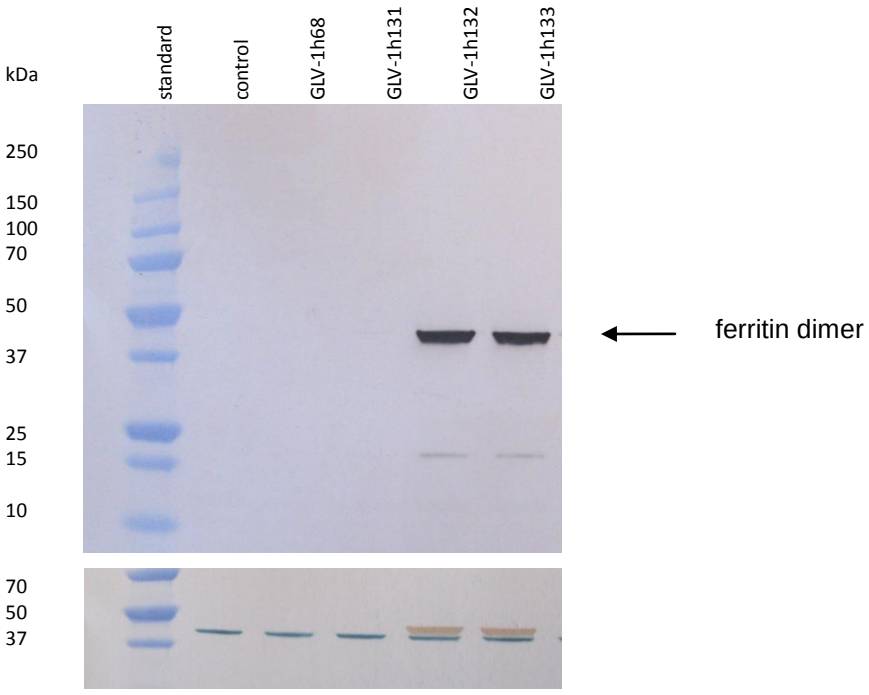

Fig. 4.5 Detection of virus-mediated human ferritin and β-actin expression by Western blot analysis in GI-101A cells

The membrane in figure 4.5 shows the detection of ferritin (above) by an anti-ferritin rabbit polyclonal antibody. Protein bands at around 20 and 40 kDa could be detected, which represent the sizes of the ferritin monomer and dimers. Similar to the results of the Coomassie staining, the ferritin protein bands were only visible in the lanes of the samples infected with viruses containing strong promoters (GLV-1h132 and GLV-1h133). The ferritin-encoding virus strain GLV-1h131 has a weak promoter and the ferritin expression is not strong enough to be visible using this colorimetric detection method. The blot below shows the β-actin expression on the same membrane which proves that the gel was loaded with the same amount of protein in each well.

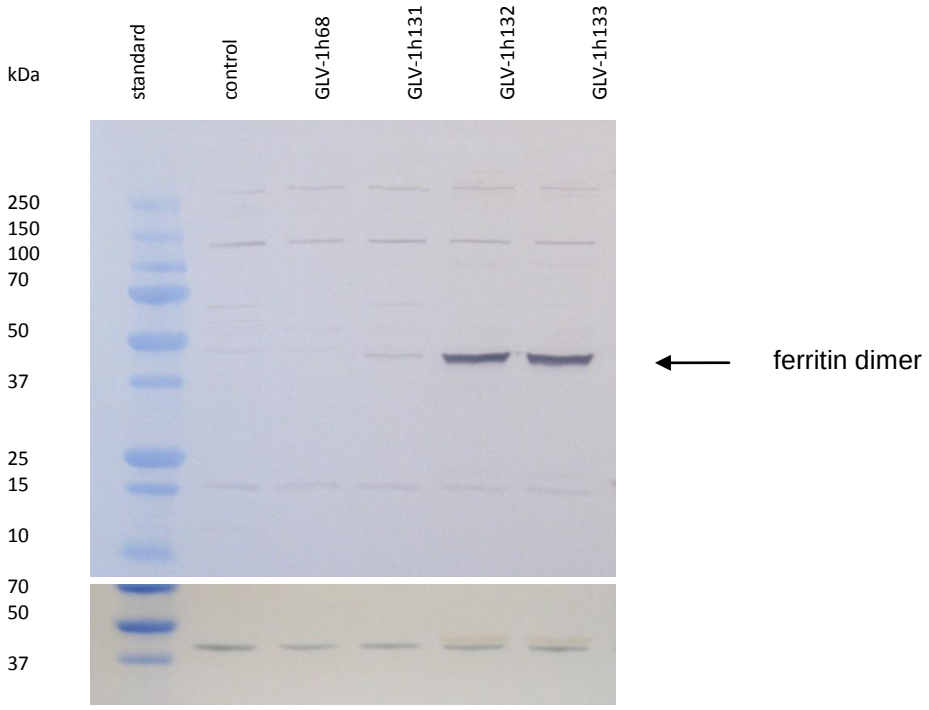

Fig. 4.6 Detection of virus-mediated human ferritin and β-actin expression by Western blot analysis in A549 cells

On the Western blot in figure 4.6 the virus-mediated ferritin expression is shown in infected A549 cells. The picture shows strong protein bands at around 40 kDa, which represent the size of the ferritin dimers. The ferritin protein bands were clearly visible for the virus strains with strong promoters (GLV-1h132 and GLV-1h133). The ferritin-harboring virus GLV-1h131 shows only a very slight ferritin band because of the weak promoter, which controls the ferritin expression in this virus. The blot on the bottom shows the detection of the β-actin expression on the same membrane which proves that the gel was loaded with the same amount of protein in each well.

4.1.1.2.3 Native PAGE

Native PAGE is a protein gel electrophoresis method, in which the proteins keep their native form. The study of proteins in their native form is useful in cases like ferritin,

which consists of a complex of 24 subunits. Western blots show only monomers or dimers of the ferritin protein. To investigate if the complex of 24 subunits is formed correctly, native gel electrophoresis was performed.

The samples were prepared from cell lysates of infected and uninfected GI-101A cells by using the NativePAGE™ Sample Prep Kit from Invitrogen. The NativePAGE™ Novex Bis-Tris Gel system (Invitrogen) was used to perform electrophoresis. For the detection of the ferritin complex via Western blot a primary ferritin antibody and a secondary anti-rabbit antibody were used. Another native PAGE gel with the same samples was stained with Coomassie Blue.

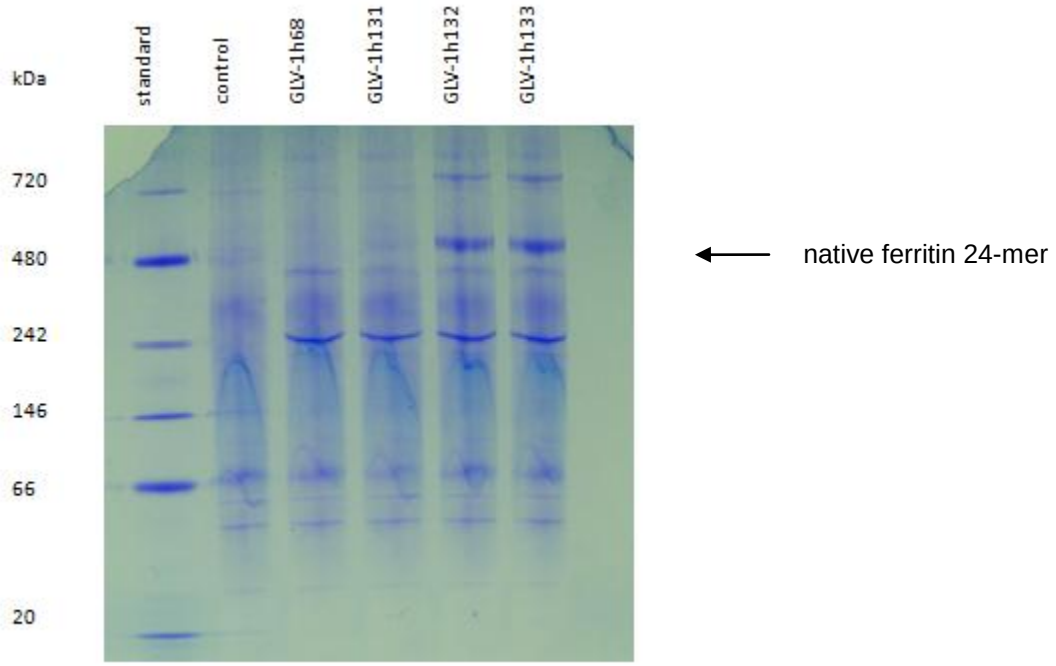

Fig. 4.7 Coomassie staining following native gel electrophoresis with infected GI-101A samples: ferritin encoding virus strains

In figure 4.7 the protein bands of the native ferritin protein were visualized on a native gel stained with Coomassie Blue. The native ferritin 24-mer could be detected with a size of approximately 500 kDa in lysates of GLV-1h132- and GLV-1h133-infected cells.

Another band double the size could be detected in the same samples which might represent a multimer. The band at around 242 kDa, which could be seen in every virus-infected sample might represent a vaccinia specific protein.

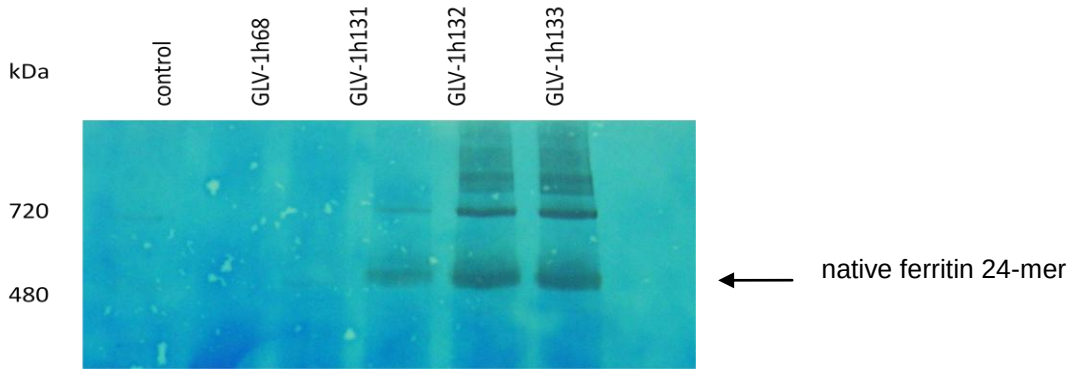

Fig. 4.8 Detection of virus-mediated human ferritin expression by native Western blot analysis in GI-101A cells

The native blot in figure 4.8 also showed bands with the size of 500 kDa representing the ferritin complex and its multimers. These results of the native PAGE experiments proof that the 500 kDa 24-mer of ferritin subunits is assembled correctly from the virus-induced expression of heavy and light subunits.

4.1.1.2.4 ELISA

To investigate whether the ferritin protein, expressed by virus-infected cells is recognized by a ferritin antibody an ELISA (Enzyme-linked immunosorbant assay) was performed. In this technique antibodies are used to bind specific antigens coated to a cell culture plate and detect them by a colorimetric reaction. As a reference a commercially available ferritin protein is used in a known protein concentration.

The assay was performed in 96-well plates. Cells were infected at an MOI of 5 and harvested after 1, 12, 24 and 48 hours post infection. The wells of the 96-well plate were coated with 10 µg/ml total protein. After incubation overnight at 4 ˚C the plate was

washed and consequently incubated with an anti-ferritin and an anti-rabbit antibody. After the color reaction with TMB and HCl the absorbance was measured with a microplate reader at 450 nm.

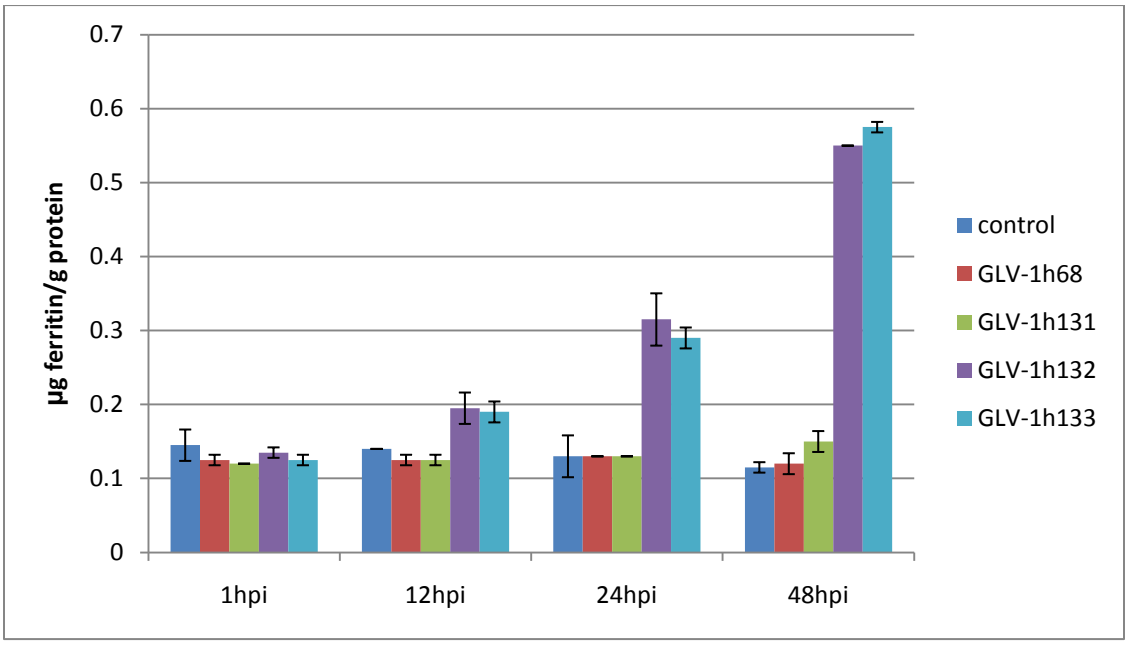

Fig. 4.9 Detection of human ferritin protein in infected GI-101A cell culture samples at different time points after infection

Figure 4.9 shows the ferritin expression in infected GI-101A cells after 1, 12, 24, and 48 hours post infection as averages of measurements in triplicate with standard deviation. All samples show ferritin expression in the range of 0.1 µg ferritin per g protein at all time points. After twelve hours of infection an increased expression of ferritin in cells could be seen for the virus strains GLV-1h132 and GLV-1h133. This difference was even more pronounced after 24 hours and even more after 48 hours of infection. Similar to the results of the Western blots the difference of the promoter strengths between the weak synthetic early promoter and the stronger synthetic early/late and synthetic late promoters could be seen clearly. The result of the ELISA proves that the ferritin protein was functionally expressed in GLV-1h131, GLV-1h132, and GLV-1h133-infected cells.

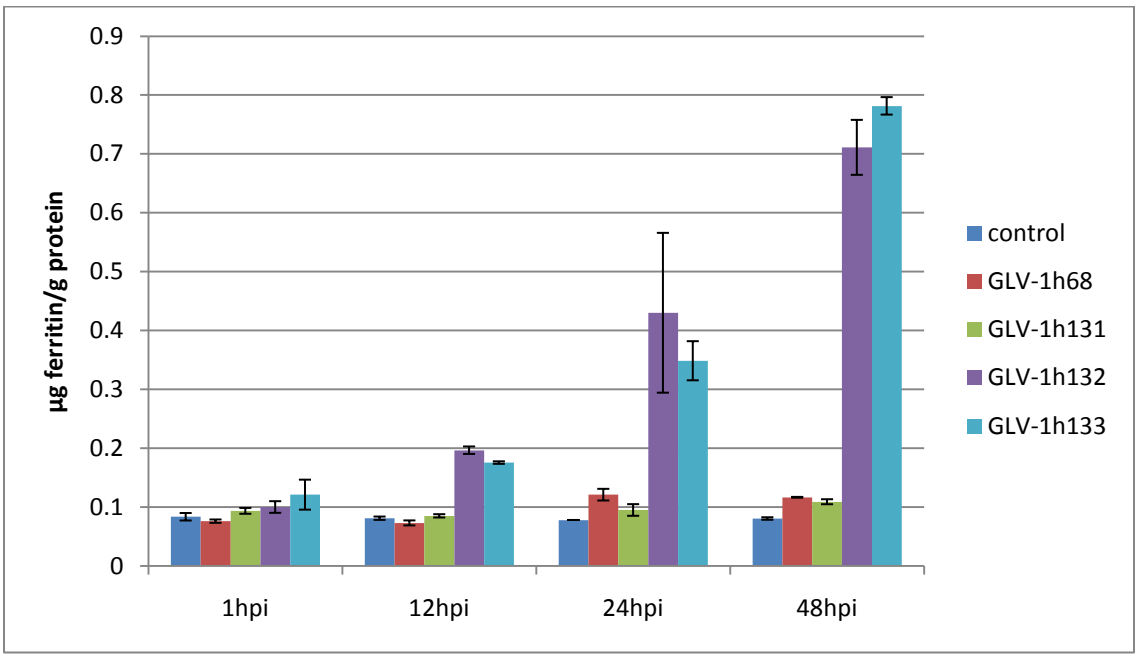

Fig. 4.10 Detection of human ferritin protein in infected A549 cell culture samples at different time points after infection

In Figure 4.10 the same experiment was performed in A549 cells. GLV-1h132- and GLV-1h133-infected cells express significantly more ferritin than the uninfected control and the GLV-1h68-infected cells. The graph looks very similar to the result in GI-101A cells even though the ferritin expression in uninfected and GLV-1h68-infected cells was slightly stronger in GI-101A cells and infection with the ferritin-encoding viruses led to a slightly better expression in A549 cells compared to GI-101A cells.

4.1.2 Virus-mediated Bacterioferritin Expression

GLV-1h110, GLV-1h111, and GLV1h112 are virus strains that express bacterioferritin in infected cells under control of different promoters (synthetic early, synthetic early/late and synthetic late vaccinia promoters for GLV-1h110, GLV-1h111, and GLV-1h112, respectively) in the HA locus. GLV-1h113 contains a “humanized” version of

bacterioferritin under control of the synthetic early/late promoter, in which the codon usage of the DNA sequence was optimized for expression in human cells. The *E. coli* bacterioferritin, which was inserted into the genome of these virus strains was shown to enhance T2 contrast in MRI measurements of murine tumors colonized with *E. coli* (Hill *et al*., in preparation) and could also be useful for MRI contrast of virus-infected tumors through delivery of the *bacterioferritin* gene by the virus.

4.1.2.1 Analysis of Viral Replication in the Cancer Cell Lines GI-101A and A549

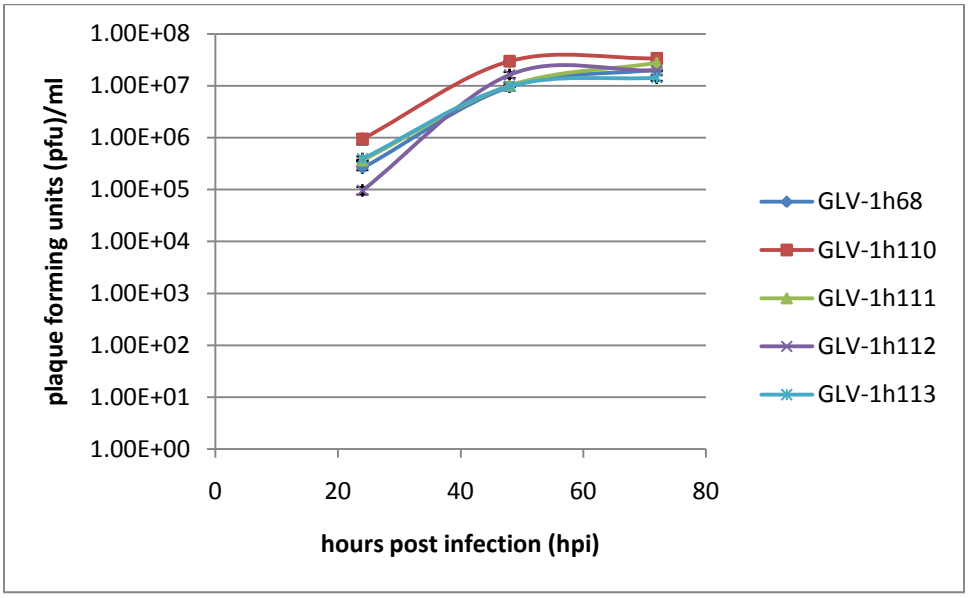

Fig. 4.11 Replication of GLV-1h110, GLV-1h111, GLV-1h112, and GLV-1h113 in comparison to GLV-1h168 in GI-101A cells

Figure 4.11 shows a replication assay performed in GI-101A cells with the virus strains GLV-1h110, GLV-1h111, GLV-1h112, and GLV-1h113. Viral titers in the cells of all infected cell samples were found to be increasing with time during the course of infection. All of the used viruses have a comparable replication rate to the parental virus

strain GLV-1h68. The replication assay shows that GI-101A cells can efficiently be infected with the used viruses in this experimental setup.

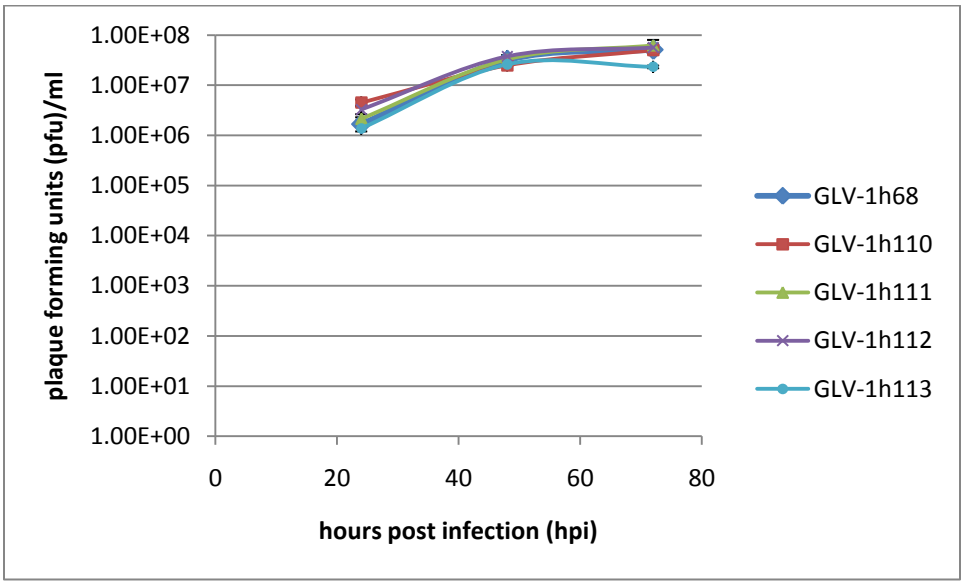

Fig. 4.12 Replication of GLV-1h110, GLV-1h111, GLV-1h112, and GLV-1h113 in comparison to GLV-1h68 in A549 cells

Figure 4.12 shows the result of the replication assay of the viruses GLV-1h110, GLV-1h111, GLV-1h112, and GLV-1h113 in the A549 cell line. The replication of the viruses in A549 cells is very similar to the replication in GI-101A cells, as shown above (figure 4.11). Viral titers in the cells increased markedly during the course of infection and the replication of the bacterioferritin-harboring viruses was comparable to the parental virus GLV-1h68. The replication assay demonstrates that, additionally to GI-101A cells, A549 cells can efficiently be infected with the used viruses in this experimental setup.

4.1.2.2 Analysis of Recombinant Protein Expression in Infected Cell Cultures

4.1.2.2.1 Coomassie Staining of Protein Gels

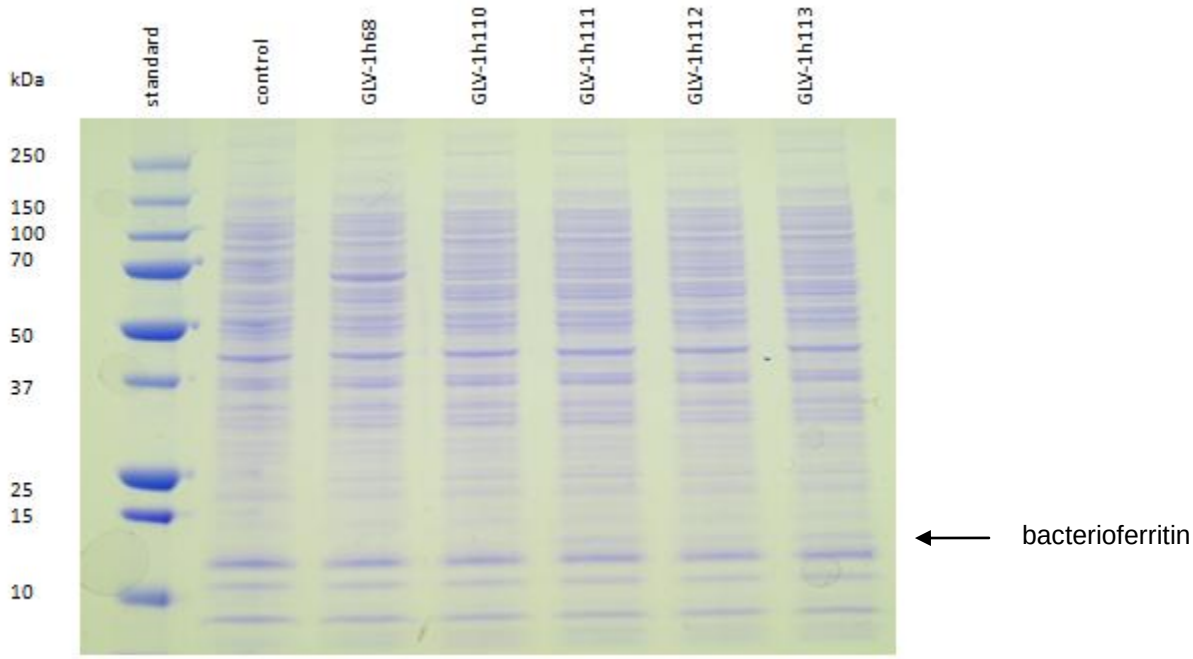

Fig. 4.13 Coomassie staining of SDS-PAGE performed with infected GI-101A cell culture samples: bacterioferritin-encoding virus strains

The next step to characterize the virus strains further was to analyze the protein expression. For this purpose cell lysates of GI-101A cells infected with the different virus strains harboring bacterioferritin genes were loaded on gels and stained with Coomassie dye. As shown in figure 4.13 an extra band between 10 and 15 kDa could be detected in GLV-1h111-, GLV-1h112-, and GLV-1h113-infected cell lysates, which was not detectable in the other samples. This represents the size of the bacterioferritin monomer. Similar to the ferritin-carrying virus GLV-1h131 (paragraph 4.1.1.2.1), GLV-1h110 is the virus construct with a weak promoter which does not lead to enough bacterioferritin expression in the cells to be detectable on the stained protein gel.

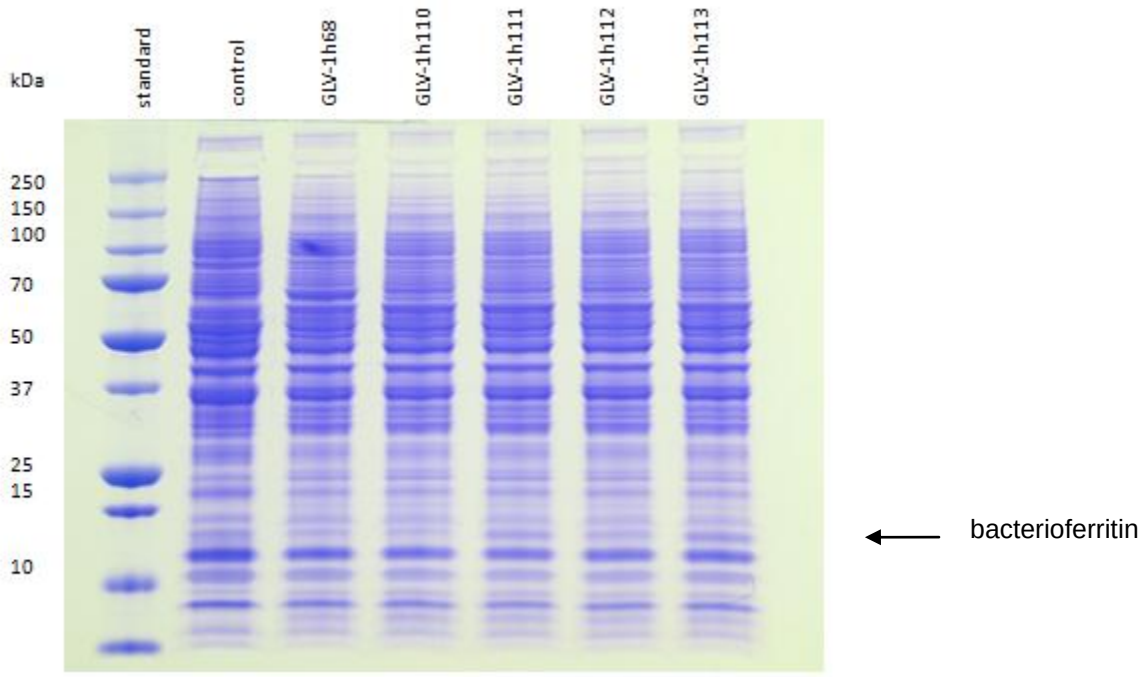

Fig. 4.14 Coomassie staining of SDS-PAGE performed with infected A549 cell culture samples: bacterioferritin-encoding virus strains

The cell lysates infected with the viruses that mediate bacterioferritin expression (GLV-1h110, GLV-1h111, GLV-1h112, and GLV-1h113) show a bacterioferritin band between 10 and 15 kDa. Comparable to results from infection of GI-101A cells shown before (figure 4.13), GLV-1h110-infected A549 cells do not express enough bacterioferritin to be shown on the gel because of the weaker promoter.

4.1.2.2.2 Western Blot

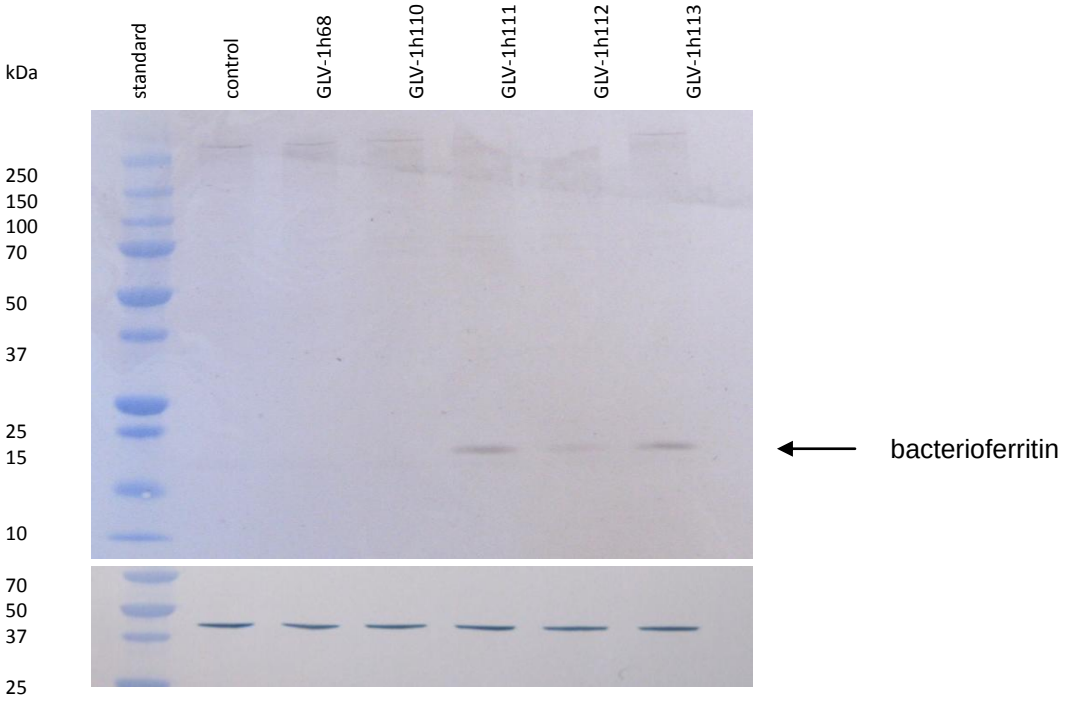

Fig. 4.15 Detection of virus-mediated bacterioferritin and β-actin expression by Western blot analysis in GI-101A cells

Due to the lack of a commercially available antibody against bacterioferritin, a serum was used for the Western blot experiments, which was produced from mice injected with purified bacterioferritin protein. The Western blot shown in figure 4.15 was performed using the self-made bacterioferritin serum (1:10 dilution) to detect of virus-mediated bacterioferritin expression in GI-101A cells and subsequently a β-actin antibody. Unfortunately, the mouse serum did not show strong binding affinities to the proteins blotted on the membrane, which led only to an overall weak signal. Nevertheless, a clear expression in the GLV-1h111- and GLV-h113-infected cells and also a weaker expression in the GLV-1h112-infected cells could be shown. This is due to the fact that in the genome of these virus strains, the gene is under the control of the stronger synthetic early/late and late promoters. Samples from GLV-1h110-infected

cells in which the gene is controlled by the weakest promoter did not show bacterioferritin expression using this detection method. The blot shown below was incubated with β-actin antibody to show that the gel was evenly loaded with protein.

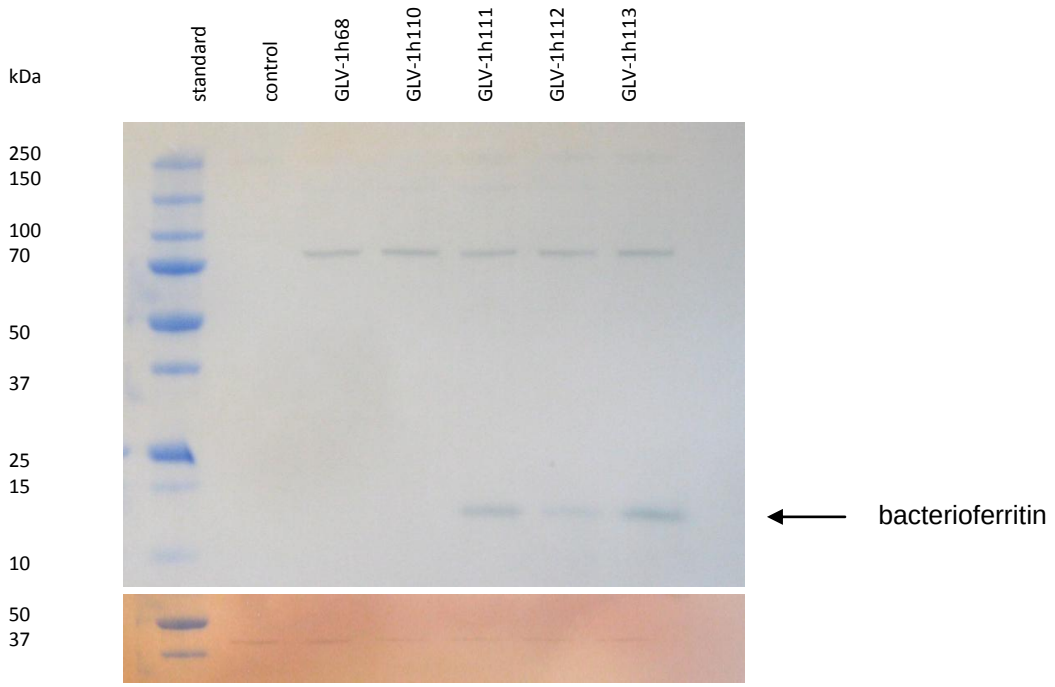

Fig. 4.16 Detection of virus-mediated bacterioferritin and β-actin expression by Western blot analysis in A549 cells

Figure 4.16 shows a Western blot performed with samples derived from virus-infected A549 cells using again the self-made serum raised against bacterioferritin and a β-actin antibody to determine bacterioferritin expression in this cell line. It could clearly be shown that the strongest bacterioferritin expression can be detected in GLV-1h111 and GLV-h113-infected cells. This goes in line with the high strength of the promoter which controls the expression of bacterioferritin in these virus strains. In GLV-1h112 the bacterioferritin gene is controlled by a weaker promoter and accordingly the Western blot shows a less pronounced protein band for the GLV-1h112-infected cell lysates. In

lysates of the GLV-1h110-infected cells with the weakest promoter no expression could be detected using this detection method. The blot shown below in figure 4.16 was incubated with a β-actin antibody as a gel loading control.

4.1.3 Virus-mediated Transferrin Receptor Expression

GLV-1h22 was constructed by inserting the human transferrin receptor gene and GLV-1h114 and GLV-1h115 contain the murine version of the transferrin receptor gene under the control of two different promoters. The transferrin receptor is a major protein of the iron uptake into the cells and cells expressing the transferrin receptor were shown to be useful as a marker for MR Imaging (Moore *et al*., 2001).

4.1.3.1 Analysis of Viral Replication in GI-101A and A549 Cells

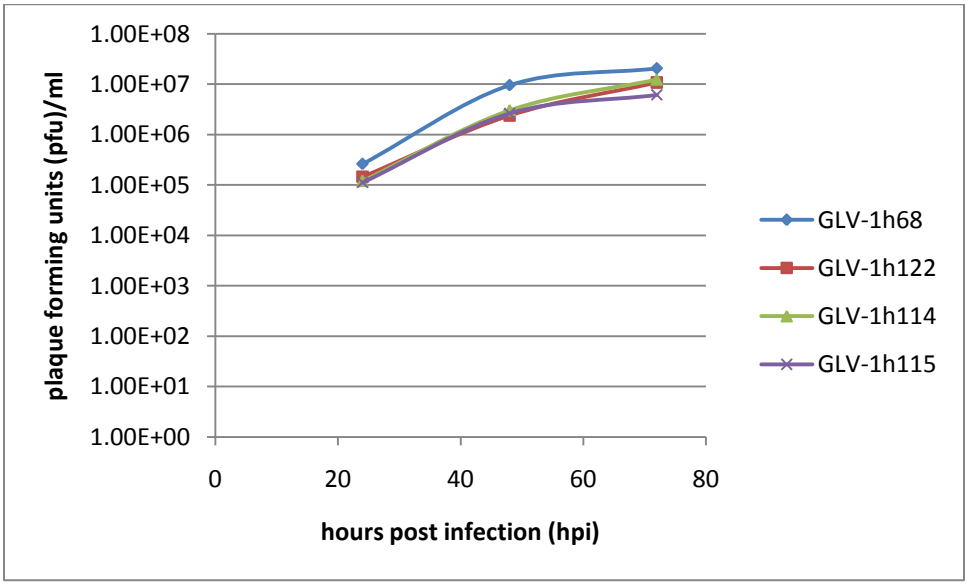

Fig. 4.17 Replication of GLV-1h22, GLV-1h114, and GLV-1h115 in comparison to GLV-1h68 in GI-101A cells

As described above, it is interesting to investigate whether new virus strains show a different replication efficiency in cell culture due to the insertion of a new gene. Figure 4.17 shows the replication efficiency of the viruses which carry the transferrin receptor gene GLV-1h122, GLV-1h114, and GLV-1h115 in comparison to the parental virus strain GLV-1h68. They were shown to efficiently replicate in the GI-101A cell line and the replication rate was similar to that of the GLV-1h68, although GLV-1h68 was replicating slightly faster in these cells. Viral titers in the cells of all infected cell samples showed an increase during the time of infection. This result shows that GI-101A cells can efficiently be infected with these new viruses and the viruses are able to replicate in this cell line.

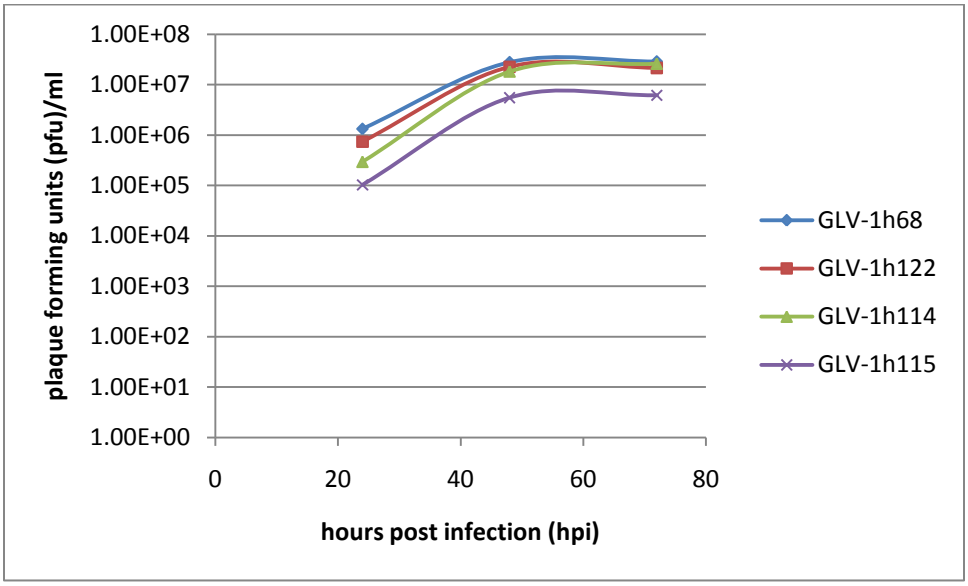

Fig. 4.18 Replication of GLV-1h22, GLV-1h114, and GLV-1h115 in comparison to GLV-1h68 in A549 cells

Figure 4.18 shows the replication of the transferrin receptor-encoding viruses GLV-1h122, GLV-1h114, and GLV-1h115 in comparison to GLV-1h68 in A549 cells. All virus strains efficiently replicate in the A549 cell line and the replication rate was similar to that of the parental virus GLV-1h68, which was replicating slightly faster in A549 cells,

as previously shown for GI-101A cells (figure 4.17). The viral titers in the cells of all infected cell samples increased with the time during the course of infection. This shows that all the transferrin receptor-encoding viruses can efficiently infect and replicate in A549 cells.

4.1.3.2 Analysis of Recombinant Protein Expression in Infected Cell Cultures

4.1.3.2.1 Coomassie Staining of Protein Gels

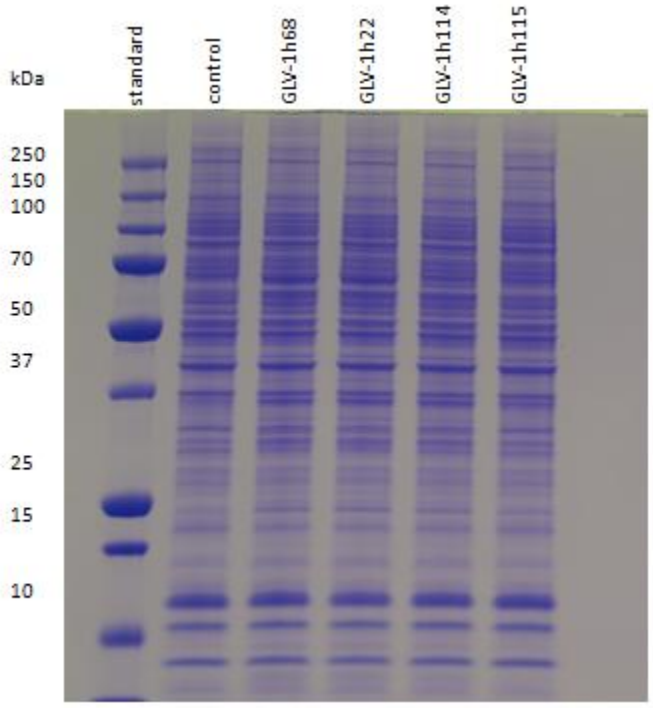

Fig. 4.19 Coomassie staining of SDS-PAGE performed with infected GI-101A cell culture samples: transferrin receptor-encoding virus strains

The transferrin receptor is also a protein that is present in every cell type and even over expressed fast proliferating cells, including cancer cells (Lok and Loh, 1998). Its size is

95 kDa. To investigate the successful expression of the transferrin receptor in virus-infected cells, cell lysates were analyzed by SDS-PAGE and subsequent Coomassie staining. Figure 4.19 shows the Coomassie staining of a gel with GI-101A cell lysate after infection with the viruses. There is no virus-induced overexpression of the protein visible on the Coomassie stained gel, which might be explained by the fact that there are multiple bands in the same protein size range on the gel which might overlap the protein band of the transferrin receptor.

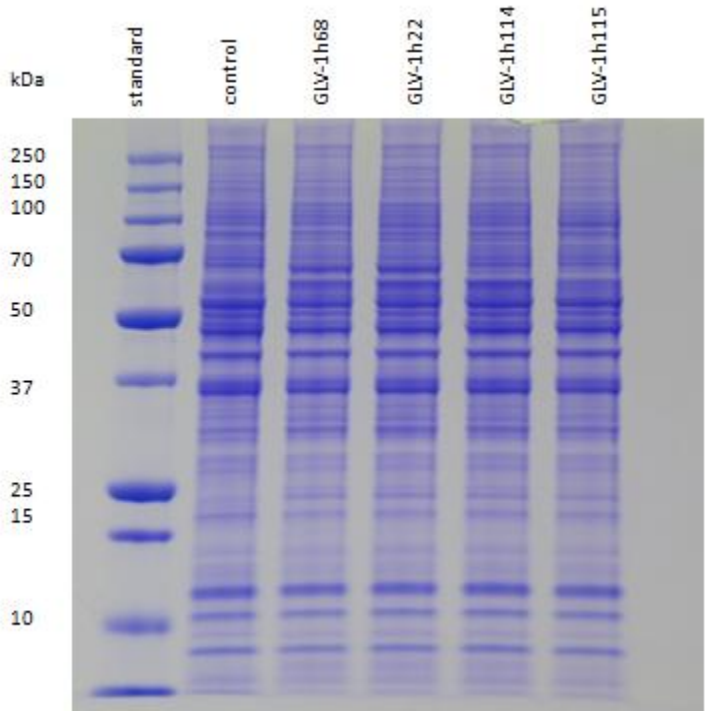

Fig. 4.20 Coomassie staining of SDS-PAGE performed with infected A549 cell culture samples: transferrin receptor-encoding virus strains

Figure 4.20 shows a Coomassie-stained protein gel with cell lysates from infected A549 cells with transferrin receptor encoding viruses. No virus-induced overexpression of the protein was visible on the Coomassie stained gel similar to what was previously shown for GI-101A cells (figure 4.19). A slightly bigger band could be detected in the lysate from GLV-1h115-infected cells, which could be explained by the fact that GLV-1h115 is

the virus strain that carries the mouse transferrin receptor gene under the control of the strong synthetic early/late promoter.

4.1.3.2.2 Western Blot

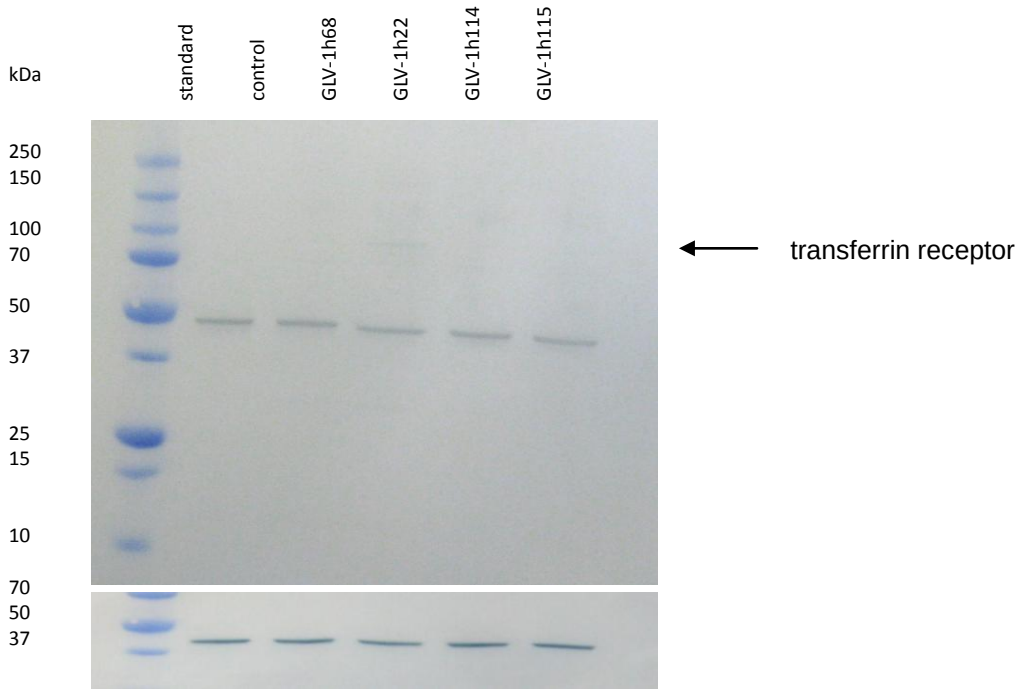

Fig. 4.21 Detection of virus-mediated human transferrin receptor and β-actin expression by Western blot analysis in GI-101A cells

After the Coomassie gel analysis of protein samples did not show any detectable expression of the transferrin receptor in infected cells, a Western blot was performed using transferrin receptor antibody. Figure 4.21 shows the Western blot of samples deriving from GI-101A cells infected with the group of viruses that mediate transferrin receptor expression. The transferrin receptor expression could only be shown by a very slight band with the correct size of the transferrin receptor (95 kDa) in the lane where

GLV-1h22-infected samples were loaded. GLV-1h22 is the human transferrin receptor expression-mediating virus. Infection with the mouse transferrin receptor-encoding viruses GLV-1h114 and GLV-1h115 did not result in any signal using that antibody, which is supposed to detect human and murine versions of the protein. The antibody did result in a signal at around 50 kDa. The β-actin blot on the bottom shows that the gel was loaded with an equal amount of protein in every well.

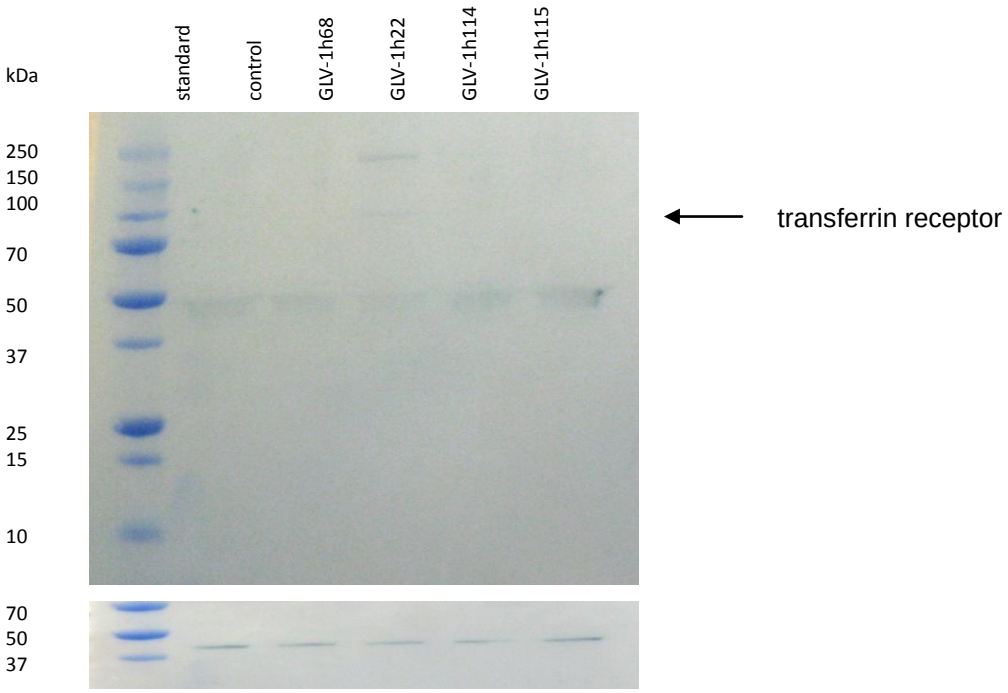

Fig. 4.22 Detection of virus-mediated human transferrin and β-actin expression by Western blot analysis in A549 cells

Figure 4.22 shows the Western blot of A549 cell lysates infected with transferrin receptor-encoding viruses. Similar as for the GI-101A-derived protein samples (Figure 4.20), only the GLV-1h22-infected cells showed a very slight transferrin receptor band on the Western blot. The β-actin blot on the bottom shows that the gel was loaded with an equal amount of protein in every well.

4.1.4 Virus-mediated Ferritin and Transferrin Receptor Expression

GLV-1h154 carries the genes that encode bacterioferritin and human transferrin receptor, GLV-1h155 the human ferritin H-chain gene and the human transferrin receptor gene. GLV-1h156 and GLV-1h157 infected cells both express the mouse transferrin receptor and bacterioferritin or human ferritin H-chain, respectively. The rationale for generating these virus strains was to combine the effect of an iron storage protein with that of an iron transport protein and thus accumulate even more iron in infected tumor cells.

4.1.4.1 Analysis of Viral Replication in GI-101A and A549 Cells

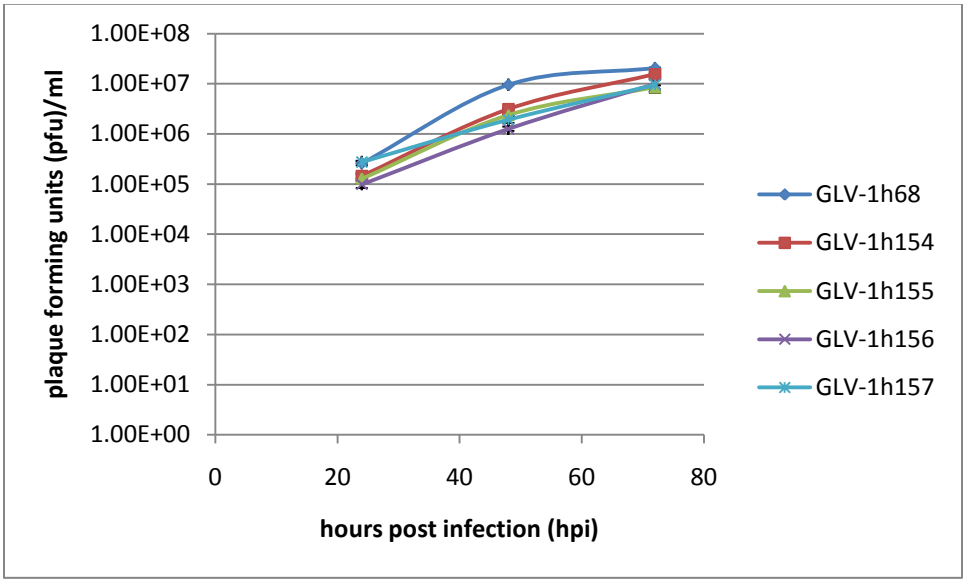

Fig. 4.23 Replication of GLV-1h154, GLV-1h155, GLV-1h156, and GLV-1h157 in comparison to GLV-1h68 in GI-101A cells

Figure 4.23 demonstrates the result of the replication assay of the viruses GLV-1h154, GLV-1h155, GLV-1h156, and GLV-1h157 in comparison to GLV-1h68 in GI-101A cells.

It can be stated that all the used viruses in this experiment efficiently replicate in the GI-101A cell line. Viral titers in the cells increased considerably during the course of infection. All of the used virus strains have a similar replication rate. The replication assay shows that GI-101A cells can efficiently be infected with all the viruses that were used in this experiment.

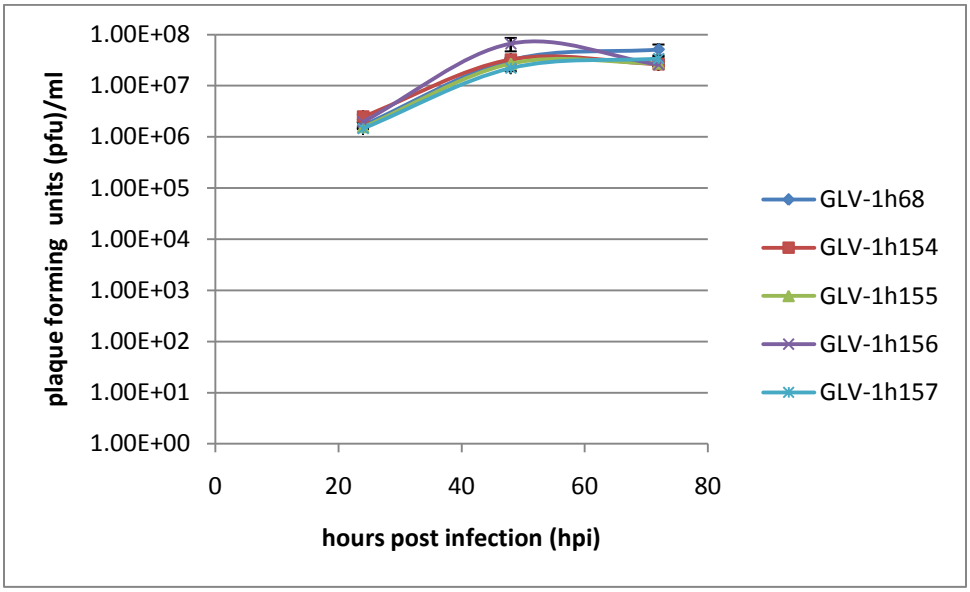

Fig. 4.24 Replication of GLV-1h154, GLV-1h155, GLV-1h156, and GLV-1h157 in comparison to GLV-1h68 in A549 cells

The replication assay performed in A549 cells infected with the viruses GLV-1h154, GLV-1h155, GLV-1h156, and GLV-1h157 in comparison to GLV-1h68 is shown in figure 4.24. It can be stated that all the used viruses in this experiment efficiently replicated also in the A549 cell line. Viral titers in the cells grew considerably during the course of infection. All of the used virus strains have a comparable replication rate. The replication assay proves that A549 cells can efficiently be infected with the used viruses in this experiment.

4.1.4.2 Analysis of Recombinant Protein Expression in Infected Cell Cultures

4.1.4.2.1 Coomassie Staining of Protein Gels

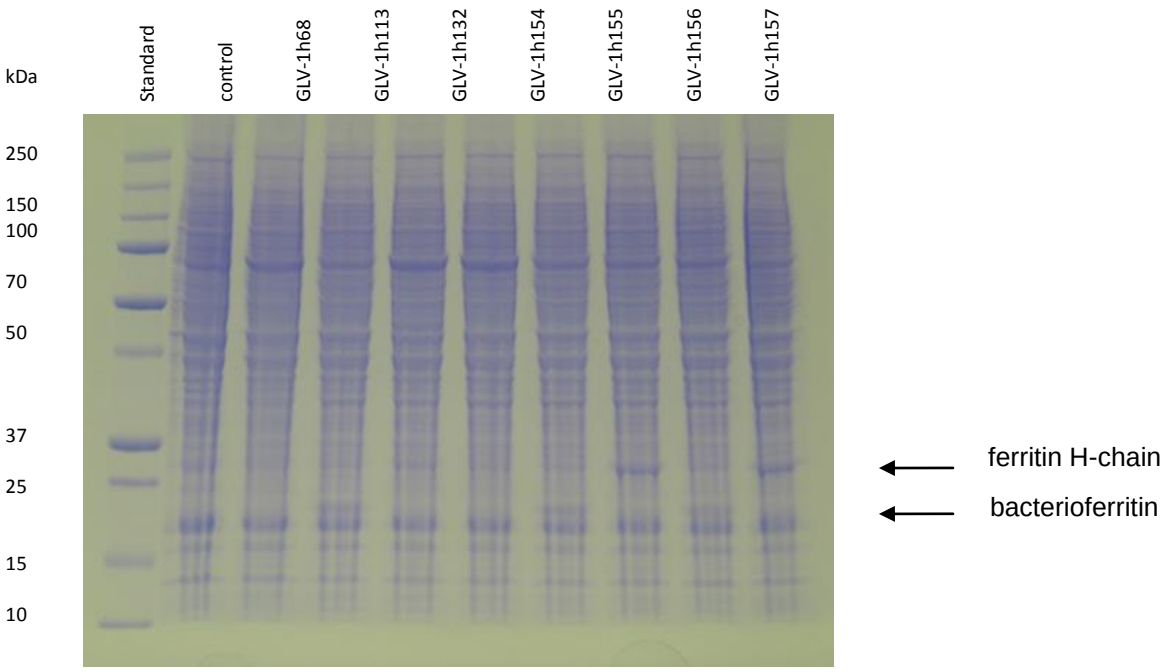

Fig. 4.25 Coomassie staining of SDS-PAGE performed with infected GI-101A cell culture samples: ferritin- and transferrin receptor-encoding virus strains

To investigate the successful expression of recombinant proteins in virus-infected cells, SDS-PAGE gels were loaded with lysates from virus-infected cells and then stained with Coomassie dye. The gel in figure 4.25 shows, next to uninfected control, cell lysates infected with the control virus GLV-1h68, GLV-1h113 and GLV-1h132, and the cell lysates of cells infected with the four viruses that were generated with combinations of transferrin receptors and ferritins. GLV-1h154 and GLV-1h156 carry the gene for bacterioferritin whose expression was detectable as a band between 10 and 15 kDa. GLV-1h155- and GLV-1h57-infected cells express the human ferritin heavy chain. The

ferritin heavy chain protein band could also clearly be detected by Coomassie staining. Ferritin and bacterioferritin bands on the gel are marked by arrows. GLV-1h54 and GLV-1h155 additionally expressed the human transferrin receptor in infected cells and GLV-1h156 and GLV-1h157 express the mouse transferrin receptor in addition to the ferritins. As already shown in figure 4.19 and 4.21, the transferrin receptor protein band cannot be clearly distinguished on the protein gel.

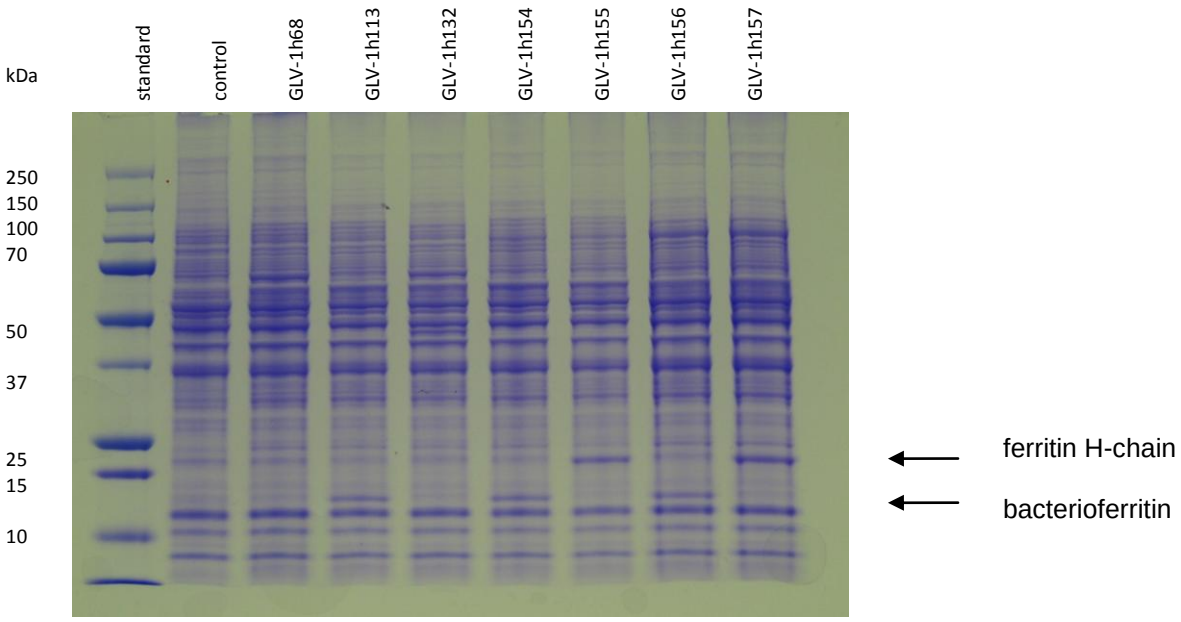

Fig. 4.26 Coomassie staining of SDS-PAGE performed with infected A549 cell culture samples: ferritin- and transferrin receptor-encoding virus strains

The gel in figure 4.26 shows cell lysates from uninfected cells and cells infected with control virus GLV-1h68, GLV-1h113 and GLV-1h132, and with the four viruses that were generated with combinations of transferrin receptors and ferritins. GLV-1h154 and GLV-1h156 carry the gene for bacterioferritin. A band between 10 and 15 kDa could be seen which represents this protein. GLV-1h155 and GLV-1h57 infected cells express the human ferritin heavy chain. The ferritin heavy chain protein band could also clearly

be detected by Coomassie staining. Ferritin and bacterioferritin bands on the gel are marked by arrows. GLV-1h54 and GLV-1h155 additionally express the human transferrin receptor in infected cells and GLV-1h156 and GLV-1h157 expressed the mouse transferrin receptor in addition to the ferritins. As already shown in figure 4.19 and 4.21, the transferrin receptor protein band could not be clearly distinguished on the protein gel.

4.1.5 Virus-mediated Ferritin Light Chain Expression

GLV-1h186 was generated by inserting the gene for the ferritin light chain with a thymidine cytidine insertion at the position 498 into the vaccinia virus sequence and GLV-1h187 carries the wild type ferritin light chain as a control. It was shown that the expression of this mutant form of the ferritin light chain led to iron overload in transgenic mice (Vidal *et al*., 2008).

4.1.5.1 Analysis of Viral Replication in GI-101A and A549 Cells

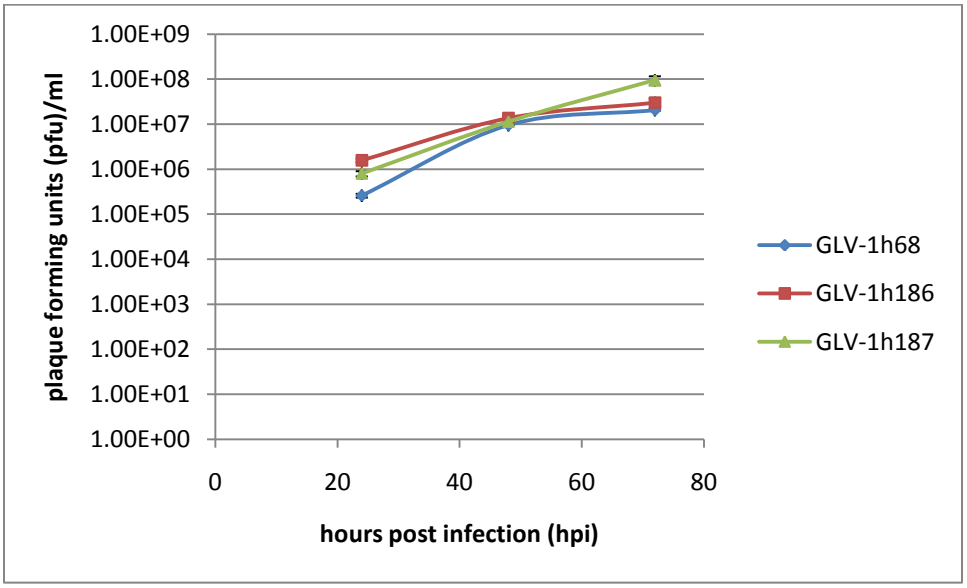

Fig. 4.27 Replication of GLV-1h186 and GLV-1h187 in comparison to GLV-1h68 in GI-101A cells

Figure 4.27 shows the replication efficiency of the virus strains GLV-1h186 and GLV-1h187 in comparison to the parental virus strain GLV-1h68. Viral titers in the cells increased clearly during the time of infection. All viruses in this experiment replicate in GI-101A cells in a similar fashion. The replication assay clearly shows that GI-101A cells can efficiently be infected with all viruses in this experiment.

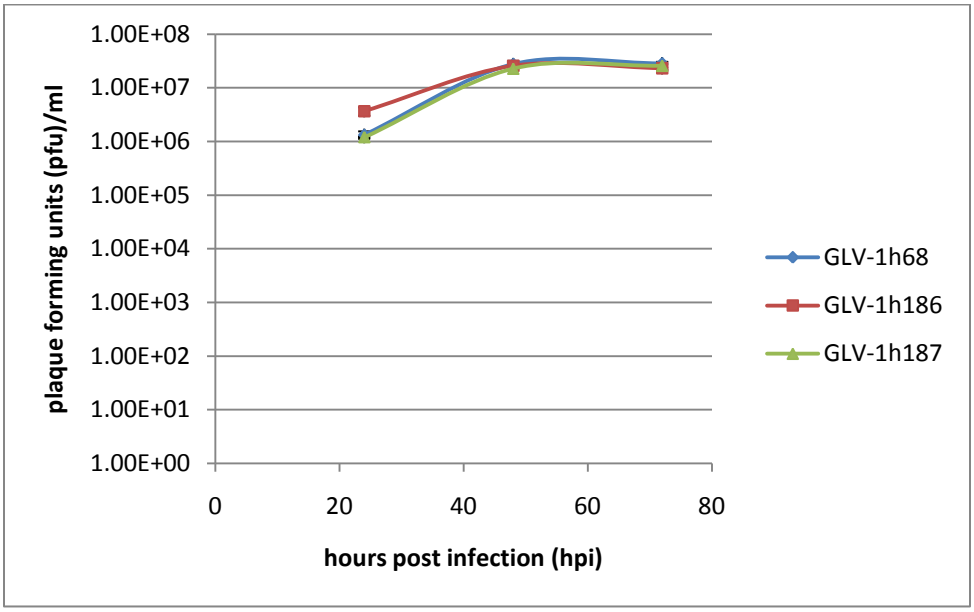

Fig. 4.28 Replication of GLV-1h186 and GLV-1h187 in comparison to GLV-1h68 in A549 cells

Figure 4.28 displays that GLV-1h186 and GLV-1h187 can efficiently replicate in the A549 cell line, comparable to GLV-1h68. Viral titers in the cells increased markedly during the course of infection. All of the used viruses replicate in A549 cells in a similar fashion. The replication assay shows that A549 cells can efficiently be infected with the used viruses in this experimental setup.

4.1.5.2 Analysis of Recombinant Protein Expression in Infected Cell Cultures

4.1.5.2.1 Coomassie Staining of Protein Gels

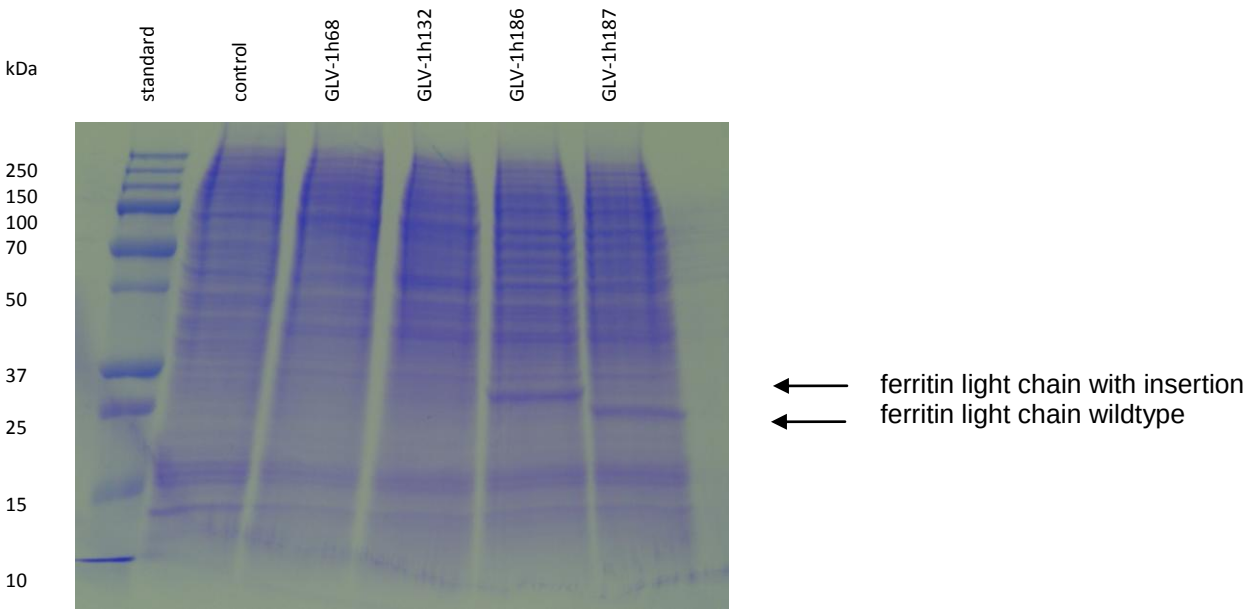

Fig. 4.29 Coomassie staining of SDS-PAGE performed with infected GI-101A cell culture samples: ferritin light chain-encoding virus strains

To investigate whether the infection of the cancer cell lines with the virus leads to efficient expression of the recombinant proteins, an SDS-PAGE was performed with cell lysates of virus-infected cells and appropriate controls and stained with Coomassie dye. Figure 4.29 shows clearly the bands of the ferritin light chain around 20 kDa in the GLV-1h186 and GLV-1h187 lanes. GLV-1h186 is the virus strain, which contains an insertion in the sequence of the ferritin light chain and therefore produced a larger protein band than GLV-h187, which carries the wildtype gene.

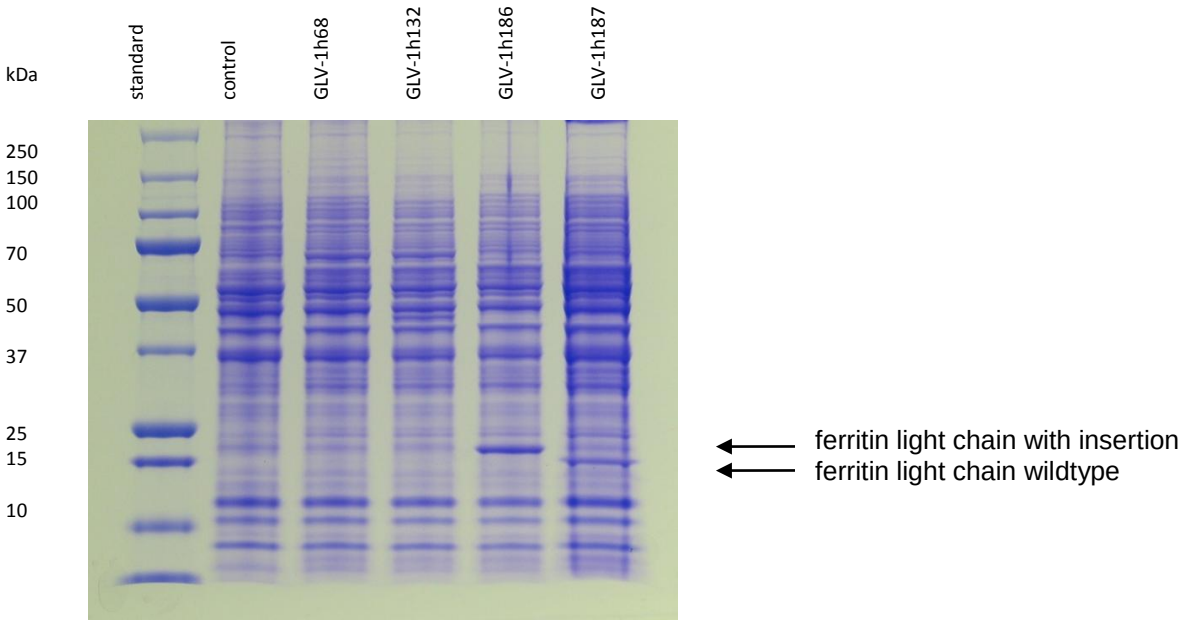

Fig. 4.30 Coomassie staining of SDS-PAGE performed with infected A549 cell culture samples: ferritin light chain-encoding virus strains

Figure 4.30 shows clearly the bands of the ferritin light chain around 20 kDa in the GLV-1h186 and GLV-1h187 lanes. GLV-1h186 is the virus strain, which contains an insertion in the sequence of the ferritin light chain and therefore produced a larger protein band than the GLV-h187, which carries the wildtype gene as a control.

4.1.6 Virus-mediated Divalent Metal Transporter Expression

The divalent metal transporter 1 gene was inserted in the parental virus strain GLV-1h68 to generate GLV-1h102. The divalent metal transporter is a major protein of iron uptake in duodenal cells and is hoped to lead to iron accumulation when expressed by virus-infected tumor cells.

4.1.6.1 Analysis of Viral Replication in GI-101A and A549 Cells

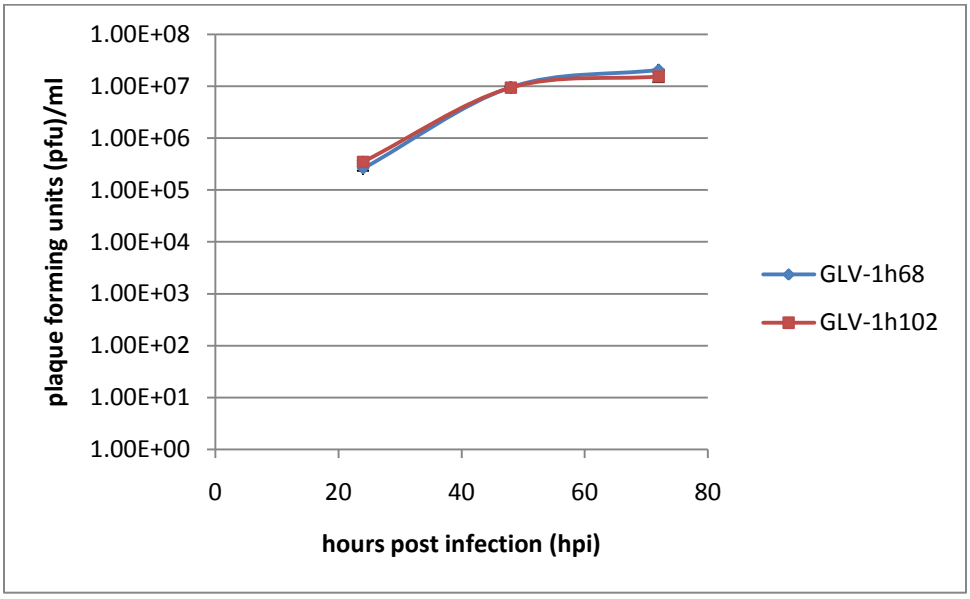

Fig. 4.31 Replication of GLV-1h68 and GLV-1h102 in GI-101A cells

Figure 4.31 shows the replication efficiency of the virus strain GLV-102 in the GI-101A cell line in comparison to the parental virus GLV-1h68. Viral titers in the cells increased visibly during the course of infection. The replication assay shows that GI-101A cells can efficiently be infected with the viruses in this experimental setup. The virus can also efficiently replicate in GI-101A cells.

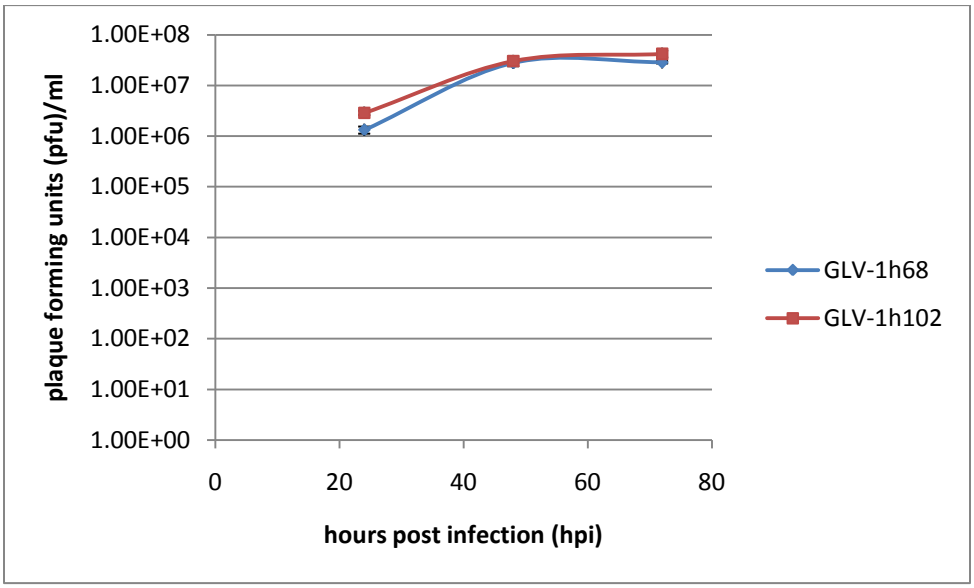

Fig. 4.32 Replication of GLV-1h68 and GLV-1h102 in A549 cells

The results of the replication assay performed with GLV-1h168 and GLV-1h102 are shown in figure 4.32. GLV-1h102 replicated efficiently in the A549 cell line comparable to the parental virus GLV-1h68. Viral titers in the cells increased considerably in the first 48 hours and then stayed at a constant level. The replication assay shows that also A549 cells can efficiently be infected with GLV-1h102 in this experimental setup.

4.1.6.2 Analysis of Recombinant Protein Expression in Infected Cell Cultures

4.1.6.2.1 Coomassie Staining of Protein Gels

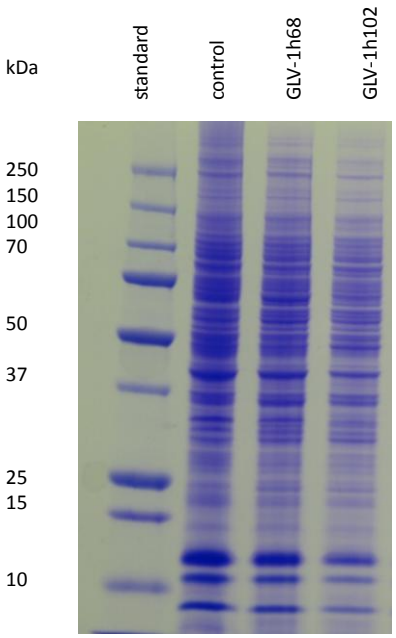

Fig. 4.33 Coomassie staining of SDS-PAGE performed with infected GI-101A cell culture samples: divalent metal transporter-encoding virus strain

Cell lysates of virus-infected cells were analyzed in a SDS-PAGE gel by Coomassie staining. No significant difference in the protein bands of the samples in figure 4.33 could be detected. The DMT1 protein has an estimated molecular weight of 65 kDa. DMT1 in the virus strain GLV-1h102 is expressed under the control of the synthetic early promoter, which is a weak vaccinia promoter, and therefore the protein product of DMT1 cannot be detected in infected GI-101A cells by the relatively insensitive method of Coomassie staining.

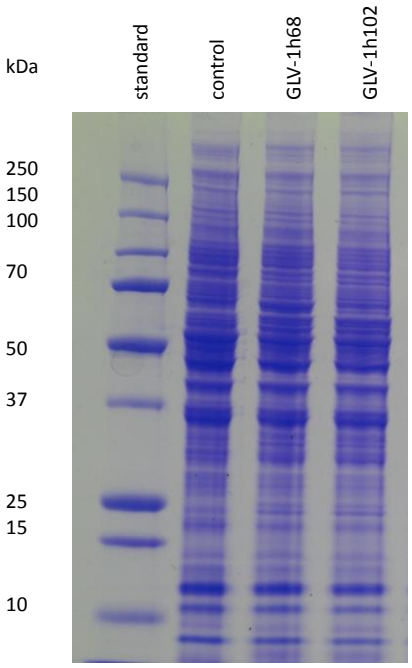

Fig. 4.34 Coomassie staining of SDS-PAGE performed with infected A549 cell culture samples: divalent metal transporter-encoding virus strain

Figure 4.34 shows a protein gel made with A549 cell lysates infected with the virus GLV-1h102. The recombinant protein could not be detected by Coomassie Blue staining in any of the cell lines tested. Therefore, a more sensitive method has to be used for the detection of this protein that is expressed under the control of the relatively weak synthetic early vaccinia promoter.

Western blot analysis was also performed with lysates from GLV-1h102-infected GI-101A and A549 cells, but showed no detectable expression of DMT1 (data not shown).

4.1.6.2.2 Analysis of Gene Transcription by RT-PCR

Due to the fact, that the protein expression could not be detected in Coomassie-stained protein gels and Western blots a different approach was chosen to prove gene expression in cell culture after delivery of the gene to the cells by the virus. Instead of

protein expression analysis, a more sensitive method that shows gene expression on a transcriptional level was used. RT-PCR is a technique, using a reverse transcriptase enzyme to produce cDNA from RNA, which is isolated from infected cell culture samples. The cDNA is then used as a template for a PCR reaction and the PCR product is analyzed with an agarose gel and photographed under UV light. In this study two iron accumulating proteins could not be detected by Western blot. One of them was DMT1 expressed by GLV-1h102. Both proteins are expressed under the control of a synthetic early vaccinia promoter which is not very strong. This could be the reason for the unsuccessful detection by Western blot.

For the RT-PCR GI-101A cells were infected with the viruses GLV-1h102 and GLV-1h68 as a control. After 24 hours the RNA was isolated from the cell lysates. The cDNA was synthesized from the RNA and used as a in a PCR reaction together with specific primers for each of the desired genes that were analyzed. The PCR product was loaded on an agarose gel to visualize the DNA bands.

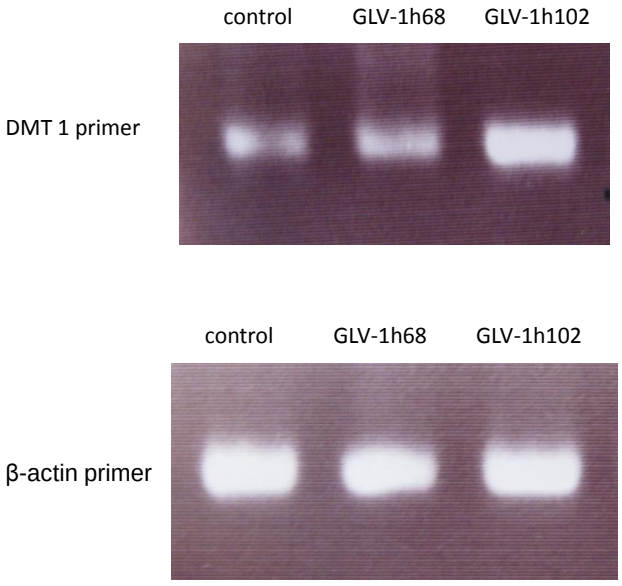

Fig. 4.35 RT-PCR products analyzed by agarose gel electrophoresis

Figure 4.35 shows DNA gels from PCR products of the RT-PCR reactions. The gel shown on the top was loaded with RT-PCR reactions originating from isolated RNA of uninfected control (lane 1), infected with GLV-1h68 (lane 2), or infected with the DMT1-expressing virus GLV-1h102 (lane 3). There are bands in every lane which can be explained by the fact that DMT1 is expressed in many different cell types (Testa, 2002). In the sample infected with GLV-1h102 the *dmt1* gene expression was upregulated in comparison with the controls. The second photo shows the RT-PCR reaction repeated with the same cDNA samples using specific β-actin primers as a loading control. All lanes show similar amounts of total DNA loaded on the gel.

4.1.7 Virus-mediated MagA Expression

GLV-1h184 was generated by transfection of GLV-1h68 with a vector that contained the bacterial gene *magA* from *Magnetospirillum magnetotacticum*. The *magA* gene is under the control of the synthetic early promoter. MagA was shown to be sufficient to produce magnetic nanoparticles in mammalian cells, making it a candidate as MRI reporter (Zurkya *et al*., 2008).

4.1.7.1 Analysis of Viral Replication in GI-101A and A549 Cells

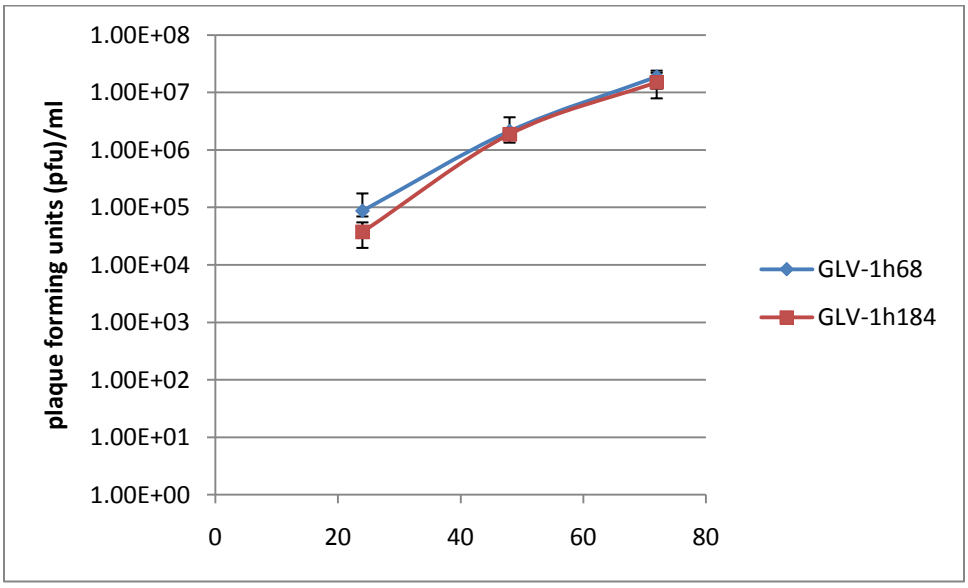

Fig. 4.36 Replication of GLV-1h68 and GLV-1h84 in GI-101A cells

To find out whether the insertion of the *magA* gene leads to a change in the replication ability of the new virus strain, replication assays were performed.

The replication of the virus GLV-1h84 in GI-101A cells is illustrated in figure 4.36. It was shown that GLV-1h184 replicated efficiently in the GI-101A cell line, comparable to the parental virus GLV-1h68. Viral titers in the cells increased considerably during the course of infection. The replication assay proved that GI-101A cells could efficiently be infected with this virus in this experimental setup.

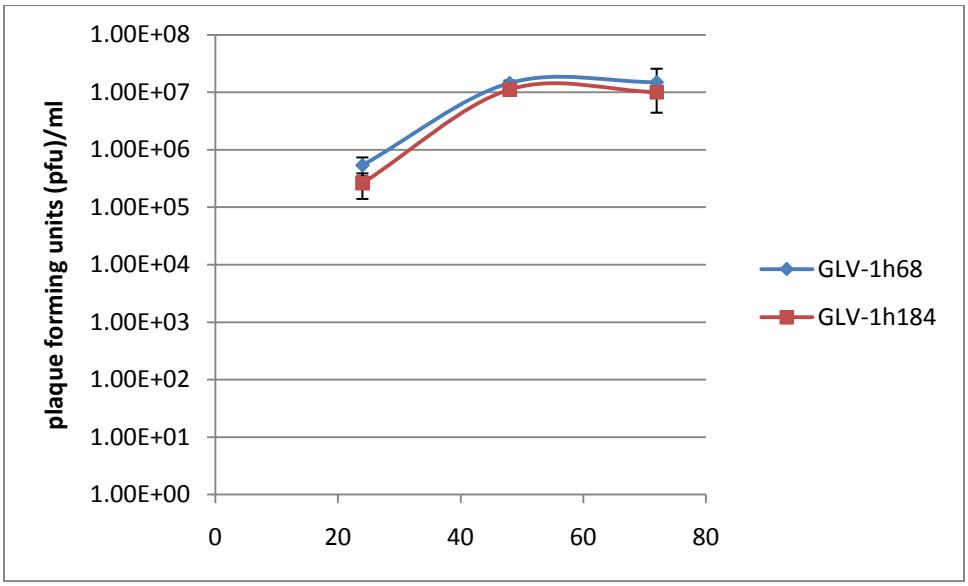

Fig. 4.37 Replication of GLV-1h68 and GLV-1h184 in A549 cells

In Figure 4.37 it is shown that GLV-1h184 replicated efficiently in the A549 cell line and that it replicated in a very similar fashion compared to the parental virus GLV-1h68. Viral titers in the cells increased visibly during the time of infection, mostly in the first 48 hours. The replication assay showed that A549 cells could efficiently be infected with this virus in this experimental setup.

4.1.7.2 Analysis of Recombinant Protein Expression in Infected Cell Cultures

4.1.7.2.1 Coomassie Staining of Protein Gels

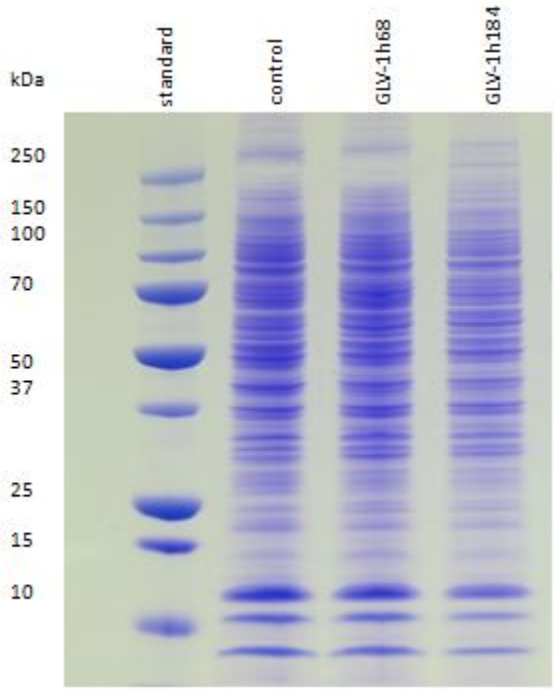

Fig. 4.38 Coomassie staining of SDS-PAGE performed with infected GI-101A cell culture samples: *magA*-encoding virus strain

After characterizing the replication pattern in cancer cell lines it was investigated whether the protein can be detected in a Coomassie-stained gel from virus-infected cell lysates. Figure 4.38 shows a protein gel loaded with samples from uninfected and infected with GLV-1h68 and GLV-1h184 GI-101A cells. The *magA* gene in the recombinant virus strain GLV-1h84 is controlled by the weak synthetic early promoter and is not expressed in a sufficient amount for detection by this technique. The MagA protein has an estimated molecular weight of 45 kDa.

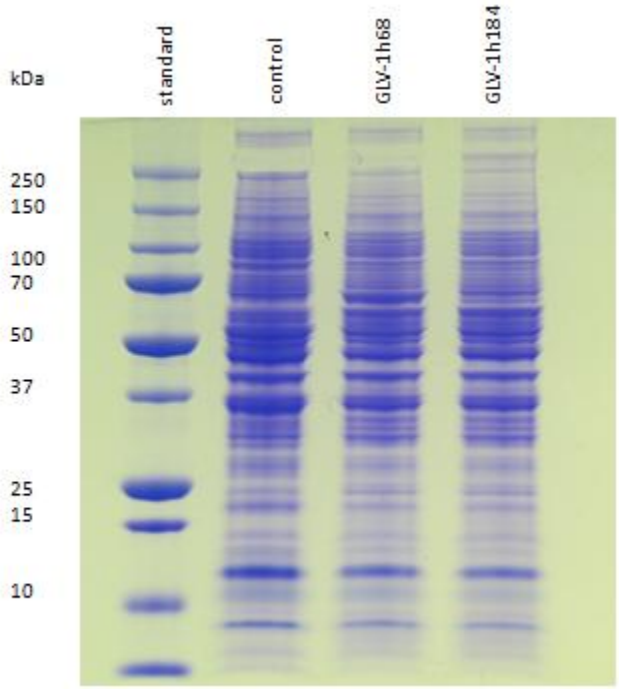

Fig. 4.39 Coomassie staining of SDS-PAGE performed with infected A549 cell culture samples: *magA*-encoding virus strain

Figure 4.39 is a protein gel made with A549 cell lysates of uninfected cells and cells infected with the viruses GLV-1h68 and GLV-1h184. As described above for the experiments performed in GI-101A cells, there was no MagA protein detectable in lysates from A549 cells infected with the GLV-1h184 virus.

4.1.7.2.2 Analysis of Gene Transcription by RT-PCR

Since MagA could not be detected with protein analytical methods a new approach was chosen to detect the expression of *magA* on a transcriptional level using RT-PCR. The *magA* gene is expressed in GLV-1h184-infected cells under the control of the synthetic early vaccinia promoter, which is weaker compared to the synthetic early/late and synthetic late promoter. This could be the reason for the unsuccessful detection by Western blot.

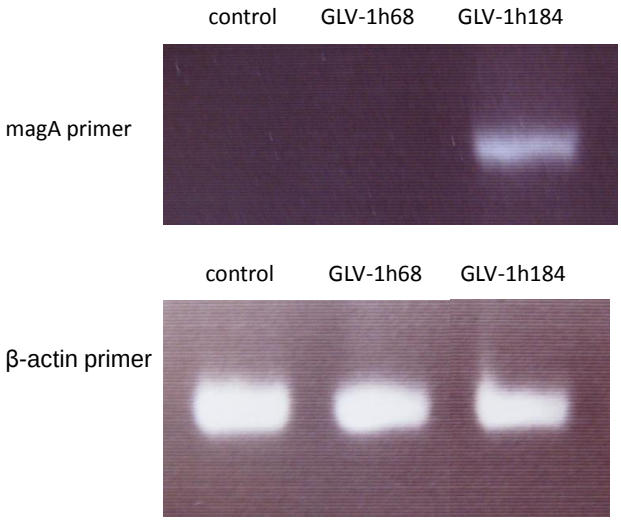

Fig. 4.40 RT-PCR products analyzed by agarose gel electrophoresis

Figure 4.40 shows DNA agarose gels made from PCR products of the RT-PCR reaction. The upper gel was loaded with RT-PCR reactions originating from isolated RNA of uninfected control (lane 1), infected with GLV-1h68 (lane 2), and infected with the *magA*-expressing virus GLV-1h184 (lane 3). GLV-1h184-infected cells express *magA*, which is a gene from *Magnetospirillum magnetotacticum* and therefore not naturally expressed in human cells. There is a band in the third lane, which proves that the *magA* gene is inserted and transcribed from the DNA of the vaccinia virus GLV-1h184. The RT-PCR reaction was repeated with all samples using β-actin primers as a loading control. All lanes show similar amounts of DNA loaded in the gel.

4.2 Heavy Metal Measurements

After the expression of all the iron accumulating proteins mediated by virus infection in cell culture was verified the aim was to characterize the ability of the different viruses to trigger accumulation of iron in infected cells due to the inserted genes. Therefore different methods of iron measurements were performed with virus-infected cells. Only the experiments performed with virus strains that led to a significant difference in the ability of infected cells to collect iron are shown in this paragraph. These are also the virus strains that were chosen for the *in vivo* studies later.

4.2.1 Iron Determination of Infected Cell Cultures by QuantiChrom™ Iron Assay

The QuantiChrom Iron Assay is a commercially available iron assay which utilizes a chromogen forming a blue colored complex specifically with Fe^{2+}. Free Fe^{3+} present in the sample is reduced to Fe^{2+}, thus allowing the assay to detect total iron concentration. The intensity of the color, measured at 590 nm, is directly proportional to the iron concentration in the sample over the concentration range determined by a standard curve.

For the iron determination experiment GI-101A cells seeded in 6-well plates were infected with viruses and harvested after 24 hours. The cell lysates were used to perform the assay according to the manufacturer's instructions.

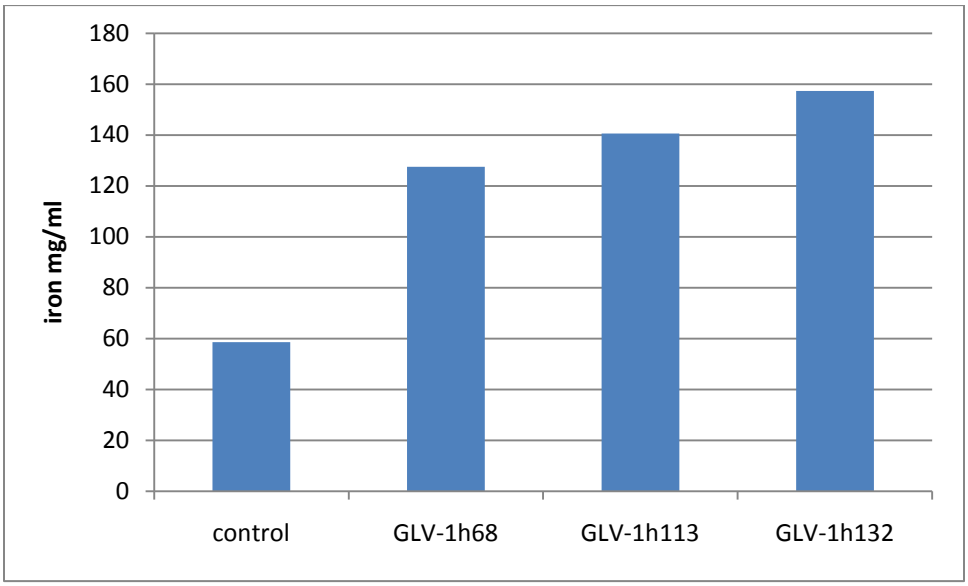

Fig. 4.41 QuantiChrom™ Iron Assay of GI-101A cells 24 hours post infection using different virus strains

The result of the QuantiChrom™ iron assay showed a significant increase of iron content in all infected cell samples in comparison to the uninfected control. The differences in iron accumulation between the virus-infected cells were not very pronounced, whereas GLV-1h132-infected cell lysates show the highest iron content and GLV-1h68 the least. This higher concentration of GLV-1h68-infected cells compared to mock-infected cells is remarkable because no iron accumulating genes were inserted into the genome of GLV-1h68.

4.2.2 Iron Determination of Infected Cell Cultures by Ferrozine Assay

The Ferrozine Assay is a method for the detection of iron in samples. Ferrozine reacts with divalent iron to form a stable magenta complex which is soluble in water and can be used for the direct determination of iron in water (Stookey, 1970).

Twenty-four hours after infection of cells with viruses an iron supplement was added to the cells. One, 6, 12 and 24 hours after addition of the supplement the cells were

harvested, washed and resuspended in 1% Triton-X. A protein assay was performed in order to be able to calculate the amount of iron per amount of total protein. Equal amounts of cell lysate were used to perform the ferrozine Assay. The absorption was measured at 562 nm with a microplate reader.

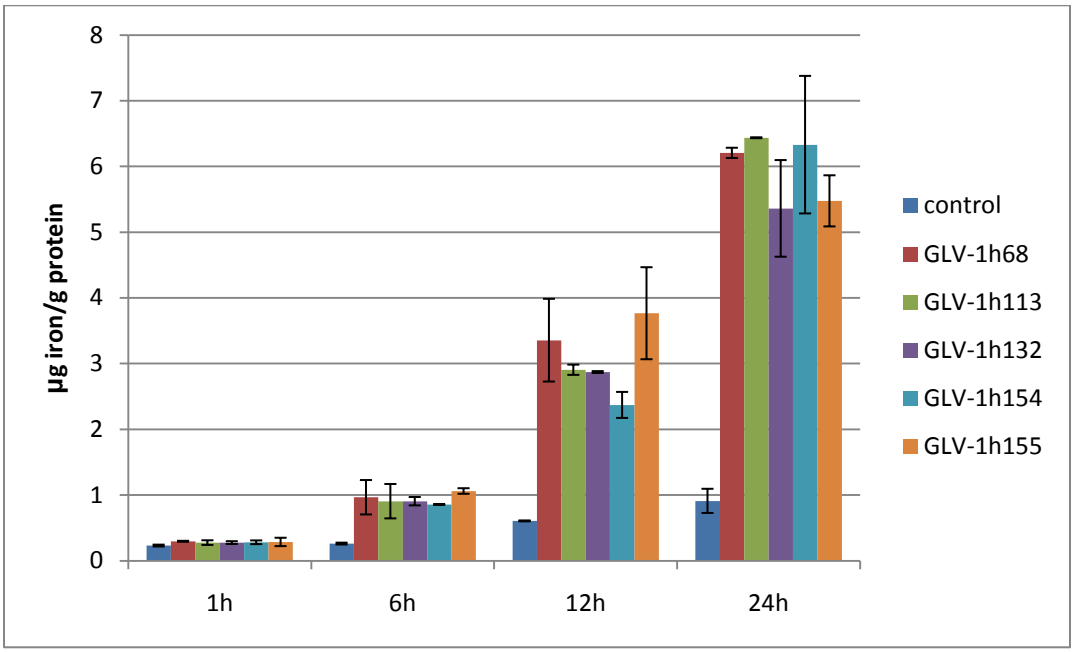

Fig. 4.42 Detection of iron in infected GI-101A cell culture samples at different times after infection by ferrozine assay

Figure 4.42 shows the iron concentrations of the different GI-101A cell lysate samples determined by the Ferrozine assay. The averages of triplicate measurements are presented with standard deviation in µg iron per g protein. A significant increase in iron concentration could be seen continually from 6 hours until 24 hours after iron supplementation. All virus samples accumulated more iron in the infected cells, even the control virus GLV-1h68, which does not mediate expression of any recombinant iron accumulating protein. The same effect of GLV-1h68 was already shown in the QuantiChrom™ iron assay.

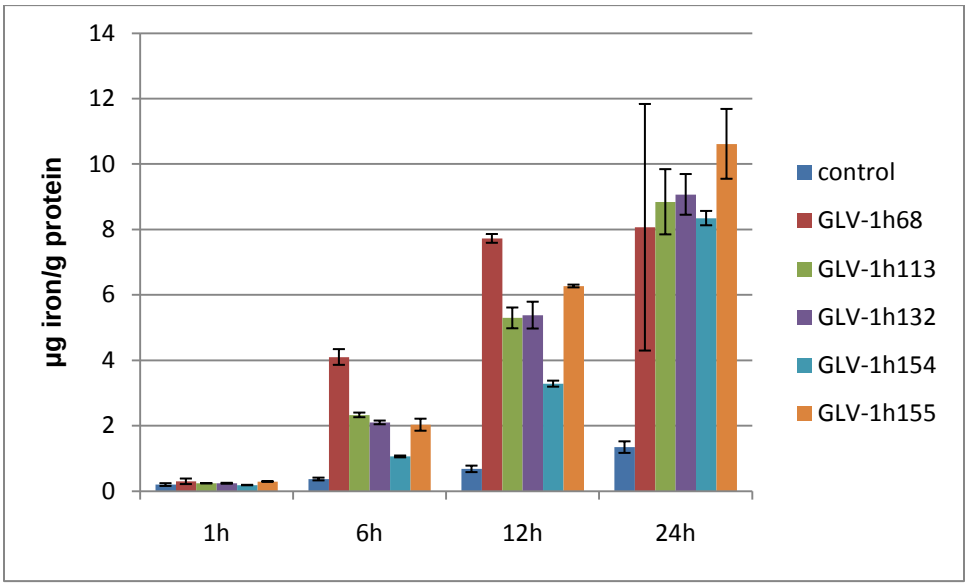

Fig. 4.43 Detection of iron in infected A549 cell culture samples at different times after infection by ferrozine assay

The ferrozine assay with A549 cell lysates showed a very similar result as for GI-101A cells. All virus-infected cells accumulated more iron than the uninfected control cells over time, including the cells infected with the control virus GLV-1h68.

4.2.3 Inductively Coupled Plasma Mass Spectrometry (ICP-MS) Measurements of Infected Cell Cultures

ICP-MS is an analytical technique used for elemental determinations. ICP-MS combines a high temperature inductively-coupled plasma source with a mass spectrometer. With this method the metal content can be detected in a much more sensitive way than the assays used before.

Forty-eight hours after infection with different virus strains and 24 hours after supplementation with iron or manganese, cells were washed twice with cold PBS and then lysed with 1% Triton-X in water. The samples were treated with benzonase and the protein concentration was determined using the Biorad protein assay. The samples were then treated with proteinase K and incubated with concentrated nitric acid on ice to

precipitate all the remaining proteins. The volume was brought to 2 ml by adding water. After sterile filtration the samples were measured by Uwe Gbureck of the Department of Functional Materials in Medicine and Dentistry, University of Würzburg.

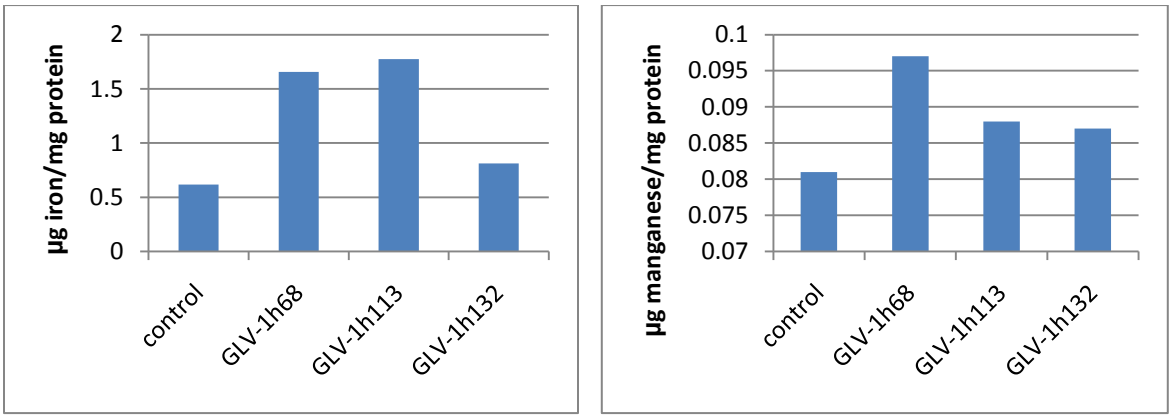

Fig. 4.44 Iron and manganese ICP-MS measurements

The ICP-MS measurements shown in figure 4.44, were performed detecting iron and manganese. The iron determination showed that cells, which were infected with GLV-1h68 exhibited a similar or even higher level of iron content compared to GLV-1h113- or GLV-1h132-infected cells. In fact, GLV-1h132-infected cells showed only a slightly more effective iron accumulation than uninfected control cells. For the manganese measurements GLV-1h68-infection led to a significantly higher manganese concentration, whereas infection with GLV-1h113 and GLV-1h132 resulted in only a slight increase in manganese content in the cells compared to uninfected control cells.

4.2.4 Heavy Metal Accumulation Using a Synthetic Phytochelatin

To test the capability of the synthetic phytochelatin EC20 as a heavy metal-collecting peptide, experiments were performed with a bacteria strain carrying a plasmid encoding the EC20 peptide. The advantage of working with bacteria in this project instead of vaccinia virus was that the effects could be investigated much more easily and time

efficient with bacterial cultures than the time consuming generation of new virus strains. After the successful metal accumulation was shown in this system, the generation of new virus strains could still be an option.

4.2.4.1 Bacterial Growth Curve

Before performing any experiments with different bacterial strains, similar to working with viruses, it was reasonable to determine and compare their growth curves. For this experiment two different bacterial strains were used. The *E. coli* Omnimax pTolC, which contains a plasmid with a gene for the surface protein TolC (German and Misra, 2001) and *E. coli* Omnimax pTolc-EC20, which additionally contains a gene for the heavy metal-accumulating synthetic phytochelatin EC20 (Bae *et al*., 2001) fused to the surface protein TolC, were used.

From overnight cultures in LB medium with 50 µg/ml kanamycin new cultures were inoculated with a 1:100 dilution. These cultures were shaken at 37 ˚C and the OD_{600} measured every hour with a spectrophotometer.

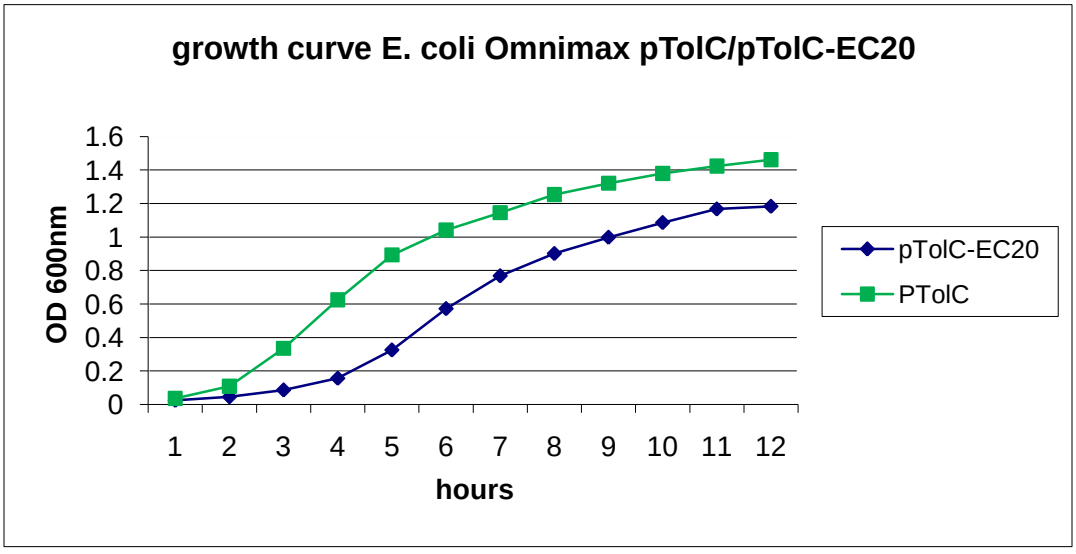

Fig. 4.45 Growth curve of the two bacterial strains *E. coli* Omnimax pTolC and *E. coli* Omnimax pTolC-EC20

Figure 4.15 shows the growth behavior of the two bacterial strains *E. coli* Omnimax pTolC and *E. coli* Omnimax pTolC-EC20. Both bacterial strains showed the characteristical growth pattern including lag-, log- and stationary phase. The *E. coli* Omnimax pTolC-EC20 showed a growth delay and did not reach the same optical density in the stationary phase compared to *E. coli* Omnimax pTolC.

4.2.4.2 Heavy Metal ICP-MS Measurements of Bacterial Cultures

ICP-MS is a very sensitive method to measure the heavy metal concentration in samples. Since EC20 is a peptide, which was shown to bind heavy metals (Bae *et al*., 2001), the bacterial strains were grown in LB medium with different heavy metal supplements. The final concentration of $FeCl_3$, $MnSO_4$, $CuSo_4$, and $CdCl_2$ in the different media was 5 µM. Cultures were grown at 37˚C for six hours and then washed and prepared for ICP-MS measurement. The measurements were done by Uwe Gbureck of the Department of Functional Materials in Medicine and Dentistry, University of Würzburg.

Sample Label (and supplement)	Fe57 ppb	Mn55 ppb	Cu63 ppb	Cd111 ppb
water	39.1106	0.109	0.155	0.0493
control -	1621.834	55.3462	29.2027	1.6204
control Fe	1713.615	53.81	36.6472	1.451
control Mn	1370.137	1150.534	25.0973	2.1277
control Cu	1480.886	62.9167	339.382	1.7422
control Cd	902.9441	31.3571	18.9629	896.0973
EC20 -	1676.928	48.9748	30.3038	1.6382
EC20 Fe	2087.084	54.4494	29.076	1.6577
EC20 Mn	1680.746	1233.193	38.9911	2.3972
EC20 Cu	1432.698	57.1271	387.6741	4.0706
EC20 Cd	1122.177	26.8486	23.0593	1030.982

Fig. 4.46 ICP-MS measurement of bacterial cultures of *E. coli* Omnimax pTolC and *E. coli* Omnimax pTolC-EC20 grown with different metal supplements (Analytes which were supplemented in the respective cultures are highlighted)

Figure 4.46 displays a table of the ICP-MS results. On the left it shows the bacterial strains with the different supplements. Control represents the control bacteria *E. coli* Omnimax pTolC and EC20 represents the strain *E. coli* Omnimax pTolC-EC20. In the first row the values for water are shown as a reference. The relevant values for this experiment are highlighted. All the measurements show an increase of at least 7% of heavy metal accumulation in the EC20-expressing *E. coli* strain.

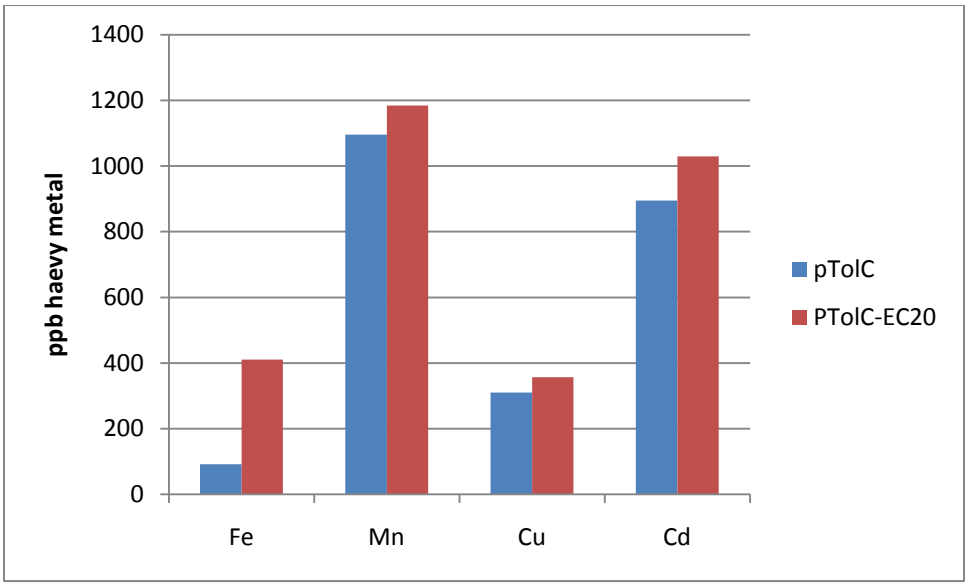

Fig. 4.47 ICP-MS measurement of bacterial cultures of *E. coli* Omnimax pTolC and *E. coli* Omnimax pTolc-EC20 grown with different metal supplements

Figure 4.47 is a chart created from the results of the ICP-MS measurement from figure 4.46. The values of the cultures without supplement were subtracted from the values measured with supplement. It can clearly be seen that *E. coli* Omnimax pTolc-EC20 accumulated a higher amount of all heavy metals tested than the control bacteria in this experiment.

4.3 *In vivo* Studies

4.3.1 Production of Mouse Serum against Bacterioferritin for Western Blots

During the time frame of this work no antibody was commercially available for bacterioferritin. To overcome this issue, an antiserum was generated in mice. BALB/c mice were injected with the purified protein mixed with Freund's Incomplete Adjuvant once every two weeks. Serum was collected from the mice after six weeks from the first injection.

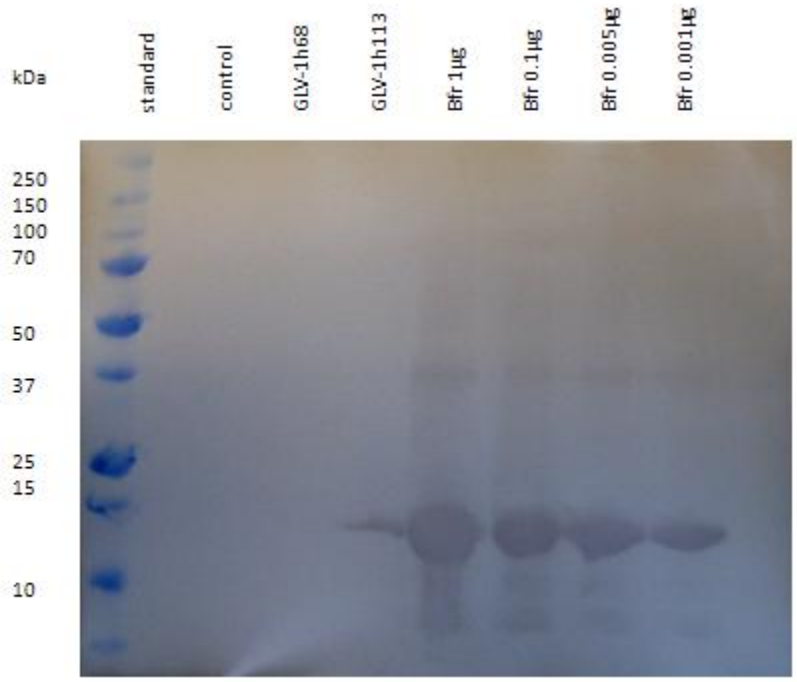

Fig. 4.48 Detection of different bacterioferritin protein dilutions and virus-mediated bacterioferritin expression by Western blot with mouse serum

To test the binding affinity of the raised antibodies in the mouse serum, a Western blot was performed with samples of uninfected and GLV-1h68- and GLV-1h113-infected

cells as well as different dilutions of purified bacterioferritin protein as a positive control. For the immunological detection the obtained mouse serum was used as primary antibody in a 1:10 dilution. A HRP-conjugated anti-mouse antibody was used as secondary antibody. As shown in figure 4.48 all dilutions of the purified bacterioferritin protein could be detected. Also, the virus-induced expression of bacterioferritin in GLV-1h113-infected cells could be visualized clearly.

4.3.2 Determination of Virus Distribution by Plaque Assay

The biodistribution of virus in the mice was analyzed 24 days after injection with the viruses by performing standard plaque assays with lysates from the A549 tumors and different organs (spleen, liver, lung, heart). The results of the plaque assays are shown in figure 4.48.

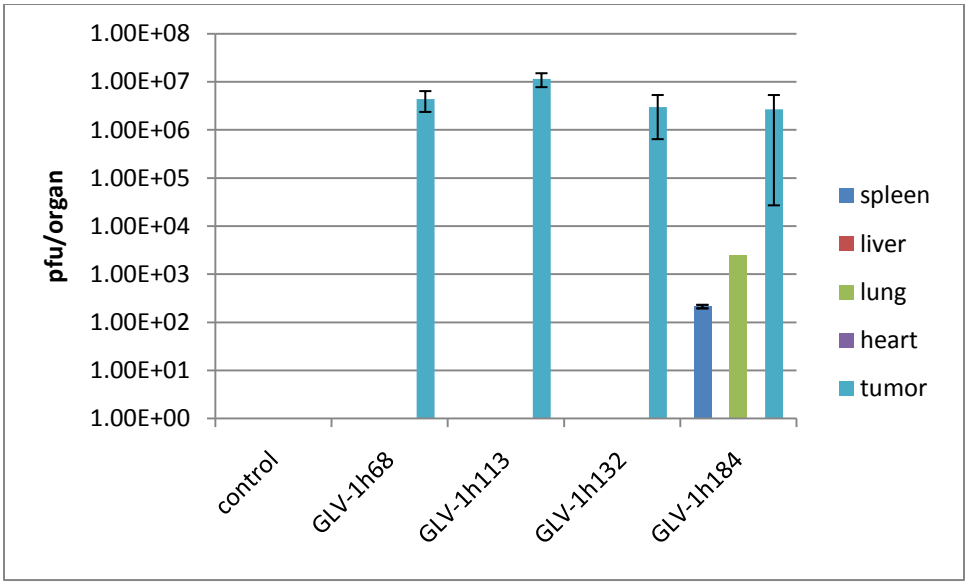

Fig. 4.49 Biodistribution of virus particles in A549 tumors and mouse organs in plaque forming units per organ

Figure 4.49 shows the biodistribution analysis of tumors and organs in plaque forming units per organ. Overall, it could be found that the virus was rapidly cleared from most of the organs except tumors. Only in the GLV-1h184-infected group, virus could be found in spleen and lung. The virus titers in the tumors reached between 10^6 and 10^7 pfu/tumor. The titers in lung and spleen were 3 and 4-log lower than those detected in tumors. In liver and heart no virus particles were detected by standard plaque assay. This finding proves that the viruses are mainly accumulating in the tumors and not in the rest of the body.

4.3.3 Western Blot of Tumor Samples

To find out whether the recombinant proteins delivered by the virus strains can also be expressed successfully *in vivo*, A549 tumor lysates were further analyzed in Western blots. An antibody against human ferritin and the bacterioferritin antiserum were used for the detection. An antibody against β-actin was used as a loading control.

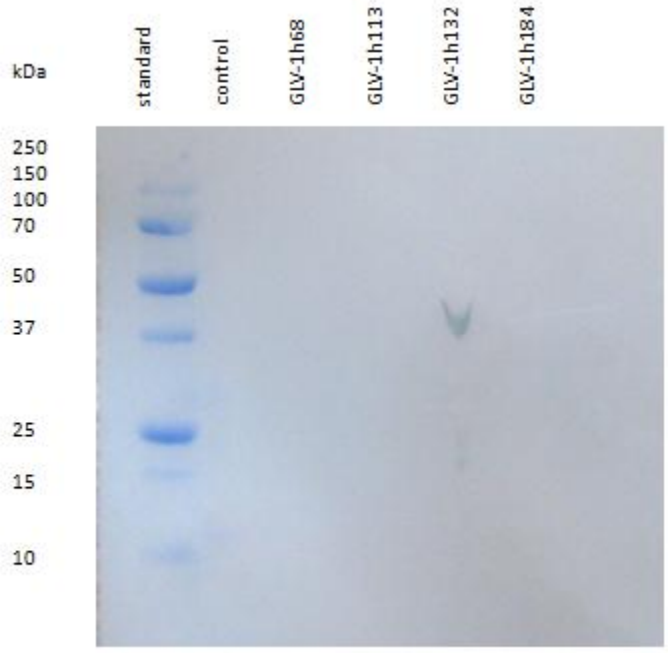

Fig. 4.50 Detection of virus-mediated human ferritin expression by Western blot analysis in A549 tumors

The Western blot in figure 4.50 shows the detection of ferritin in the infected tumor sample. The protein band of the ferritin dimer with a size of 40 kDa could clearly be detected in GLV-1h132-infecetd tumors. This Western blot proves that there is enough human ferritin expressed in the infected A549 tumor to be detected using this method.

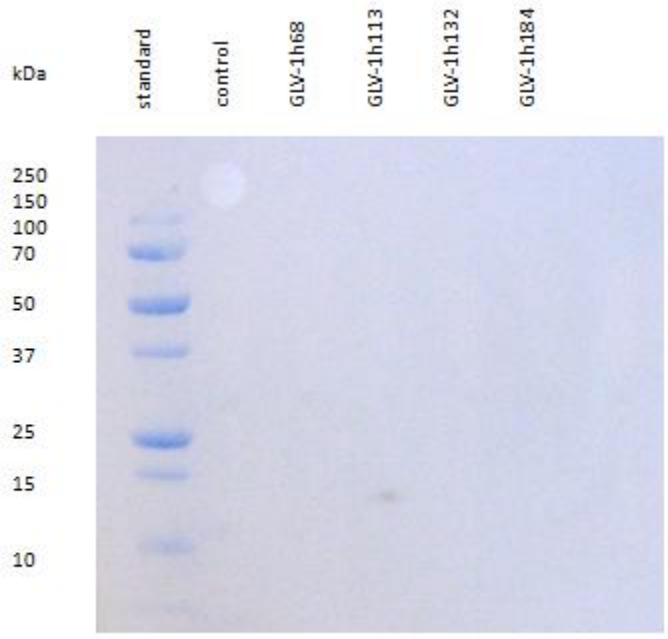

Fig. 4.51 Detection of virus-mediated bacterioferritin expression by Western blot analysis in A549 tumors

Figure 4.51 shows a Western blot which was incubated with an anti-bacterioferritin mouse serum. The band representing bacterioferritin is very weak because of the nature of the self-made serum but still detectable with this relatively insensitive colorimetric detection method.

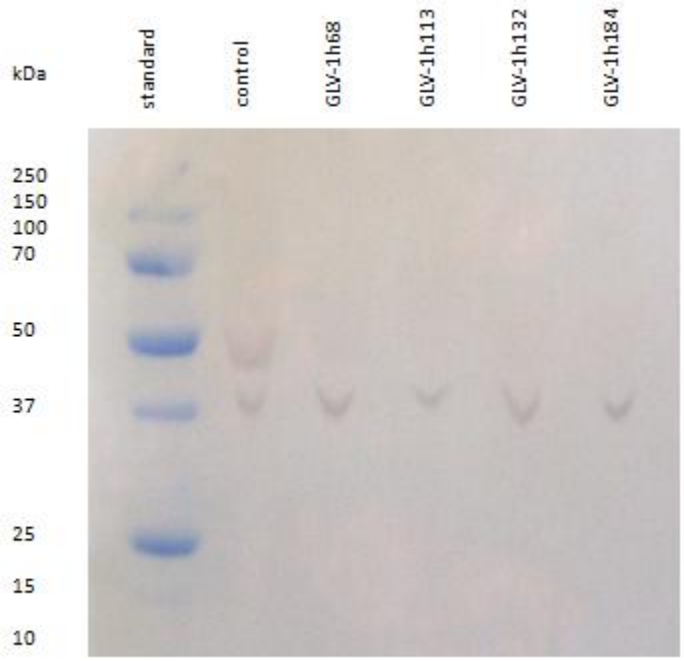

Fig. 4.52 Detection of β-actin expression by Western blot analysis in A549 tumors

As a loading control the blot was incubated with a β-actin antibody. Figure 4.52 shows that the gel was loaded evenly in all wells.

4.3.4 Ferrozine Assay of Tumor Samples

To determine whether the virus-mediated overexpression of iron-accumulating proteins resulted in an enhanced iron concentration in the tumor samples, a ferrozine assay was performed. The tumor lysates were treated in the same way as the cell lysates for the ferrozine assay. The results are shown in figure 4.54 and figure 4.55.

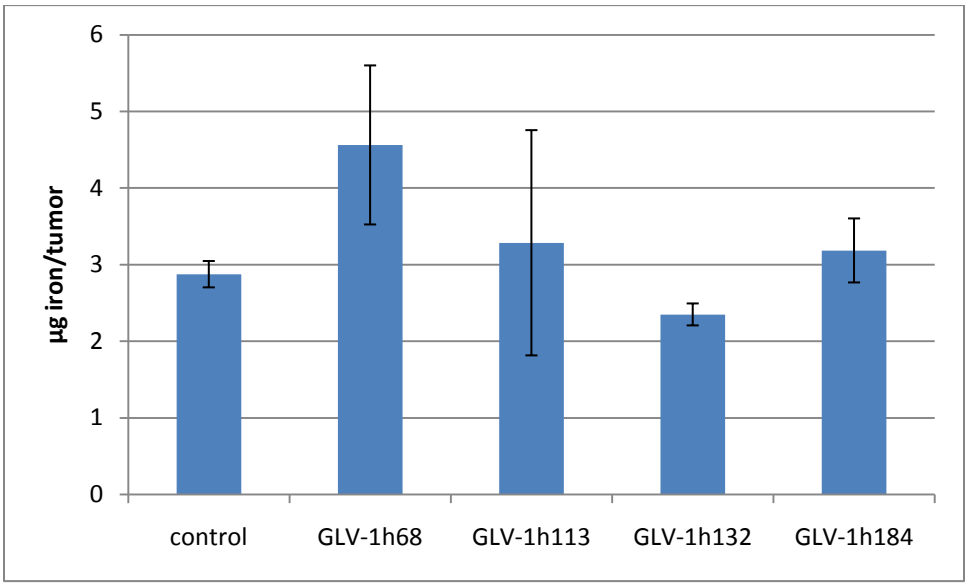

Fig. 4.53 Detection of iron in A549 tumor samples by ferrozine assay in µg iron per tumor

The results of the ferrozine iron assay show that in the GLV-1h68-infected tumors the iron concentration as highest. GLV-1h113 and GLV-1h184 had only a slight positive effect on iron accumulation and GLV-1h132 infected tumors even showed less iron than the control.

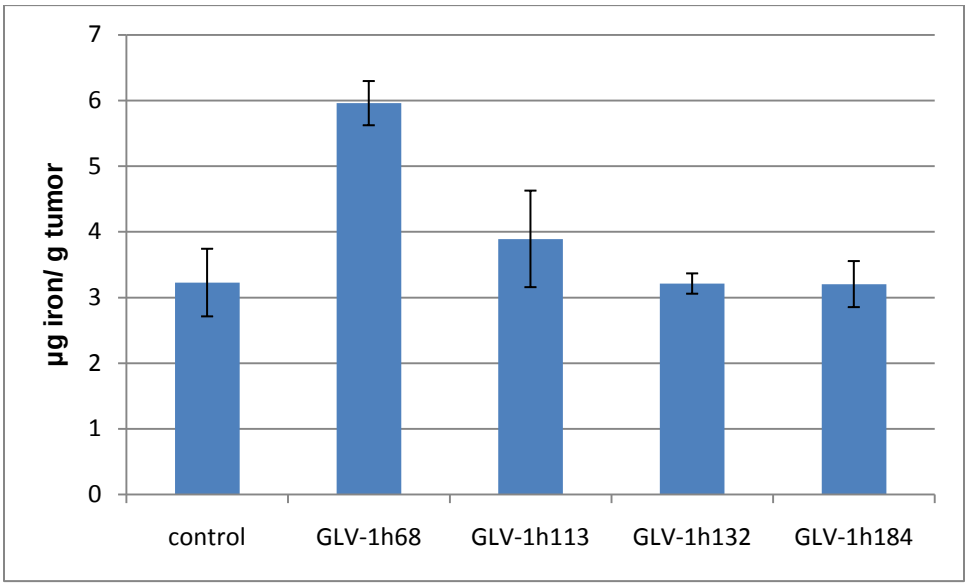

Fig. 4.54 Detection of iron in A549 tumor samples by ferrozine assay in µg iron per g tumor

Figure 4.54 shows the same results of the ferrozine assay, this time in µg iron per g tumor. GLV-1h168-infected tumors showed the highest iron concentration of all the tested groups. GLV-1h113 also seemed to have a slightly positive effect on iron accumulation.

4.3.5 Histology

Immunohistochemical studies were conducted to further evaluate viral spreading and influence of the virus infection on iron accumulation. Tumors were fixed in formalin and sectioned as previously described. Different stainings were performed with the tissue sections. All pictures are shown in a 40 x magnification.

4.3.5.1 Hematoxylin and Eosin (H&E) Staining

Hematoxylin and Eosin staining was performed with the sections of tumors. H&E is a structural staining. For the staining the basic dye hematoxylin was used, which colors basophilic structures in a blue-purple color, and alcohol-based acidic eosin Y, which

colors eosinophilic structures bright pink. Basophilic structures are the ones containing nucleic acids, such as the ribosomes and the chromatin-rich cell nucleus. Eosinophilic structures usually consist of intracellular or extracellular protein. Most of the cytoplasm is eosinophilic but the cytoplasmatic regions rich in RNA are basophillic. Clear areas in the stained sections represent water, carbohydrates, lipids or gas.

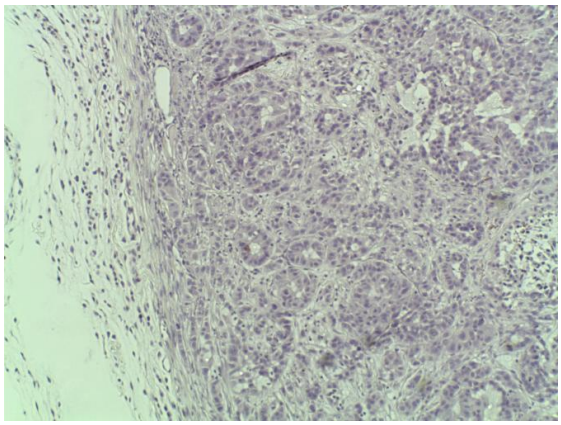

Uninfected control

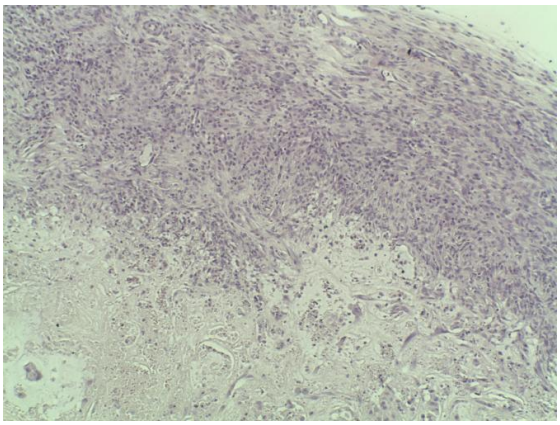

GLV-1h68-infected

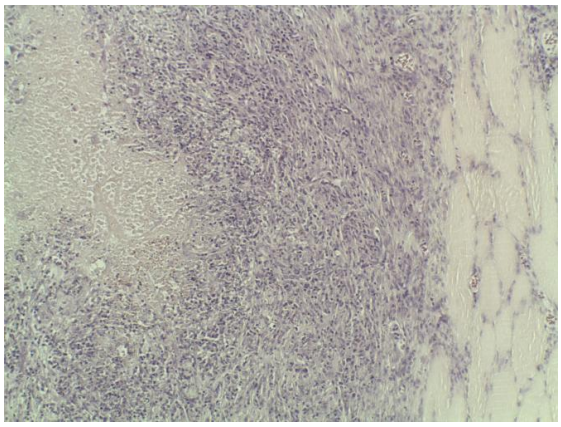

GLV-1h113-infected

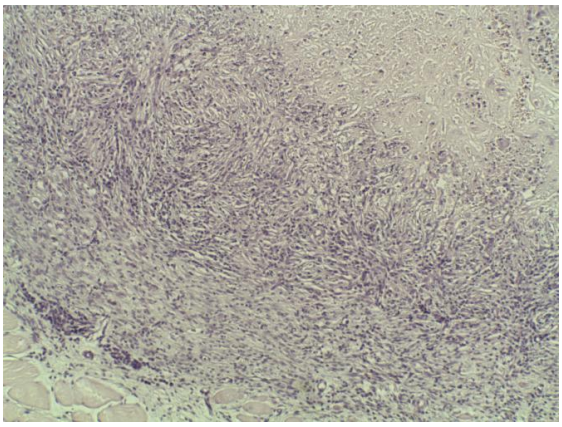

GLV-1h132-infected

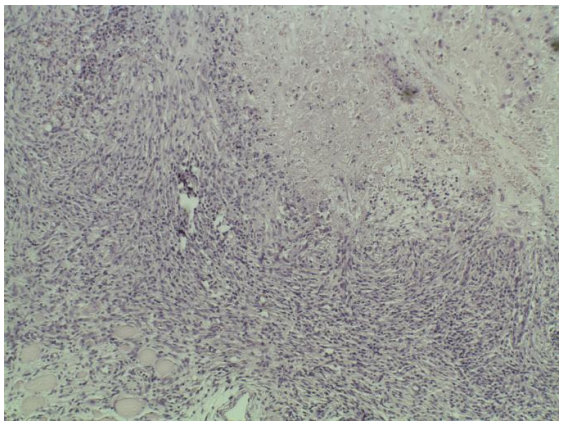

GLV-1h184-infected

Fig. 4.56 Histological H&E staining of A549 tumor sections 21 days after virus injection

The H&E staining in figure 4.55 shows the typical structures of tumors. Cancer cell nuclei vary greatly in size because they are genetically destabilized. Often that results in very large nuclei. In the infected tumors more necrotic areas can be seen as in the uninfected control. Cell death can be detected by necrotic debris or nuclear dust. Muscle is sometimes seen on the edge of the tumor and is stained pink. The different virus strains used in this study did not show any significant differences in the H&E staining.

4.3.5.2 Immunohistochemical Staining of Vaccinia Virus and Prussian Blue Iron staining

The staining of vaccinia virus infected areas of the tumors using a vaccinia specific antibody was performed to investigate if all tumors were infected by the virus and to compare whether the infected areas correlate with areas of high iron content. It is important to see whether and how much of the tumors are infected by the respective virus strain to determine whether iron accumulating effects are likely to result from the virus infection or if other mechanisms are responsible. Prussian Blue is a staining method to detect iron, which leads to a blue staining of the iron present in a tissue. The

additional DAB intensification results in a better visible dark brown color of the same staining. Figure 4.57 shows both stainings in direct comparison.

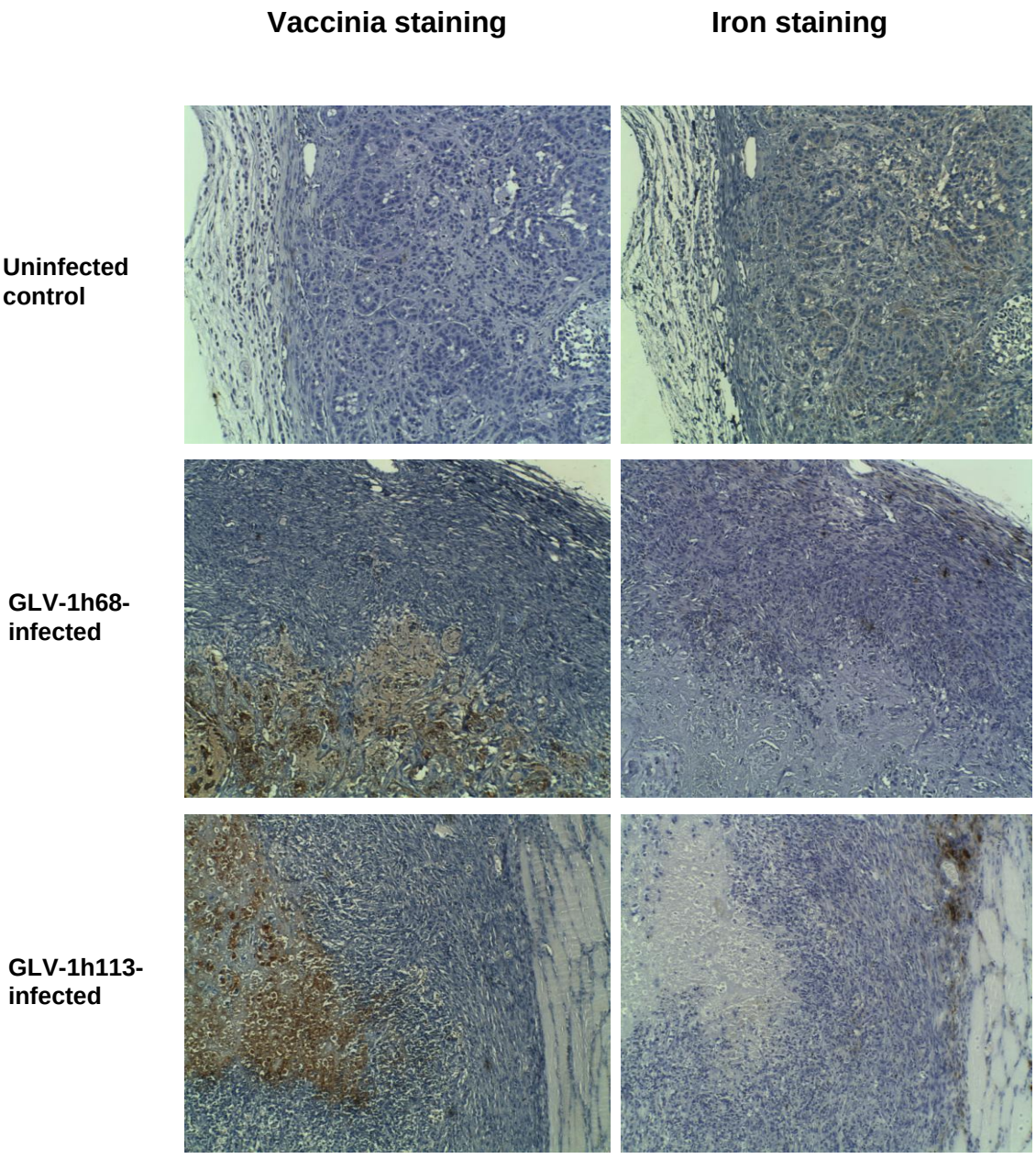

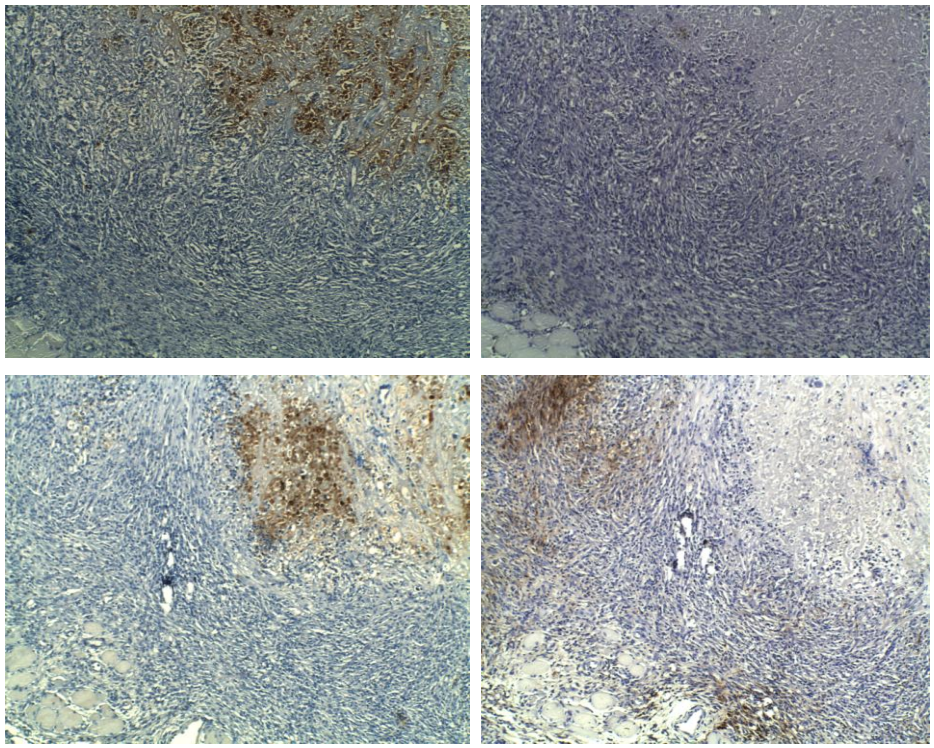

Fig. 4.57 Immunohistochemical vaccinia staining and Prussian Blue Iron staining of A549 tumor sections 21 days after virus injection

The photos of the sections, which were stained with vaccinia antibody shown in figure 4.57 on the left side display, that all the tumors of mice that were injected with virus show large areas of virus infection. The staining of the uninfected control resulted in no vaccinia-specific staining.

The iron staining of the tumor sections, shown on the right side of the illustration led to a dark brown staining of some areas in the tumors. In the uninfected control tumors there was no significant staining visible. In contrary to the ferrozine assay shown in figure 4.54 and 4.55, the highest iron content detected by this method was observed in GLV-1h184-infected tumors.

The comparison of the vaccinia staining with the iron staining led to the conclusion that the areas with high iron content were not overlapping with the virus-infected areas. The

iron accumulation effect seemed to be not a direct result of the virus-mediated overexpression of iron-accumulating proteins according to this experiment.

4.3.5.3 Immunohistochemical Staining of Ferritin

Another immunohistochemical staining was performed using a ferritin antibody. The technique that was used was similar to the vaccinia staining. Areas in the tumor that contain high amounts of ferritin are shown as a dark brown staining. The ferritin staining is shown on the right side of figure 4.58 next to the vaccinia staining on the left, which is shown as a comparison.

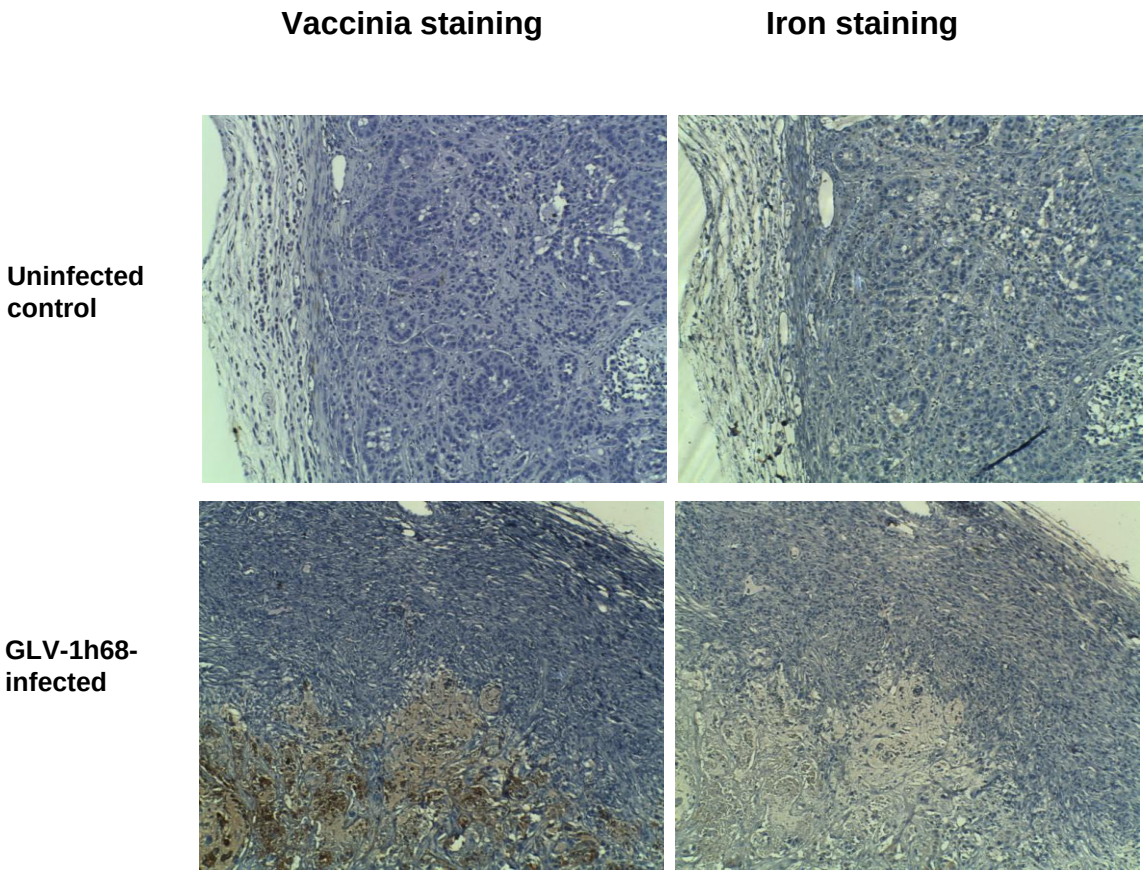

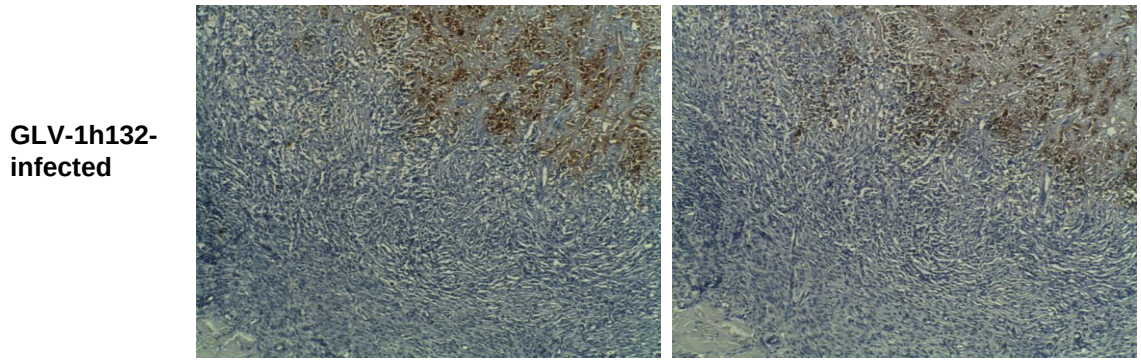

Fig. 4.58 Immunohistochemical staining of ferritin in comparison to vaccinia staining of A549 tumor sections 21 days after virus injection

The ferritin staining shows a clear overexpression of ferritin by infection with the virus GLV-1h132 in comparison to GLV-1h68 and in the uninfected control. The overexpression of ferritin correlated directly with the areas, which were shown to be infected by the virus, as shown on the left side of the illustration.

4.4 MRI Measurements

The MRI measurements are the central experiment of this work. The aim of the study was to accumulate enough iron in the tumors with one of the newly constructed virus strains to be able to detect the virus-infected tumors with MRI technology.

Mice were implanted with tumors on both sides on the lower back and injected with the viruses three weeks after tumor implantation. The mice were supplemented with iron (0.1 mg) every other day and seven days after the injection they were measured with the seven Tesla scanner. After 21 days another MRI measurement was performed with the same mice. Unfortunately, the second measurement could only be performed with a three Tesla scanner because the seven Tesla scanner used for the initial measurement

was out of order. All measurements were done by Miriam Scadeng at the Center for functional MRI of UCSD.

4.4.1 Seven Tesla Measurements

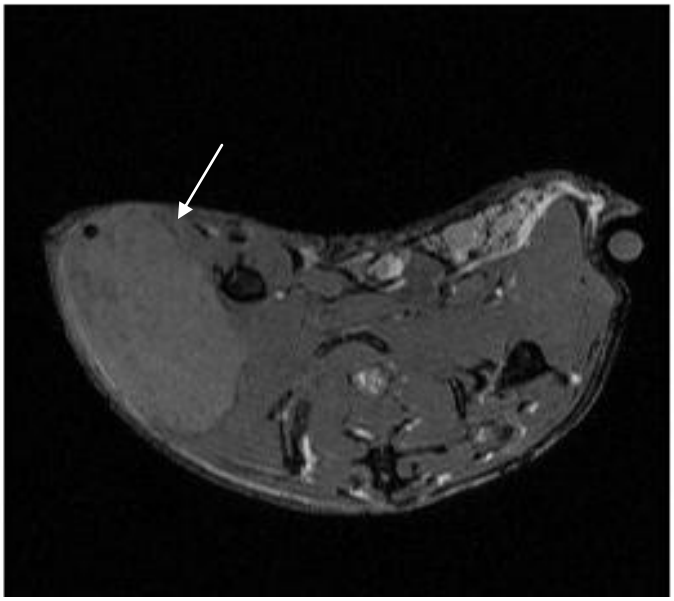

Fig. 4.59 Untreated control

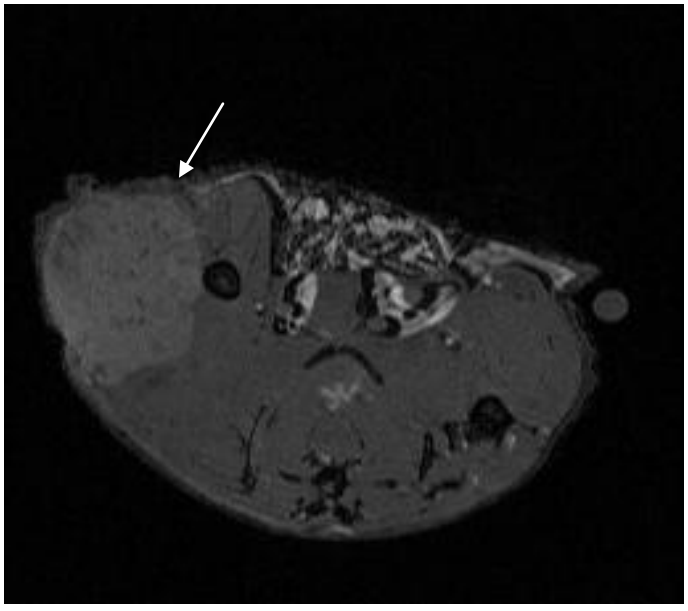

Fig. 4.60 GLV-1h68-treated tumor

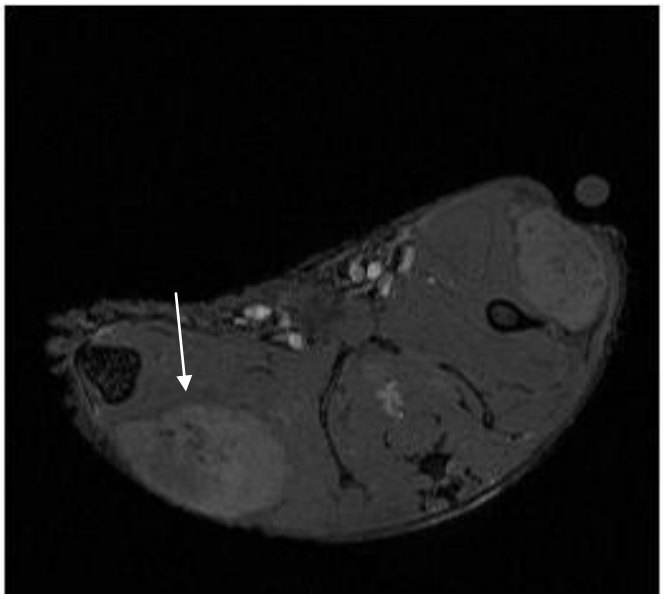

Fig. 4.61 GLV-1h113-treated tumor

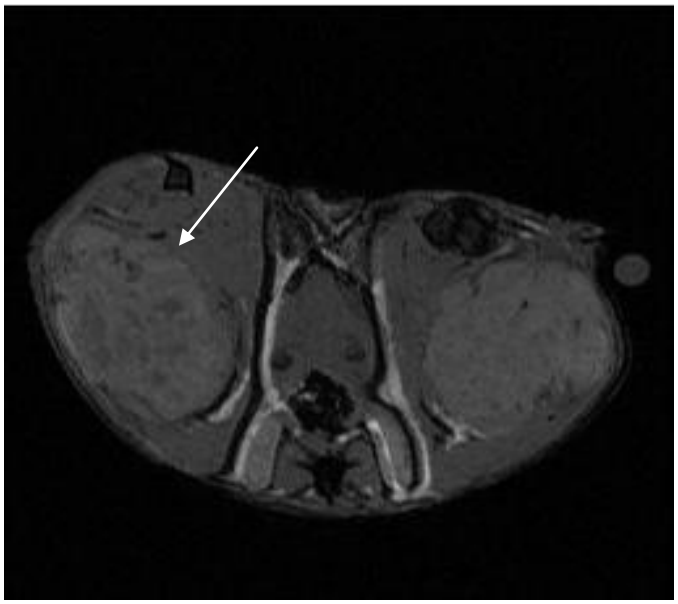

Fig. 4.62 GLV-1h132-treated tumor

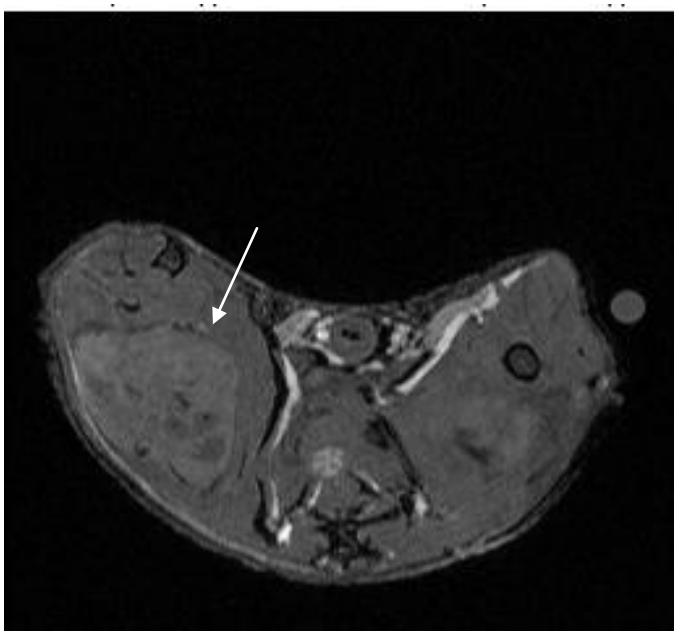

Fig. 4.63 GLV-1h184-treated tumor

The seven Tesla measurements show T2-weighted FISP images of five differently treated mice seven days after virus injection. A FISP measurement uses parameters which are very sensitive for iron but not very sensitive for motion. The darker the image the higher is the iron content using these scanning parameters. Every caption (figures 4.59 - 4.63) shows at least one tumor on the left flank of the mouse body. White arrows point to the tumors. According to these captures in the uninfected control tumor fewer dark areas could be detected than in all the virus-infected tumors shown. Considering the fact that each tumor was scanned in many different slices, it is difficult to find a conclusion on the overall effect of the infection by the different virus strains on iron accumulation only by eye. Therefore it is important to use a quantitative method to measure the overall tumor and compare different treatments. Figure 4.65 shows a quantitative analysis of T2 relaxation times that was obtained by using Paravision 4.0 software. Iron accumulation shortens the T2 relaxation time.

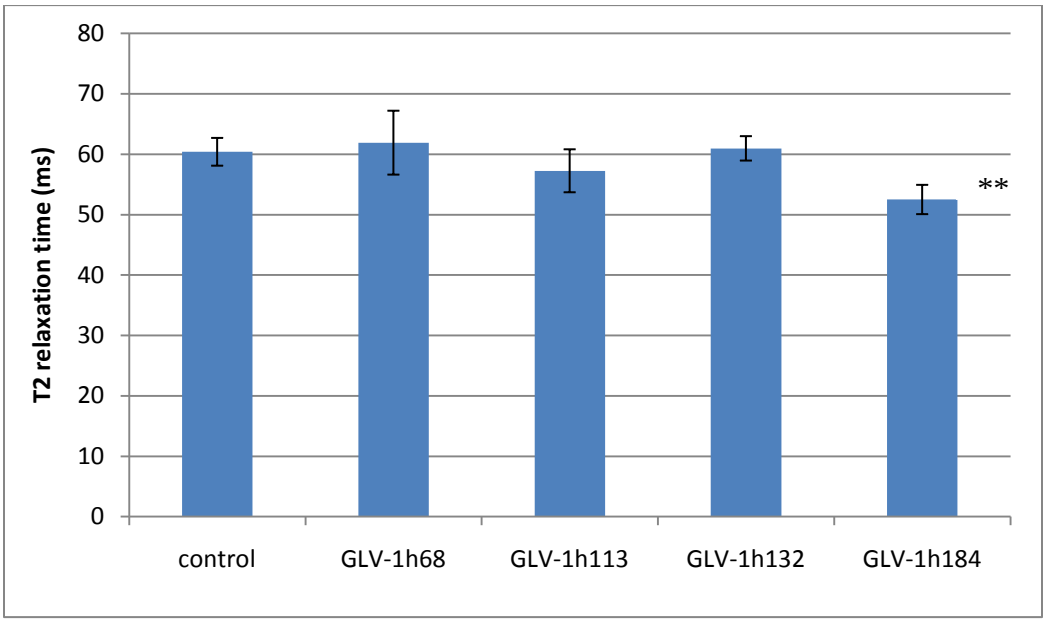

Fig. 4.64 T2 relaxation time of tumors seven days after virus injection with seven Tesla scanner (P<0.01)**

The quantitative data analysis showed T2 relaxation times in ms which were shortened in GLV-1h113- and significantly shortened in GLV-1h184-infected tumors (figure 4.64). These are the viruses that mediate bacterioferritin and MagA expression in infected cells, respectively. The values were calculated from T2 maps (TR 2000ms, TE 10-160ms) using small ROI's with Paravision 4.0 software. Values of six ROI's were averaged and the values are shown in the graph with standard deviations.

Figure 4.65 shows the *R2* values for these tumors, which is the relaxation rate. It can be stated that GLV-1h113 and GLV-1h184 decreased T2 and increased *R2*, which is a sign for higher iron content in the tumors.

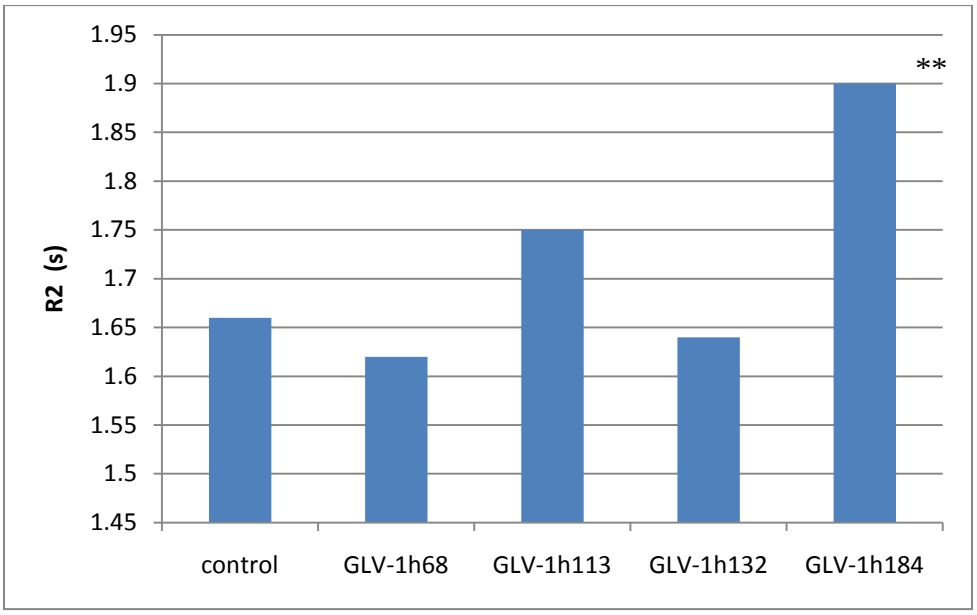

Fig. 4.65 *R2* relaxation rate (*R2*=1/T2) of tumors seven days after virus injection with seven Tesla scanner (*P*<0.01)**

The illustration of the *R2* relaxation rate values in seconds shows the differences even clearer.

4.4.2 Three Tesla Measurements

The three Tesla measurements were performed with a GE human scanner 21 days after virus injection.

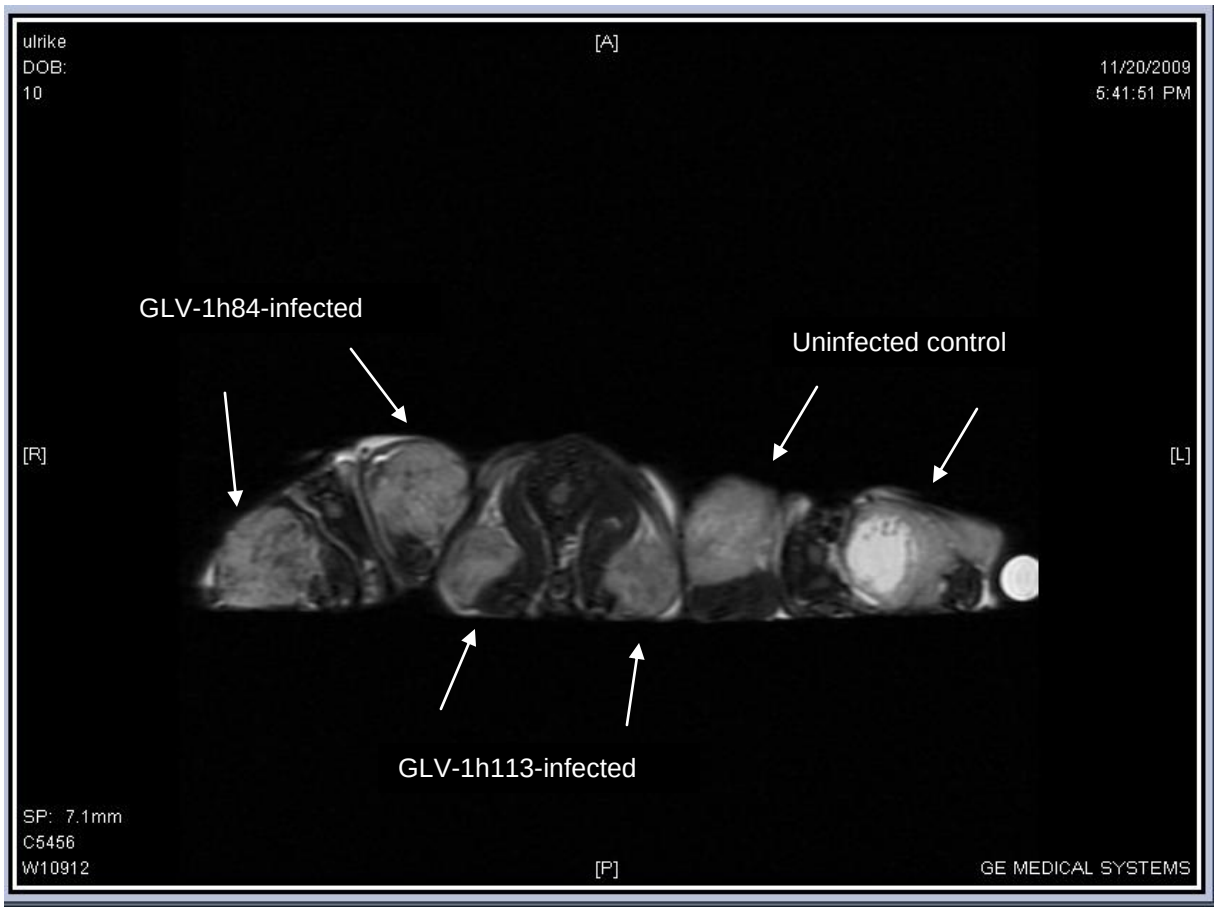

Fig. 4.66 T2 measurement of uninfected and GLV-113- and GLV-1h84-injected mice 21 days after injection

Figure 4.66 shows three mice measured at the same time with two tumors on each side of the body. The mouse on the right side of the picture is the uninfected control mouse. The mouse in the middle was injected with the virus GLV-1h113 and the mouse on the left side of the image was injected with GLV-1h184. In the right tumor of the control mouse a large cystic area could be seen, which could not be included in the data analysis. The tumors on the right (GLV-1h184-injected mouse) contained more and darker areas in the tumors which are a sign for more iron accumulated in the tumor. Also the tumors in the middle (GLV-1h113-injected mouse) appeared darker than the control tumors.

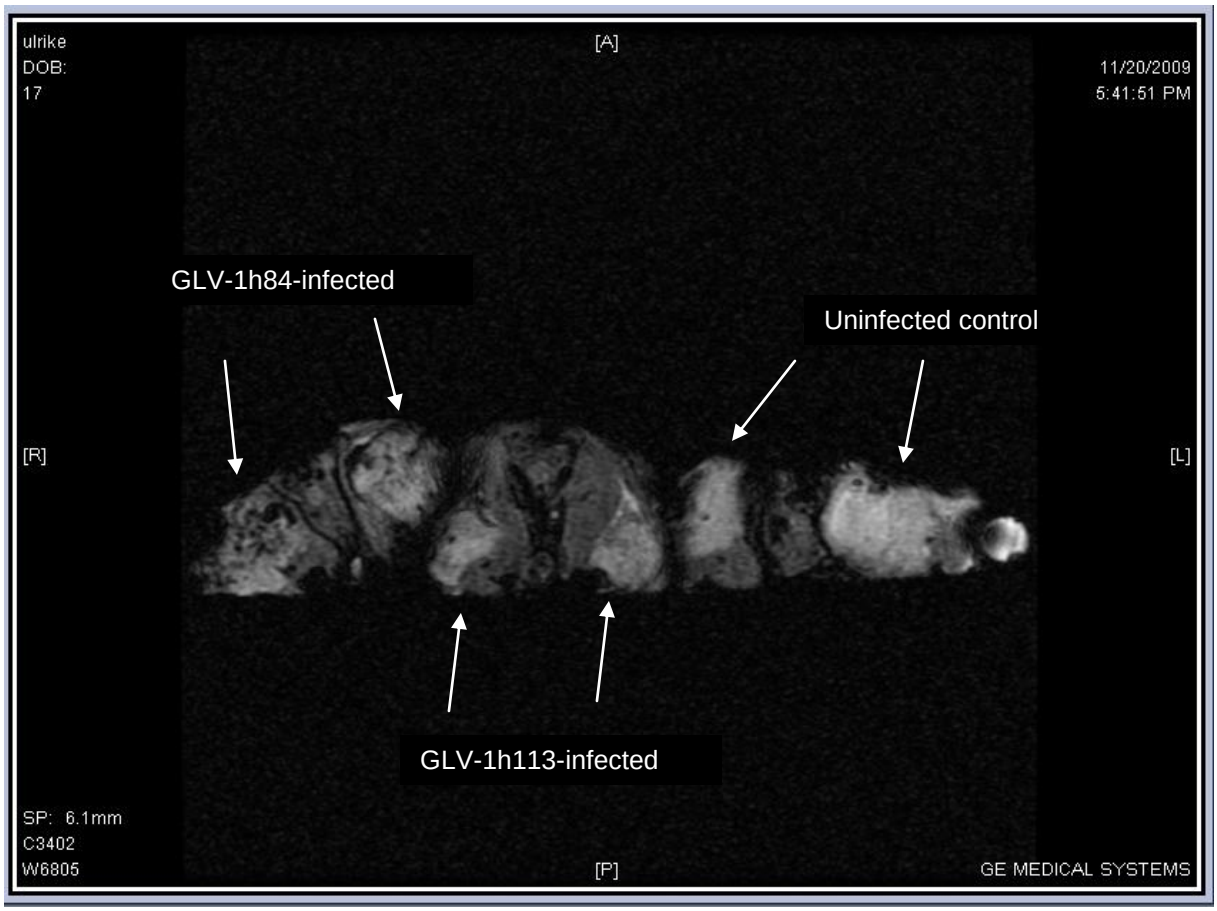

Fig. 4.67 T2* measurement of uninfected and GLV-113- and GLV-1h84-injected mice 21 days after injection

Figure 4.67 is a T2* measurement which is using different parameters than the measurement shown in the image before. The results went in line with the previously shown measurements in figure 4.67. The cystic area was not that clearly visible with these parameters but the more iron-sensitive settings showed more dark spots.

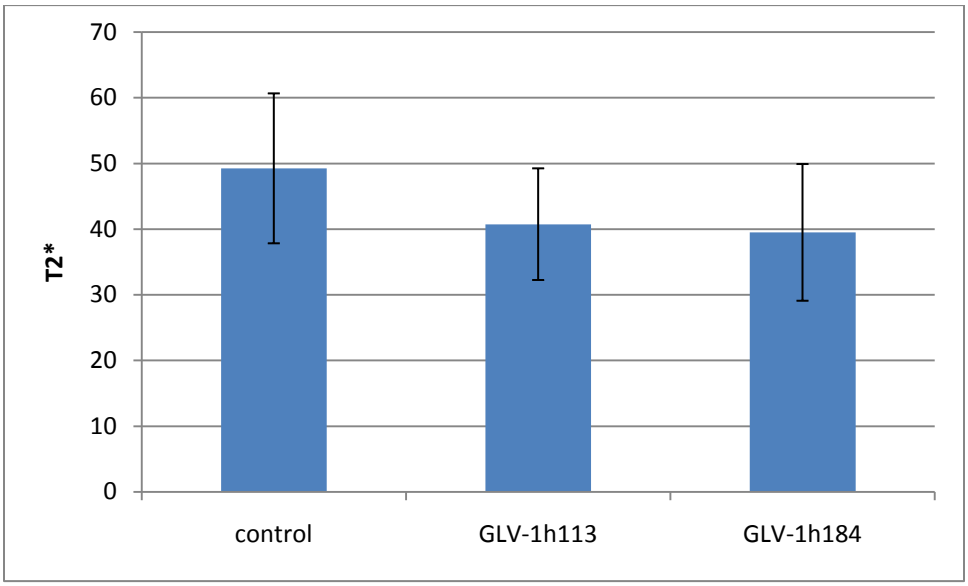

Fig. 4.68 T2* values

Figure 4.68 shows the T2* data quantitatively analyzed in a graph. The values were obtained with GE software using small ROI's. The averages and standard deviation of the T2 values of six ROI's are shown in the graph. Tumors infected with both viruses, GLV-1h113 and GLV-1h184 showed clearly shortened T2* times in comparison to the uninfected control tumors.

5 Discussion

It was recently shown that vaccinia virus is able to infect and replicate specifically in cancer cells (Yu *et al*., 2004, Kirn and Thorne, 2009). The generation of new recombinant virus strains allows the expression of different proteins by the virus-infected cancer cells. This includes for example proteins which have antitumor effects and proteins which enable real-time imaging of the tumor progression or regression.

Early detection of tumors and metastases is crucial for the survival of a cancer patient. Luminescent proteins like luciferases or fluorescent proteins like GFP can be used to add optical imaging capability to viral strains (Luker at al., 2005; Gross and Piwnica-Worms, 2005). For deep tissue imaging, which is more useful for tumor diagnosis, reporter genes have to be inserted in the virus genome that are detectable with Positron Emission Tomography (PET) or Magnetic Resonance Imaging (MRI). CT, MRI and PET scans are all diagnostic tools to non-invasively investigate the body. CT is today the mostly used technique in oncological imaging. X-rays are used to create a detailed picture of the body's tissues and structure of organs. Limitations of CT are the use of harmful X-rays and the limited soft tissue contrast outside of the lung, which can make the detection of metastases or tumors in the surrounding tissues difficult.

PET scans measure emissions from positron-emitting molecules. Before the scan, substances that bind to target structures (e.g. enzymes, transporters, etc.) in the body are labeled with radioisotopes. They are injected into the blood stream and taken up in greater concentrations by areas of tissues which express the target structures. The PET scan shows molecular function and activity but not structure, and can thus show differences between normal and abnormal or live versus dead tissue. However, there is a risk of misinterpretation due to the uptake of the radiotracer in muscle or fat tissue. Another disadvantage is the use of ionizing radiation by the radioactive tracer.

MRI is a diagnostic technique that provides three dimensional images of organs and structures with high soft tissue contrast and high special resolution without using harmful X-rays or other radiation. As a disadvantage contrast agents usually have to be

administered to patients to provide better contrast. By delivering the contrast agent via infection by the virus, these difficulties can be avoided.

In this study it was attempted to create recombinant virus strains with metal-accumulating capabilities for tumor detection via MRI technology. New virus strains were generated harboring different iron-collecting genes and were tested for their usefulness in cell culture and *in vivo*. The aim of this work was to compare and evaluate the potential of these viruses to be used in cancer detection.

5.1 Ferritin-encoding Viruses Were Able to Replicate and Mediate Ferritin Expression in the Cancer Cell Lines GI-101A and A549

Ferritin is the major iron storage protein and was shown to provide MRI contrast in C6 glioma tumors (Cohen *et al*., 2005). Recombinant vaccinia virus strains harboring the two ferritin subunits were generated to test if these effects can also be caused by ferritin overexpression in tumors mediated by vaccinia viruses. GLV-1h131, GLV-1h132, and GLV-1h133 carry the genes that encode for the human ferritin H- and L-subunits linked by a 2A sequence under the control of the three different vaccinia promoters, the synthetic early promoter, the synthetic early/late promoter, and the synthetic late promoter.

In an initial experiment, the course of replication of GLV-1h131, GLV-1h132, and GLV-1h133 was compared to the replication behavior of the parental virus strain GLV-1h68 in the cell lines GI-101A and A549. The viral titers of infected cells at different time points were obtained using standard plaque assay. It can be stated that the recombinant virus constructs that mediate ferritin expression in infected cells, were able to replicate efficiently in GI-101A breast carcinoma and A549 lung carcinoma cells. The replication behavior of the new virus strains was comparable to the parental virus strain GLV-1h68. Both cell lines showed very similar viral titers at each time point, however the replication of the viruses in A549 cells was slightly more effective than in GI-101A cells. Since both cell lines were infected with equal amounts of virus (MOI 0.01), these findings indicate that A549 might be a cell line that divides and grows faster than the GI-101A cell line and thus provides more cells for the replication of more viruses. Forty-eight hours post

infection viral titers in infected cells decreased resulting in a plateau phase, which indicates that by that time almost every cell was infected and replication was slowed down. GLV-1h131 showed a slower replication than the other ferritin-encoding virus strains and also no plateau at 48 hours post infection in both cell lines. Since the use of the synthetic early promoter in this viral strain cannot explain the observed differences and the fact that this phenomenon was observed in cell lysates of both cell lines, it might be that additional mutations were acquired in this particular strain. However, the chance of mutations happening is very unlikely which leads to the conclusion that the amount of added virus might not have been equal to the amount of the other viruses. This could result from an inaccurate determination of the virus titer before the infections.
The virus-mediated ferritin expression was analyzed by using three different protein analytical techniques. Both the Coomassie staining of SDS-PAGE gels and the Western blot analysis with GI-101A cells and with A549 cells showed the same results. The viruses that induce ferritin expression under the control of the strong synthetic early/late and synthetic late promoters (GLV-1h132 and GLV-1h133) resulted in a strong signal that most likely represents the protein band of the ferritin dimer at 40 kDa, consisting of the light and the heavy chain subunits that are still linked to each other. The ferritin-encoding virus controlled by the weak synthetic early promoter did not result in any signal, which can be explained by the insensitivity of the techniques, by which the analysis was performed (colorimetric instead of ECL-mediated Western blot detection) and the lower expression levels of the recombinant protein caused by the expression under the control of a weak vaccinia promoter. The genes encoding the two ferritin subunits are connected by the linker sequence 2A, which is originating from the picornavirus foot-and-mouth disease virus and is used in molecular biology to create polycistronic mRNAs for coexpression of two proteins. Insertion of picornaviral 2A sequences into mRNAs cause ribosomes to skip formation of a peptide bond at the junction of the 2A and downstream sequences, leading to the production of two proteins from a single open reading frame (Funston *et al*., 2008). It leads to approximately equal expression of the proteins upstream and downstream of the 2A site (de Felipe *et al*., 2006). The finding that the two subunits are still connected after expression by virus-infected cells gathered from SDS-PAGE and Western blot was the reason to investigate

that the ferritin complex consisting of 24 subunits can be assembled correctly. The confirmation was obtained by performing a different kind of protein gel electrophoresis, native PAGE, which detects proteins in their native and non-denatured form. The native gel stained with Coomassie Blue and the native Western blot both showed the strongest protein bands at the size of approximately 500 kDa, which is the correct size of the ferritin 24-mer. There were also weaker protein bands double that size, which might represent multimers of ferritin. Thus, it can be assumed that a functional complex is formed after expression in virus-infected cells.

Additionally a different protein analytical method was performed using the ferritin-encoding viruses. In an ELISA antibodies are used to detect a specific antigen, in this case ferritin. The analysis of the ferritin expression by ELISA revealed that twelve hours post infection the first detectable overexpression could be detected. Results in GI-101A cells and in A549 cells were very similar. Twenty-four and 48 hours after infection the differences between GLV-1h132-infected cells and controls were even more pronounced. The only difference was a slightly enhanced expression of ferritin in A549 compared to GI-101A cells which were infected with the ferritin-encoding viruses, even though in GI-101A cells the uninfected and GLV-1h89-infected cells expressed slightly more ferritin to begin with. Infection with GLV-1h131 did not result in any detectable overexpression of ferritin in both cell lines. One reason for this is that GLV-1h131 encodes ferritin under the control of the weak synthetic early promoter. Another reason could be that the virus titer was not determined correctly. A lower MOI results in a decreased overall expression of recombinant protein in the sample. The analysis of the replication of GLV-1h131 confirm that possibility because it showed less virus particles in infected cells at all time points in both cell lines. The promoter strength and time of activation is also reflected in the amount of protein produced. The weak synthetic early promoter leads to less expressed protein. The strong synthetic early/late promoter in GLV-1h132 led to a higher expression in the earlier time points (twelve and 24 hours) but at after 48 hours the synthetic late promoter led to a more efficient expression of ferritin in GLV-1h133-infected cells. This phenomenon could be observed in both cell lines.

Overall it can be stated that the ferritin-encoding viruses are able to infect and replicate in GI-101A and A549 cells and in addition to that mediate the expression of ferritin according to the strength and time of activation of the promoters controlling its expression in the different virus strains.

5.2 Bacterioferritin-encoding Viruses Were Able to Replicate and Mediate Bacterioferritin Expression in the Cancer Cell Lines GI-101A and A549

The *E. coli* bacterioferritin was shown to enhance T2 contrast in MRI measurements of murine tumors colonized with *E. coli* (Hill *et al*., in preparation). By inserting the bacterioferritin gene into the genome of vaccinia viruses it was investigated if this approach could also be useful for enhancing MRI contrast in virus-infected tumors. GLV-1h110, GLV-1h111, and GLV1h112 are virus strains that express bacterioferritin in infected cells under control of different promoters (synthetic early, synthetic early/late and synthetic late vaccinia promoters for GLV-1h110, GLV-1h111, and GLV-1h112, respectively) in the HA locus. GLV-1h113 contains a “humanized” version of bacterioferritin under control of the synthetic early/late promoter, in which the codon usage of the cDNA sequence was optimized for expression in human cells.

After generation of the bacterioferritin-encoding viruses, the first step was to analyze their replication behavior. This was done by performing standard plaque assays. The analysis revealed that GLV-1h110, GLV-1h111, GLV-1h112, and GLV-1h113 were able to infect and replicate in GI-101A and A549 cells. The virus titers increased with the time until a plateau was reached between 48 and 72 hours post infection. This indicates that all cells in the wells were infected by the virus and replication was slowed down. The replication behavior of all bacterioferritin-encoding viruses was comparable to the replication of the parental virus strain GLV-1h68 in both cell lines used. Thus, the integration of the bacterioferritin gene had no influence on the replication efficiency of the new virus strains.

The next step to characterize the virus strains was to investigate the virus-induced bacterioferritin expression. This was done by performing SDS-PAGE and Western blotting. These protein-analytical experiments revealed that the bacterioferritin protein

was expressed by virus-infected cells as expected. The amount of protein detected on the gels and blots corresponded to the strength of the promoters which controlled the bacterioferritin expression in the used viruses. The bacterioferritin expression in GLV-1h110-infected cells could not be detected using these methods, which is due to the weak promoter strength of the synthetic early promoter and, as already discussed above, also to the insensitivity of the method. GLV-1h111- and GLV-1h113-infection resulted in the strongest bands on both, the gels and the blots, because in these viruses the protein is under the control of the strongest of the three vaccinia promoters used in this study, the synthetic early/late promoter. These virus strains only differ in the sequence of the bacterioferritin gene inserted in the vaccinia genome. GLV-1h111 contains the *E. coli* bacterioferritin gene and GLV-1h113 carries a codon-optimized version of the bacterioferrritin gene for a possibly more effective expression in human cells. It could be shown that this difference did not affect the replication behavior of the viruses and did not lead to a detectable difference in the expression of the recombinant proteins in infected GI-101A and A549 cells. In GLV-1h112-infected cells the bacterioferritin band on the gels and blots were detectable but slightly weaker. In this virus strain the bacterioferritin gene is under the control of the synthetic late promoter, which was shown to lead to a weaker expression compared to the synthetic early/late promoter. Overall the signals on the Western blots were relatively weak, which is due to the serum which was used for detection of this protein. There was no bacterioferritin antibody available at that time which was the reason for generating anti-bacterioferritin mouse serum by injecting mice multiple times with purified bacterioferritin protein. Obviously the obtained serum did not show as strong binding affinities to the protein as a commercially available antibody.

From these experiments it can be concluded that all used virus strains showed a very similar infection and replication behavior and that the recombinant proteins could be successfully expressed in GI-101A and A549 cancer cells by infection with these viruses.

5.3 Transferrin Receptor-encoding Viruses Were Able to Replicate and Mediate Transferrin Receptor Expression in the Cancer Cell Lines GI-101A and A549

The transferrin receptor is a major protein involved in iron metabolism, especially iron uptake into the cell. It was shown to be useful as a marker for MR Imaging (Moore *et al*., 2001). GLV-1h22 was constructed by inserting the human transferrin receptor gene into the viral genome. GLV-1h114 and GLV-1h115 contain the murine version of the transferrin receptor gene under the control of two different promoters.

Before starting any experiments with these virus strains the infection and replication behavior was investigated by performing plaque assays. The analysis of the replication of GLV-1h22, GLV-1h114, and GLV-1h115 revealed that all of the used virus strains in this experiment were able to infect and replicate in GI-101A and A549 cells. The viral titers in the infected cells were similar to those of cells infected with the parental virus strain GLV-1h68 and increased until a plateau was reached between 48 and 72 hours post infection. The same phenomenon was already described for the previously mentioned viruses and can be explained from the fact that all cells in the wells were infected at that time which slowed down the further replication of the viruses.

After proving that all transferrin receptor-encoding viruses were able to infect and replicate efficiently in the two cell lines, the expression of the foreign genes was tested by Coomassie staining of SDS gels and Western blotting. The analysis of Coomassie-stained protein gels revealed no major differences in the protein bands. All samples loaded in the gel, including the uninfected control, showed multiple protein bands at around 95 kDa which is the molecular weight of the transferrin receptor protein. The reason for that is the expression of the transferrin receptor in every cell type, especially in fast proliferating cells like cancer cells (Lok and Loh, 1998), which were used in these experiments. However, there was a slightly stronger band at around 95 kDa detectable in the lane of the cell lysate infected with GLV-1h115. In the genome of GLV-1h115 the strong synthetic early/late promoter controls the transferrin receptor expression in contrary to the weak synthetic early promoter which controls the transferrin receptor expression in GLV-1h114, which could explain the band. GLV-1h114 and GLV-1h115 contain the murine transferrin receptor gene and GLV-1h22 carries the human corresponding gene. There is no difference in the molecular weight because the

sequence is almost homologous. On the Western blots these bands at 95 kDa could not be detected in all samples, only a very slim band in the lane that was loaded with the human transferrin-encoding virus GLV-1h22-infected cells. A possible reason for this result is the suitability of the antibody against the transferrin receptor used in this experiment. It was supposed to detect human and mouse transferrin receptor but even in very low dilutions it did not show a good signal. The blot performed with β-actin antibody showed a band in all lanes, which proves that enough amount of protein samples were loaded to show an overexpression of the virus-mediated protein and that the samples were loaded evenly in all wells of the gel.

5.4 Ferritin- and Transferrin Receptor-encoding Viruses Were Able to Replicate and Mediate Ferritin and Transferrin Receptor Expression in the Cancer Cell Lines GI-101A and A549

To combine the possible effects of virus-mediated expression of an iron storage and an iron transport protein on iron accumulation, four new recombinant ferritin- and transferrin-expressing virus strains were generated. GLV-1h154 carries the genes that encode bacterioferritin and human transferrin receptor, GLV-1h155 the human ferritin H-chain gene and the human transferrin receptor gene. GLV-1h156 and GLV-1h157 infected cells both express the mouse transferrin receptor and bacterioferritin or human ferritin H-chain, respectively.

After the generation of these new virus strains the infection and replication efficiency was tested in GI-101A and A549 cells by plaque assays. All viruses in this experiment showed increasing viral titers at all time points and in both cell lines tested. It could be shown that all four virus strains exhibited a similar replication behavior to the parental virus strain GLV-1h68. Thus, the additional payload of two foreign genes in the vaccinia genome did not interfere with the infection and replication capabilities of the viruses.

The analysis of the expression of these foreign genes delivered by the different virus strains in infected cells was conducted by SDS-PAGE and subsequent Coomassie staining of the gels. On the gels loaded with infected cell lysates of both cell lines, the ferritin H-chain overexpression of GLV-1h155 and GLV-1h157-infected cells could be

seen clearly at 21 kDa. Also the bacterioferritin expression could be detected in cell lysates infected with GLV-1h154 and GLV-1h156 between 10 and 15 kDa on the gel. As already mentioned in the previous paragraph about transferrin receptor-expressing virus strains, the overexpression of this protein mediated by the recombinant viruses could not clearly been shown by this protein analytical method. One reason for that could be that the transferrin receptor is expressed in every cell type, especially in fast proliferating cells like cancer cells (Lok and Loh, 1998). This method is not sensitive enough to show only slight differences in protein expression and thus could not visualize the overexpression of the transferrin receptor mediated by the virus strains GLV-1h154, GLV-1h155, GLV-1h156, and GLV-1h157.

5.5 Ferritin Light Chain-encoding Viruses Were Able to Replicate and Mediate Ferritin Light Chain Expression in the Cancer Cell Lines GI-101A and A549

It was shown that expression of a mutant form of the ferritin light chain led to iron overload in transgenic mice (Vidal *et al*., 2008). This mutation consists of an insertion of a thymidine (T) and a cytidine (C) at position 498 in its open reading frame. To investigate if this approach also leads to a higher iron accumulation than the wild type light chain when delivered by vaccinia virus, two new recombinant virus strains were generated. GLV-1h186 carries the ferritin light chain-encoding gene with the insertion and GLV-1h187 carries the wild type ferritin light chain-encoding gene to be used as a control.

As a first step in the characterization of these new virus strains the replication efficiency in comparison with the parental virus strain GLV-1h68 was tested. The infection of GI-101A and A549 cells was analyzed at different time points by plaque assays. It could be shown that all used viruses were able to infect and replicate in cells of both cell lines. The replication behavior of both ferritin light chain-encoding virus strains was shown to be similar to that of GLV-1h68. It can be stated that the insertion of these genes into the genome of the parental virus GLV-1h68 did not affect the infection and replication capabilities of these viruses.

Coomassie staining of protein gels was performed to analyze the protein expression of these foreign genes delivered by the viruses. The gels loaded with infected GI-101A and A549 cells showed clear bands that represent the ferritin light chain in the lanes loaded with cell lysates infected by the respective viruses. Infection of cells with GLV-1h186 led to a protein band with a slightly bigger molecular weight in comparison to infection with GLV-1h187. The difference in the molecular weight due to the insertion of two nucleotides, which caused a shift in the reading frame, could clearly be shown in the stained protein gels.

5.6 Divalent Metal Transporter-encoding Viruses Were Able to Replicate in the Cancer Cell Lines GI-101A and A549 and Mediate Expression of DMT in Infected Cells

The divalent metal transporter is another major protein in the uptake of iron and is hoped to lead to iron accumulation when expressed by virus-infected tumor cells. The gene encoding the divalent metal transporter 1 (DMT1) was inserted in the parental virus strain GLV-1h68 to generate GLV-1h102.

In the replication analysis performed by using plaque assays the virus GLV-1h102 was shown to infect and replicate in GI-101A and A549 cells in an almost identical manner than the parental virus strain GLV-1h68. Infection of both cell lines showed increasing viral titers correlating with the time of infection. Between 48 and 72 hours post infection a plateau was reached when all cells were infected by the viruses and replication was slowed down. This result proved that the insertion of the *dmt1* gene into the genome of the parental virus GLV-1h68 did not interfere with the replication capabilities of this virus.

The detection of the DMT1 expression by SDS-PAGE and Coomassie staining was not successful. The molecular mass of DMT1 is estimated to be 65 kDa and could not be shown clearly on the stained gels. One explanation for this result could be that DMT1 is expressed in many different cell types (Testa, 2002) and that one of the bands with the molecular mass of 65 kDa that were visible in all lanes represents the DMT1 expression and the method is just not sensitive enough to visualize the overexpression of this

protein mediated by the virus GLV-1h102. An additional argument that supports this explanation is that DMT1 is expressed under the control of the weak synthetic early promoter, which does not lead to enough protein expression to be detected by this relatively insensitive method. To prove that this protein is expressed by GLV-1h102-infected cells, a more sensitive method had to be used. RT-PCR is a method that is used to detect gene expression on a transcriptional level. cDNA is made from isolated mRNA and can be then amplified by PCR using specific primers, which makes it a very sensitive technique. The result of the RT-PCR revealed a DNA band on the agarose gel loaded with the PCR products from reactions with the DMT1 primers in all lanes. That means that also the uninfected control cells and the cells infected with GLV-1h68 showed DMT-1 expression. This finding goes in line with the previously mentioned expression of DMT1 in many different cell types (Testa, 2002). However, the band on the gel in the lane of the PCR product deriving from GLV-1h102-infected cells was stronger even though the same reaction using the β-actin primers led to three bands with the same intensity. This proves that the virus GLV-1h102 leads to overexpression of the DMT1 protein in infected cells and that the technique of RT-PCR is sensitive enough to show these differences in gene expression even though GLV-1h102 contains the weak synthetic early promoter upstream of the *dmt1* gene.

5.7 MagA-encoding Viruses Were Able to Replicate in the Cancer Cell Lines GI-101A and A549 and Mediate *magA* Expression in Infected Cells

MagA is a protein of the bacterium *Magnetospirillum magnetotacticum* which was shown to be sufficient to produce magnetic nanoparticles in mammalian cells. This property was used in a study showing its capability as an MRI reporter (Zurkya *et al*., 2008). To investigate if this property could also be useful when expressed by infected tumor cells the recombinant virus strain GLV-1h184 encoding this protein was generated.

As already shown for the other viruses the first step in the characterization of a new virus strain is the analysis of the infection and replication behavior in cancer cells in comparison to the parental virus GLV-1h68. This analysis showed a very similar

replication of the MagA-encoding virus strain GLV-1h84 compared to that of GLV-1h68. Infection of both cell lines resulted in a similar number of plaques of both viruses at each time point. Thus, it was shown that the insertion of the *magA* gene in the virus genome did not affect the replication capability of this virus.

After the replication behavior was investigated, the expression of MagA by GLV-1h184-infected tumor cells was analyzed. In Coomassie-stained protein gels the MagA expression was not detectable in infected GI-101A and A549 cells similar to what was shown for DMT1 as described in section 5.6. The MagA protein has a predicted molecular mass of 45 kDa. No protein band corresponding to this molecular weight could be identified. The explanation for the unsuccessful detection by SDS-PAGE could be the expression of the MagA protein under the control of the weak synthetic early promoter, which does not lead to sufficient protein expression for detection by this technique as already shown for all the virus strains that contain this promoter described above. Due to the lack of detection the more sensitive method RT-PCR, which shows gene expression on a transcriptional level was utilized. The RT-PCR analysis led to a successful detection of *magA*. The agarose gel which was loaded with PCR products of uninfected, GLV-1h68-infected and GLV-1h184-infected samples, showed a clear band only in the lane of the GLV-1h84- infected sample. The use of the same samples for a RT-PCR with β-actin primers led to three bands comparable in size and intensity, which proves that the same amount of PCR product was loaded on the gel. It can be stated that the infection with the virus GLV-1h84 therefore most probably results in the expression of the bacterial protein MagA in the used cancer cells.

5.8 Iron Measurements Showed Enhanced Iron Accumulation in Virus-infected Cells

As a next step after the characterization of all virus strains that were used in this study, their ability to collect iron in tumor cells for a possible detection by MRI technology was investigated in cell culture. For this purpose different iron assays were performed. The first assay was the commercially available QuantiChrom™ Iron Assay, which measures the total iron concentration of a sample by forming a blue colored complex with iron that

can be measured using a microplate reader. The assay performed with samples from uninfected and GLV-1h68-, GLV-1h113-, and GLV-1h132-infected cells 24 hours post infection revealed an iron concentration which was at least twice as high in samples infected by all the different virus strains as in uninfected control cells. The differences between the used virus strains in iron accumulation were not very pronounced. This leads to the question why GLV-1h68-infection has such an effect even though no iron-accumulating genes were inserted in its genome.

The same observation was made using the ferrozine iron assay. Ferrozine reacts with divalent iron and forms a stable magenta complex which can be used for the determination of iron in solutions (Stookey, 1970). Uninfected cells and with GLV-1h68-, GLV-1h113-, GLV-1h132-, GLV-1h154-, and GLV-1h155-infected cells were harvested one, six, twelve, and 24 hours post infection and the samples were analyzed using that assay. It was shown that the difference in iron concentration between uninfected and infected cells was first apparent six hours post infection. The difference was more pronounced after twelve hours, and 24 hours post infection the iron accumulation reached the maximum. The different iron-accumulating viruses did not exhibit significant differences in iron concentration, not even when compared to GLV-1h68. The result in A549 cells resembled the result in GI-101A cells greatly; with the only difference that in A549 cells the overall iron concentration was higher. As already described A459 cells grow faster and thus can accumulate more iron in more cells.

The ICP-MS measurements, which were performed detecting iron and manganese, showed a similar result for the iron accumulation. Cells that were infected with GLV-1h68 exhibited a similar or even higher level of iron content compared to GLV-1h113- or GLV-1h132-infected cells. In fact, GLV-1h132-infected cells showed only a slightly more effective iron accumulation than uninfected control cells. For the manganese measurements the only virus strain whose infection led to a significant higher manganese concentration was also the parental virus strain GLV-1h68. Infection with GLV-1h113 and GLV-1h132 resulted in only a slight increase in manganese content in the cells.

The fact that infection with GLV-1h68 led to a similar or even more effective accumulation of iron (and manganese) in infected cells compared to all the virus strains

that were genetically modified for the purpose of accumulating iron in infected cells, is remarkable. This finding could be a result of the changes in iron metabolism that happen after viral infection. Although in contrast to bacteria or fungi, viruses do not require iron, infected host cells require iron to synthesize the viral particles. After infection, hosts have several ways to withhold iron from invading cells. These are the upregulation of iron-binding proteins, lowering iron in body fluids and withdrawing iron from invaded host cells (Weinberg, 1996). In a study from 1994 it was shown by Cemeriglu and Ozsoylu that children with chicken pox exhibited a decrease in serum iron and transferrin iron saturation and an increase in serum ferritin. These values returned to normal after recovery from the disease (Cemeriglu and Ozsoylu, 1994). In a different study on vaccinia virus it was shown that Interferon-γ, which is produced in response to virus infection, induced the synthesis of nitric oxide. Nitric oxide was found to inhibit viral DNA synthesis, late gene expression and virus particle formation. This observation could be reversed by administering ferrous sulfate (Karupiah and Harris, 1995). Correspondingly iron overload leads to increased risk of infection by compromising immune defense mechanisms. Due to this observation iron chelators were proposed in the treatment for viral infections. Vaccinia virus specifically was shown to be impaired by iron chelation, which resulted in inhibition of viral late proteins and DNA synthesis (Romeo *et al*., 2001). Some viruses were also shown to target proteins of iron metabolism, for example some viruses use TfR as cellular receptor. The picornavirus mengo virus was found to induce ferritin synthesis and cause an increase in the cellular iron (Mulvey *et al*., 1996). It was also suggested by studies in our group that infection with GLV-1h68 results in TfR overexpression (Horbaschek, 2009, Worschech, personal communication). For the manganese accumulation the explanation is the same, because manganese uses some of the same uptake mechanisms as iron.

In summary it can be stated that virus infection alone can cause iron (and possibly manganese) overload and this could be a reason for elevated concentrations in GLV-1h68-infected cells.

5.9 Heavy Metal Measurements Showed that the Synthetic Phytochelatin EC20 Led to Heavy Metal Accumulation in Bacterial Cultures

It was shown that synthetic phytochelatins have the capability to bind metals (Bae and Mehra, 1997). One study described the construction and characterization of recombinant *E. coli* strains that bind functional synthetic phytochelatins on the cell surface and showed that these synthetic phytochelatins give a metal-binding capability to the host cells and lead to a higher accumulation of cadmium than the wild type cells (Bae *et al*., 2001). In this study EC20, a synthetic phytochelatin with 20 cysteines, was used to accumulate different metals in bacteria. EC20 was genetically integrated into an outer loop of the *E. coli* surface protein TolC. The advantage of working with bacteria on this project instead of vaccinia virus was that the effects could be investigated much more easily and time efficient with bacterial cultures than the time consuming generation of new recombinant virus strains. For this experiment two different bacterial strains were used. The *E. coli* Omnimax pTolC, which contains a plasmid with a gene for the surface protein TolC (German and Misra, 2001) and *E. coli* Omnimax pTolC-EC20, which additionally contains a gene for the heavy metal-accumulating synthetic phytochelatin EC20 (Bae *et al*., 2001) fused to the surface protein TolC, were used. Similar to the procedure when creating new virus strains, the growth behavior of the two bacterial strains was investigated first. Both bacterial growth curves showed the characteristic growth pattern including lag-, log- and stationary phase. However, the *E. coli* Omnimax pTolC-EC20 showed a growth delay and did not reach the same optical density in the stationary phase compared to *E. coli* Omnimax pTolC. This finding might be due to the additional payload of the EC20-encoding gene in the slower growing strain *E. coli* Omnimax pTolC-EC20 or a reduced functionality in the important outer membrane protein TolC due to the EC20 insertion.

For the actual heavy metal measurement by ICP-MS, which is a very sensitive technique for metal determination in a sample, the optical density of the two strains was adjusted before the different heavy metal supplements $FeCl_3$, $MnSO_4$, $CuSO_4$, and $CdCl_2$ were added. The obtained values for the heavy metal concentration in the bacterial cultures showed that that *E. coli* Omnimax pTolC-EC20 strain showed enhanced accumulation of all used heavy metals of at least 7% when compared to the

control strain *E. coli* Omnimax pTolC. The most pronounced difference could be shown for cadmium, as described in the study published by Bae *et al*. (2001).

Overall, it can be stated that the heavy metal accumulation by using the synthetic phytochelatin EC20 in *E. coli* was successful. Since it could be proven to work in bacteria, the next step could be to use this system for metal accumulation in vaccinia virus-infected tumor cells. A recombinant EC20-encoding vaccinia virus strain could possibly be generated and tested for its ability to collect detectable amounts of metals in infected tumors for a possible diagnostic purpose.

5.10 Virus Particles in Infected Xenograft Mice Were Mainly Found in the Tumors

For the *in vivo* experiments only the most promising virus strains were used. These were GLV-1h68 as a control virus, the codon-optimized bacterioferritin-encoding virus GLV-1h113, the ferritin-encoding virus GLV-1h132, and GLV-1h184, which encodes *magA*. The major requirement for these virus strains to be used as a diagnostic tool in live mice and eventually in humans is that the viruses are infecting, replicating, and also inducing expression of iron-accumulating proteins only in tumor cells. All the newly generated virus strains are expected to have this property, which was already shown for the parental virus GLV-1h68 (Zhang *et al*., 2007). One reason for this behavior is the attenuation that comes from a deletion of the thymidine kinase gene in vaccinia virus that leads to dependence of the virus on cellular thymidine expression, which is overexpressed in tumor cells (Buller *et al*, 1985).

To confirm this assumption plaque assays were performed with tumor and organ lysates from uninfected and infected mice 24 days after intravenous injection of the viruses. The experiment showed that up to $1x10^7$ viral particles were found in the tumors of all virus-infected mice. All tested viral strains led to similar amounts of virus particles in the tumors. As expected no virus particles could be detected in uninfected control mice. The only group of mice that showed virus particles in organs other than the tumor, was the group infected with GLV-1h184. Viral particles were found in lung and spleen, however the titers were 3 and 4-log lower than in the tumors. This finding could possibly also be an indication of metastases in the lungs or spleen, which were targeted by the virus.

Plaque assays from liver and heart lysates did not lead to detection of virus in these organs. These results demonstrated that the viruses almost exclusively infected and replicated in tumor cells and are cleared by the immune system in the rest of the body, which makes them perfect candidates for tumor diagnosis.

5.11 Recombinant Viral Proteins Were Expressed in Tumors of Infected Mice

After the biodistribution *in vivo* was investigated the next question was whether the recombinant proteins are expressed in detectable amounts in virus-infected tumors. To solve this question tumor lysates were analyzed by Western blot using different antibodies. The analysis showed that the ferritin protein and the bacterioferritin protein could clearly be detected in GLV-1h132- and GLV-1h113-infected tumors, respectively. The signal on the blot obtained by incubating with anti-bacterioferritin mouse serum was slightly weaker than the one obtained from incubation with ferritin antibody because the serum which was used for detection did not show very strong binding affinities to the protein. The same difficulties were encountered when using this mouse serum for the detection of bacterioferritin in the protein expression studies in cell culture as already mentioned in section 5.2. The Western blot performed by using β-actin antibody served as a loading control to prove that the same amounts of total protein were loaded on the gel and the signals actually result from expression mediated by the viruses. In summary it could be proven that ferritin and bacterioferritin were expressed by virus-infected tumor cells.

5.12 Iron Measurements of Tumor Lysates Showed Significantly Enhanced Iron Accumulation Only in GLV-1h68-infected Tumors

Following the procedure in cell culture the third step of *in vivo* experiments was the determination of iron accumulation in uninfected and infected tumors. The iron content of the tumors was measured by performing a ferrozine assay with tumor lysates. The measurement revealed that the only significantly enhanced iron accumulation came from infection with GLV-1h68, the control virus strain with no inserted gene for iron

collection. This remarkable result was already described in cell culture studies but became even more pronounced in the tumors. The reason for this behavior of GLV-1h68-infected cells could be that viral infection alone was shown to lead to changes in iron metabolism as already discussed in the paragraph 5.8. In contrary to the measurement in cell culture, where GLV-1h68 led to a similar amount of iron collected in the infected cells as by the other virus strains, GLV-1h68 seemed to be the only virus enhancing iron accumulation significantly. GLV-1h113 and GLV-1h184 were shown to slightly enhance the iron concentration in the respective tumors.

5.13 Histological Staining Showed that Iron Accumulation Did Not Correlate with Virus Infection in the Tumors

For the histological analysis of the tumors four different staining procedures were performed. H&E staining helped visualize the general structure of the tumors and identified the virus-infected areas as areas of dead tumor cells. Additionally immunohistochemical stainings with a vaccinia and a ferritin antibody were performed with the tumor sections. These studies confirmed that all tumors that were dissected from virus-injected mice, showed large areas of virus infection. The ferritin staining revealed that ferritin overexpression could only be found, as expected, in ferritin-encoding virus GLV-1h132-infected tumors. In GLV-1h132-infected tumors these areas of ferritin overexpression corresponded directly with the areas of vaccinia virus infection, which proves again that the ferritin expression was mediated by the virus GLV-1h132.

Furthermore the iron present in the tumor sections was stained by Prussian Blue iron staining. The performed staining did not lead to clear results. However, it can be stated that the uninfected tumors seemed to have less iron content than the infected tumors. It could be observed that the areas of stained iron clearly did not correlate to the virus-infected areas in any of the infected tumors. Iron accumulation according to this experiment seemed not to be a direct result of virus-mediated overexpression of the iron-accumulating proteins. However, it still seemed to be an effect resulting from infection because staining of non infected tumors did not lead to a comparable staining of iron in the tumors. The finding obtained from the iron assays in cell cultures as well

as *in vivo* support this observation because they showed no difference in iron accumulation between GLV-1h68 and the virus strains encoding iron-accumulating proteins. As already discussed in the paragraph 5.8 this could be due to general effects of viral infection on iron metabolism and iron withholding strategies by host cells to inhibit viral replication.

5.14 MRI Measurements Showed Shortened T2 and T2* Relaxation Times in Tumors Infected by Viruses that Mediate Iron Accumulation

The central experiment and aim of this study were the MRI measurements with virus-infected mice. The newly generated iron-accumulating virus strains were analyzed for their potential to create contrast (iron appears dark on T2–weighted images) in scans of infected tumors. Their usefulness for tumor diagnosis by MRI technology should be evaluated.

Two different measurements were performed, the first scan being done with a seven Tesla small animal scanner seven days post infection and the second scan using a three Tesla human scanner 21 days after virus injection. The T2-weighted FISP images obtained from the seven Tesla measurements showed five differently treated mice seven days after virus injection. According to these images in the uninfected control tumor fewer dark areas could be detected than in all the virus-infected tumors. Considering the fact that each tumor was scanned in many different slices, it is difficult to get to a conclusion on the overall effect of the viruses on iron accumulation only by eye. Therefore this data was analyzed quantitatively to measure the overall tumor and compare different treatments. The quantitative data analysis showed that T2 relaxation times were shortened in GLV-1h113- and significantly shortened in GLV-1h184-infected tumors. These are the virus strains that mediate bacterioferritin and MagA expression in infected cells, respectively. In contrary to the histological stainings an effect on MRI contrast could be successfully shown for these two virus strains.

The results of the three Tesla measurements two weeks after the seven Tesla measurements were very similar. The tumors of the GLV-1h184-injected mouse contained more and darker areas in the tumors which are a sign for more iron

accumulated in the tumor. Also the tumors of the GLV-1h113-injected mouse appeared darker than the control tumors. In the right tumor of the control mouse a large cystic area could be seen, which could not be included in the data analysis. In the quantitative data analysis tumors infected with both viruses, GLV-1h113 and GLV-1h184, showed clearly shortened T2* relaxation times in comparison to the uninfected control tumors. Thus, also the human three Tesla scanner was able to detect the differences in relaxation times resulting from infection with GLV-1h113 and GLV-1h184 compared to uninfected tumors.

Overall these results are very promising for future tumor diagnostics using oncolytic vaccinia viruses, especially the finding that the differences in T2 relaxation could not only be detected with a seven Tesla small animal scanner but also with a three Tesla human scanner which is used in the clinic today. Also the fact, that the oncolytic vaccinia viruses, which are administered intravenously are able to find and infect the tumors is an important factor not only for tumor diagnosis but also for detecting metastases that are distant from the primary tumor. However, some aspects of this system still have to be optimized. To be able to see borders of tumors, which would be important for detection of tumors and metastasis, but also to monitor the effects of different treatments, it would be advantageous to find a way to infect the whole tumor and not only areas of it. It would also be beneficial to accumulate even more iron in the tumors to get a more significant difference in T2 relaxation times. There is also the possibility to use other metals (like manganese) as contrast agents which use some of the same uptake systems as iron and also lead to enhanced MRI contrast. The goal for the future has to be to generate oncolytic vaccinia viruses armed with genes encoding anti-tumor proteins and diagnostic proteins and thus combine these two crucial aspects of cancer treatment for a better chance of patient recovery thanks to diagnosis in earlier stages of cancer and better monitoring of the course of the disease and effects of treatments.

Literature

Abboud, S. & Haile, D. J. (2000) A novel mammalian iron-regulated protein involved in intracellular iron metabolism. *J Biol Chem,* **275:** 19906-12.

Aisen, P., Enns, C. & Wessling-Resnick, M. (2001) Chemistry and biology of eukaryotic iron metabolism. *Int J Biochem Cell Biol,* **33:** 940-59.

Anderson, G. J., Frazer, D. M. & McLaren, G. D. (2009) Iron absorption and metabolism. *Curr Opin Gastroenterol,* **25:** 129-35.

Andrews, N. C. (1999) The iron transporter DMT1. *Int J Biochem Cell Biol,* **31:** 991-4.

Andrews, N. C. (2000) Iron homeostasis: insights from genetics and animal models. *Nat Rev Genet,* **1:** 208-17.

Andrews, N. C. (2008) Forging a field: the golden age of iron biology. *Blood,* **112:** 219-30.

Andrews, S. C., Le Brun, N. E., Barynin, V., Thomson, A. J., Moore, G. R., Guest, J. R. & Harrison, P. M. (1995) Site-directed replacement of the coaxial heme ligands of bacterioferritin generates heme-free variants. *J Biol Chem,* **270:** 23268-74.

Andrews, S. C., Robinson, A. K. & Rodriguez-Quinones, F. (2003) Bacterial iron homeostasis. *FEMS Microbiol Rev,* **27:** 215-37.

Arakaki, A., Nakazawa, H., Nemoto, M., Mori, T. & Matsunaga, T. (2008) Formation of magnetite by bacteria and its application. *J R Soc Interface,* **5:** 977-99.

Arosio, P. & Levi, S. (2002) Ferritin, iron homeostasis, and oxidative damage. *Free Radic Biol Med,* **33:** 457-63.

Bae, D. S., Gennings, C., Carter, W. H., Jr., Yang, R. S. & Campain, J. A. (2001) Toxicological interactions among arsenic, cadmium, chromium, and lead in human keratinocytes. *Toxicol Sci,* **63:** 132-42.

Bae, W., Chen, W., Mulchandani, A. & Mehra, R. K. (2000) Enhanced bioaccumulation of heavy metals by bacterial cells displaying synthetic phytochelatins. *Biotechnol Bioeng,* **70:** 518-24.

Bae, W., Mehra, R. K., Mulchandani, A. & Chen, W. (2001) Genetic engineering of Escherichia coli for enhanced uptake and bioaccumulation of mercury. *Appl Environ Microbiol,* **67:** 5335-8.

Barbeito, A. G., Garringer, H. J., Baraibar, M. A., Gao, X., Arredondo, M., Nunez, M. T., Smith, M. A., Ghetti, B. & Vidal, R. (2009) Abnormal iron metabolism and oxidative stress in mice expressing a mutant form of the ferritin light polypeptide gene. *J Neurochem,* **109:** 1067-78.

Bazylinski, D. A. & Frankel, R. B. (2004) Magnetosome formation in prokaryotes. *Nat Rev Microbiol,* **2:** 217-30.

Bazylinski, D. A., Frankel, R. B., Heywood, B. R., Mann, S., King, J. W., Donaghay, P. L. & Hanson, A. K. (1995) Controlled Biomineralization of Magnetite (Fe(inf3)O(inf4)) and Greigite (Fe(inf3)S(inf4)) in a Magnetotactic Bacterium. *Appl Environ Microbiol,* **61:** 3232-3239.

Bellini, S. (1963) Su di un particolare comportamento di batteri d'acqua dolce. *Instituto di Microbiologia dell'Universita di Pavia*

Blakemore, R. (1975) Magnetotactic bacteria. *Science,* **190:** 377-9.

Bradley, W. G. Fundamentals of MRI Part I

Bradley, W. G. Fundamentals of MRI Part II
Bradley, W. G. Fundamentals of MRI Part III
Brooks, R. A., Vymazal, J., Goldfarb, R. B., Bulte, J. W. & Aisen, P. (1998) Relaxometry and magnetometry of ferritin. *Magn Reson Med,* **40:** 227-35.
Broyles, S. S. (2003) Vaccinia virus transcription. *J Gen Virol,* **84:** 2293-303.
Buller, R. M., Smith, G. L., Cremer, K., Notkins, A. L. & Moss, B. (1985) Decreased virulence of recombinant vaccinia virus expression vectors is associated with a thymidine kinase-negative phenotype. *Nature,* **317:** 813-5.
Camaschella, C. & Silvestri, L. (2008) New and old players in the hepcidin pathway. *Haematologica,* **93:** 1441-4.
Carrondo, M. A. (2003) Ferritins, iron uptake and storage from the bacterioferritin viewpoint. *EMBO J,* **22:** 1959-68.
Cemeroglu, A. P. & Ozsoylu, S. (1994) Haematologic consequences of viral infections including serum iron status. *Eur J Pediatr,* **153:** 171-3.
Chen (2006) MRI basics
Chen, N., Zhang, Q., Yu, Y. A., Stritzker, J., Brader, P., Schirbel, A., Samnick, S., Serganova, I., Blasberg, R., Fong, Y. & Szalay, A. A. (2009) A novel recombinant vaccinia virus expressing the human norepinephrine transporter retains oncolytic potential and facilitates deep-tissue imaging. *Mol Med,* **15:** 144-51.
Chiancone, E., Ceci, P., Ilari, A., Ribacchi, F. & Stefanini, S. (2004) Iron and proteins for iron storage and detoxification. *Biometals,* **17:** 197-202.
Cohen, B., Dafni, H., Meir, G., Harmelin, A. & Neeman, M. (2005) Ferritin as an endogenous MRI reporter for noninvasive imaging of gene expression in C6 glioma tumors. *Neoplasia,* **7:** 109-17.
Conrad, M. E., Umbreit, J. N. & Moore, E. G. (1999) Iron absorption and transport. *Am J Med Sci,* **318:** 213-29.
Faber, C. (2001) Living Lodestones: Magnetotactic bacteria
de Felipe, P., Luke, G. A., Hughes, L. E., Gani, D., Halpin, C. & Ryan, M. D. (2006) E unum pluribus: multiple proteins from a self-processing polyprotein. *Trends Biotechnol,* **24:** 68-75.
De Freitas, J. M. & Meneghini, R. (2001) Iron and its sensitive balance in the cell. *Mutat Res,* **475:** 153-9.
Douglas, T, Ripoli, D. R. (1998) Calculated Electrostatic Gradients in recombinant human H chain ferritin*. Protein Sci* pp.1083-91
Drakesmith, H. & Prentice, A. (2008) Viral infection and iron metabolism. *Nat Rev Microbiol,* **6:** 541-52.
Enns, C. A. & Sussman, H. H. (1981) Physical characterization of the transferrin receptor in human placentae. *J Biol Chem,* **256:** 9820-3.
Erlitzki, R., Long, J. C. & Theil, E. C. (2002) Multiple, conserved iron-responsive elements in the 3'-untranslated region of transferrin receptor mRNA enhance binding of iron regulatory protein 2. *J Biol Chem,* **277:** 42579-87.
Falkner, F. G. & Moss, B. (1990) Transient dominant selection of recombinant vaccinia viruses. *J Virol,* **64:** 3108-11.
Falkner, W. Basic principles of MRI
Fleming, R. E., Britton, R. S. (2006) Iron Imports. VI. HFE and regulation of intestinal iron absorption. *Am J Physiol Gastrointest Liver Physiol*. **290**:590-94

Frazer, D. M. & Anderson, G. J. (2005) Iron imports. I. Intestinal iron absorption and its regulation. *Am J Physiol Gastrointest Liver Physiol,* **289:** G631-5.

Frentzen, A., Yu, Y. A., Chen, N., Zhang, Q., Weibel, S., Raab, V. & Szalay, A. A. (2009) Anti-VEGF single-chain antibody GLAF-1 encoded by oncolytic vaccinia virus significantly enhances antitumor therapy. *Proc Natl Acad Sci U S A,* **106:** 12915-20.

Funston, G. M., Kallioinen, S. E., de Felipe, P., Ryan, M. D. & Iggo, R. D. (2008) Expression of heterologous genes in oncolytic adenoviruses using picornaviral 2A sequences that trigger ribosome skipping. *J Gen Virol,* **89:** 389-96.

Ganz, T. & Nemeth, E. (2006) Iron imports. IV. Hepcidin and regulation of body iron metabolism. *Am J Physiol Gastrointest Liver Physiol,* **290:** G199-203.

Garber, D., O'Mara, L., Zhao, J., Gangadhara, S., An, I., Feinberg, M. B. (2009) Expanding repertoire of the repertoire of modified vaccinia ankara-based vaccine vectors via genetic complementation strategies. *PloS one*. **4** (5)

Garrick, M. D., Garrick L. M. (2004) Divalent Metal Transporter DMT1. *Membrane Transporter Diseases*. pp.107-22 Kluwer

Genove, G., DeMarco, U., Xu, H., Goins, W. F. & Ahrens, E. T. (2005) A new transgene reporter for in vivo magnetic resonance imaging. *Nat Med,* **11:** 450-4.

Genove, G., DeMarco, U., Xu, H., Goins, W. F. & Ahrens, E. T. (2005) A new transgene reporter for in vivo magnetic resonance imaging. *Nat Med,* **11:** 450-4.

German, G. J. & Misra, R. (2001) The TolC protein of Escherichia coli serves as a cell-surface receptor for the newly characterized TLS bacteriophage. *J Mol Biol,* **308:** 579-85.

Giannetti, A. M. & Bjorkman, P. J. (2004) HFE and transferrin directly compete for transferrin receptor in solution and at the cell surface. *J Biol Chem,* **279:** 25866-75.

Giard, D. J., Aaronson, S. A., Todaro, G. J., Arnstein, P., Kersey, J. H., Dosik, H. & Parks, W. P. (1973) In vitro cultivation of human tumors: establishment of cell lines derived from a series of solid tumors. *J Natl Cancer Inst,* **51:** 1417-23.

Gossuin, Y., Burtea, C., Monseux, A., Toubeau, G., Roch, A., Muller, R. N. & Gillis, P. (2004) Ferritin-induced relaxation in tissues: an in vitro study. *J Magn Reson Imaging,* **20:** 690-6.

Gossuin, Y., Muller, R. N. & Gillis, P. (2004) Relaxation induced by ferritin: a better understanding for an improved MRI iron quantification. *NMR Biomed,* **17:** 427-32.

Gross, S. & Piwnica-Worms, D. (2005) Spying on cancer: molecular imaging in vivo with genetically encoded reporters. *Cancer Cell,* **7:** 5-15.

Gunshin, H., Mackenzie, B., Berger, U. V., Gunshin, Y., Romero, M. F., Boron, W. F., Nussberger, S., Gollan, J. L. & Hediger, M. A. (1997) Cloning and characterization of a mammalian proton-coupled metal-ion transporter. *Nature,* **388:** 482-8.

Hanahan, D. & Weinberg, R. A. (2000) The hallmarks of cancer. *Cell,* **100:** 57-70.

Harrison, P. M. & Arosio, P. (1996) The ferritins: molecular properties, iron storage function and cellular regulation. *Biochim Biophys Acta,* **1275:** 161-203.

Harrison, P. M. & Arosio, P. (1996) The ferritins: molecular properties, iron storage function and cellular regulation. *Biochim Biophys Acta,* **1275:** 161-203.

Harrison, S. C., Alberts, B., Ehrenfeld, E., Enquist, L., Fineberg, H., McKnight, S. L., Moss, B., O'Donnell, M., Ploegh, H., Schmid, S. L., Walter, K. P. & Theriot, J. (2004) Discovery of antivirals against smallpox. *Proc Natl Acad Sci U S A,* **101:** 11178-92.

Hentze, M. W., Muckenthaler, M. U. & Andrews, N. C. (2004) Balancing acts: molecular control of mammalian iron metabolism. *Cell,* **117:** 285-97.

Hesselink, J. R. Basic principles of MR imaging

Hodge, J. W. & Schlom, J. (1999) Comparative studies of a retrovirus versus a poxvirus vector in whole tumor-cell vaccines. *Cancer Res,* **59:** 5106-11.

Holowczak, J. A. & Joklik, W. K. (1967) Studies on the structural proteins of vaccinia virus. I. Structural proteins of virions and cores. *Virology,* **33:** 717-25.

Holowczak, J. A. & Joklik, W. K. (1967) Studies on the structural proteins of vaccinia virus. II. Kinetics of the synthesis of individual groups of structural proteins. *Virology,* **33:** 726-39.

Horbaschek (2009) Dissertation, Universität Würzburg

Hurst, J., Maniar, N., Tombarkiewicz, J., Lucas, F., Roberson, C., Steplewski, Z., James, W. & Perras, J. (1993) A novel model of a metastatic human breast tumour xenograft line. *Br J Cancer,* **68:** 274-6.

IUPAC (1997) Compendium of Chemical Terminology

Jemal, A., Siegel, R., Ward, E., Hao, Y., Xu, J. & Thun, M. J. (2009) Cancer statistics, 2009. *CA Cancer J Clin,* **59:** 225-49.

Karupiah, G. & Harris, N. (1995) Inhibition of viral replication by nitric oxide and its reversal by ferrous sulfate and tricarboxylic acid cycle metabolites. *J Exp Med,* **181:** 2171-9.

Kim, J. H., Oh, J. Y., Park, B. H., Lee, D. E., Kim, J. S., Park, H. E., Roh, M. S., Je, J. E., Yoon, J. H., Thorne, S. H., Kirn, D. & Hwang, T. H. (2006) Systemic armed oncolytic and immunologic therapy for cancer with JX-594, a targeted poxvirus expressing GM-CSF. *Mol Ther,* **14:** 361-70.

Kirn, D. H. & Thorne, S. H. (2009) Targeted and armed oncolytic poxviruses: a novel multi-mechanistic therapeutic class for cancer. *Nat Rev Cancer,* **9:** 64-71.

Klausner, R. D., Van Renswoude, J., Ashwell, G., Kempf, C., Schechter, A. N., Dean, A. & Bridges, K. R. (1983) Receptor-mediated endocytosis of transferrin in K562 cells. *J Biol Chem,* **258:** 4715-24.

Komeili, A., Li, Z., Newman, D. K. & Jensen, G. J. (2006) Magnetosomes are cell membrane invaginations organized by the actin-like protein MamK. *Science,* **311:** 242-5.

Korentsky, A., Lin, Y, Scharle, H, Jaenisch, R. (1996) Proc ISMRM, **4**:5471

Larrick, J. W. & Cresswell, P. (1979) Modulation of cell surface iron transferrin receptors by cellular density and state of activation. *J Supramol Struct,* **11:** 579-86.

Lawrence, C. M., Ray, S., Babyonyshev, M., Galluser, R., Borhani, D. W. & Harrison, S. C. (1999) Crystal structure of the ectodomain of human transferrin receptor. *Science,* **286:** 779-82.

Lee, P. L., Gelbart, T., West, C., Halloran, C. & Beutler, E. (1998) The human Nramp2 gene: characterization of the gene structure, alternative splicing, promoter region and polymorphisms. *Blood Cells Mol Dis,* **24:** 199-215.

Luker, K. E., Hutchens, M., Schultz, T., Pekosz, A. & Luker, G. D. (2005) Bioluminescence imaging of vaccinia virus: effects of interferon on viral replication and spread. *Virology,* **341:** 284-300.

Matsumoto, Paul, S (2005) *Journal of Clinical Education*. **82**:1660

Matsunaga, T., Okamura, Y., Fukuda, Y., Wahyudi, A. T., Murase, Y. & Takeyama, H. (2005) Complete genome sequence of the facultative anaerobic magnetotactic bacterium Magnetospirillum sp. strain AMB-1. *DNA Res,* **12:** 157-66.

McCart, J. A., Puhlmann, M., Lee, J., Hu, Y., Libutti, S. K., Alexander, H. R. & Bartlett, D. L. (2000) Complex interactions between the replicating oncolytic effect and the enzyme/prodrug effect of vaccinia-mediated tumor regression. *Gene Ther,* **7:** 1217-23.

McKenzie, B., Hediger, M. A. (2004) SLCII family of H+-coupled metal-ion transporters NRAMP1 and DMT1. *Pfluegers Arch.* **447** (5):590-579

McShane, H., Pathan, A. A., Sander, C. R., Goonetilleke, N. P., Fletcher, H. A. & Hill, A. V. (2005) Boosting BCG with MVA85A: the first candidate subunit vaccine for tuberculosis in clinical trials. *Tuberculosis (Edinb),* **85:** 47-52.

Meyron-Holtz, E. G., Ghosh, M. C., Iwai, K., LaVaute, T., Brazzolotto, X., Berger, U. V., Land, W., Ollivierre-Wilson, H., Grinberg, A., Love, P. & Rouault, T. A. (2004) Genetic ablations of iron regulatory proteins 1 and 2 reveal why iron regulatory protein 2 dominates iron homeostasis. *EMBO J,* **23:** 386-95.

Missirlis, F., Kosmidis, S., Brody, T., Mavrakis, M., Holmberg, S., Odenwald, W. F., Skoulakis, E. M. & Rouault, T. A. (2007) Homeostatic mechanisms for iron storage revealed by genetic manipulations and live imaging of Drosophila ferritin. *Genetics,* **177:** 89-100.

Moore, A., Josephson, L., Bhorade, R. M., Basilion, J. P. & Weissleder, R. (2001) Human transferrin receptor gene as a marker gene for MR imaging. *Radiology,* **221:** 244-50.

Moorthy, V. S., Imoukhuede, E. B., Keating, S., Pinder, M., Webster, D., Skinner, M. A., Gilbert, S. C., Walraven, G. & Hill, A. V. (2004) Phase 1 evaluation of 3 highly immunogenic prime-boost regimens, including a 12-month reboosting vaccination, for malaria vaccination in Gambian men. *J Infect Dis,* **189:** 2213-9.

Morrissey, J. J., Raney, S. (1998) A metastatic breast tumor cell line, GI-101A, is estrogen receptor positive and responsive to estrogen but resistant to tamoxifen. *Cell Biol Int* **22**(6): 413-9

Mulvey, M. R., Kuhn, L. C. & Scraba, D. G. (1996) Induction of ferritin synthesis in cells infected with Mengo virus. *J Biol Chem,* **271:** 9851-7.

Munoz, M., Villar, I, Garcia-Erce, J. A. (2009) An update on iron physiology. *W J Gastroentero*, **15**(27):4617-26.

Murau (2004) *J Gen Virol* **85**:911-9

Nemeth, E. & Ganz, T. (2006) Regulation of iron metabolism by hepcidin. *Annu Rev Nutr,* **26:** 323-42.

Omary, M. B. & Trowbridge, I. S. (1981) Covalent binding of fatty acid to the transferrin receptor in cultured human cells. *J Biol Chem,* **256:** 4715-8.

Pantopoulos, K. (2004) Iron metabolism and the IRE/IRP regulatory system: an update. *Ann N Y Acad Sci,* **1012:** 1-13.

Park, B. H., Hwang, T., Liu, T. C., Sze, D. Y., Kim, J. S., Kwon, H. C., Oh, S. Y., Han, S. Y., Yoon, J. H., Hong, S. H., Moon, A., Speth, K., Park, C., Ahn, Y. J., Daneshmand, M., Rhee, B. G., Pinedo, H. M., Bell, J. C. & Kirn, D. H. (2008) Use of a targeted oncolytic poxvirus, JX-594, in patients with refractory primary or metastatic liver cancer: a phase I trial. *Lancet Oncol,* **9:** 533-42.

Peyssonnaux, C., Zinkernagel, A. S., Schuepbach, R. A., Rankin, E., Vaulont, S., Haase, V. H., Nizet, V. & Johnson, R. S. (2007) Regulation of iron homeostasis by the hypoxia-inducible transcription factors (HIFs). *J Clin Invest,* **117:** 1926-32.

Ponka, P. (1999) Cellular iron metabolism. *Kidney Int Suppl,* **69:** S2-11.

Qian, Z. M., Li, H., Sun, H. & Ho, K. (2002) Targeted drug delivery via the transferrin receptor-mediated endocytosis pathway. *Pharmacol Rev,* **54:** 561-87.

Qian, Z. M. & Tang, P. L. (1995) Mechanisms of iron uptake by mammalian cells. *Biochim Biophys Acta,* **1269:** 205-14.

Roberts, K. L. & Smith, G. L. (2008) Vaccinia virus morphogenesis and dissemination. *Trends Microbiol,* **16:** 472-9.

Romeo, A. M., Christen, L., Niles, E. G. & Kosman, D. J. (2001) Intracellular chelation of iron by bipyridyl inhibits DNA virus replication: ribonucleotide reductase maturation as a probe of intracellular iron pools. *J Biol Chem,* **276:** 24301-8.

Rosel, J. & Moss, B. (1985) Transcriptional and translational mapping and nucleotide sequence analysis of a vaccinia virus gene encoding the precursor of the major core polypeptide 4b. *J Virol,* **56:** 830-8.

Santambrogio, P., Levi, S., Arosio, P., Palagi, L., Vecchio, G., Lawson, D. M., Yewdall, S. J., Artymiuk, P. J., Harrison, P. M., Jappelli, R. & et al. (1992) Evidence that a salt bridge in the light chain contributes to the physical stability difference between heavy and light human ferritins. *J Biol Chem,* **267:** 14077-83.

Sargent, P. J., Farnaud, S. & Evans, R. W. (2005) Structure/function overview of proteins involved in iron storage and transport. *Curr Med Chem,* **12:** 2683-93.

Schaegger, H., von Jagow, G. (1991) Blue native electrophoresis for isolation of membrane protein complexes in enzymatically active form. *Anal Biochem.* **199**(2):223-31

Schenck, J. F. (2003) Imaging of brain iron by magnetic resonance. *J Neurosci* **207** 99-102

Schneider, C., Owen, M. J., Banville, D. & Williams, J. G. (1984) Primary structure of human transferrin receptor deduced from the mRNA sequence. *Nature,* **311:** 675-8.

Schneider, C., Sutherland, R., Newman, R. & Greaves, M. (1982) Structural features of the cell surface receptor for transferrin that is recognized by the monoclonal antibody OKT9. *J Biol Chem,* **257:** 8516-22.

Schramm, B. & Locker, J. K. (2005) Cytoplasmic organization of POXvirus DNA replication. *Traffic,* **6:** 839-46.

Scieczkarsky, S. B., Whittaker, G. R. (2005) Viral entry. *Curr Top Microbiol Immunol*. **285**:1-23

Shen, Y. & Nemunaitis, J. (2005) Fighting cancer with vaccinia virus: teaching new tricks to an old dog. *Mol Ther,* **11:** 180-95.

Smith, C. L., Dunbar, P. R., Mirza, F., Palmowski, M. J., Shepherd, D., Gilbert, S. C., Coulie, P., Schneider, J., Hoffman, E., Hawkins, R., Harris, A. L. & Cerundolo, V.

(2005) Recombinant modified vaccinia Ankara primes functionally activated CTL specific for a melanoma tumor antigen epitope in melanoma patients with a high risk of disease recurrence. *Int J Cancer,* **113:** 259-66.

Smith, G. L. & Moss, B. (1983) Infectious poxvirus vectors have capacity for at least 25 000 base pairs of foreign DNA. *Gene,* **25:** 21-8.

Sodeik, B., Doms, R. W., Ericsson, M., Hiller, G., Machamer, C. E., van 't Hof, W., van Meer, G., Moss, B. & Griffiths, G. (1993) Assembly of vaccinia virus: role of the intermediate compartment between the endoplasmic reticulum and the Golgi stacks. *J Cell Biol,* **121:** 521-41.

Stern, W. & Dales, S. (1974) Biogenesis of vaccinia: concerning the origin of the envelope phospholipids. *Virology,* **62:** 293-306.

Stookey, L. (1970) Two new spectrophotometric reagents for copper. *Talanta,* **17:** 644-7.

Sutherland, R., Delia, D., Schneider, C., Newman, R., Kemshead, J. & Greaves, M. (1981) Ubiquitous cell-surface glycoprotein on tumor cells is proliferation-associated receptor for transferrin. *Proc Natl Acad Sci U S A,* **78:** 4515-9.

Suzuki, T., Okamura, Y., Calugay, R. J., Takeyama, H. & Matsunaga, T. (2006) Global gene expression analysis of iron-inducible genes in Magnetospirillum magneticum AMB-1. *J Bacteriol,* **188:** 2275-9.

Tenhunen, R., Grasbeck, R., Kouvonen, I. & Lundberg, M. (1980) An intestinal receptor for heme: its parital characterization. *Int J Biochem,* **12:** 713-6.

Testa, U. (2002) Recent developments in the understanding of iron metabolism. *Hematol J,* **3:** 63-89.

Testa, U. (2002) Proteins of Iron Metabolism

Theurl, I., Ludwiczek, S., Eller, P., Seifert, M., Artner, E., Brunner, P. & Weiss, G. (2005) Pathways for the regulation of body iron homeostasis in response to experimental iron overload. *J Hepatol,* **43:** 711-9.

Thomas (2008)

Thorne, S. H., Hwang, T. H., O'Gorman, W. E., Bartlett, D. L., Sei, S., Kanji, F., Brown, C., Werier, J., Cho, J. H., Lee, D. E., Wang, Y., Bell, J. & Kirn, D. H. (2007) Rational strain selection and engineering creates a broad-spectrum, systemically effective oncolytic poxvirus, JX-963. *J Clin Invest,* **117:** 3350-8.

Thorne, S. H., Tam, B. Y., Kirn, D. H., Contag, C. H. & Kuo, C. J. (2006) Selective intratumoral amplification of an antiangiogenic vector by an oncolytic virus produces enhanced antivascular and anti-tumor efficacy. *Mol Ther,* **13:** 938-46.

Tolonen, N., Doglio, L., Schleich, S. & Krijnse Locker, J. (2001) Vaccinia virus DNA replication occurs in endoplasmic reticulum-enclosed cytoplasmic mini-nuclei. *Mol Biol Cell,* **12:** 2031-46.

Torti, F. M. & Torti, S. V. (2002) Regulation of ferritin genes and protein. *Blood,* **99:** 3505-16.

Trowbridge, I. S. & Omary, M. B. (1981) Human cell surface glycoprotein related to cell proliferation is the receptor for transferrin. *Proc Natl Acad Sci U S A,* **78:** 3039-43.

Uzel, C. & Conrad, M. E. (1998) Absorption of heme iron. *Semin Hematol,* **35:** 27-34.

Verga Falzacappa, M. V., Vujic Spasic, M., Kessler, R., Stolte, J., Hentze, M. W. & Muckenthaler, M. U. (2007) STAT3 mediates hepatic hepcidin expression and its inflammatory stimulation. *Blood,* **109:** 353-8.

Vidal, R., Miravalle, L., Gao, X., Barbeito, A. G., Baraibar, M. A., Hekmatyar, S. K., Widel, M., Bansal, N., Delisle, M. B. & Ghetti, B. (2008) Expression of a mutant form of the ferritin light chain gene induces neurodegeneration and iron overload in transgenic mice. *J Neurosci,* **28:** 60-7.

Vymazal, J., Zak, O., Bulte, J. W., Aisen, P. & Brooks, R. A. (1996) T1 and T2 of ferritin solutions: effect of loading factor. *Magn Reson Med,* **36:** 61-5.

Wang, J. & Pantopoulos, K. (2002) Conditional derepression of ferritin synthesis in cells expressing a constitutive IRP1 mutant. *Mol Cell Biol,* **22:** 4638-51.

Wein, L. M., Wu, J. T. & Kirn, D. H. (2003) Validation and analysis of a mathematical model of a replication-competent oncolytic virus for cancer treatment: implications for virus design and delivery. *Cancer Res,* **63:** 1317-24.

Weinberg, E. D. (1996) Iron withholding: a defense against viral infections. *Biometals,* **9:** 393-9.

Weinberg, E. D. (2007) The Biology of Cancer

Weissleder, R., Moore, A., Mahmood, U., Bhorade, R., Benveniste, H., Chiocca, E. A. & Basilion, J. P. (2000) In vivo magnetic resonance imaging of transgene expression. *Nat Med,* **6:** 351-5.

Wessling-Resnik, M. (2006) Iron Imports. III. Transfer of Iron from the mucosa into circulation. *Am J Physiol Gastrointest Liver Physiol*. **290** (1)

Yu, Y. A., Shabahang, S., Timiryasova, T. M., Zhang, Q., Beltz, R., Gentschev, I., Goebel, W. & Szalay, A. A. (2004) Visualization of tumors and metastases in live animals with bacteria and vaccinia virus encoding light-emitting proteins. *Nat Biotechnol,* **22:** 313-20.

Zenk, M. H. (1996) Heavy metal detoxification in higher plants--a review. *Gene,* **179:** 21-30.

Zhang, Q., Yu, Y. A., Wang, E., Chen, N., Danner, R. L., Munson, P. J., Marincola, F. M. & Szalay, A. A. (2007) Eradication of solid human breast tumors in nude mice with an intravenously injected light-emitting oncolytic vaccinia virus. *Cancer Res,* **67:** 10038-46.

Zurkiya, O., Chan, A. W. & Hu, X. (2008) MagA is sufficient for producing magnetic nanoparticles in mammalian cells, making it an MRI reporter. *Magn Reson Med,* **59:** 1225-31.

Acknowledgements

First I want to thank Prof. Dr. Szalay for giving me the opportunity to work on such an interesting and exciting project and for his supervision and continuous encouragement. He was always available for every little question and constantly cared about my well-being in the lab and also outside of the lab.
Next I would like to thank all the members of Genelux Corporation for their help and support and for a great work atmosphere. Especially I want to thank Dr. Zhang, Dr. Chen and Dr. Yu for their guidance and very helpful discussions. I also would like to thank Terry and Jason for always providing the cells perfectly and making life in the lab a lot easier and Melody for her help with animal experiments. I want to thank Alexa for always being interested in my project and willing to help and for her friendship in and outside the lab. I also want to thank her for proof-reading this thesis. Camha I want to thank for helping with all the organizational things and for her friendship throughout the three years.
I am very grateful for the stipend provided by Genelux Corporation and the opportunity to work and live in San Diego for the time of the thesis.
For the fruitful collaboration and lots of late hours and her patience performing the MRI scans I want to thank Miriam Scadeng of the University of California, San Diego. I also want to thank Uwe Gbureck of the University of Würzburg for performing the ICP-MS measurements.

In der Würzburger “Zweigstelle” möchte ich mich vor allem bei Prof. Dr. Grummt bedanken für die Unterstützung und die netten Worte während meiner Doktorarbeit und auch beim Korrigieren dieser Arbeit. Ich danke Prof. Dr. Krohne ganz herzlich für die Zustimmung mein Zweitgutachten zu verfassen. Jochen möchte ich für die liebe Betreuung per Email, am Telefon und bei manchen San Diego-Besuchen mit vielen guten Tipps und Hilfestellungen danken. Ausserdem bin ich sehr dankbar für seine Hilfe beim Verfassen dieser Arbeit. Meinen “Mitstreitern”, die mir in meiner Zeit in Würzburg (und in San Diego) liebe Freunde geworden sind, Andrea, Caro, Viki und Rike möchte ich für die schöne Arbeitsatmosphäre und ihre Freundschaft trotz der Entfernung

danken. Vielen lieben Dank auch an Anneli, dafür dass sie auf alle Fragen immer eine Antwort hatte und für ihre Hilfsbereitschaft. Bei allen anderen Mitgliedern der Arbeitsgruppe an der Uni Würzburg möchte ich mich auch für die gute Zusammenarbeit und immer nette Atmosphäre bedanken.

Am Ende möchte ich vor allem meinen Eltern, Karin und Bernie mit Familien danken, dafür dass sie mich immer am Telefon, mit Post und durch Besuche motiviert und unterstützt haben und die auch durch die Entfernung bedingte Schwierigkeiten immer gerne für mich in Kauf genommen haben.